DYNAMIC RESPONSE OF HIGHWAYS AND AIRPORT PAVEMENTS TO FALLING WEIGHT DEFLECTOMETER LOADING

by

REZA SALAHI

A Thesis Submitted for the Degree of

Master of Science

Department of Civil Engineering

University of Glasgow

October 1989

in the Name of the Almighty

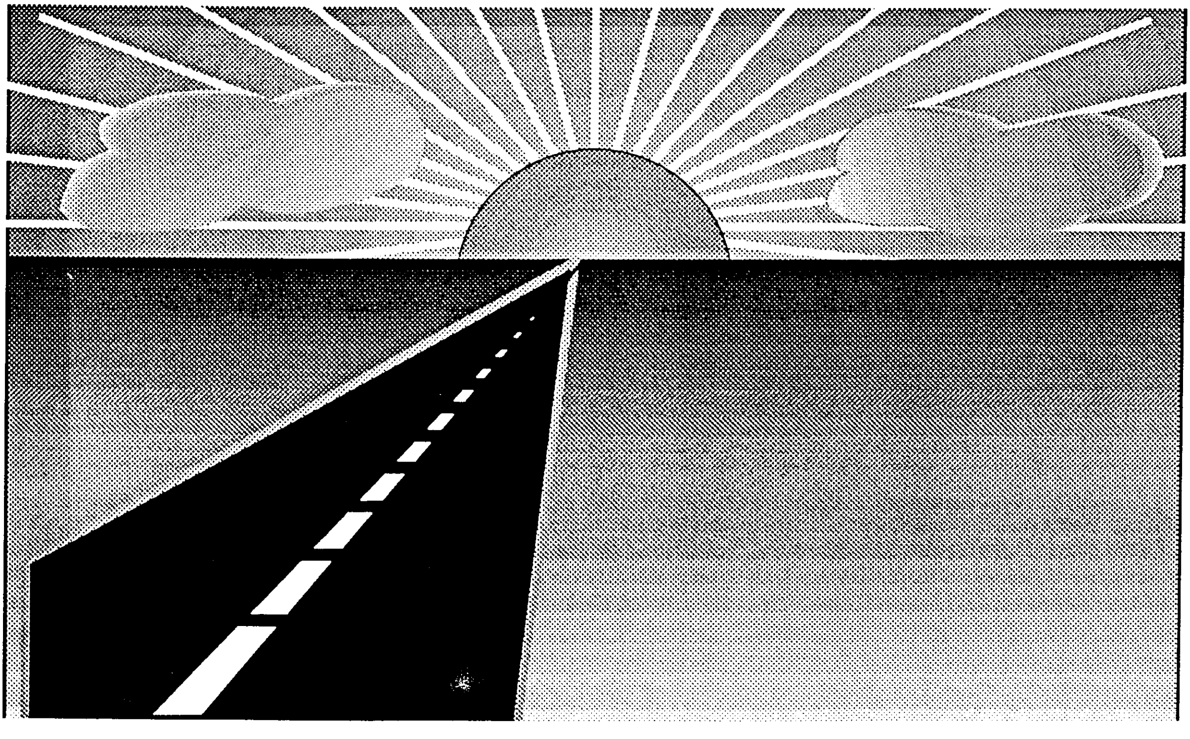

TO MY PARENTS AND

MY FAMILY

ACKNOWLEDGEMENT

The author would like to express his appreciation to the Head of Department, Dr. D R GREEN for the provision of facilities in the Department of Civil Engineering at Glasgow University where the work described in this thesis was carried out.

The author is grateful to his supervisor Dr. T G DAVIES for his advice and guidance during the course of this study and Professor D MUIR WOOD for his interest in this work.

My gratitude is also due to my friends Dr. G B Khaskheli, Dr. H Khachatourian, T S Cheng, Y K To, A Bouazza, S Djellab and M Bendehgane for their discussions and comments.

My special thanks are due to my wife Maureen for her encouragement throughout.

Finally, my deepest appreciations are reserved for my parents' support throughout the years at home and abroad.

SUMMARY

An elasto-dynamic analysis of pavement response to Falling Weight Deflectometer (FWD) impact is presented. The analysis is based on the Fourier series synthesis of a solution for periodic loading of elastic or visco-elastic horizontally layered strata. The method is applied to selected flexible and rigid pavement sections.

Pavement deflection predictions at several geophone locations for various pavements are presented. Comparison between dynamic and static deflection predictions reveal the importance of inertial effects in the prediction of pavement response. Conventional static analysis can yield significantly different results and, therefore may lead to erroneous (unconservative) predictions of pavement moduli back-calculated from deflection data.

Deflection basins together with deflection contours for several pavements are also presented in order to give an insight into the progressive deformation of pavements during and after FWD impact.

NOTATION

Major symbols used in the text are listed below. Others are defined as they first appear.

a_o	Constant load in the Fourier series
a_n	Fourier coefficient
b_n	Fourier coefficient
C	Dashpot constant
Do	Peak centroidal deflection
D900	Deflection at 900 mm from the centroid
D1800	Deflection at the outermost station (1800 mm from the centroid)
E	Young's modulus
E^*	Complex Young's modulus
e	Natural base
F	Falling weight deflectometer force magnitude
F_o	Peak applied force
F_n	Amplitude of the n^{th} harmonic of the Fourier series
G	Shear modulus
G^*	Complex shear modulus
g	Acceleration due to gravity
H	Subgrade thickness
h	Falling weight drop height Pavement layer thickness
i	Imaginary number $(\sqrt{-1})$
K_n	System impedance for the n^{th} harmonic
k	Spring constant of FWD

M Magnification factor
Mass of the falling weight

N Number of terms in the Fourier series

l Number of pavement sublayers

s Compression of the spring under static condition

T Time period

T_P Pulse duration

T_R Rest duration

t Time

t_q Quiescent period

U_o Peak displacement

u_i i^{th} cartesian component of the displacement

$\ddot{u}$ Acceleration

V_R Rayleigh wave velocity

x Displacement vector

z Spring compression

$\ddot{z}$ Acceleration due to the falling weight

****

β Damping

$\delta_{dynamic}$, δ_{static} Dynamic and static displacements

ϵ Strain

ϵ_o Peak strain

λ, μ Lame's constants

υ Poisson's ratio

π Constant (= 3.1415926)

ρ Mass density

σ stress

Φ Phase angle difference between the load and displacement

ω Circular frequency of excitation

CONTENTS

CHAPTER TWO: DYNAMIC ANALYSIS

CHAPTER THREE: NUMERICAL IMPLEMENTATION

CHAPTER FOUR: RESULTS

CHAPTER ONE INTRODUCTION

1.1 PREAMBLE

The effectiveness of pavement rehabilitation programmes is contingent upon the accurate assessment of pavement integrity. Non-Destructive Testing (NDT) techniques are used widely for this purpose and currently much attention is being devoted to dynamic loading tests [3,4,12,20,21,23,24,35,40,41,42,43]. These tests can be categorised into two main divisions :-

(i) Loading tests in which pavement deformations are measured and,

(ii) Loading tests in which the speed of the propagating surface waves are measured (seismic tests), [33,34,50].

These latter tests are less attractive due to, amongst other factors, their complexity and high cost. In this thesis, we shall concentrate on tests of the former type and, in particular, the falling weight deflectometer (FWD) test.

The falling weight deflectometer is a trailer mounted device (Fig. 1.1.a) and consists essentially of a large mass which is constrained to fall freely from a height of about 200 mm on to a spring-loaded plate resting on the pavement surface (Fig. 1.1.b). The falling weight is cylindrical in shape and weighs approximately 1000 Newtons. The impact is transmitted via a rubber pad over a steel load platen to the pavement surface. The deflection of the pavement surface at several locations is then measured by seismic transducers (geophones), (Fig. 1.2). The impulsive load has a relatively short duration (30-40 msec), (Fig. 1.3) which is intended to simulate the passage of a wheel load. The maximum force amplitude can be varied in the range 10-30 KN, yielding a corresponding peak acceleration of the FWD (falling mass) in the range of 10-30 g. Detailed descriptions of this device are given in the literature [2,28,41,42].

The FWD device has been used for evaluation of the structural condition of asphalt and concrete pavements [5,8,9,17,25,29] in Europe and the USA. It is also useful for determining the structural performance of highly loaded pavements such as those found at airfields as well as assessing the remaining life of sections of highway pavements where a need for more detailed investigations (and possible remedial work) has been identified.

Before examining the responses of different pavements to the FWD testing device in more detail, it is useful to review basic pavement construction practices in order to focus attention on the key difficulty in this subject area, namely the characterisation of individual pavement layer properties from the overall pavement response.

Pavements are classified into two main categories; flexible and rigid. Flexible pavements have asphalt contact surfaces and are usually composed of several layers (Fig. 1.4). Four-layer flexible pavements consist of four main layers; bituminous surfacing, roadbase, subbase and subgrade (Fig. 1.5.a). The surfacing is generally subdivided into a wearing course and a base course. The roadbase and subbase are sometimes constructed in composite form using different materials designated the upper and lower roadbase or upper and lower subbase (Fig. 1.5.b) [37,39]. Three-layer flexible pavements consist of relatively thin wearing surfaces built over base courses and subbases which rest upon compacted subgrades (Fig. 1.6).

Rigid pavements, because of their rigidity, tend to distribute vehicular loads over a relatively wide area of the subgrade. Since the major portion of the load capacity is supplied by the slab itself, the strength of the concrete is critically important.

Three-layer rigid pavements consist of reinforced concrete slabs laid over a subbase and subgrade although a thin bituminous surfacing (wearing course) may also be provided to improve ride characteristics (Fig. 1.7). Not infrequently the subbase is omitted resulting in a two-layer structure (Fig. 1.8), since the vertical stress at the slab-subgrade interface is usually only about 30% of the applied pressure at the surface [11,53].

1.2 LITERATURE REVIEW

This review is not exhaustive although it does cover a wide range of papers related to Falling Weight Deflectometer testing and methods of data interpretation.

1.2.1 General use of the FWD

The FWD has been used increasingly to assess pavement conditions during the last decade. Some recent researchers include: Hoffman and Thompson (1982,1983); Ullidtz and Stubstad (1985), Roesset and Shao (1985); Mamlouk and Davies (1985,1986); Kulkarni et al (1986), Foxworthy and Darter (1986), Uddin et al, (1986); and Brown (1987,1988).

Bohn [1,2] was amongst the first researchers to use the FWD to investigate the surface stiffnesses (Eo) of three (Denmark) road sections at various asphalt temperatures (8 Degrees C to 20 Degrees C). He found that the surface stiffness values obtained (based on the static interpretation of the FWD) were highly dependent upon both temperature and the thickness of the asphalt layer. Hoffman and Thompson [20-22] carried out an investigation into pavement characterisation using several non-destructive devices and obtained their best results with the FWD. Their work is described in detail in the following sections. Ullidtz and Stubstad [49] used an iterative technique to evaluate pavement layer moduli from FWD data. They reported that this method yielded satisfactory results. Kulkarni et al [29] used the FWD device to predict the occurrence of cracking on paved Alaskan highways. The FWD was found to be a better indicator of the damage potential to highway surfaces than a single measurement of surface deflection under the load centre (i.e. static loading). Foxworthy and Darter [17] employed the FWD to test some rigid airfield pavements. Consistent load-deformation measurements were obtained for a wide variety of conditions.

1.2.2 Comparison of the FWD with other non-destructive tests

Deflection data obtained from different types of device differ, and this fact necessitates the identification of the factors which affect pavement response to different loading modes [21,23]. Each device has its own advantages and disadvantages, some of which are discussed below.

1/ A. Claessen et al (1976)

Claessen et al carried out a comparative study of various non-destructive testing devices and found the FWD to be the most efficient in providing rational data for pavement evaluation purposes. Full details of the road sections investigated and the various devices employed are given in [8]. Some of these devices are briefly reviewed here for completeness.

The Benkelmann Beam (BB) is essentially a static loading device and is therefore not representative of real traffic loading, thereby reducing its value as a means of pavement evaluation. Another drawback of the BB test is the effect on the deflection measurements of movements of the beam supports resting in the deflection bowl which gives rise to inaccurate results. In Fig. 1.9 the FWD deflections are plotted against the (corrected) BB deflections. It can be seen that the deflection per unit force in the BB test is two to three times as large as that of the FWD. In Fig. 1.10 the subgrade moduli E3 obtained from FWD deflections are compared with those obtained from BB measurements. It is seen that ;

$$E3\ (FWD) \simeq 2.5\ E3\ (BB) \qquad (1.1)$$

This indicates that the BB test results have grossly underestimated the subgrade moduli. In Fig. 1.11 the asphalt layer thickness h1 derived from the FWD deflections (h1 FWD) (using the chart given in Fig. 1.13) has been plotted against the actual thickness (h1 actual). Similarly Fig. 1.12 shows the asphalt layer thickness h1 values derived from BB deflections (h1 BB) (also using Fig. 1.13) plotted against those of the actual pavement. The asphalt layer thickness (h1) values derived from the FWD experiments are in fair agreement with the actual thicknesses, whereas those calculated from BB deflections are generally greater than the actual values.

The Lacroix Deflectograph (LD) is also a static device which measures the deflection under the dual wheels of a truck in much the same way as the BB; the main difference being that the measurements are taken at a constant low truck speed (2-4 Km/h). The movement of the supports and the load on the front wheels have major effects on the deflection values and presetting (correction) similar to that for the BB is imperative prior to taking any measurements. With this device however, significant errors, particularly for thick pavement structures have been recorded. Figs. 1.14 and 1.15 show some typical results obtained for different road sections using the LD compared with those measured using the FWD. Although a better correlation exists between the LD and the FWD (Fig. 1.14) than between the FWD and the Benkelmann beam (Fig. 1.9) there are still significant discrepancies.

The Dynaflect device, on the other hand, exerts a dynamic load of low amplitude at a fixed frequency on the pavement. Some of the drawbacks of this device include its inability to simulate heavy traffic and its tendency to generate layer resonances. The Road Vibration Machine (RVM) [sometimes known as the Road Rater (RR)] also exerts a dynamic force but differs from the Dynaflect in its ability to apply loads of varying amplitudes and frequencies. It is an expensive piece of equipment and the measurements are time consuming. In Fig. 1.16, the FWD deflection per unit force is plotted as a function of the RVM deflection obtained after extrapolation to zero frequency. This extrapolation enabled a comparison between the FWD and the RVM to be carried out and the correlation is seen to be very good. Claessen et al also investigated several road sections using the FWD and the surface wave (SW) propagation technique. The subgrade modulus derived from surface wave propagation measurements (E3 SW) has been plotted versus the moduli obtained from the FWD test (E3 FWD), (Fig. 1.17). Although there is some degree of scatter, the overall results show reasonable agreement. Despite this, steady state techniques generally remain less popular than the FWD because of their complexity and cost.

2/ M. S. Hoffman and M. R. Thompson (1982)

Hoffman and Thompson [21] tested several conventional flexible pavements using various non-destructive testing devices. Correlations and comparisons between the NDT devices such as the Road Rater and the FWD are highlighted here.

The comparative study between the FWD and the Road Rater deflections was performed on 12 different American Association of State Highway Officials (ASSHO) in-service pavement sections. The RR was operated at an 8-Kip (8,000 lbf) peak-to-peak load and a frequency of 15 Hz, and the FWD was operated at an 8-Kip load (plus or minus five percent). The test data showed that the FWD and RR centreplate deflections (Do) were highly correlated (Fig. 1.18) while Fig. 1.19 also shows the good correlation between the FWD and RR deflection-basin areas. Fig. 1.19 shows the deflection-load relationship for moving trucks, RR and the FWD for the AASHO test road sections in the study. Truck speeds ranged from 6 to 36 mph. Pavement surface deflections (for different test road sections) obtained under moving trucks (shown in Fig. 1.20) were found to be largely independent of truck speeds (Fig. 1.21) for speeds less than 20 mph. The deflections decreased at higher truck speeds furnishing clear evidence of the importance of pavement inertia. RR deflections shown in Fig. 1.20 correspond to both the peak and the lowest operating frequencies. At the 8-Kip load level, RR deflections were about 25% lower than moving-truck deflections. They also found that on average, the moving-truck and the FWD deflections were in close agreement. A similar study on moving-truck and FWD deflections was reported earlier in references 2 and 21.

3/ <u>M. S. Hoffman (1983)</u>

Hoffman [23] used pavement deflection data from several non-destructive testing devices to identify the factors which affect pavement response to different loading modes of which Fig. 1.22 is an example. It shows the centreplate deflection results of the Road Rater load and frequency sweep test as well as the results of FWD load sweep tests for three in-service pavement sections (Sherrard, Monticello and Deland). The FWD tends to give higher deflections than the Road Rater. Hoffman's studies showed that since the loading mode and load intensity were highly significant parameters in the structural evaluation of the pavements, it was therefore imperative to carry out tests to simulate real loading conditions as closely as possible. Comparisons between different non-destructive testing devices indicated that the FWD best simulated the pavement response under real loading conditions.

1.2.3 Comparison of the FWD with moving wheel loads

A moving wheel load may be regarded as producing a series of impulses at adjacent points along the direction of travel [46]. Since these disturbances are propagated along the pavement surface at high speed, the deflection under the moving wheel load will be affected by the impulses imparted to the pavement at earlier times. Clearly, wheel loads develop stresses within the body of the pavement that vary with time and the movement of the pavement is opposed by inertial forces due to its mass (body forces). The object of the comparison between the (stationary) FWD testing device and a moving wheel load is to find out whether the FWD can simulate the pavement response under real (moving wheel) loading conditions. Some studies are reviewed here in order to give an insight into the differences between the FWD and moving wheel loads.

1/ A. Bohn et al (1972)

Bohn et al [2] used two sets of measurements to demonstrate the close correlation between FWD and moving wheel loads. The first set of measurements was taken in Holland, where photo-electric equipment was used to measure the deflection due to a passing wheel load while the second set was undertaken in Denmark, using an accelerometer. They concluded that there was one principal difference between the effect of the FWD and the effect of a moving wheel, namely that the stresses due to the latter in the deeper layers of the road construction had an appreciably greater duration. Bohn et al introduced the concept of the "Conical Dispersion Pattern" which advances with the wheel load, thereby causing a steadily increasing pressure in the underlying layers before the wheel reaches the point in question. Fig. 1.23 illustrates typical data from their studies. It is apparent that the pulse widths in the FWD test were virtually constant regardless of the depth while under the moving wheel the corresponding (recorded) pulse widths increased progressively with depth. Figs. 1.24 and 1.25 show the deflections recorded under a moving wheel load travelling at approximately 40 Km/h and the FWD, respectively. The impulse width of the surface deflection is 26 msec for the FWD and several hundred msec for the moving wheel load. Fig. 1.26 shows a series of points which represent a simple average of a number of tests performed at various sections (1-7). Good correlations between the FWD and the moving wheel tests were obtained.

Bohn et al concluded that in order to draw definitive conclusions, additional experiments (especially on roads having thick asphalt layers) were needed.

2/ M. S. Hoffman and M. R. Thompson (1982)

An accelerometer implanted in the pavement's surface was used to check the FWD data-acquisition system and to generate deflection data for moving trucks travelling at various speeds. All the tests were performed on selected AASHO road test sections [21]. The simultaneous measurement of FWD surface deflections with the accelerometer and the FWD centreplate sensor produced similar results (Fig. 1.27). The agreement indicated that both measuring techniques provided reliable results. Accelerometer outputs were then used to generate acceleration, velocity, and deflection signals under moving trucks (Fig. 1.28) and FWD impact (Fig. 1.29). Hoffman and Thompson concluded that the recorded truck load signals had a longer 'pulse' duration than those of the FWD; typical values at 50 mph were estimated at 120 msec whereas FWD pulses were of the order of 30 msec. From the corresponding diagrams of Fig. 1.28, truck load signals started at the edge of the deflection basin zone of influence suggesting that the stiffer the pavement, the longer the equivalent truck pulse duration. Perhaps the most significant result of this study is illustrated in Fig. 1.30 which shows the relationship between the ground acceleration amplitude (mm/s2) and centreplate deflection caused by the FWD blows determined from accelerometer measurement. From Fig. 1.30 it may be observed that (a) the FWD-imposed ground accelerations can reach values of up to 4 times g and, (b) there are different relationships between acceleration and deflection for different sections. These results suggest that inertial effects under FWD blows can be significant and may need to be included in theoretical analyses of pavement assessment.

3/ M. S. Hoffman (1983)

Hoffman [23] tested several pavements in Ottawa, Illinois (USA) subjected to impulse loading (FWD) and moving truck loading. Referring to his earlier work in 1982 [21], (Fig. 1.28-1.30), he discussed the importance of the inertial characteristics of pavements. Hoffman found that recorded acceleration signals for moving wheels were in general, about one-tenth of the FWD imposed acceleration, whereas their pulse durations were 3-5 times longer than those of the FWD thereby mobilising more "mass" and a higher pavement damping ratio than the FWD (due to the large "area of influence" of a moving load). He concluded that although the FWD approximates the actual wheel load more closely than other devices, it is basically a "Fixed-In-Place" device that cannot exactly simulate a moving wheel since, as noted earlier, a moving wheel produces surface deformation in advance of the wheel whilst the FWD cannot produce deflections before the load is applied. Nevertheless, the FWD has been found to best simulate a moving wheel load by several researchers [2,8,21,25].

4/ <u>B. Sebaaly et al (1985)</u>

Sebaaly et al [41] compared experimental data obtained from FWD tests and truck loads [21] with the results of a numerical model which included the inertia of pavements. The results of their study are depicted in Fig. 1.31. To a good degree of accuracy, all three cases studied exhibited a linear response to increasing load and there was very good correlation between FWD deflection data and those measured for the moving wheel loads. The theoretical FWD predictions yielded higher pavement deflections than those induced by truck loading in two cases (AASHO-845, 874) but lower deflections in the third (AASHO-872).

1.2.4 FWD measurements in and between wheel tracks

Fig. 1.32 shows the results of one of five (German road sections I-V) surveys carried out using the FWD which underlines the importance of the measurement locations (i.e. nearside wheel track or lane centre) on the interpretation of FWD test data [8]. Table 1.1 shows the results obtained for road sections I-V. Differences between the centroidal deflections (Do), Q600 (the ratio of deflection at 600 mm from the centroid (i.e. D600) to the centroidal deflection Do) as well as subgrade stiffnesses (E3) for the nearside wheel track and the lane centre indicate the extent of damage caused to the pavement by traffic. This study is particularly relevant to overlay design [5,6], (Fig. 1.33). Table 1.1 shows that (for all five sections) subgrade stiffnesses in the wheel track are 20-50% lower than those of the lane centre (i.e. between the wheel tracks)

1.2.5 Overlay design using the FWD

The key to adequate overlay design is to determine the condition of existing pavements, i.e. performance criteria (deformation and cracking) is needed to link pavement characteristics to load applications. Overlay design based on empirical relationships [27,49,52] between pavement response (load) and pavement performance (deformation, cracking and rutting) are usually restricted to specific pavements. To overcome the disadvantages and the inaccuracies of these methods, improved evaluation methods have been developed based on FWD measurements e.g. [9]. A brief note on these developments is given in the sequel.

1/ A. Claessen et al (1976,1977)

Claessen et al used the Shell Design Charts (first published in 1963 for flexible pavements) to study several road sections [8,9]. The pavement properties derived from FWD deflection measurements were used with the Shell Design Charts to determine overlay thickness. Fig. 1.34 shows the variation of asphalt layer thickness (h1) against those of unbound base layers (h2) for a constant subgrade modulus E3 (110 MPa) derived from FWD deflection data. N represents the traffic data and design life. Fig. 1.35 also shows the design charts used to derive pavement design life and the required overlay (asphalt) thickness (h1) for different subgrade moduli (E3); the upper chart is applicable to pavements without granular base layers whilst the lower chart is applicable to pavements with granular base layer thicknesses (h2) of 300 mm. Overlay thicknesses derived using the FWD device were compared with those of other devices such as the Lacroix Deflectograph (LD) shown in Fig. 1.36. These were generally found to underestimate the overlay thicknesses compared with the FWD. Fig. 1.37 shows the result of an overlay thickness survey carried out using the FWD on a Nijkerk pavement. A consistent deflection trend exists (at surveyed positions 1-19) both before and after the application of the overlay indicating the consistency of the FWD deflection results.

2/ R. C. Koole (1979)

Koole [28] described an overlay design method based on FWD measurements in which the principles of the Shell Pavement Design Manual [44] were incorporated. The pavement structure was schematized as a three-layer model (Fig. 1.38). The top layer represents the asphalt layer, the second layer represents the base materials (granular or cementicious) and the third (infinitely deep), the subgrade. With the aid of the multi-layer elastic computer program BISAR, deflection interpretation charts were derived of which Fig. 1.39 is an example. (BISAR calculates the stresses and strains in the pavements by a trial and error iteration procedure). From Fig. 1.39, pavement properties may be determined from a number of surface deflection measurements. In view of the large number of variables, this procedure cannot be readily generalised, despite the fact that only three distinct layers have been assumed in the analysis.

3/ K. R. Peattie (1979)

Peattie [36] presented similar overlay design charts (Fig. 1.40) based on the FWD measurements to those described in references [9,28,44]. The pavement was represented by a three-layer elastic system in which the value of Poisson's ratio in all layers was 0.35. The second layer thickness h2 (200 mm) was measured by coring, and it was assumed that the modulus of the unbound layer E2 was 2.5 times that of the subgrade E3 (30 MPa). The procedure is confined to a limited number of variables (for a three-layer pavement structure) thereby limiting its applicability.

4/ S. F. Brown (1987)

Brown [5] described an overlay design procedure based on the FWD test. His iterative design method is based on, (a) the determination of layer thicknesses and stiffnesses from coring and back-analysis using the FWD charts, (b) the adjustment of asphalt stiffnesses for differences between the testing temperature and design loading time (30 Km/h for FWD) and design temperatures and loading time and, (c) the assessment of pavement life based on both cracking (Nt) and deformation (Nz) criteria [6]. The decision on whether to design a new pavement structure or to opt for an overlay is governed by cracking and deformation criteria. New pavement construction is required if the cracking criterion is critical but an overlay suffices when deformation becomes critical. The flow diagrams summarised in Figs. 1.41 and 1.42 illustrate this approach to pavement evaluation and overlay design.

1.2.6 FWD test data interpretation (Empirical)

Data obtained from FWD measurements can be interpreted and used as an empirical tool in order to assess the performance and integrity of existing pavements. Some examples of this type of work are presented here.

1/ P. Ullidtz and R. N. Stubstad (1985)

Ullidtz and Stubstad [49] investigated the performance of pavements by means of an Analytical-Empirical (mechanistic) approach using FWD data. The analysis included the prediction of future functional conditions of pavement structures (fatigue and cracking), determination of the elastic moduli for each material in the pavement structure, and calculation of critical stresses or strains in each material. Ullidtz and Stubstad used the Dynatest 8000 FWD along with the ELMOD computer program to assess pavements. The ELMOD analysis procedure is based on the use of the Method of Equivalent Thickness (MET) which converts pavement layers overlying the subgrade into an equivalent layer of the same stiffness as the subgrade by varying the layer thicknesses [47]. The Boussinesq equations are then used to calculate stresses, strains and deflections at various positions. (The ELMOD program can only analyse two and three-layered structures; it fails to analyse structures with a lean concrete roadbase layer, a common type of structure for heavily trafficked roads). An iterative procedure based on the above method was employed to determine layer thicknesses from measured deflection basins. Changes in moduli due to seasonal fluctuations in temperature and moisture content were incorporated into the ELMOD program. Ullidtz and Stubstad found the weakest part of their method lay in relating the empirical relationships between pavement performance (roughness, rutting and cracking) to the pavement response (stresses and strains). One drawback of this conventional procedure is the assumption of a static (peak) load instead of the dynamic force produced by the impact of the falling weight (deflectometer).

2/ R. B. Kulkarni et al (1986)

Kulkarni et al [29] used the data obtained from the FWD deflection basin measurements and fatigue cracking observations in pavements to develop a fatigue cracking prediction model for Alaskan highways. Careful selection of the data obtained (by screening and data grouping) over a period of 2-3 months during the thawing season was used to correlate the deflection basin profile to fatigue cracking. The results of the studies carried out by the Alaska Department of Transportation and Public Facilities (DOTPF) staff indicated that the deflection basin developed by the FWD was a better indicator of the damage potential to highway surfaces than a single measurement of surface deflection under the load centre (i.e. static loading).

1.2.7 Influence of temperature on FWD test data interpretation

1/ A. Claessen et al (1976)

Fig. 1.43 shows the results of a typical survey carried out into the effect of temperature variation on FWD measurements [8]. The variation in the deflection values was the same for both March and August testing months, but the centroidal deflection values were higher in August than in March. The German State Road Research Institute used this survey in conjunction with other similar surveys to investigate the structural integrity of six (three-layered) road sections (A1-A3, B1-B3). The values of asphalt surface thickness h1 and subgrade modulus E3 were derived from the FWD deflections, (Table 1.2) and the asphalt modulus E1 was determined from Fig. 1.44 which describes the relationships between asphalt modulus and temperature (and loading time) for a typical mix composition. Agreement between actual values of asphalt surface thickness (from construction reports) and calculated values (using a similar chart to that of Fig. 1.13) for the A-sections were found to be fair. In the B-sections, larger differences between actual and calculated values of h1 were found and interpretation of h1 and E3 were not possible for pavements at high temperatures. The Institution's test results showed that, in general, it is difficult to assess the condition of pavements at higher ambient temperatures.

2/ P. T. Foxworthy and M. I. Darter (1986)

Foxworthy and Darter [17] studied the effect of temperature on the repeatability of falling weight deflectometer load and deflection measurements. Tests were carried out on a number of rigid airfield pavements. Tables 1.3 and 1.4 present a summary of the results of back-calculated dynamic Young's moduli (E) of the slab [i.e. ratio of the stress amplitude to the corresponding strain amplitude when pavements (slabs) are subjected to a harmonic loading] and the stiffnesses of the underlying support systems (moduli of subgrade reaction, K) for eight slabs at constant pavement temperature and, also, for varying temperatures ranging from 36 to 101 Degrees F. Fig. 1.45 shows that normal variations in E and K at constant temperatures encompasses the variations in E and K with temperature. Foxworthy and Darter concluded that only temperature extremes substantially influence back-calculated dynamic E and K values.

1.2.8 Static analysis of the FWD

Static analysis of the FWD is based on the Navier-Cauchy equation of equilibrium, which in cartesian indicial notation, takes the form:

$$\mu u_{i,jj} + (\lambda+\mu)\, u_{j,ij} = 0 \qquad (1.2)$$

where u_i = i-th cartesian component of the displacement (i ranges from 1 to 3)

$$u_{i,jj} = \delta^2 u_i \,/\, \delta x_j . \delta x_j \qquad \text{etc.}$$

Lame's constants μ and λ are defined as follows:

$$\lambda = E\,v \,/\, (1+v)\,(1-2v) \qquad (1.3)$$

$$\mu = G = E \,/\, 2\,(1+v) \qquad (1.4)$$

where
E = Young's modulus
G = shear modulus
v = Poisson's ratio

Equation (1.2) takes no account of inertia (due to mass) of pavements.

1/ M. S. Hoffman and M. R. Thompson (1982)

Thompson and Hoffman [22] used a static analysis of the FWD to show that it was possible, using a three-parameter model, to characterise flexible pavements by using the maximum deflection under the load (Do) and a parameter they called the 'basin area' A (Fig. 1.46). This area concept combines all the measured deflections in the basin into a single number which is essentially one half the cross-sectional area of the deflection basin taken through the centre line of the load.

$$A = 6 \; (Do + 2D1 + 2D2 + D3) \; / \; Do \qquad (1.5)$$

where Do is the peak centroidal deflection and, D1, D2 and D3 are the deflections at 300, 600 and 900 mm from the centroid respectively. The third parameter (Δ) is defined as the equivalent 9000 lb moving wheel load deflection (in mils). These parameters were then used to develop nomographs such as that shown in Fig. 1.47 to determine asphalt concrete moduli Eac and the resilient moduli Eri from the known values of A and Δ. Computation of stiffnesses from the deflection data was achieved by an iterative technique which involved successive correction of initial seed values. This procedure is vulnerable as errors are introduced at each stage of the iteration process which further distort the erroneous assumption of static loading.

1.2.9 Dynamic analysis (SDOF and continuum)

Current dynamic analyses of pavement response to surface loading can be divided into two main branches; Single Degree of Freedom (SDOF) analyses and continuum theory.

1. Single degree of freedom analysis - This is a simplified analysis in which pavements are represented by a combination of masses, springs and dashpots.

1/ R. A. Weiss (1977,1979)

Weiss [51,52] has applied the single degree of freedom dynamic theory to pavements. The major shortcoming of this method is it cannot be used to predict the deflections away from the location of the applied load. Difficulties in relating fundamental soil properties, Young's modulus (E) and Poisson's ratio (v) to parameters such as K, C and M (spring constant, dashpot viscosity and mass, respectively) is also a major problem. In short, SDOF dynamic theory can not be used as a tool to tackle complex problems.

2. Continuum theory - This analysis (using visco-elasto-dynamic continuum theory) is based on the Helmholtz's equation for steady-state vibration given by:

$$\mu u_{i,jj} + (\lambda+\mu)\, u_{j,ij} + \rho\omega^2 u_i = 0 \qquad (1.6)$$

where p = mass density

w = circular frequency of excitation

1/ M. S. Mamlouk and T. G. Davies (1984)

Mamlouk and Davies [31] were the first researchers to use a continuum elasto-dynamic theory to show that the static and dynamic responses of pavements may be materially different even at low loading frequencies. Their analysis was based on rigorous elasto-dynamic theory and the results revealed the importance of the inertial effect in pavement analyses. They presented their results in terms of the deflection ratio M (Magnification factor); where

$$M = \text{Dynamic Deflection} / \text{Static Deflection} \quad (1.7)$$

It is noteworthy that the magnification factor may be significantly greater than unity at frequencies near the resonant frequency but at higher frequencies it reduces monotonically to a value less than unity. Fig. 1.48 shows typical values of static and dynamic deflections computed at a point near to a Road Rater operating at 25 Hz. The axis labelled 'thickness' refers to the thicknesses of the individual layers of the (four-layered) pavement structure while the 'stiffness' axis refers to the stiffnesses of the individual layers. It can be seen that the deflection ratios are not the same at all radial locations. Fig. 1.49 shows that, for pavements of medium stiffness, the deflection ratios tend to increase with increasing distance away from the load. Mamlouk and Davies concluded that the dynamic deflections resulting from Road Rater excitation were complex functions of frequency, pavement properties and geometry as well as distance from the point of application of loading.

2/ J. M. Roesset and K. Y. Shao (1985)

Roesset and Shao [40] carried out an elasto-dynamic analysis of the FWD to compare the dynamic deflections with those provided by conventional static computer programs when the subbase is a homogeneous soil stratum of finite depth resting on a much stiffer rock-like material. The results of these comparisons indicated that for certain ranges of depth to bedrock a static interpretation of the FWD tests could lead to substantial errors. Fig. 1.50 shows the ratio of the dynamic to the static deflection (Wd and Ws, respectively), considering both a finite layer and a half-space for the static analyses. It can be seen that a small amount of dynamic amplification takes place particularly at points furthest from the load application. Computed deflections and the estimated moduli of the pavement for the cases studied are summarised in Table 1.5. Roesset and Shao concluded that dynamic effects were less important for the falling weight deflectometer because a broad range of frequencies were excited instead of a single one (e.g. Dynaflect).

3/ B. E. Sebaaly et al (1986)

Sebaaly et al [42] studied the response of pavements to falling weight deflectometer blows using a multidegree of freedom elasto-dynamic analysis. A Fourier synthesis solution for periodic loading was utilised and was applied to the flexible pavement section described in Tables 1.6 and 1.7. The FWD deflection measurements at various geophone locations were compared by using dynamic as well as static (zero frequency) analysis,(Figs. 1.51-1.54). The results of the study showed that the static analysis of the pavement response to the FWD resulted in average surface defections 20 to 40 percent larger than field measurements. This indicated that the static analysis of the FWD overestimates (by back-calculation from deflection data) the stiffness of the pavement layers. Sebaaly et al concluded that inertial effects are important in the prediction of pavement response.

1.2.10 Back-analysis of elastic stiffnesses from FWD deflection data

The technique used to evaluate the insitu elastic stiffness of each pavement layer is known as 'Back-Analysis'. It involves computing, by an iterative procedure, a theoretical deflection bowl which closely matches the measured one. The inertial effects of the pavement on the measured deflections (when subjected to the Road Rater and the FWD) have been studied by Hoffman and Thompson [20], Roesset and Shao [40] and Mamlouk and Davies [31]. Sebaaly et al [41,42] suggested that the back-analysis of FWD deflection could significantly overestimate (by 25-30%) the elastic stiffness of pavement layers.

1/ S. F. Brown (1987)

Brown [5] produced design charts (using FWD measurements) aimed to simplify the back-analysis (Fig. 1.55) of measured deflection bowls. Brown recognised that subgrade stiffness has a major influence on the shape of the deflection bowls (Fig. 1.56). He therefore took special care to model the subgrade layer as accurately as possible (Fig. 1.57). Fig. 1.58 shows the relationship between $E_b * h_b^3$, D1800 (E_b, h_b and D1800 are road base stiffness, roadbase thickness and deflection at 1800 mm from the centroid, respectively) and E_f (stiffness at formation) which is the basis of the design procedure. An estimated value for E_b together with the measured value of h_b (from coring) and D1800 is used to determine a first estimate of E_f. A second chart (Fig. 1.59) is then entered with the resulting deflection (D0 - D900), (D0 and D900 are deflections at the centroid and 900 mm from the centroid, respectively) to determine E_b. By trial and error, consistent values of base and subgrade stiffnesses can be obtained. This analysis excludes the inertia of pavements and a study of these charts in Chapter Four using a dynamic analysis reveals their shortcomings.

2/ W. S. Tam and S. F. Brown (1988)

Tam and Brown [47] developed a computer program PADAL (Pavement Deflection AnaLysis) at the University of Nottingham to back-analyse deflection bowls from pavement testing with the FWD. The PADAL program incorporated a rigorous iterative procedure and stringent convergence criteria to produce accurate solutions. Separate back-analysis techniques assuming the subgrade to be either linear or non-linear in behaviour, demonstrated a distinct improvement (by 10%) in accuracy for the deflection bowl match when subgrade non-linearity was introduced; the PADAL program therefore incorporates a non-linear elastic model for the subgrade.

Since the PADAL program assumes a static applied load in the calculation of surface deflection, a comparative study of the back-analysed stiffnesses from the PADAL program was carried out with the dynamic analysis method proposed by Mamlouk and Davies [31]. For this comparison, FWD deflection bowls for three structures(1-3) detailed in Table 1.8.B representing two, three and four-layered asphalt pavements respectively were chosen of which structure number 3 consisted of asphalt surfacing, lean concrete road base and combined subbase and capping layers overlying the subgrade.

Direct comparison of PADAL with the dynamic analysis was not possible, since the latter does not perform back-analysis. To enable comparisons of the aforementioned methods, Tam and Brown adopted two procedures outlined in Fig.1.60. The first procedure uses the PADAL back-analysed elastic stiffnesses in a 'forward' dynamic analysis (Fig. 1.60.a) and then compares the resulting deflection bowls with the measured one. Fig.1.61 shows the results obtained for structure number 3. Similar results were obtained for the other two structures. The second procedure involved comparison of elastic stiffnesses from the PADAL back-analysis of the measured bowls with those from back-analysis of the bowls computed by the dynamic method (Fig. 1.60.b). Table 1.8.A shows the results of these comparisons for three structures. They concluded that the effects of pavement inertia on FWD deflections were insignificant. But the results of the PADAL model show an overestimation of subgrade stiffnesses of about 10% at formation level and up to 40% at 4.6 m depth (below formation). In addition, the stiffnesses of the upper layers are generally underestimated by 5-15%.

Although these discrepancies are not large, some caution in the use of static back-analysis procedures is indicated.

1.2.11 Dynamic surface wave (seismic) analysis

A vertically oscillating mass is used to generate surface waves in the pavement and by locating successive troughs or peaks by means of transducers their wave lengths can be determined [38]. Given the frequency of vibration of the oscillating mass, the Rayleigh wave velocity can then be obtained using the equation:

$$V_R = \omega L_R \tag{1.8}$$

where

V_R = Rayleigh wave velocity

w = frequency of vibration

L_R = wave length

The stiffnesses of the pavement layers can then be obtained from Equation (1.9) below. Using this steady state technique and spectral analysis, the elastic moduli and thicknesses of different layers can be determined non-destructively and rapidly. This technique has not however gained widespread popularity, partly because of the relative sophistication required in field operation and in the interpretation of test data - despite the fact that the technique yields not only the layer stiffnesses but also their thicknesses. Some examples of this type of work are presented here for completeness.

1/ <u>W. Heukelom and C. R. Foster (1960)</u>

Heukelom and Foster [24] identified the Rayleigh wave velocities of the base, subbase and subgrade layers of a four-layer pavement structure (Fig. 1.62.a and 1.62.b) by means of the steady-state seismic technique. From this data the layer stiffnesses were found from [18];

$$V_R \simeq \sqrt{(G / p)} \qquad (1.9)$$

where

G = shear modulus

p = mass density

V_R = Rayleigh wave velocity

Further studies were carried out by Szendrei and Freeme (1970), Walker and Hudson (1971) and similar results have been reported elsewhere [46,50].

2/ <u>S. Nazarian and K. H. Stokoe (1986)</u>

Nazarian and Stokoe [34] used the surface wave technique to evaluate pavement performance. The analysis was based on Spectral Analysis of Surface Waves (SASW), (Fig. 1.63). The SASW method was utilised to determine the Young's modulus profiles of pavement structures and the underlying soils as well as the thicknesses of each layer. Fig. 1.64 shows the

Young's modulus and shear wave profiles from SASW and crosshole tests at a typical flexible pavement site. Nazarian and Stokoe concluded that the elastic moduli determined by the SASW method compare favourably with those of crosshole seismic tests. Similar studies were also reported by Heisey and Mayer (1982), [19] and Nazarian et al (1983), [33]. However, these (seismic) methods remain unpopular due to their high costs and complexity of data interpretation. One of the major difficulties in data interpretation is the fact that the loading does not at all correspond to vehicle loads and substantial corrections have to be made to the computed stiffness values to allow for non-linear small-strain effects. The majority of researchers have therefore resorted to static/dynamic non-destructive testing devices.

1.2.12 CONCLUSIONS

Pavement material characterisation procedures must be accurate, reliable and cost-effective. Many non-destructive testing devices currently used in assessing pavement integrity involve static loading which differ appreciably from real loading conditions. For this reason, amongst others, there is an increasing demand for non-destructive testing devices which simulate pavement response under moving traffic loads. Field studies have shown that the Falling Weight Deflectometer (FWD) yields good correlations with pavement deflections induced by traffic loading.

Interpretation of dynamic loading test data is difficult; the vast majority of researchers have resorted to empirical techniques or simple static analyses [5,17,24,25,29,43,49], i.e. layered elastic theory for this purpose. While the latter approach is clearly superior to empirical methods, these analyses suffer one major defect: they neglect the dynamic dimension of the loading. The significance of inertial effects under FWD blows has recently been emphasised by some researchers. Consequently, rigorous elasto-dynamic analysis (using continuum theory) which incorporate inertial effects may be a step forward towards a better interpretation of the deflection data.

1.3 OBJECTIVES

The objective of this research study is to carry out, using elasto-dynamic continuum theory, a comprehensive parametric study on the effect of changes in pavement layer stiffnesses and thicknesses on pavement response to FWD testing. The effect of changes in the FWD loading rate (i.e. pulse duration) on pavement response are also examined. The results of this study are then used to develop design charts to aid interpretation of FWD data.

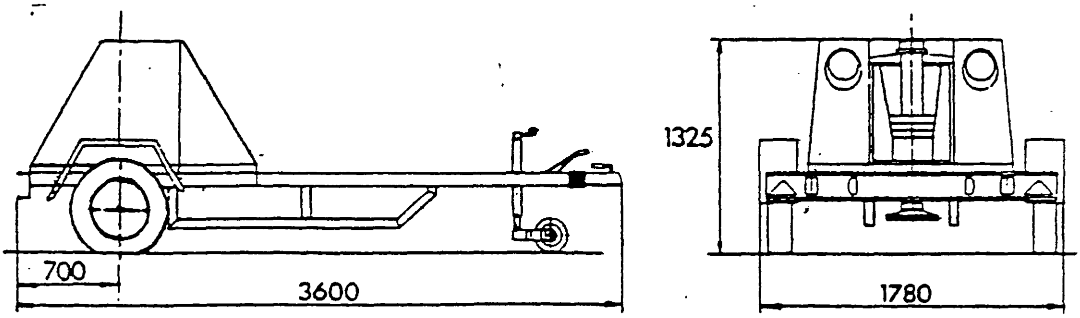

(a)

Fig.1.1- Falling Weight Deflectometer [5]

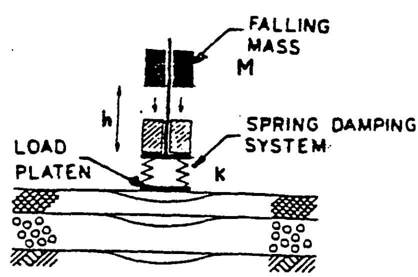

(b)

Fig 1.1- Schematic Diagram of FWD [28, 41]

where

M = mass of the falling weight (kg),
h = drop height (m), and
k = spring constant (N/m).

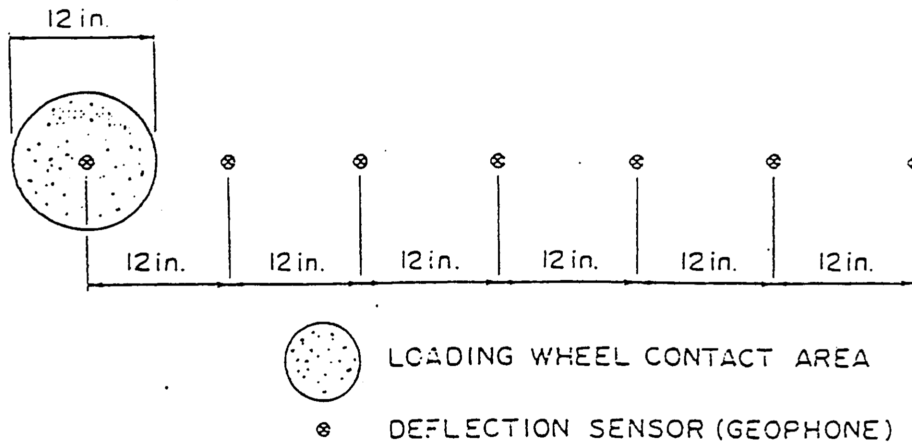

Fig.1.2 FWD-Geophone Stations[12]

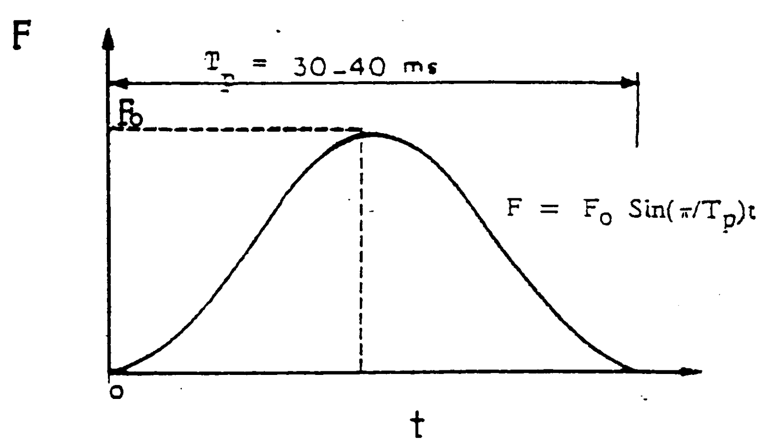

Fig. 1.3 Characteristic Shape of Load Impulse [42]

(Half-Sine-Wave)

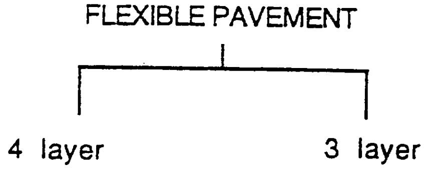

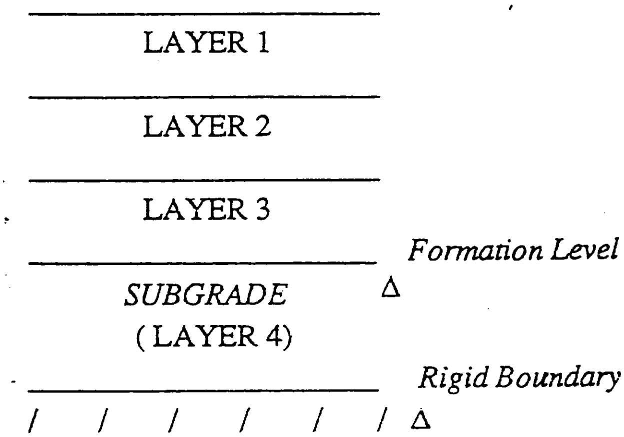

(FIG. 1.4) **FOUR LAYER FLEXIBLE PAVEMENT**

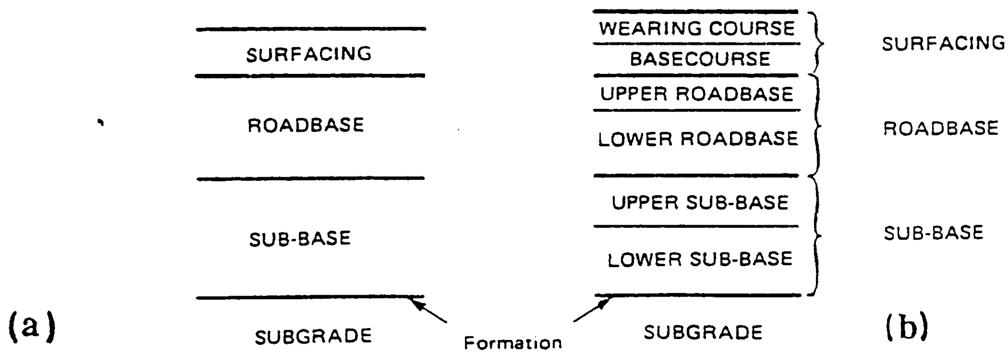

Notes:-

1. Where the roadbase is laid in two different materials as in (b) the pavement is often referred to as COMPOSITE
2. Where bituminous or unbound stone or gravel materials are used exclusively in the pavement it is often referred to as FULLY FLEXIBLE

(FIG. 1.5) Components of Flexible Pavement [11]

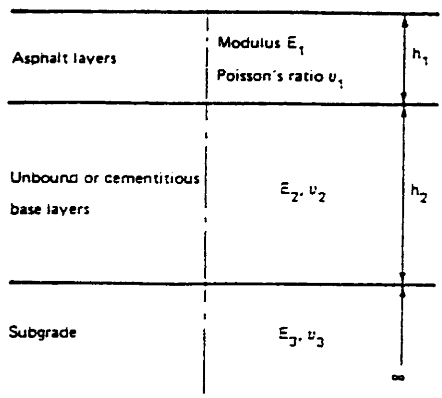

(Fig.1.6) THREE LAYER FLEXIBLE PAVEMENT [28]

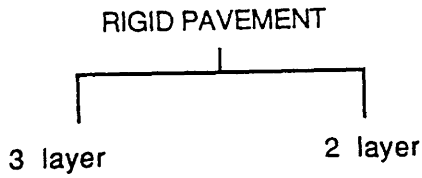

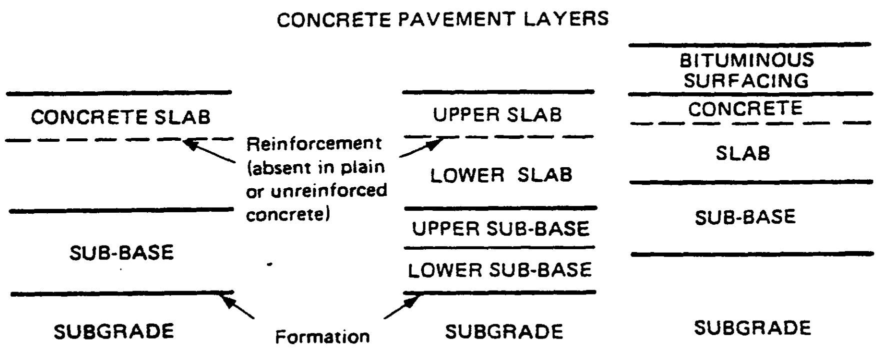

(Fig.1.7) - **Components of concrete pavement** [11]

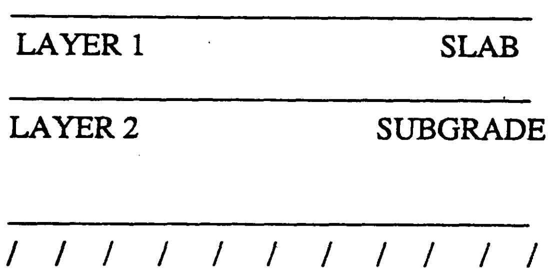

(Fig.1.8) - Two layer rigid pavement

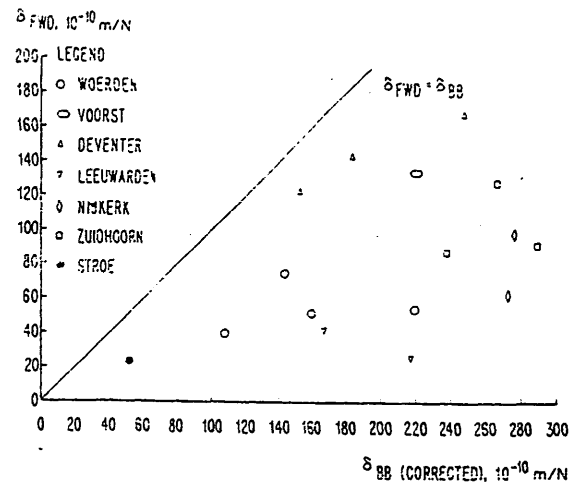

Fig. 1.9 Mean Deflections per Unit Load Under FWD in Various Road Sections Against Those Measured with BB and Corrected for Movements of Supports [8]

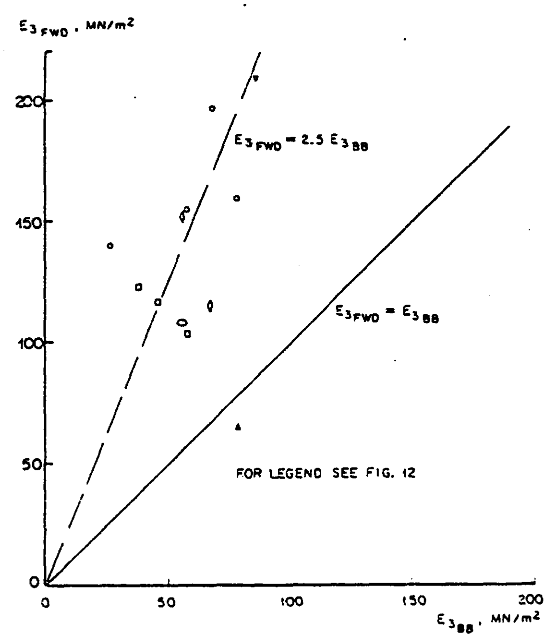

Fig. 1.10 Subgrade Moduli (E_3 FWD) Derived from FWD Deflections versus the Subgrade Moduli (E_3 BB) Determined from the BB Deflection Using h_1 FWD for the Thickness of the Top Layer. [8]

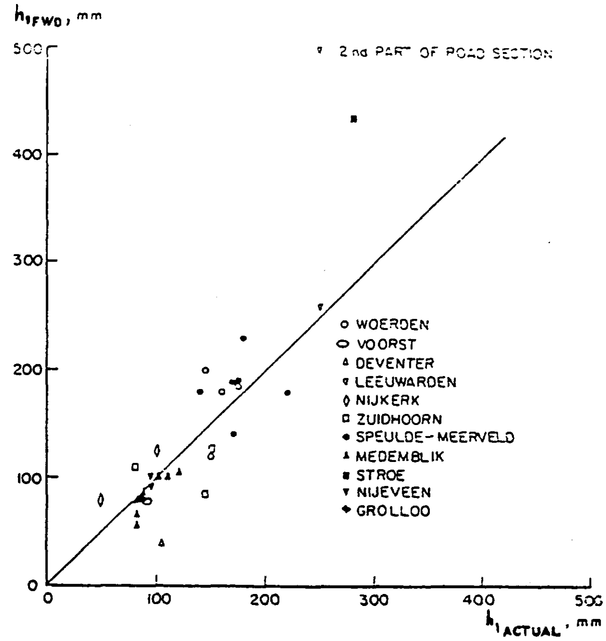

Fig. 1.11 Asphalt Layer Thickness ($h_{1\ FWD}$) Determined from the FWD Deflections versus the Actual Thickness. [8]

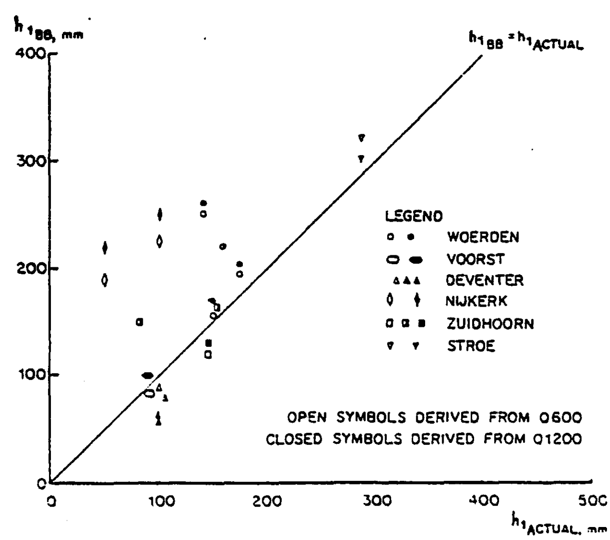

Fig. 1.12 Asphalt Layer Thickness ($h_{1\ BB}$) Derived from BB Deflections versus the Actual Thickness. [8]

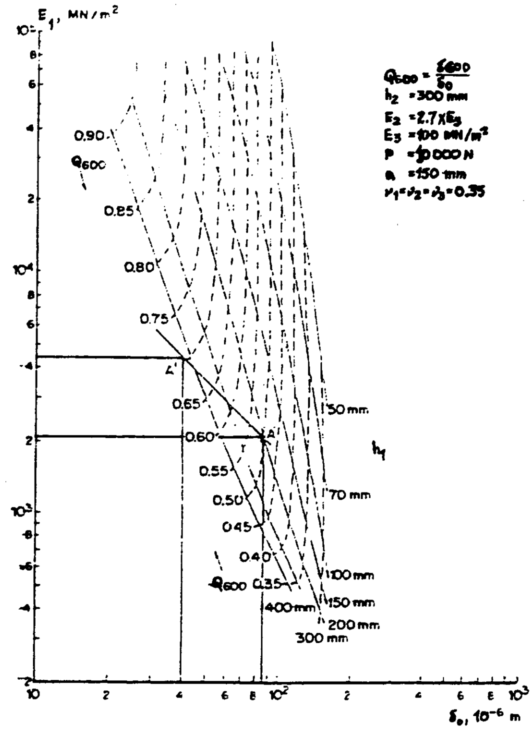

Fig. 1.13 Young's Modulus (E_1) of Asphalt Layer versus Deflection (δ_0) Under Single Test Load in Structures with Base Layer Thickness h_2 = 300 mm. [8]

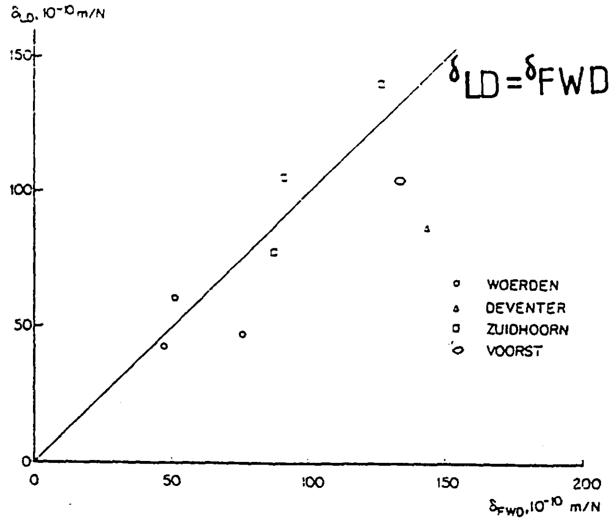

Fig. 1.14 Mean Values of the Deflections per Unit Force Measured with the LD versus Those Measured with the FWD [8]

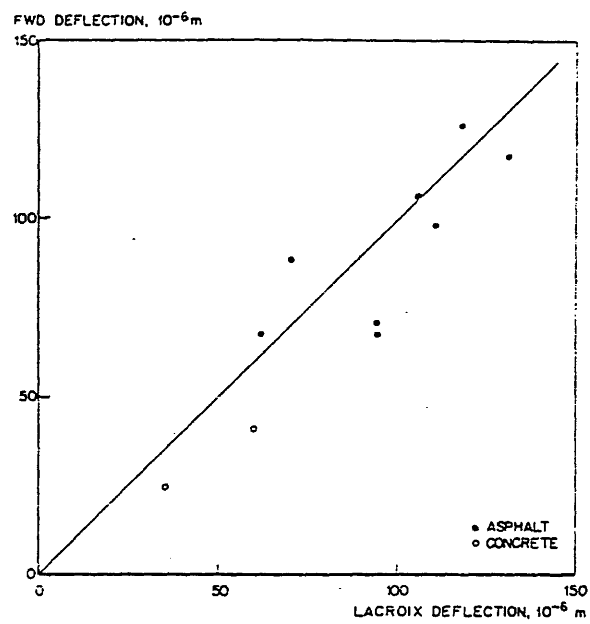

Fig. 1.15 Comparison of Measurements with the Falling Weight Deflectometer and Measurements with the GLC Lacroix Deflectograph (Deflections per 10^4 N). [8]

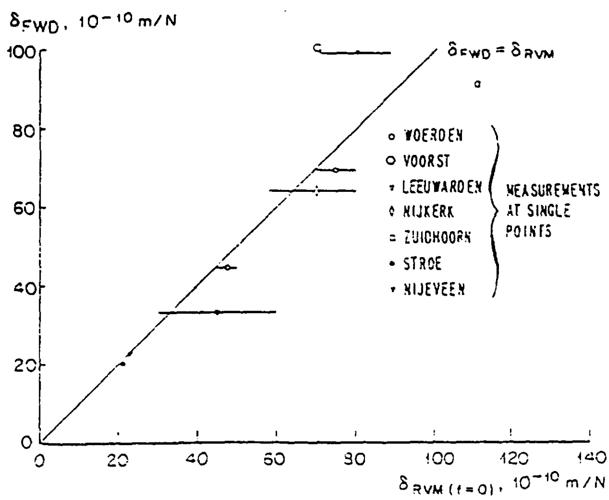

Fig. 1.16 The Deflection Under the FWD Against the Deflection Under the RVM Obtained After Extrapolation to Zero Frequency (Bars Denote Accuracy of Extrapolation to $f = 0$). [8]

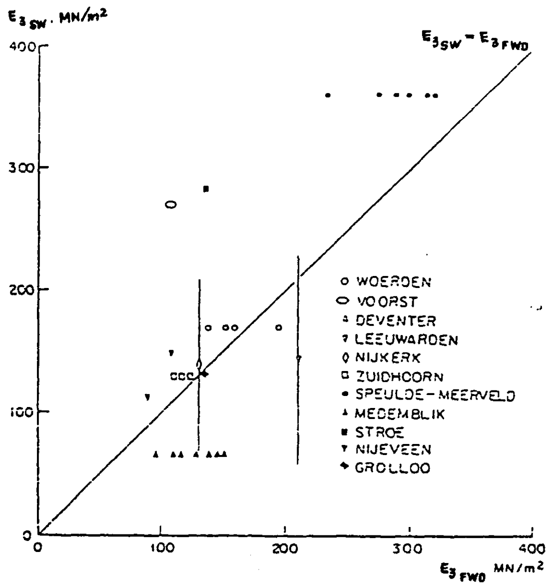

Fig. 1.17 Subgrade Modulus ($E_{3\ SW}$) Obtained in Wave Propagation Measurements versus $E_{3\ FWD}$ Derived from FWD Deflections. [8]

Fig. 1.18 Correlation between FWD and RR deflections. [21]

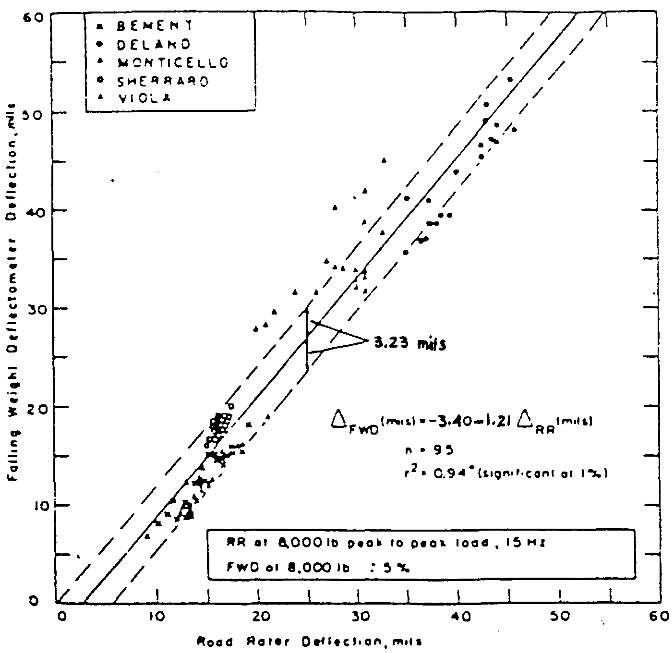

Fig. 1.19 Correlation between FWD and RR areas. [21]

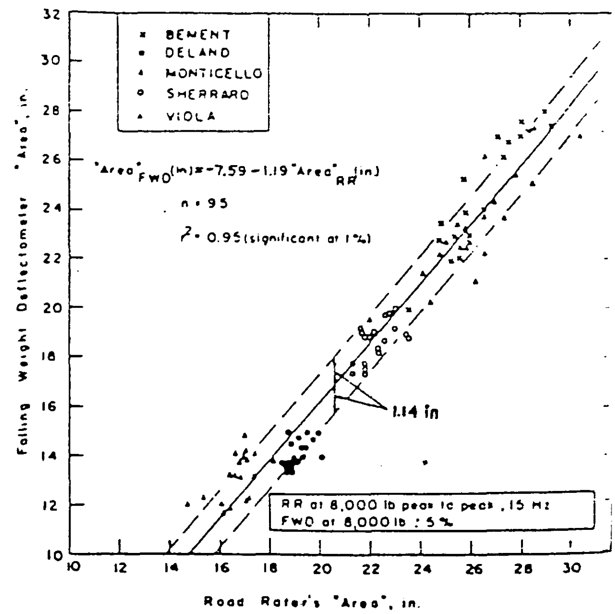

Fig. 1.20 Variation of moving-truck, RR, and FWD deflections with load. [21]

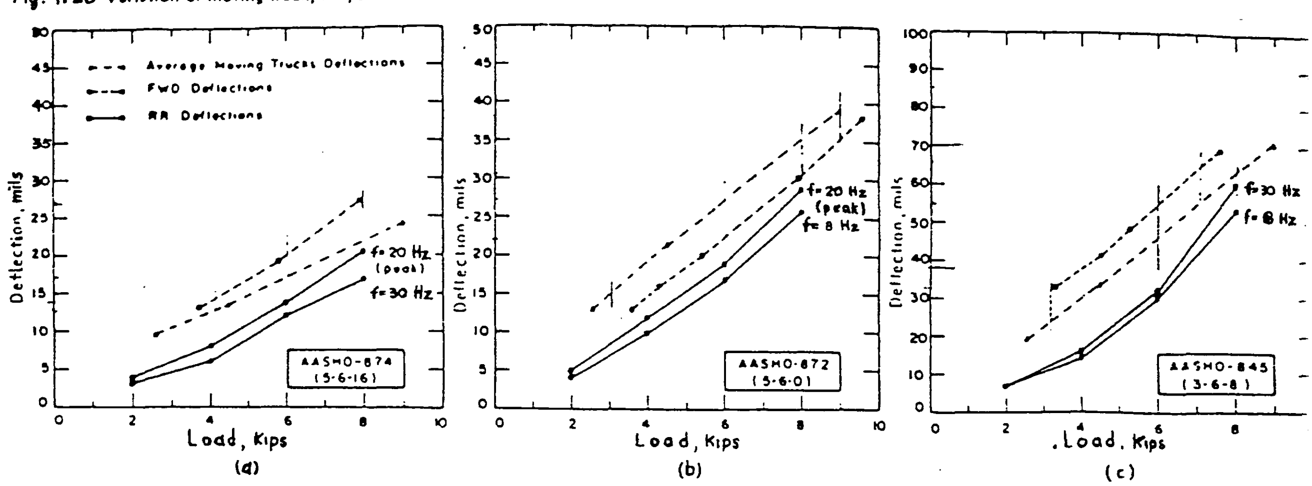

Fig. 1.21 Variation of moving-truck deflections with vehicle speed. [21]

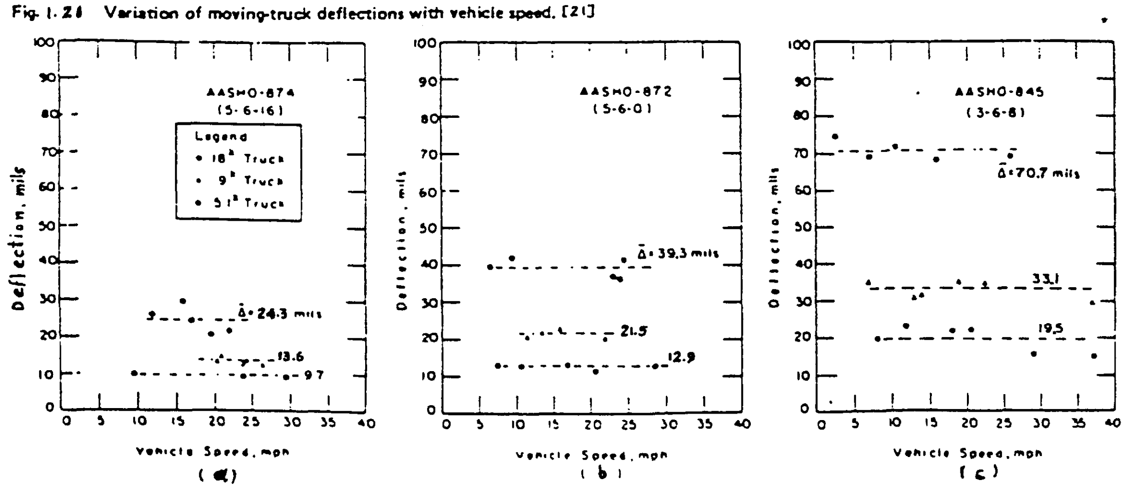

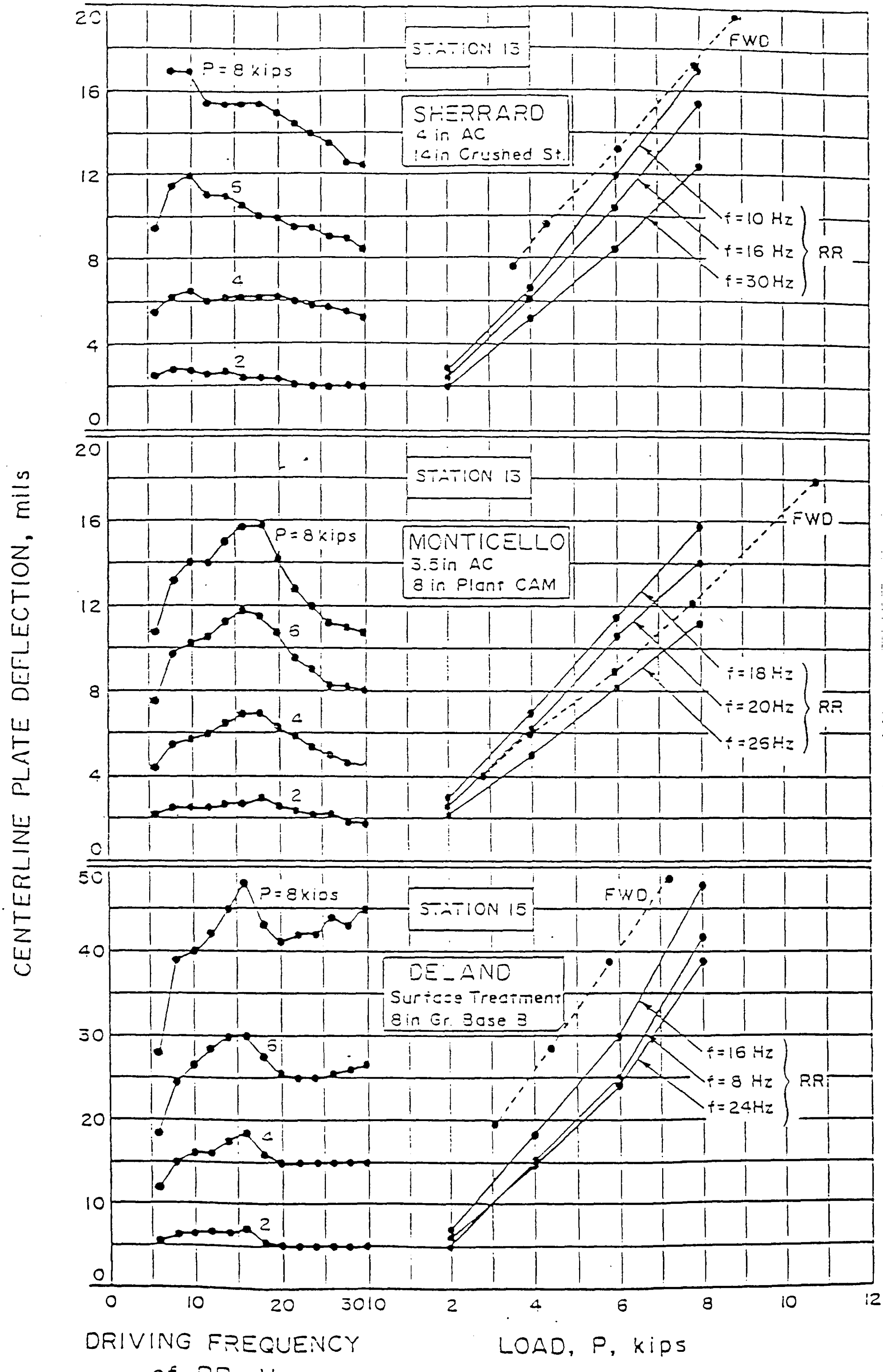

Fig. 1.22 Comparison between Road Rater and Falling Weight Deflectometer Test Data[2]

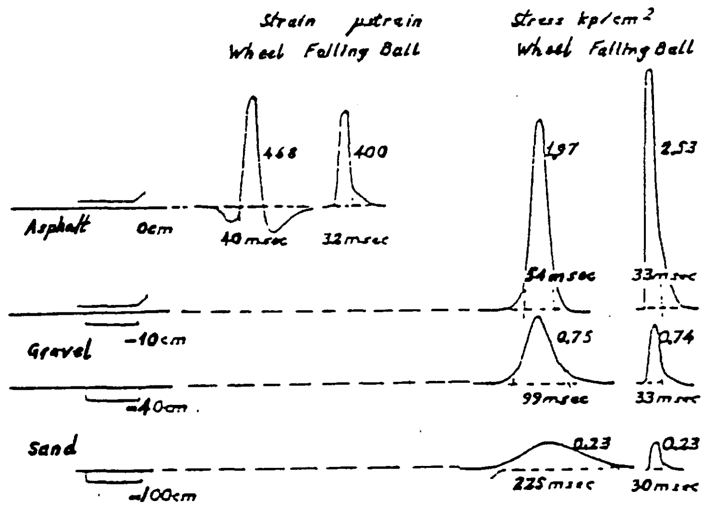

Fig. 1.23 Stress and Strain Curves from Various Depths under the Effect of the FWD and a Moving Wheel Load[2].

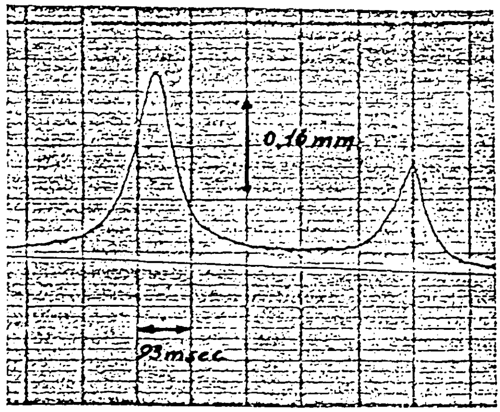

Fig. 1.24 Deflection of Road Surface Under Truck [2]

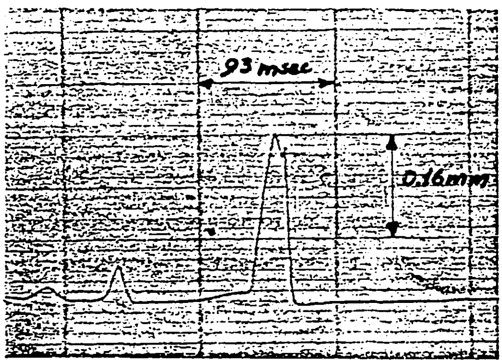

Fig. 1.25 Deflection of Road Surface Under FWD [2]

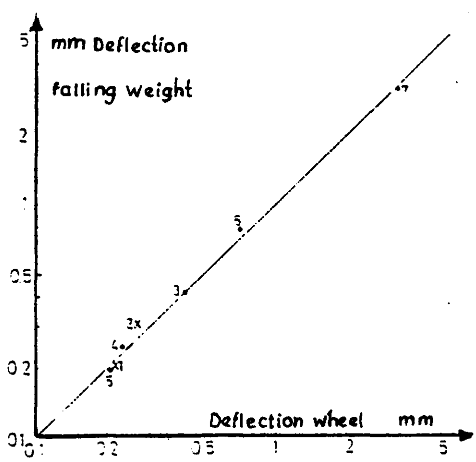

Fig. 1.26 Correlation between the FWD and Moving Wheel Deflections [2]

Fig. 1.27 FWD versus accelerometer deflections. [21]

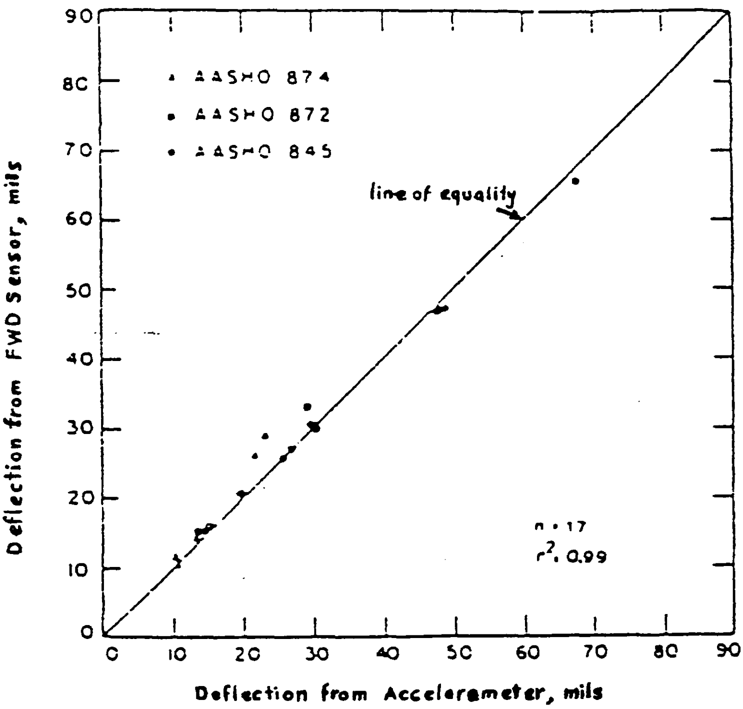

Fig. 1.28 Acceleration, velocity, and deflection signals under moving trucks. [21]

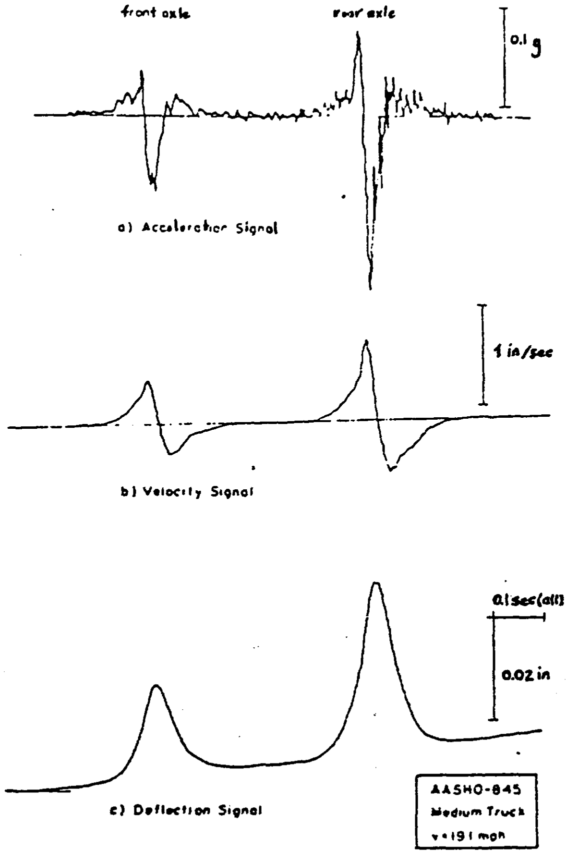

Fig. 1.29 Typical FWD acceleration and deflection signals. [21]

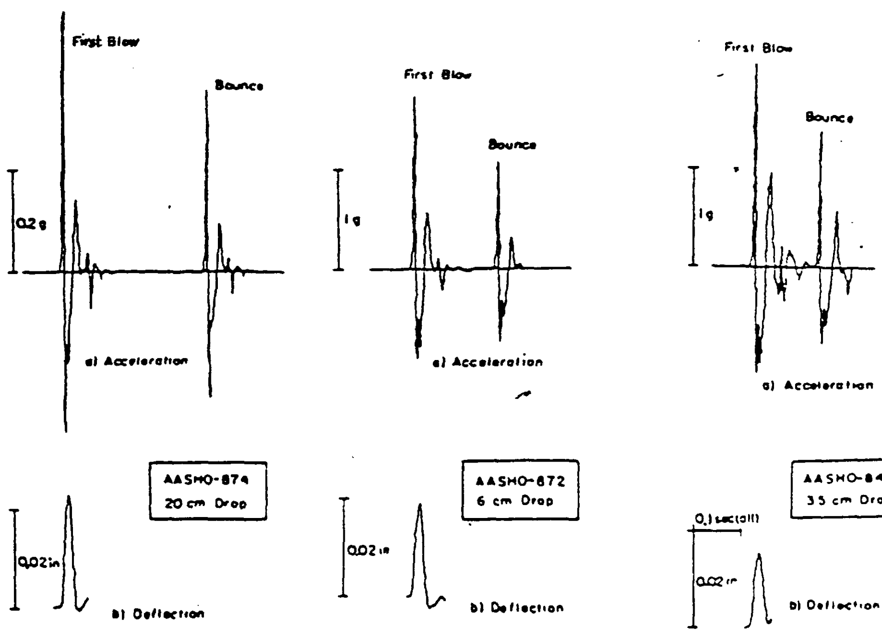

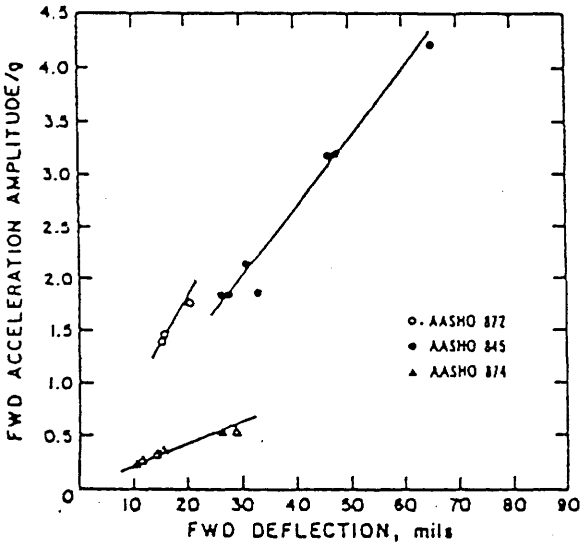

FIG.1.30 –FWD Acceleration versus FWD Deflection in AASHO Sections[21]

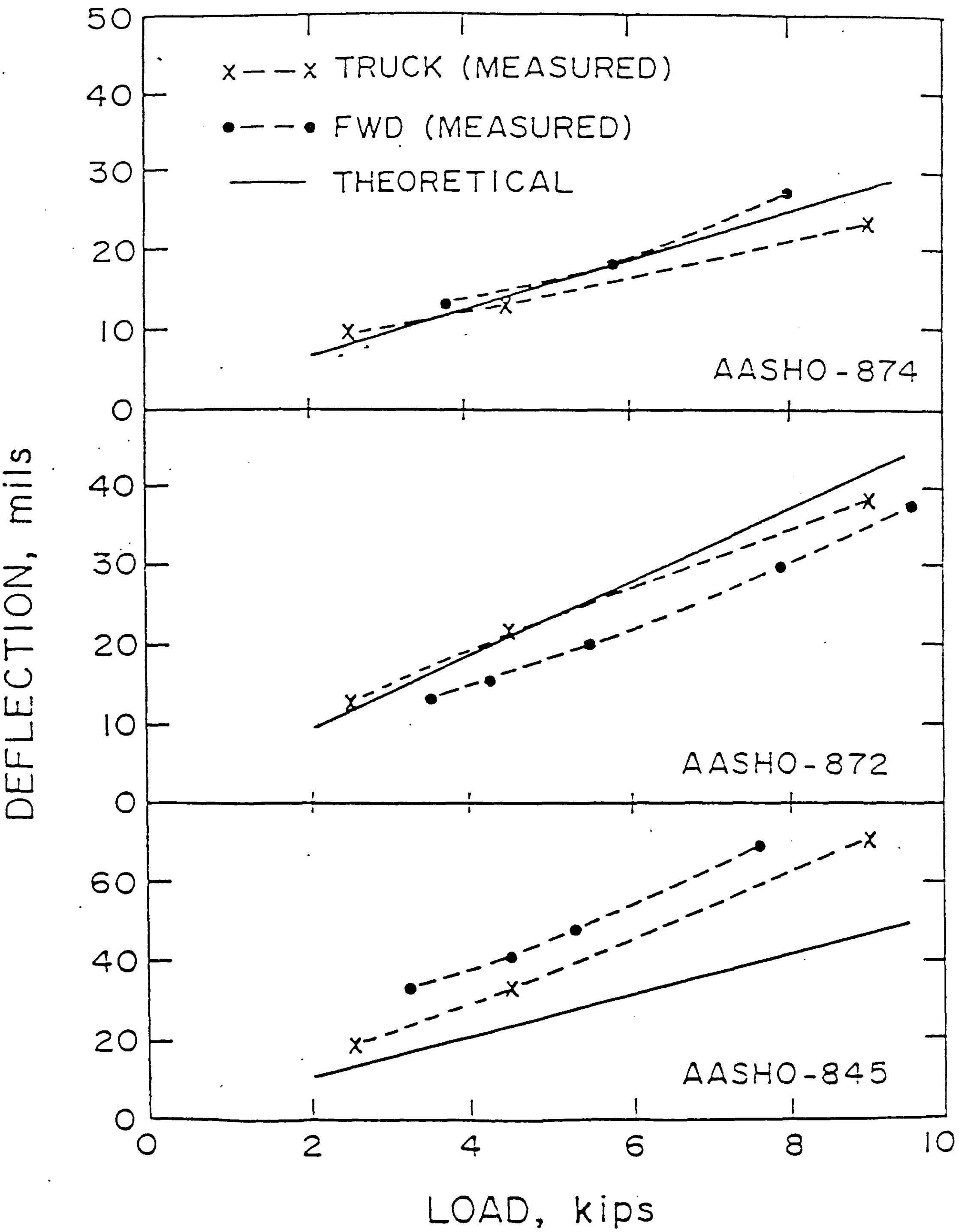

Fig. 1.31 Comparison Between Predicted and Measured Deflection Data for Selected AASHO Road Test Sections [41]

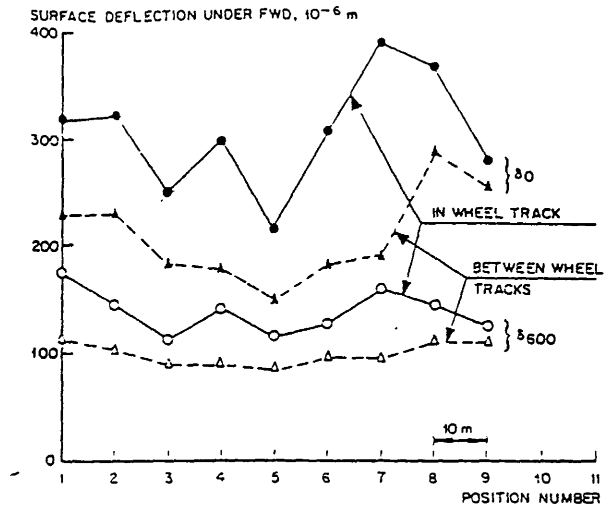

Fig. 1.32 Deflections Under the Falling Weight Deflectometer in and between Wheel Tracks at Speulde-Meerveld (Section IV). Deflections in Center of Load (δ_0), and at Radial Distance of 600 mm (δ_{600}) Temperature: 3.5 C. [8]

Table 1.1 Average FWD Data on Various Sections in Speulde-Meerveld Temperature: 3.5 C [8]

Site	h_1 obtained from cores mm	In the wheeltrack δ_0 10^{-10} m/N	v %	δ_{600}	h_1 mm	E_3 MN/m^2	Between the wheeltracks δ_0 10^{-10} m/N	v %	δ_{600}	h_1 mm	E_3 MN/m^2
I	240	54	17	0.99	165	150	47	17	0.58	165	175
II	175	70	25	0.59	150	120	53	8	0.57	155	160
IV(1)	160	95	18	0.45	100	120	74.5	6	0.46	110	150
(2)	160	95	18	0.45	100	120	55	9	0.52	140	175
V	110	185	19	0.26	50	100	100	8	0.39	85	135

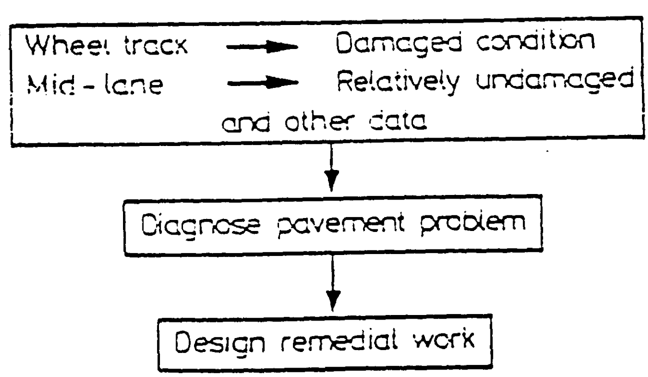

FIG. 1.33 General procedures for pavement evaluation [5]

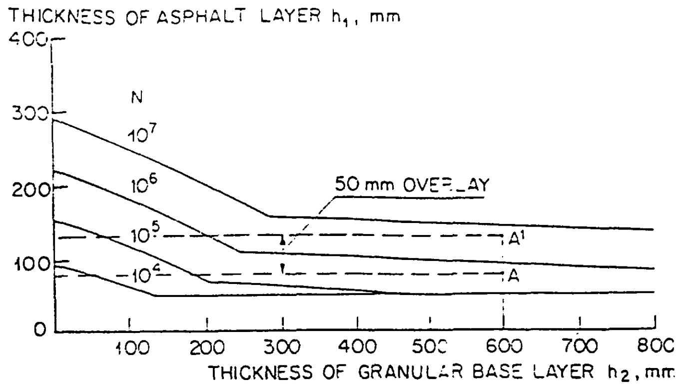

Fig. 1.34 Shell Design Chart for Subgrade Modulus E_3 = 110 MN/m^2. [9]

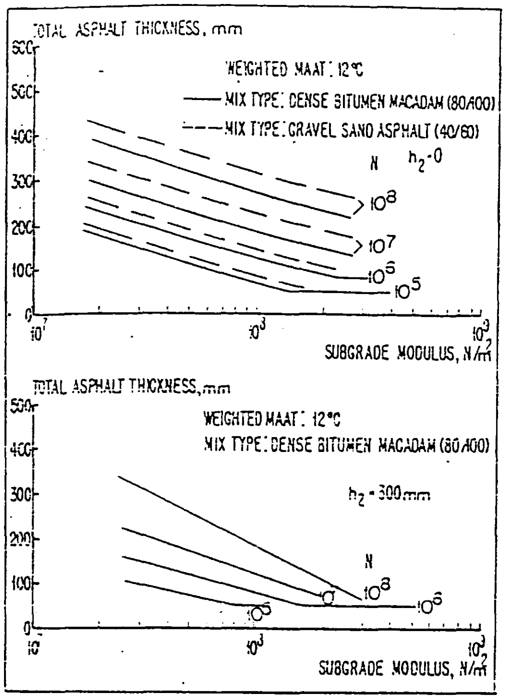

Fig. 1.35 Design charts to derive original pavement design life and overlay thickness required [9]

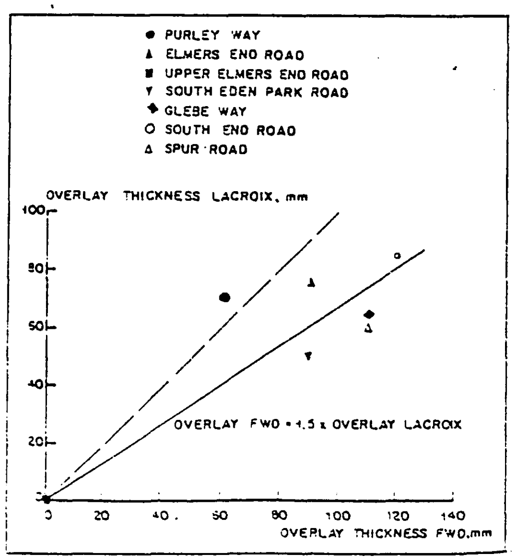

Fig. 1.36 Comparison of overlay thicknesses derived by two methods [9]

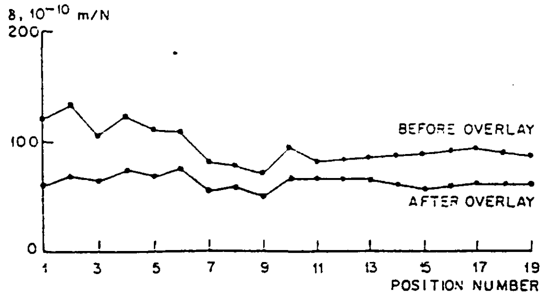

Fig. 1.37 Deflection per Unit Force in the FWD Measurements as a Function of the Position on the Pavement (Nijkerk). [9]

Fig. 1.38 Schematic representation of a pavement structure under a test load. [28]

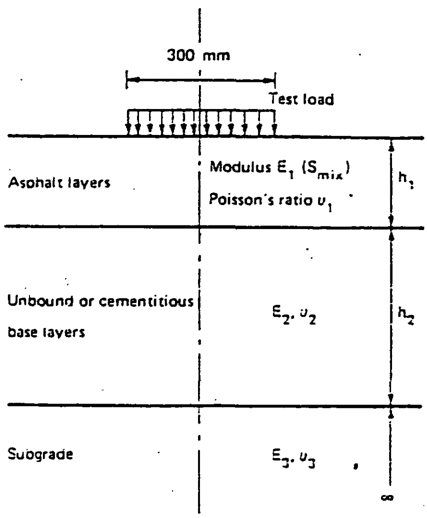

Fig. 1.39 Deflection interpretation chart. [28]

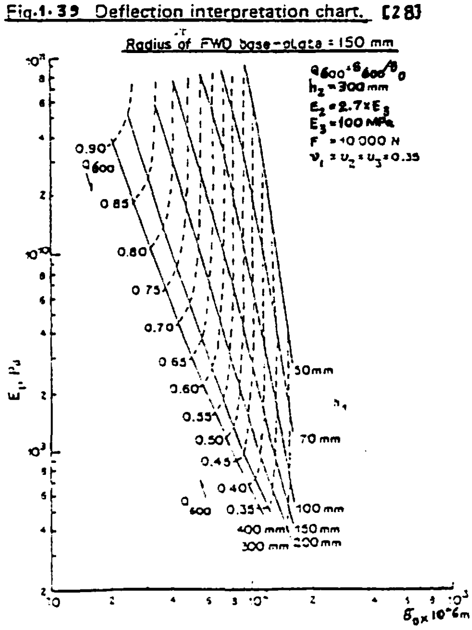

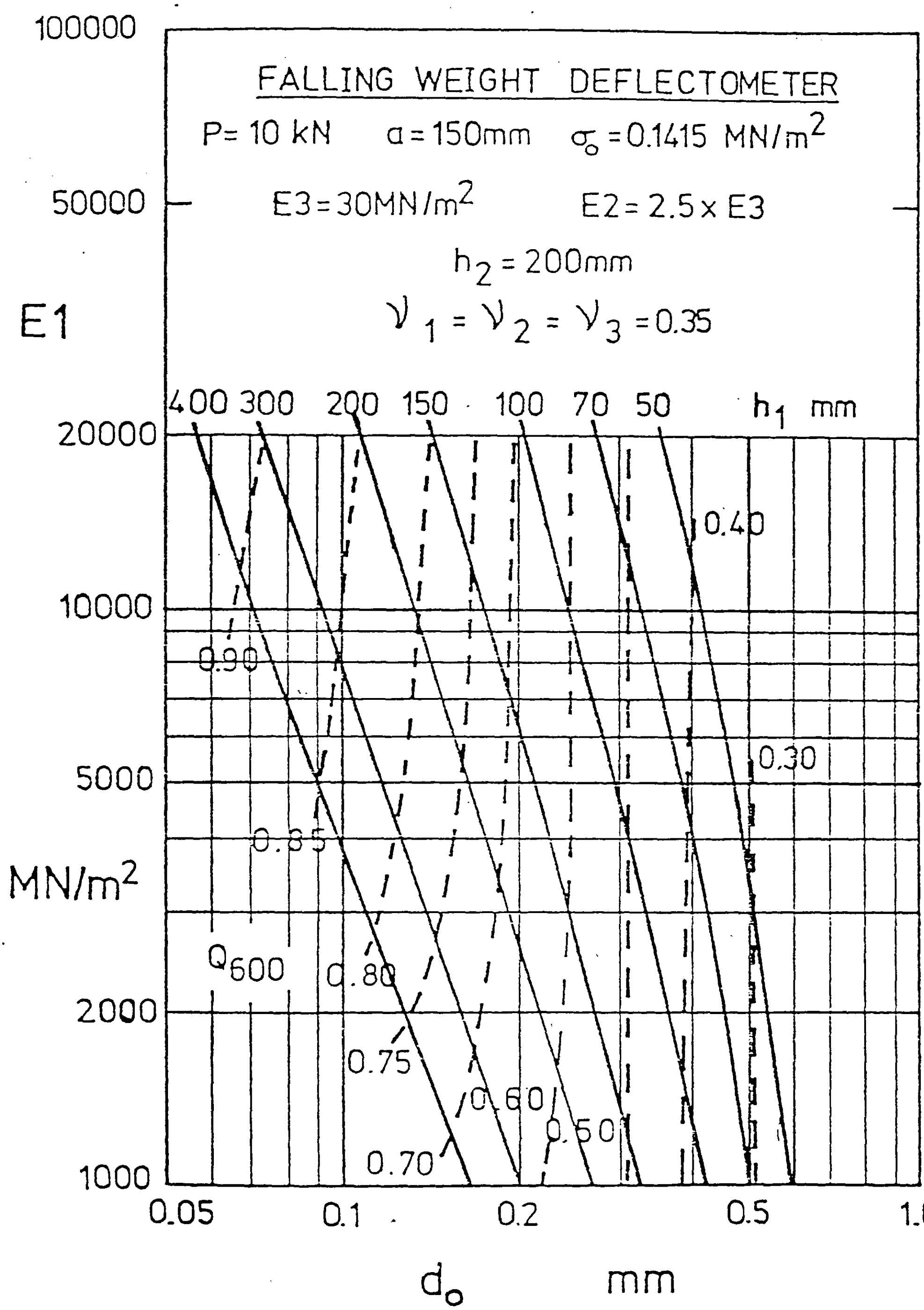

FIG.1.40 CHART FOR ESTIMATING STIFFNESS OF PAVEMENT LAYERS[36]

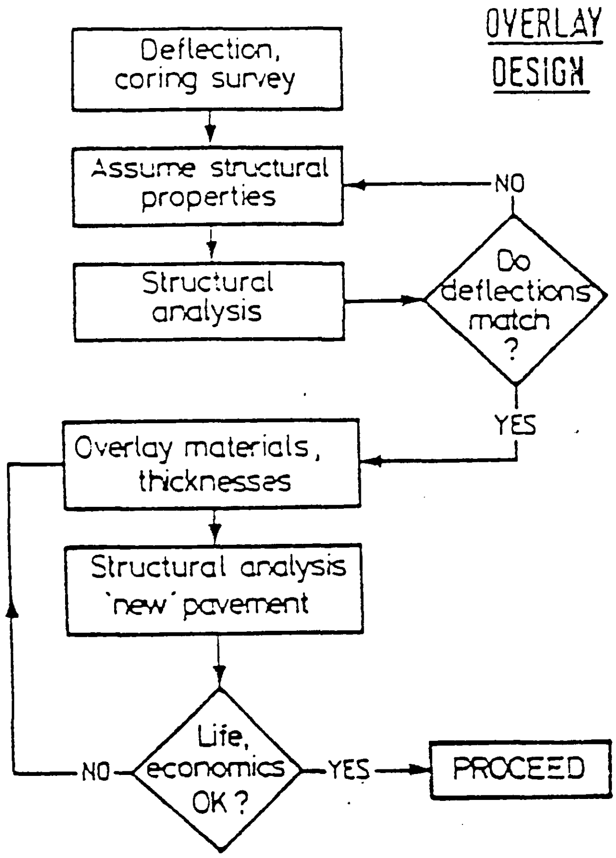

FIG. 1.41 Flow diagram of evaluation and overlay design procedure [5]

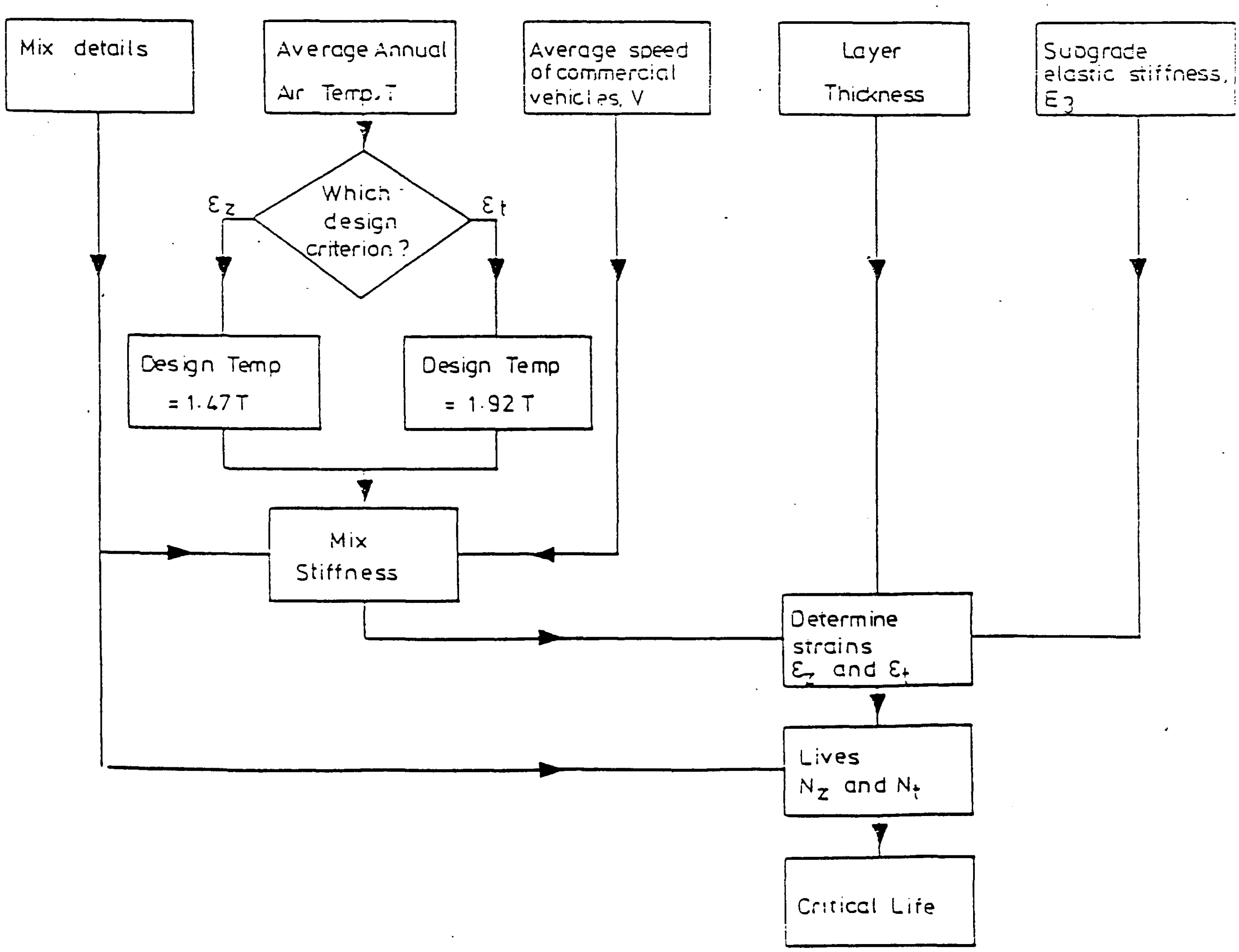

Fig.1.42 FLOW DIAGRAM OF DESIGN LIFE PROCEDURE[6]

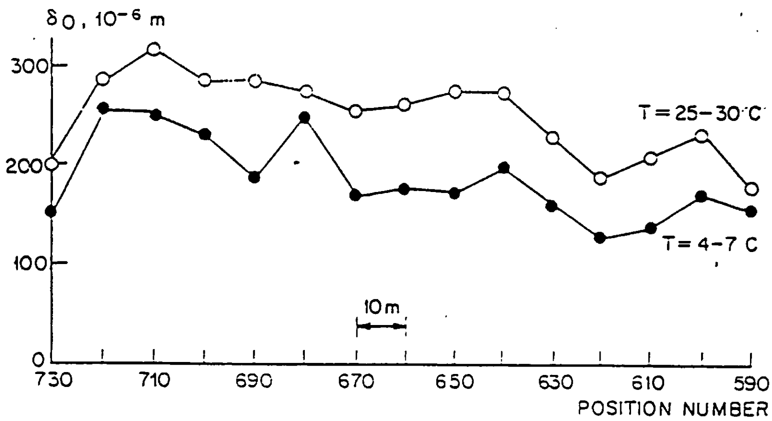

Fig. 1.43 Deflections Under the Falling Weight Deflectometer in Hilpoltstein Section A_1 in March (●) and August 1975 (○). [8]

Table 1.2 Results of FWD Measurements at Hilpoltstein [8]

Section	A_1		A_2		A_3		B_1		B_2		B_3	
Layer Thicknesses from Construction Reports h_1, mm	180		190		240		155		175		205	
h_2, mm	300		300		300		150		150		150	
Wave Propagation Measurements												
Temperature, C			5		12	20						
E_1, MN/m^2			17 000		12 000	11 500						
E_3, MN/m^2	230		250–300		230				210			
FWD Deflection Measurements												
Temperature C	7	25	7	30	7	30	4	31	4	25	4	30
δ_0, 10^{-10} m/N	58	78	45	76	37	74	39	51	40	43	34	43
V, %			16		14		25		19		14	
$q_{600} = \delta_{600}/\delta_0$	0.56	0.49	0.61	0.42	0.67	0.48	0.71	0.76	0.69	0.70	0.71	0.74
FWD Calculations												
E_1*, MN/m^2	10 000	3 000	10 000	2 000	10 000	2 000	12 000	2 000	12 000	3 000	12 000	2 000
h_1, mm	145	175	180	170	225	210	235	**	220	**	260	**
E_3, MN/m^2	140	115	160	145	160	120	140	**	140	**	150	**

* E_1 values derived from Fig. 1.44.
** To be interpreted later, on the basis of new graphs.

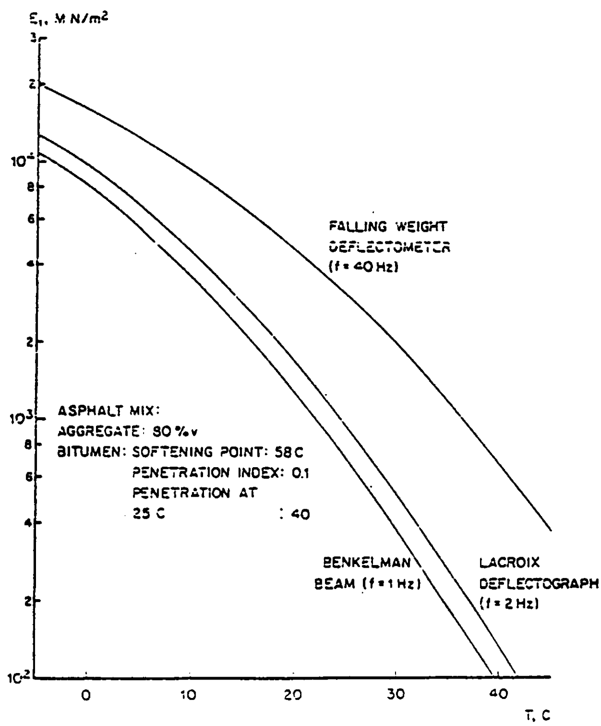

Fig. 1.44 Asphalt Modulus E_1 as a Function of the Temperature T in Different Tests. [8]

TABLE 1.3 Repeatability of Backcalculated Dynamic E and k Moduli at Constant Temperature at the Center Slab Position [17]

				k		$E \times 10^6$		
Feature	Slab No.	Pvmt Temp. (°F)	Load[a] Range	Average (pci)	Coef. of Var.	Average (psi)	Coef. of Var.	No. of Tests
T04A	1	78.6	Low	294	.19	4.2	.33	8
			Medium	280	.15	3.8	.26	8
			High	286	.11	3.6	.18	8
	2	82.2	Low	434	.09	2.9	.13	8
			Medium	349	.07	3.3	.14	8
			High	358	.07	3.2	.12	8
	3	80.8	Low	206	.14	5.5	.15	8
			Medium	205	.17	4.7	.27	8
			High	215	.12	4.6	.22	8
A05B	1	68.4	Low	181	.11	6.6	.18	9
			Medium	178	.16	6.0	.11	9
			High	190	.05	5.8	.12	9
	2	74.5	Low	156	.12	7.9	.17	8
			Medium	158	.04	6.9	.04	8
			High	181	.06	6.2	.08	8
	4	89.1	Low	125	.18	7.9	.29	8
			Medium	141	.07	6.0	.13	8
			High	150	.05	5.7	.07	8

[a]Load ranges are as follows: low, 6,000 to 9,000 lbf; medium, 14,000 to 17,000 lbf, and high, 22,000 to 26,000 lbf.

TABLE 1.4 Repeatability of Backcalculated Dynamic E and k Moduli at Various Temperatures at the Center Slab Position [17]

Feature	Slab No.	Pvmt Temp. Range (°F)	Load[a] Range (lbf)	k Average (pci)	k Coef. of Var.	E x 10^6 Average (psi)	E x 10^6 Coef. of Var.	No. of Cases
T04A	1	33.1	Low	275	.19	5.9	.31	8
		to	Medium	276	.15	4.2	.16	8
		121.8	High	316	.13	3.6	.19	8
	2	33.1	Low	422	.13	4.7	.26	8
		to	Medium	348	.12	4.4	.27	8
		121.8	High	396	.10	3.8	.27	8
	3	33.1	Low	268	.29	5.8	.38	8
		to	Medium	243	.27	1.3	.27	8
		121.8	High	261	.25	4.6	.26	8
	4	33.1	Low	448	.24	2.9	.53	5
		to	Medium	370	.13	4.4	.08	5
		121.8	High	391	.12	4.2	.12	5
A05B	1	34.2	Low	209	.17	7.1	.13	6
		to	Medium	189	.16	7.2	.13	6
		119.3	High	208	.18	6.5	.09	6
	2	34.2	Low	194	.31	9.1	.33	7
		to	Medium	176	.16	7.7	.21	7
		119.3	High	188	.08	7.6	.14	7
	3	34.2	Low	327	.23	10.0	.19	6
		to	Medium	287	.12	9.3	.24	6
		119.3	High	310	.09	8.8	.09	6
	4	34.2	Low	189	.14	7.5	.27	7
		to	Medium	173	.10	6.8	.15	7
		119.3	High	182	.07	6.8	.11	7

[a]Load ranges are as follows: low, 6,000 to 9,000 lbf; medium, 14,000 to 16,000 lbf; and high, 22,000 to 25,000 lbf.

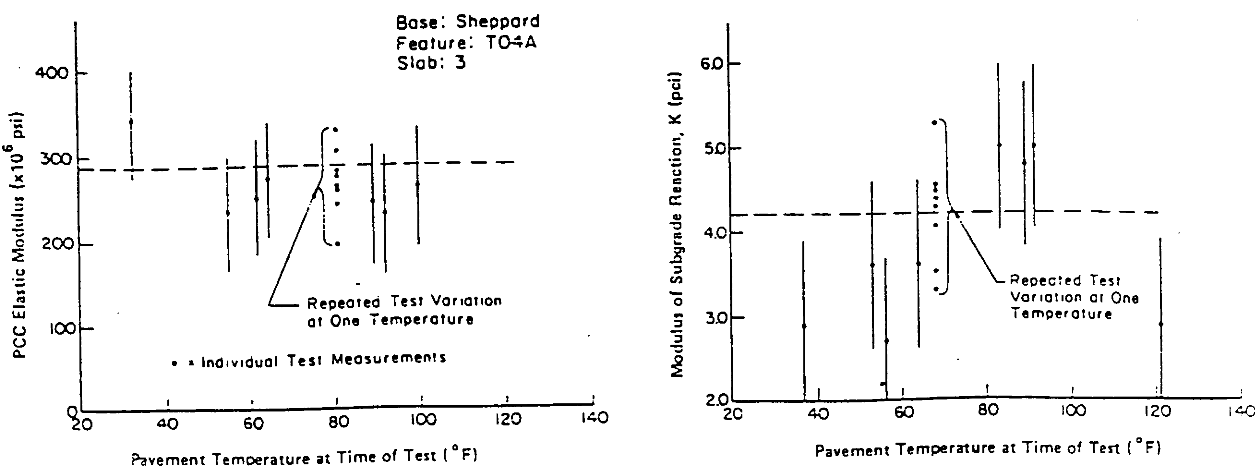

FIG. 1.45 Typical variation in E and k at constant temperature applied to single observations of E and k at various temperatures. [17]

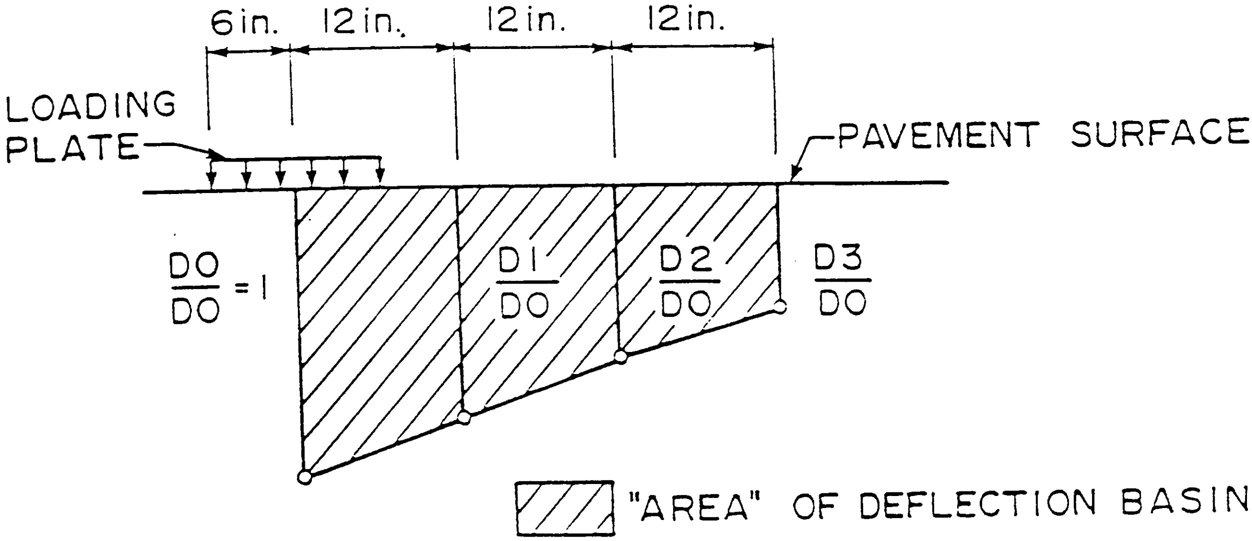

Fig.1.46 Deflection Basin Characterisation. [22]

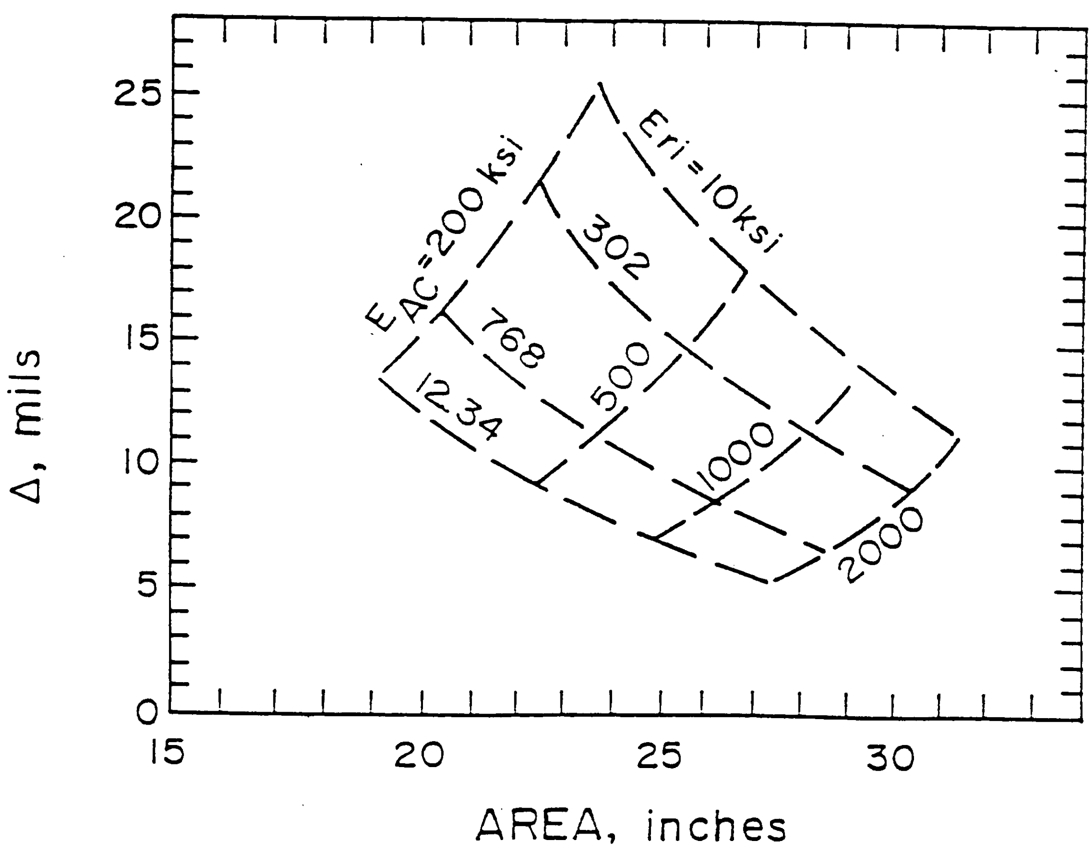

Fig.1.47 Evaluation Nomograph for a Nine Inch Thick Full-Depth AC Pavement [22]

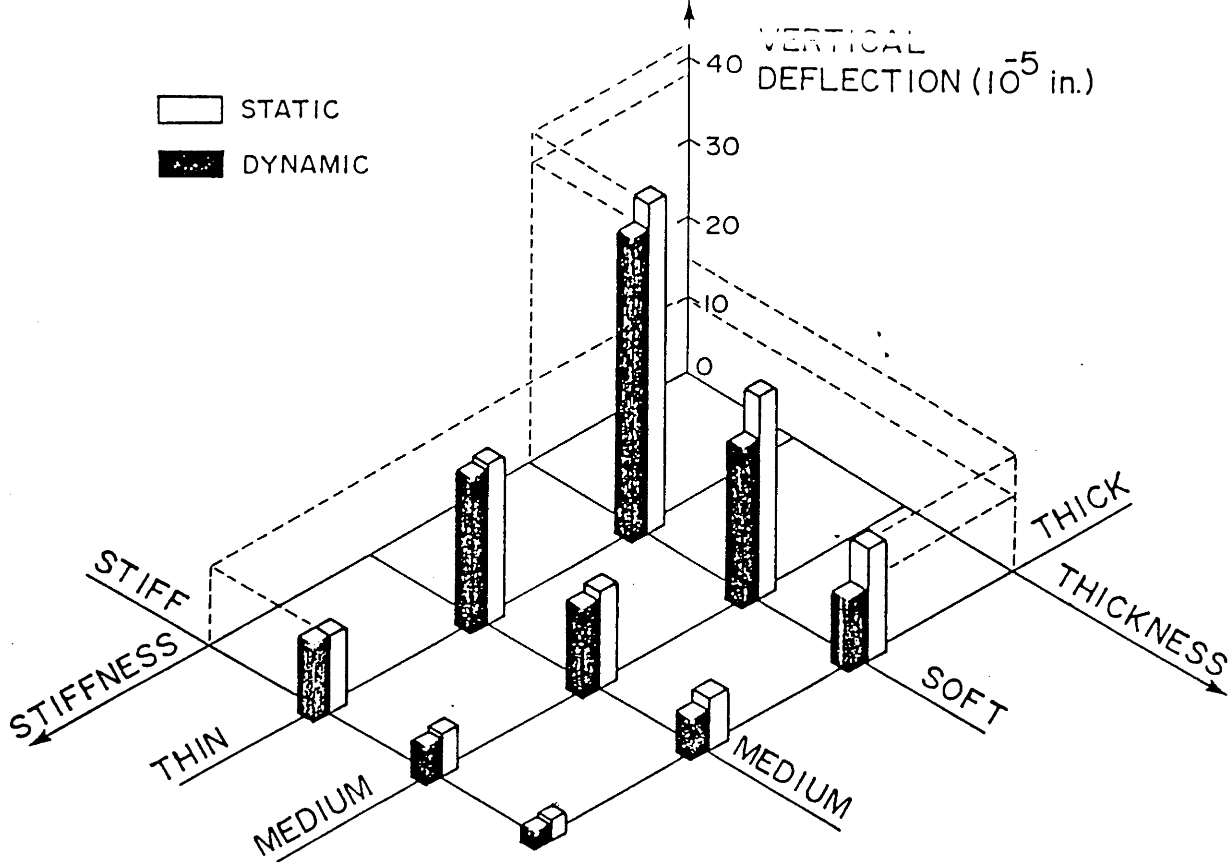

Fig. 1.48 Pavement Deflections Under Static and (25 Hz) Dynamic Loads Adjacent to the Road Rater [31]

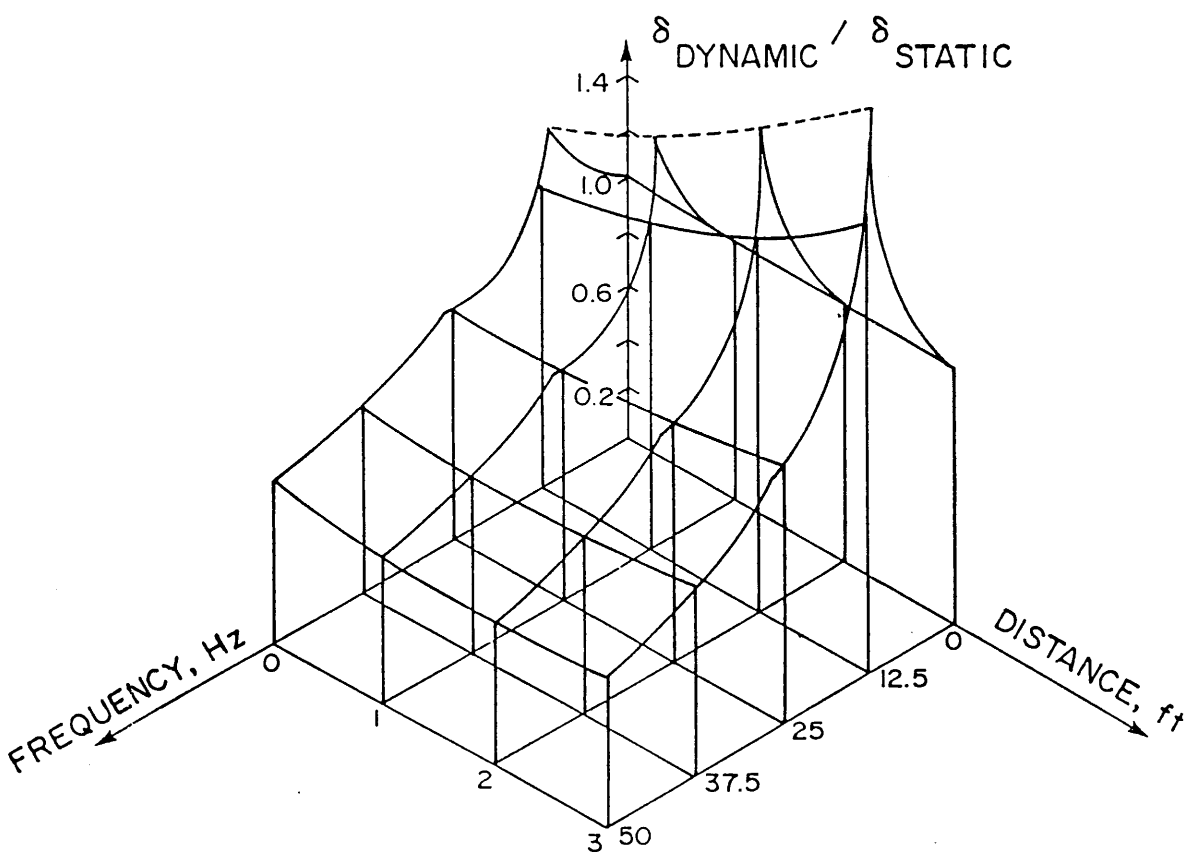

Fig. 1.49 Deflection Ratios at Various Geophone Locations of the Road Rater [31]

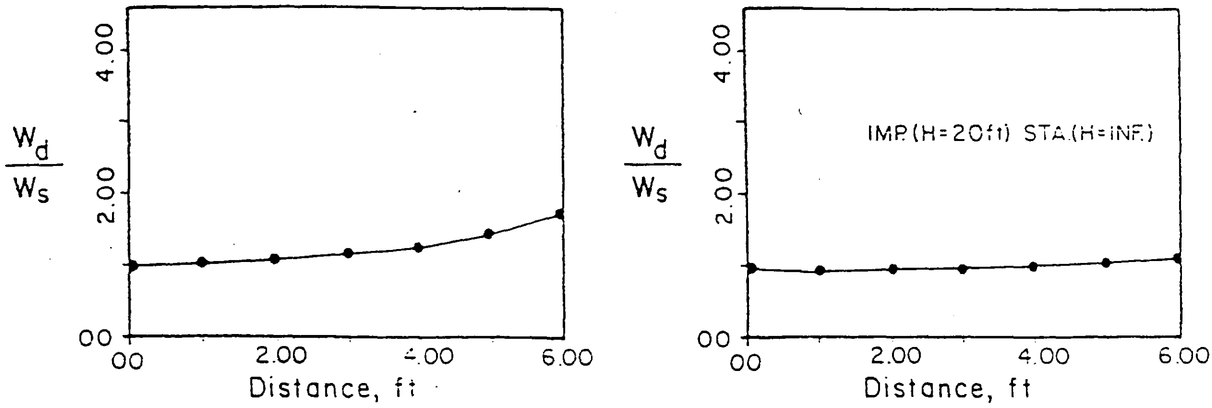

FIG. 1. 50 Ratio of dynamic (IMP) to static (H = ∞) deflections at H = 20 ft—falling weight deflectometer. [40]

TABLE 1.5 Deflection Bulbs and Estimated Elastic Moduli for Homogeneous Subbase and Different Depths to Bedrock, Falling Weight Deflectometer [40] (displacement x 10^{-8} ft)

		Distance to the Center (ft)								
	H (ft)	0	1	2	3	4	5	6	Estimated (lb/in²)	Errors (%)
Static	∞	11.54	5.139	3.141	2.180	1.611	1.253	1.015	200,000 78,500 29,000	
Dynamic	10	10.60	4.622	2.842	1.923	1.317	0.9094	0.7214	200,000 78,500 35,539	0.0
Dynamic	20	11.06	4.652	3.013	2.073	1.538	1.280	1.090	200,000 82,200 28,790	0.0 4.7 0.7
Dynamic	40	10.74	4.860	3.008	2.111	1.590	1.288	1.086	287,200 87,375 28,331	43.6 11.3 2.3
Dynamic	80	11.08	4.733	3.073	2.109	1.608	1.311	1.044	200,000 89,131 29,245	0.0 13.5 0.8

TABLE 1.6 Material Types and Layer Thicknesses of Pavement Sections [42]

Section	Layer	Type	Thickness (in.)
Bement	Surface	Asphalt concrete	4
	Base	Soil cement	6
	Subgrade	A-7-6 (24)	720[a]
Deland	Surface	Surface treatment	0.5
	Base	Granular	8
	Subgrade	A-7-6 (21)	720[a]
Monticello	Surface	Asphalt concrete	3.5
	Base	Plant-mixed CAM	8
	Subgrade	A-6 (8)	720[a]
Sherrard	Surface	Asphalt concrete	4
	Base	Crushed stone	14
	Subgrade	A-4 (6)	720[a]

[a] Assumed values.

TABLE 1.7 Pavement Material Properties [42].

Section	Layer	Moduli[a] (ksi)	Poisson's Ratio[b]	Density[b] (lb/ft^3)
Bement	Surface	170	0.35	145
	Base	1700	0.4	140
	Subgrade	7.5	0.45	115
Deland	Surface	30	0.35	145
	Base	9	0.4	140
	Subgrade	9	0.45	115
Monticello	Surface	450	0.35	145
	Base	650	0.4	140
	Subgrade	8	0.45	115
Sherrard	Surface	500	0.35	145
	Base	35	0.4	140
	Subgrade	10	0.45	115

[a] From laboratory testing.
[b] Assumed values.

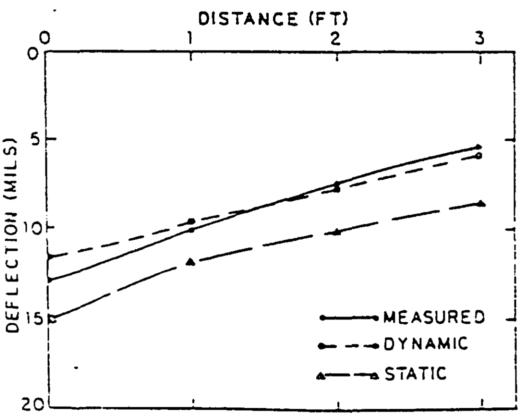

FIG. 1.51 Measured, static, and dynamic deflections at various geophone locations for Bement section. [42]

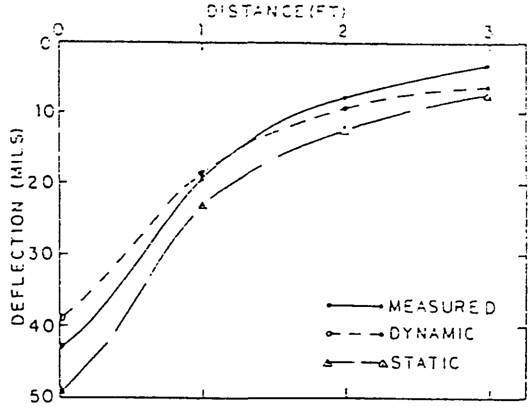

FIG. 1.52 Measured, static, and dynamic deflections at various geophone locations for Deland section. [42]

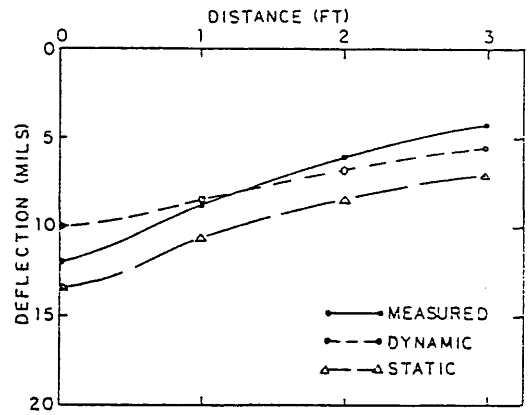

FIG 1.53 Measured, static, and dynamic deflections at various geophone locations for Monticello section. [42]

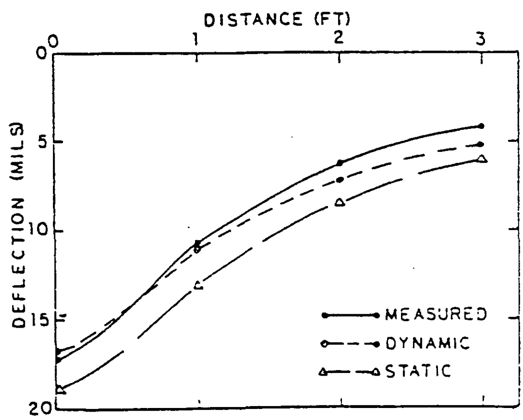

FIG. 1.54 Measured, static, and dynamic deflections at various geophone locations for Sherrard section. [42]

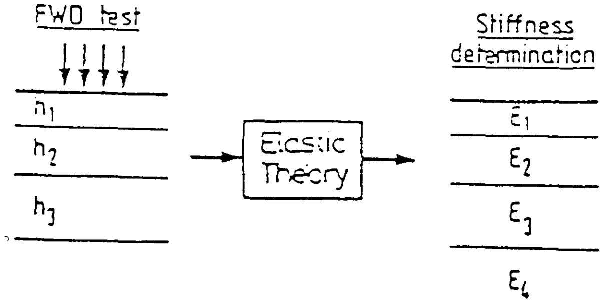

(FIG. 1.55) [5]

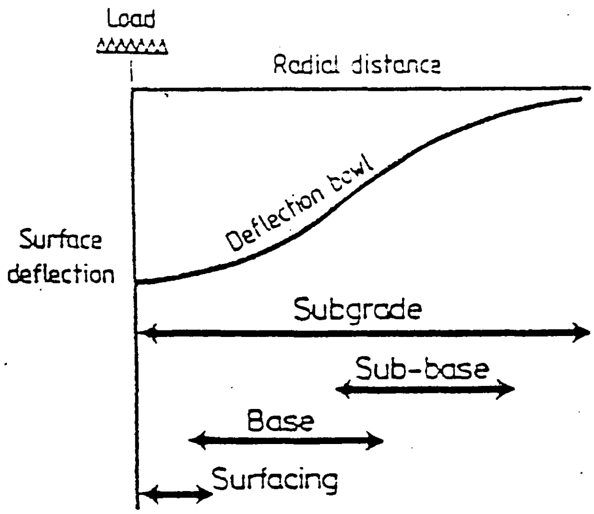

FIG. 1.56 Deflection bowl characteristics [5]

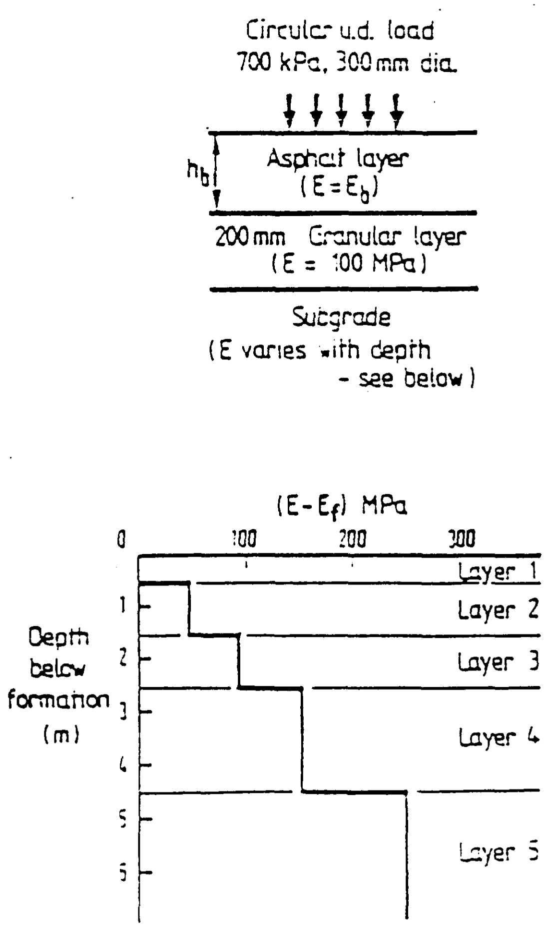

FIG. 1.57 Structural arrangement for back analysis [5]

THREE LAYER FLEXIBLE PAVEMENT

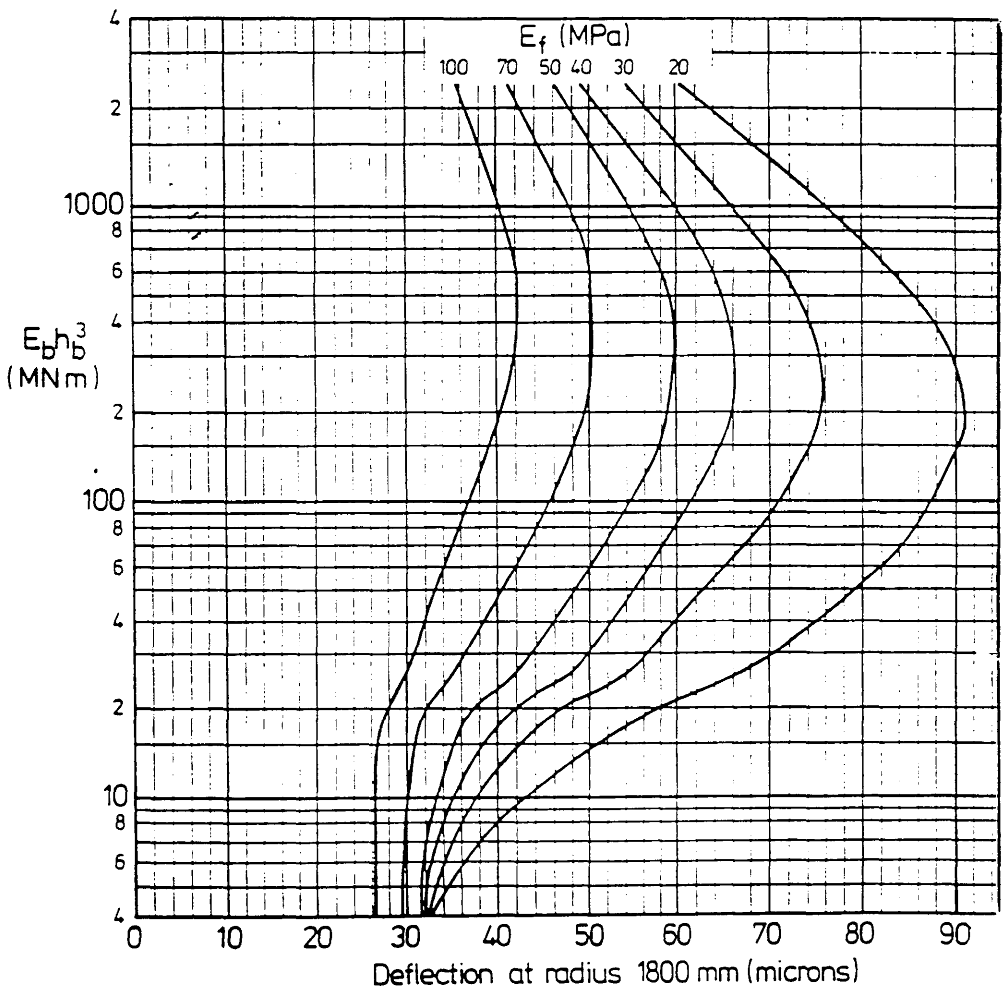

(FIG. 1.58) Chart for determination of elastic stiffness at formation level (E_f) [5]

THREE LAYER FLEXIBLE PAVEMENT

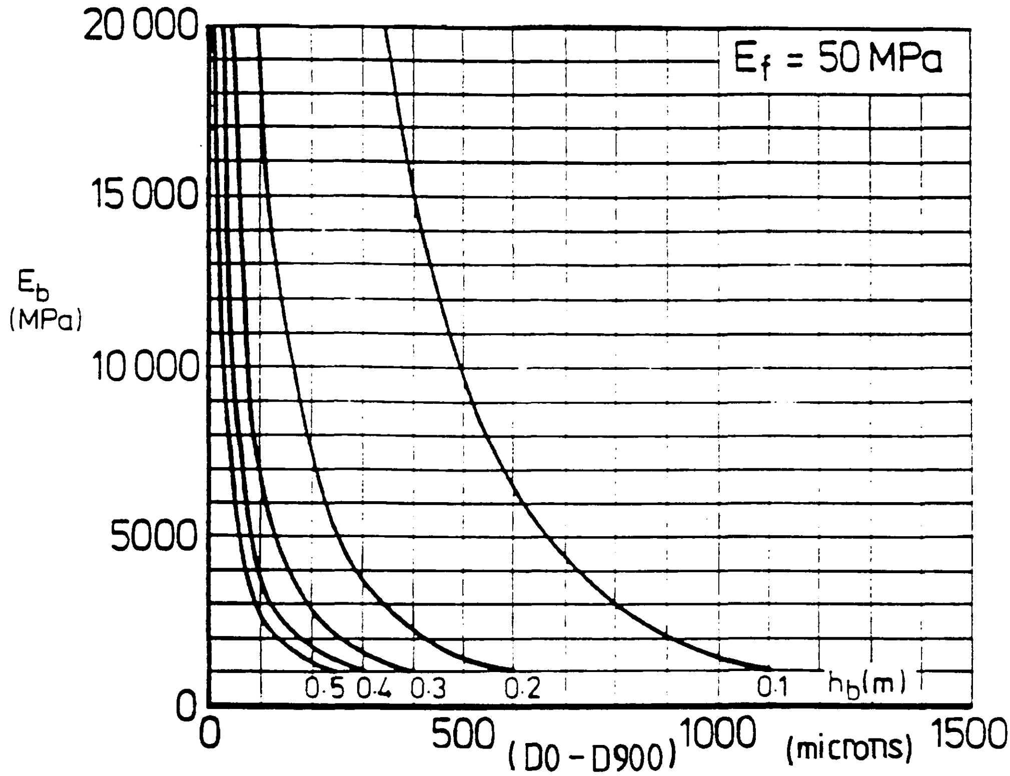

(FIG. 1.59) Chart for determination of elastic stiffness (E_b) [5]

Layer	Structure 1			Structure 2			Structure 3		
	(a)[1]	(b)[2]	difference (%)[3]	(a)[1]	(b)[2]	difference (%)[3]	(a)[1]	(b)[2]	difference (%)[3]
(A) Back-analysed stiffnesses (MPa)									
Asphaltic	3813	4331	13.6	1809	1806	-0.2	2450	2416	1.4
Lean Concrete	-	-	-	-	-	-	27450	28656	4.4
Sub-base	-	-	-	31	36	16.1	200	200	0.0
Subgrade - formation	119	135	13.4	175	164	-6.3	340	315	-7.4
- at 4.6m depth	651	392	-39.8	182	165	-9.3	840	752	-10.5
(B) Layer thicknesses (mm)									
Asphaltic	330			220			90		
Lean concrete	-			-			200		
Sub-base	-			220			370		

Note : 1. Back-analysed stiffnesses based on original measured deflection bowl.

2. Back-analysed stiffnesses based on deflection bowl from dynamic analysis.

3. difference = $\frac{(b)-(a)}{(a)} \times 100\%$

Table 1.8 Comparison of back-analysed elastic stiffnesses to illustrate dynamic inertia effects [47]

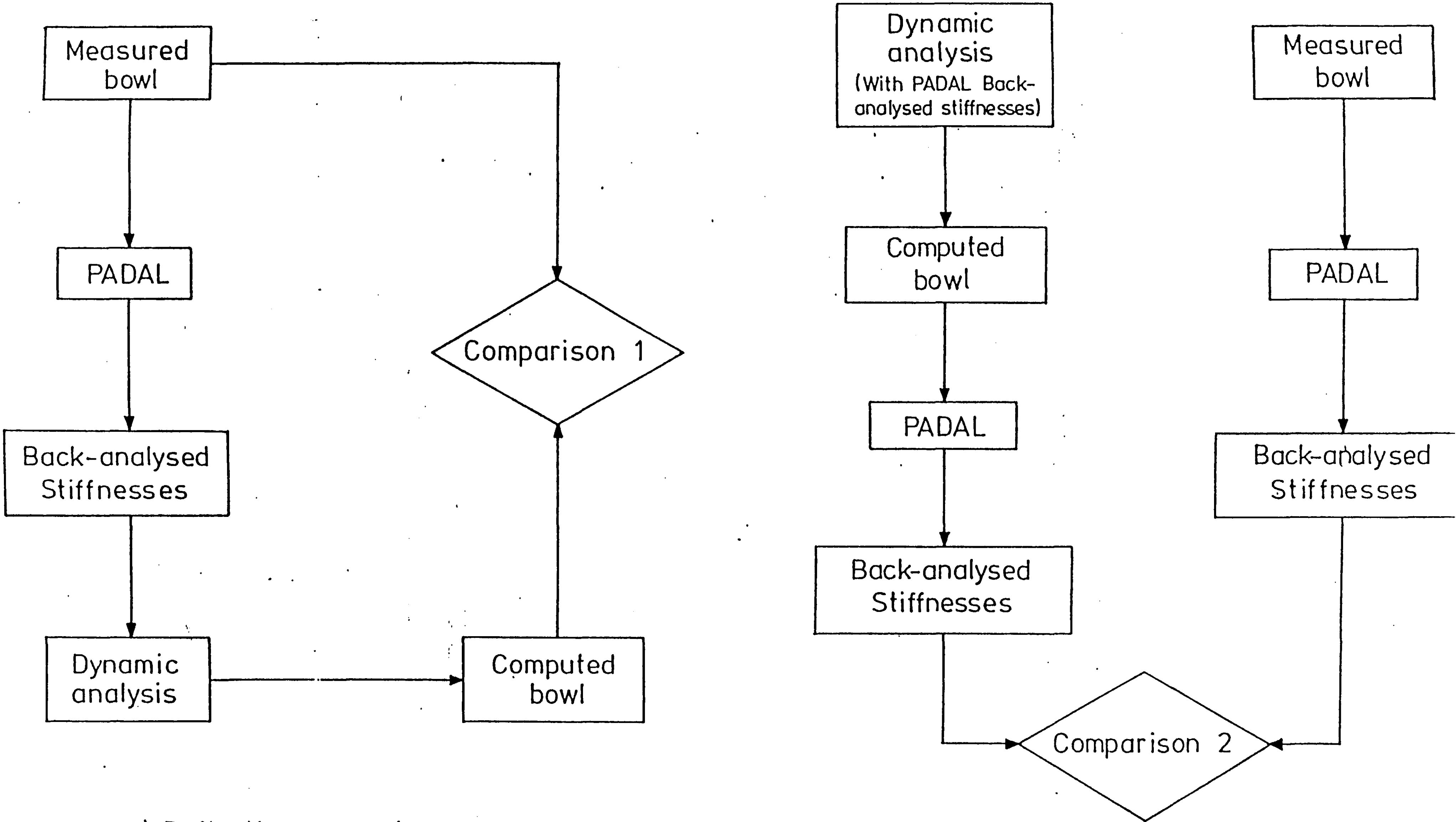

a) Deflection comparison.

b) Stiffness comparison.

Fig. 1.60 PROCEDURES FOR COMPARING PADAL AND DYNAMIC ANALYSIS [47]

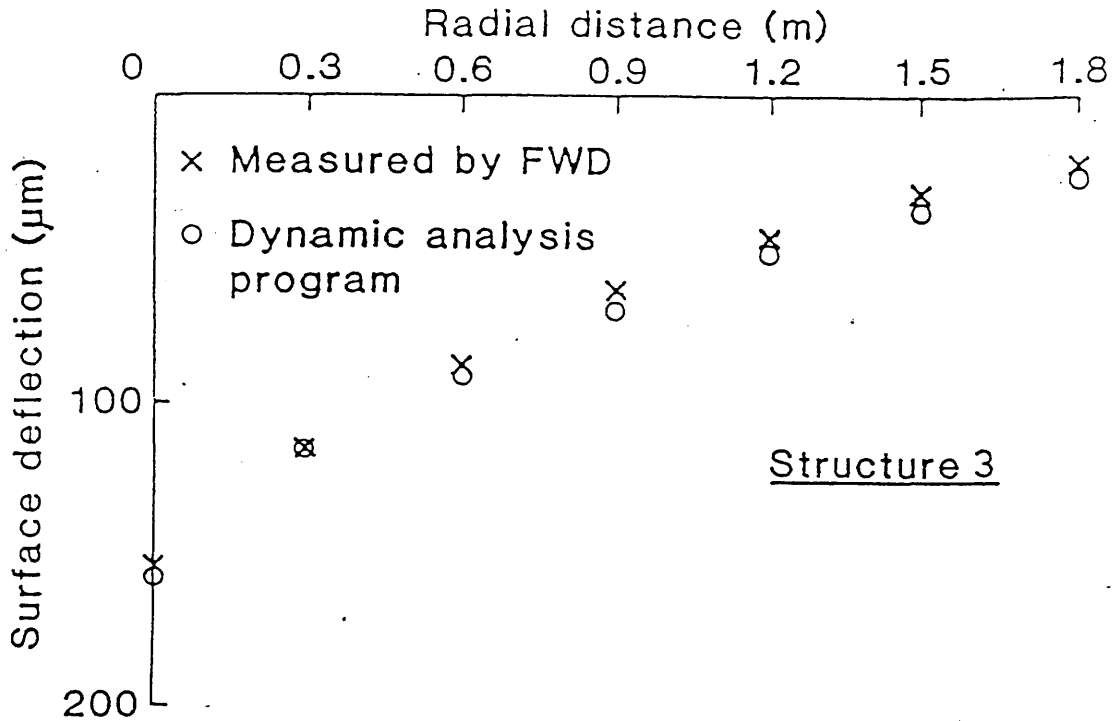

Fig.1.61 COMPARISON OF DEFLECTION BOWLS MEASURED BY FWD AND DYNAMIC ANALYSIS COMPUTATION [47]

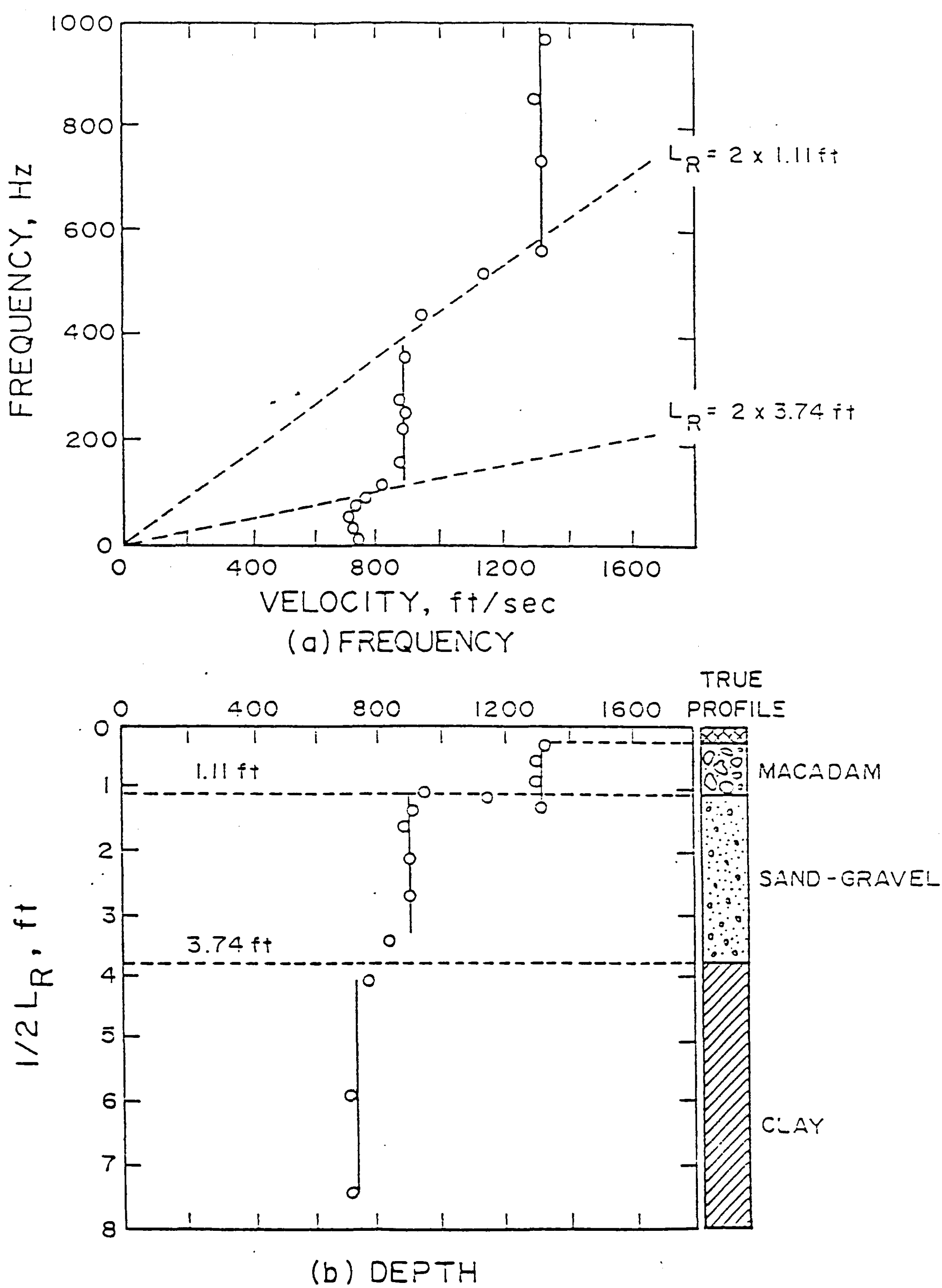

Fig. 1.62 Typical Velocity Profile Developed from Steady-State Rayleigh Wave Testing.[24]

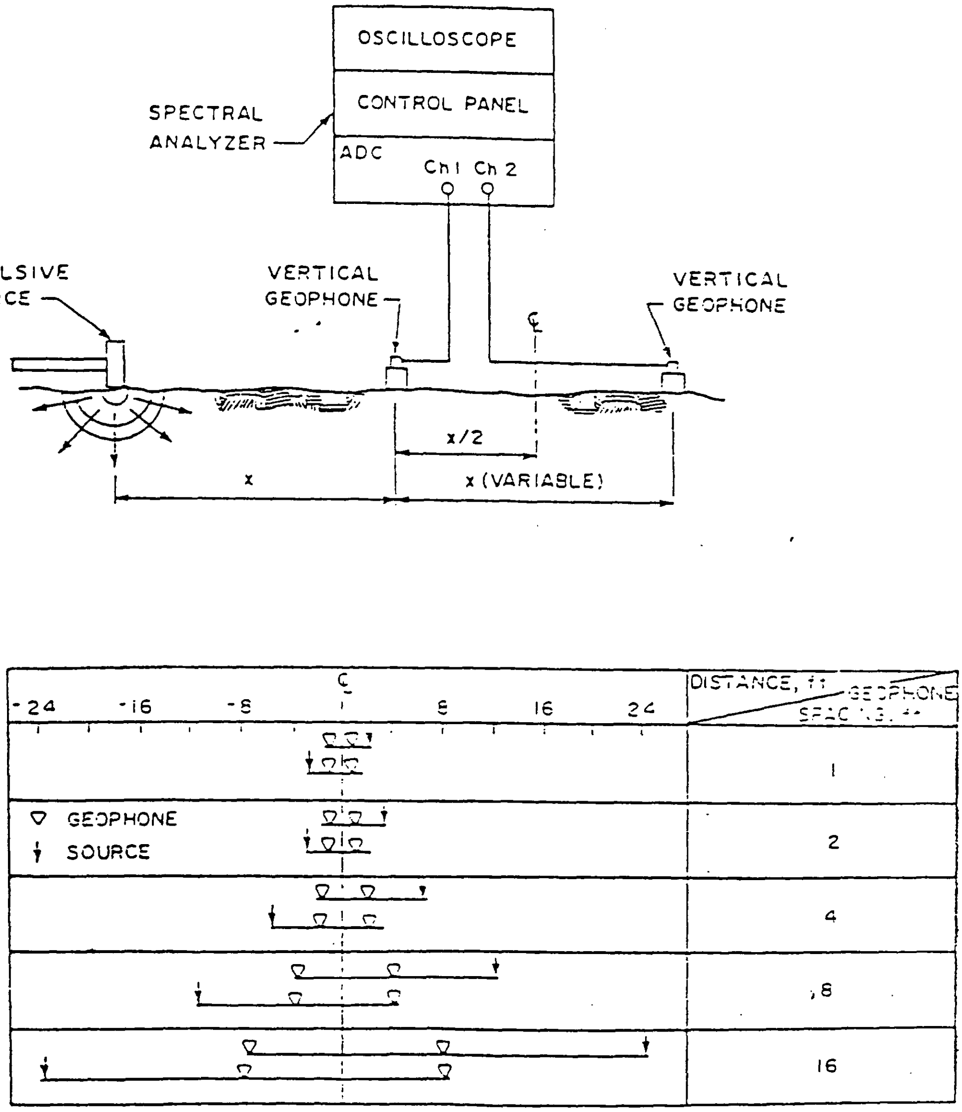

Fig.1.63Experimental Set-up for Spectral Analysis Of Surface Waves-(SASW)[34]

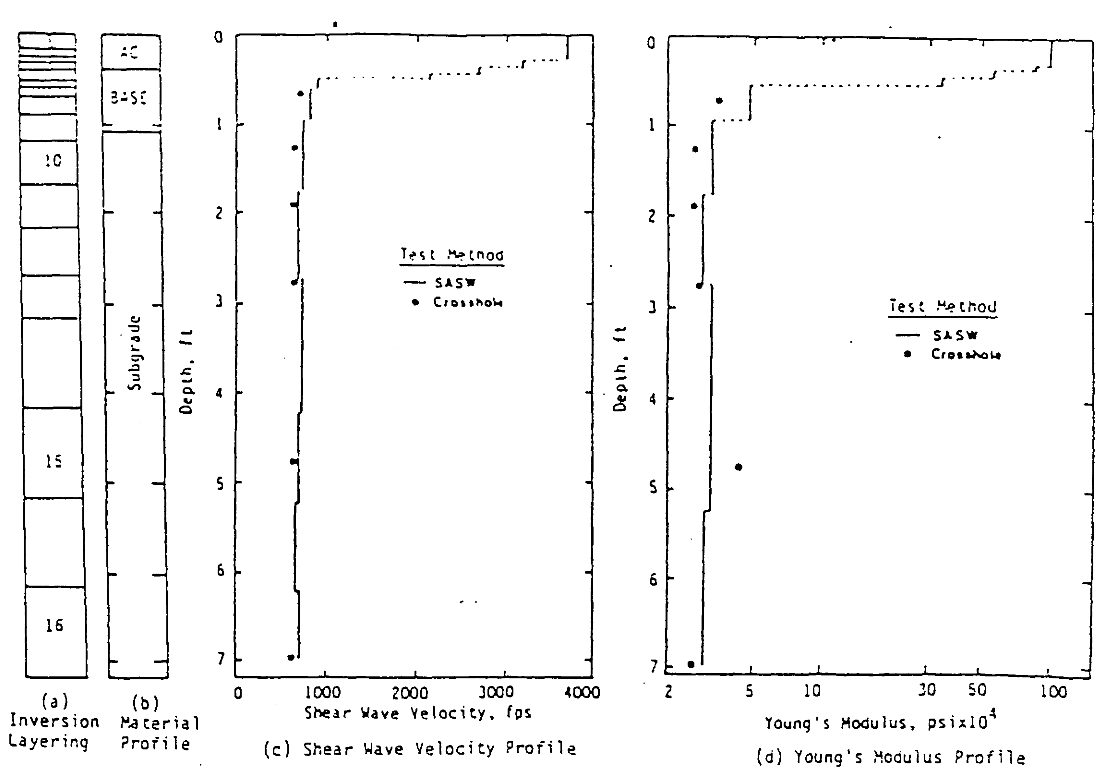

FIG. 1.64 Composite profile at flexible pavement site. [34]

CHAPTER TWO DYNAMIC ANALYSIS

2.1 INTRODUCTION

In this chapter, the elasto-dynamic analysis of pavement response (assuming visco-elastic material behaviour) to FWD blows will be described. The analysis is based on the Fourier synthesis of a solution for periodic loading of visco-elastic horizontally layered strata. The details of the computer program used in this analysis are also presented.

2.2 DYNAMICS OF FALLING WEIGHT DEFLECTOMETER

The dynamic analysis of the falling weight deflectometer comprises two distinct parts;

(i) Determination of the dynamic motion of the FWD device and,

(ii) Evaluation of the pavement response.

The former is depicted by a simple discrete mass spring model of the FWD in Fig. 2.1 ; the latter is discussed in the following section.

Mamlouk and Davies [41] showed that for a linearly elastic spring, the compression z after time t, following impact by the FWD mass is:

$$z = s[\ (1- \text{Cos}\ \omega t) + \surd\ (2h/s)\ \text{Sin}\ \omega t\ ] \qquad (2.1)$$

in which s = the compression of the spring under static conditions,

i.e. $s = M\ g\ /\ K$ (2.2)

where M = mass of the falling weight

g = acceleration due to gravity

K = spring constant

and h = drop height

w = natural frequency of oscillation of the system

$= \sqrt{(\ K\ /\ M\ )}$ (2.3)

The compression-time relation described by Equation (2.1) is shown in Fig. 2.2. The first term in Equation (2.1) represents the response of the spring if the free fall of the mass is zero (i.e. h = 0). In this case the compression of the spring reaches twice the static value (i.e. 2s). The second term is dominant for large drop heights, therefore for practical purposes the compression-time relation becomes

$$z = \surd(2hs).\mathrm{Sin}\ \omega t \tag{2.4}$$

Under these conditions, the dispacement of the FWD mass while it is in contact with the pavement, closely approximates a half-sine wave [if $z < 0$ the mass rebounds] and, since the spring force (F) is proportional to the spring compression (z), the force generated is :

$$F = \sqrt{(2hMgk)}.\sin wt \tag{2.5}$$

The maximum force is generated when $wt = \pi/2$, thus

$$Fo = \sqrt{(2hMgk)} \tag{2.6}$$

From Equations (2.5) and (2.6) we obtain

$$F = Fo \sin wt \tag{2.7}$$

The pulse width is given by

$$\begin{aligned} Tp &= \pi / w \\ &= \pi \sqrt{(M / k)} \end{aligned} \tag{2.8}$$

i.e. Tp is a function of the characteristics of the loading device.

2.3 GOVERNING EQUATIONS OF ELASTO-DYNAMICS

2.3.1 Introduction

In this analysis, the flexible pavement system is idealised as a layered visco-elastic continuum overlying bedrock at a finite depth as shown in Fig. 2.3. The system has five model parameters per layer, that is, Young's modulus (E), Poisson's ratio (v), material damping (β), mass density (p), and thickness (h). For any given pavement structure, these parameters must be defined for each layer. The assumption of material linearity and isotropy as well as the no-slip conditions at the layer interfaces are invoked.

2.3.2 The Helmholtz's Equation

Under the conditions outlined above, the relevant governing equations of the elasto-dynamics [16,41], in cartesian tensor notation, are:

(i) *Equilibrium equation*:

$$\sigma_{ij,j} + \rho\ddot{u}_i = 0 \qquad (2.9)$$

where $\rho\ddot{u}_i$ = the body force per unit volume (and $\ddot{u}$ is the body acceleration)

σ_{ij} = stress tensor, and,

the comma denotes partial differentiation with respect to the space variable, i.e.

$$\sigma_{ij,j} = \delta\sigma_{ij} / \delta x_j \tag{2.10}$$

(ii) *Hooke's law*:

$$\sigma ij = \lambda \; \delta_{ij} \; \epsilon_{kk} + 2 \; \mu \; \epsilon_{ij} \tag{2.11}$$

where $\mu = \lambda =$ Lame's constants

$\delta_{ij} =$ Kronecker delta,

$$\left\{ \begin{array}{ll} \delta_{ij} = 1 \, , & i = j \\ \delta_{ij} = 0 \, , & i \neq j \end{array} \right\}$$

Lame's constants are related to the conventional elastic constants E, G, v (Young's modulus, shear modulus and Poisson's ratio, respectively) by the relations :

$$\lambda = E\nu \; / \; (1+\nu)(1-2\nu) \tag{2.12}$$

$$\mu = G = E \; / \; 2(1+\nu) \tag{2.13}$$

(iii) *Strain-displacement relation*:

$$\epsilon_{ij} = 1/2 \; (\; u_{i,j} + u_{j,i} \;) \tag{2.14}$$

where $u_i =$ the i-th component of the displacement vector.

The strain-displacement Equation (2.14) may be substituted into Hooke's law (2.11) and the result in turn substituted into the equilibrium Equation (2.9) to produce the following equation :

$$\mu u_{i,jj} + (\lambda+\mu)\, u_{j,ij} = \rho \ddot{u}_i \tag{2.15}$$

which is called the Navier- Cauchy equation.

The direct solution of Equation (2.15), that is determination of the displacement field, u(x,t) which satisfies both the initial conditions and boundary conditions in relation to the impact of a falling weight on a multilayered pavement system is not feasible. However, a solution for the transient load problem can be obtained based on a continuum model developed in the field of seismology [26].

Mamlouk and Davies [31] have described and applied a numerical solution, devised by Kausel and Peek [26], for periodic surface loading of pavement systems from which a solution for the transient load problem can be used. Loading and displacements are assumed to be time harmonic;

$$F(t) = F\, e^{i\omega t} \tag{2.16}$$

$$u(t) = u\, e^{i\omega t} \tag{2.17}$$

where $i = \sqrt{-1}$

e = Natural base

t = time

From Equation (2.17) we obtain, by differentiation :

$$\ddot{u} = \delta^2 u \,/\, \delta t^2$$
$$= -\,\omega^2\, u(t) \qquad (2.18)$$

Substitution of Equation (2.18) into Equation (2.15) yields the reduced elasto-dynamic (Helmholtz) Equation for the steady state, namely ;

$$\mu u_{i,jj} + (\lambda+\mu)\, u_{j,ij} + \rho\omega^2 u_i = 0 \qquad (2.19)$$

The solution (integration) of this quasi-static equation yields the displacement field u(x,w), thus eliminating the time variable. The solution is best carried out in terms of complex numbers so that both the magnitude of the displacements and their phase with respect to some datum (typically, the loading cycle) are represented by a single quantity. Numerical investigation of harmonic devices by this means has successfully revealed the existence of resonant pavement responses at certain operating frequencies [12,13].

Transient loading conditions (FWD impulse) however, can be analysed by superimposing the spectrum of frequency responses using the method of Fourier synthesis. This method is discussed in Section 2.5.

2.3.3 Damping

Material damping is related to the internal energy dissipation which occurs in real materials subjected to dynamic loading. The existence of material damping, whether of a visco-elastic or hysteretic (frequency invariant damping) nature can be easily

accommodated within elasto-dynamic analyses by referring to the correspondence principle of visco-elasticity. Simply stated, this involves replacement of the elastic moduli by their complex counterparts [31,41] e.g.

$$E^* = E\ (1 + 2i\beta) \qquad (2.20)$$

$$G^* = G\ (1 + 2i\beta) \qquad (2.21)$$

where E^* = Complex Young's modulus

G^* = Complex shear modulus

β = Damping ratio

It was discovered some 20 years ago [18,38,45] that granular materials (sand, etc.) exhibit hysteretic behaviour. Typical values for the damping ratio of such soils is about 5% [38] and is somewhat lower for clay.

However, this internal energy dissipation is of secondary importance in the present problem since the major component of energy dissipation in continua results from radiation (geometric) damping. i.e. the dissipation of energy from the source of excitation to the far field (Fig. 2.4). Thus, any error in the determination of material damping or departure from assumed frequency invariance are not likely to be significant [31,41]. This is why material damping is often neglected in practice (e.g. in the analysis of machine foundation vibrations [18,30,38]), although it is included in this analysis for completeness.

2.4 TRANSIENT LOADING

2.4.1 Falling weight deflectometer loading impulse

The Falling Weight Deflectometer (FWD) loading impulse is assumed to be periodic (i.e. a forcing function that repeats itself at equal intervals of time) with period, T, which includes the loading pulse width, Tp, and a rest period, T_R, (Fig. 2.5). The rest period is chosen to be of sufficient duration that the pavement fully recovers from the deformation during this time. Therefore, the response of the pavement to each load is isolated. The relevant equation for an idealised (half-sine wave) shape of an impulse is given by:

$$F = Fo \sin (\pi t \ / \ Tp) \qquad (2.22)$$

where F = Applied load

Fo = Peak applied force

Tp = Impulse duration

The complete cycle (of duration T) must now be represented in terms of circular functions (i.e. a Fourier series).

2.4.2 Fourier series of loading impulse

The Fourier series expansion of the loading function f(t), (Fig. 2.6) may be expressed as F(t), the summation of an infinite number of sine and cosine terms;

$$F(t) = a_o/2 + \sum_{n=1}^{\infty} a_n \cos \omega_n t + \sum_{n=1}^{\infty} b_n \sin \omega_n t \qquad (2.23)$$

where $w_n = 2n\pi / T$

The coefficients a_o, a_n, and b_n may be calculated by integrating (over a period) the products of the forcing function and the sine/cosine functions thus:

$$a_o = 2 / T \int_0^T f(t) \cdot dt \qquad (2.24)$$

$$a_n = 2 / T \int_0^T f(t) . \cos (2\pi n/T) . dt \qquad (2.25)$$

$$b_n = 2 / T \int_0^T f(t) . \sin (2\pi n/T) \cdot dt \qquad (2.26)$$

The derivation of the above constants (for the loading function shown in Fig. 2.6) is presented in Appendix -A- and only the final results are given here for brevity:

$$a_o = \frac{4}{\pi} \frac{T_p}{T} \qquad (2.27)$$

$$a_n = \frac{2A}{T} \left(\frac{\cos (BT_p) + 1}{A^2 - B^2} \right) \qquad (2.28)$$

$$b_n = \frac{2A}{T} \left[\frac{\sin (B\ T_p)}{A^2 - B^2} \right] \qquad (2.29)$$

where

$$A = \pi / Tp$$

$$B = 2\pi n / T$$

$$= Wn$$

It is worth noting that the coefficients a_n and b_n become singular if the constants A and B are equal. This condition occurs when the period T is an even multiple of the pulse width Tp and , therefore, some care must be exercised in the choice of period in order to avoid numerical difficulties. This point is addressed again in Chapter Three.

2.5 FOURIER SYNTHESIS

Since any loading impulse can be expressed in terms of a Fourier series (by decomposing the load into a series of harmonic loading cycles), the solutions for each term of this periodic (time-harmonic) series [Equation (2.23)] can be superposed (assuming linearity) in order to construct the transient response [10]. In other words, the displacement response u(t), of a pavement to a dynamic forcing function f(t) can be obtained by means of Fourier synthesis.

2.5.1 Loading and displacement

Fig. 2.7 shows the periodic loading function F(t) and periodic displacement U(t):

$$F(t) = F_o \, Cos(\omega t) \tag{2.30}$$

$$U(t) = U_o \, Cos(\omega t - \Phi) \tag{2.31}$$

where Fo = Peak applied force (force amplitude)

Uo = Peak displacement (diplacement amplitude)

w = Circular frequency of excitation

Φ = Phase angle between the load and displacement.

For the n-th harmonic, the above equations can be written as:

$$F_n(t) = F_n \cos(\omega_n t) \tag{2.32}$$

$$U_n(t) = U_n \cos(\omega_n t - \Phi_n{}^u) \tag{2.33}$$

where Φ_n^u = is the phase lag between the n-th harmonic forcing function and the corresponding displacement response as shown in the complex plane in Fig. 2.8.

Combining Equations (2.32) and (2.33) we obtain the system's impedance Kn for the n-th harmonic as follows:

$$U_n = K_n \cdot F_n \tag{2.34}$$

where
$$K_n = (Un\ /\ F_n)\ e^{-i\Phi_n{}^u} \tag{2.35}$$

The Fourier series representation of the forcing function F(t) in Equation (2.23) can be rewritten as:

$$F(t) = \sum_{n=1}^{\infty} F_n \cos(\omega_n t - \Phi_n{}^f) \tag{2.36}$$

where Fn = the amplitude of the n-th harmonic of the Fourier series

Φ_n^f = phase angle of the n-th harmonic of the Fourier series.

2.5.2 Superposition

The superposition procedure is performed for convenience in complex arithmetic by transforming Equation (2.36) as follows:

$$F(t) = \sum_{n=1}^{\infty} F_n \cdot e^{i(\omega_n t - \Phi_n f)} \qquad (2.37)$$

that is, the loading function is decomposed into an infinte series of harmonic functions (of different frequency Wn and phase angle ϕ). By superposition, the final solution is the vector sum of each displacement harmonic, hence:

$$U(t) = \sum_{n=1}^{\infty} U_n \qquad (2.38)$$

$$= \sum_{n=1}^{\infty} K_n \cdot F_n \cdot e^{i(\omega_n t - \Phi_n f)} \qquad (2.39)$$

Combining Equations (2.35) and (2.39) we obtain:

$$U(t) = \mathrm{Re}\left\{ \sum_{n=1}^{\infty} U_n \cdot e^{i(\omega_n t - \Phi_n f - \Phi_n u)} \right\} \qquad (2.40)$$

In practice, about 10 terms of the series is sufficient to obtain a solution to engineering accuracy. This is illustrated in more detail in Chapter Three.

2.6 LAYERED THEORY

2.6.1 Introduction

Solution of the elasto-dynamic problems of continua subjected to dynamic loads available so far are applicable to solids of relatively simple geometry, such as full spaces, half-spaces and finite homogeneous strata. The complexities introduced by layering can only be solved numerically using complicated integral formulations.

The numerical solutions currently available are described briefly in the sequel.

2.6.2 Exact Numerical solutions

These solutions are based on the use of the Transfer Matrix in the frequency-wavenumber domain. For arbitrary loadings, the loads have to be resolved in their temporal and spatial Fourier Transforms, assuming both to be harmonic in time and space. Thus, the first step in the computation is to find the harmonic displacements at the layer interfaces due to unit harmonic loads. In the Stiffness Matrix method expounded by Kausel and Roesset (1981), the external loads applied at the layer interfaces (i.e. between the layers having arbitrary thicknesses) are related to the displacements at these locations through stiffness matrices which are functions of both frequency of excitation and wavenumber. This latter method offers several advantages over earlier approaches, namely, it does not suffer from numerical instabilities at high frequencies, allows specifications of multiple loads at various elevations, and requires consideration of only half as many degrees of freedom. However, in both methods, the transfer functions (Green's functions in the frequency-wavenumber domain) are evaluated at discrete intervals and the Green's function are computed by direct integration over wavenumber.

2.6.3 The Discrete Thin-Layer Method

In this method due to Kausel and Peek [26], the soil is subdivided into thin layers within which the displacments are assumed to vary linearly in the direction normal to the layer interfaces. The formulation of the Green's functions in the wavenumber domain then results in algebraic expressions. Hence, the integral transforms can be evaluated in closed form so that explicit expressions are obtained for these functions in the spatial domain. That is, explicit expressions for layer stiffness matrices are formed (using the Stiffness Matrix method - explained earlier) with numerical functions of the frequency, the horizontal wavenumber and material properties. For a soil system consisting of N layers (N + 1 interfaces) a global stiffness matrix can be assembled by summing the contributions of the layer matrices at each interface, as well as the half-space stiffness (impedance) matrix. The result is a system of equations of the form:

$$\begin{bmatrix} K11 & K12 & . & . & & & \\ & K21 & K22 & K23 & . & & \\ & . & K32 & K33 & K34 & . & \\ & . & . & . & . & . & \\ & & & & & & Kn+1,\ n+1 \end{bmatrix} \begin{bmatrix} U1 \\ U2 \\ U3 \\ . \\ Un+1 \end{bmatrix} = \begin{bmatrix} P1 \\ P2 \\ P3 \\ . \\ Pn+1 \end{bmatrix} \qquad (2.41)$$

in which

$$Uj = \begin{Bmatrix} Ux \\ Uy \\ iUz \end{Bmatrix}_j \qquad \text{and} \qquad Pj = \begin{Bmatrix} Px \\ Py \\ iPz \end{Bmatrix}_j \qquad (2.42)$$

are the displacement and external load vectors at the j-th interface, and Kjj are 3*3 submatrices of the global stiffness matrix (the $i = \sqrt{-1}$ factor in front of Uz and Pz is introduced to attain symmetric stiffness matrices). Analogous equations can also be written in cylindrical coordinates. In compact form:

$$K.U = P \qquad (2.43)$$

For given sources P, which are expressed in the frequency-wavenumber domain, the Green's functions U are solved by Gaussian elimination of the tridiagonal, symmetric stiffness matrix K. This corresponds formally to the solution

$$U = K^{-1} . P \qquad (2.44)$$

For a half-space, two adjoining half-spaces, or a homogeneous stratum over an elastic half-space, one can solve for U in closed form.

2.7 COMPUTER PROGRAM

The numerical technique due to Kausel and Peek [26] provides a relatively economical means for solving the harmonic loading problem. The solution involves subdivision of the layered system into artificial sublayers of sufficient thinness so that the implicit assumption of a linear variation of displacement in the direction of layering between the adjacent interfaces of these layers become tenable. For each sublayer a stiffness matrix is formed and these are then assembled to form a global stiffness matrix. The solution provides the displacement magnitudes (and phases) at any location within the pavement structure.

2.7.1 Description

The computer program PULSE used in this study, comprises approximately 2000 FORTRAN (77) statements with some 17 subroutines. The solution is carried out in the frequency-wavenumber domain by resolving the loads and displacements in terms of their temporal and spatial Fourier Transforms (assuming them to be both harmonic in time and space). The stiffness matrices (in the transfer domain), for each sublayer, are then assembled in a global stiffness matrix form, i.e. as an eigenvector expansion. Finally, the inverse (Hankel) tranformation is utilised to compute the displacements in the (real) spatial domain. The Hankel transform Fn (λ) of $f(r)$ is defined as:

$$Fn(\lambda) = \mathcal{H}n(f) = \int_0^\infty r\ Jn\ (\lambda r)\ f(r)\ dr \qquad (2.45)$$

where Jn (λr) is the Bessel function of the first kind of order n.

Using integration by parts, the Hankel transform renders the Bessel differential equation into algebraic form, that is:

$$Hn = \left[\frac{d^2f}{dr^2} + \frac{1}{r}\ \frac{df}{dr} - \frac{n^2f}{r^2} \right] = -\lambda^2\ Fn\ (\lambda) \qquad (2.46)$$

The inverse Hankel transform is

$$f(r) = \mathcal{H}n^{-1}(Fn) = \int_0^\infty \lambda \, Jn\,(\lambda r)\; Fn\,(\lambda)\; d\lambda \qquad (2.47)$$

2.7.2 Enhancement

In order to solve the transient loading problem, the computer program was enhanced (see Appendix -C-) by the provision of a preprocessor which performed the Fourier decomposition of the FWD loading impulse and then called the main program to compute the harmonic response to each term of the series.
A postprocessor was then written to superpose these harmonic loading solutions at discrete instants of time through the loading cycle. The entire superposition was performed in complex arithmetic. The final solution yields displacements at various radial positions on the pavement surface as a function of time.

2.8 CONCLUSIONS

A dynamic analysis of the pavement response to FWD blows (assuming visco-elastic material behaviour) based on Fourier synthesis has been described in this Chapter. The procedure involves the solution of Helmholtz's harmonic equations for each loading component of the Fourier series expansion of the transient loading impulse (using the so-called discrete layer approach) and superposing the harmonic responses.

The computer program which has been developed for this study (based on the original program of Kausel and Peek) calculates pavement deflections resulting from FWD impact directly beneath the load and at arbitrary selected points elsewhere on the pavement surface.

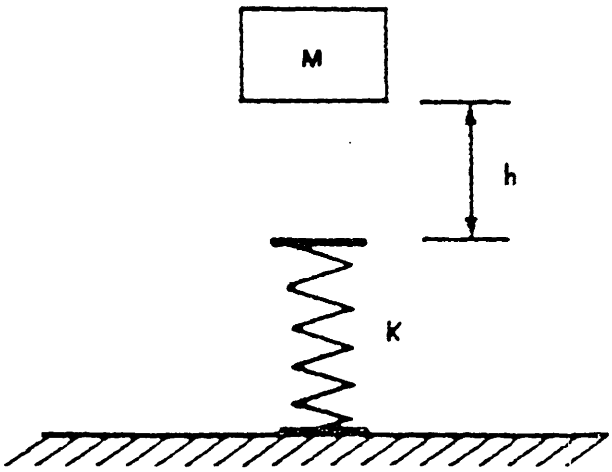

FIG 2.1 Discrete mass-spring model of FWD [12,41]

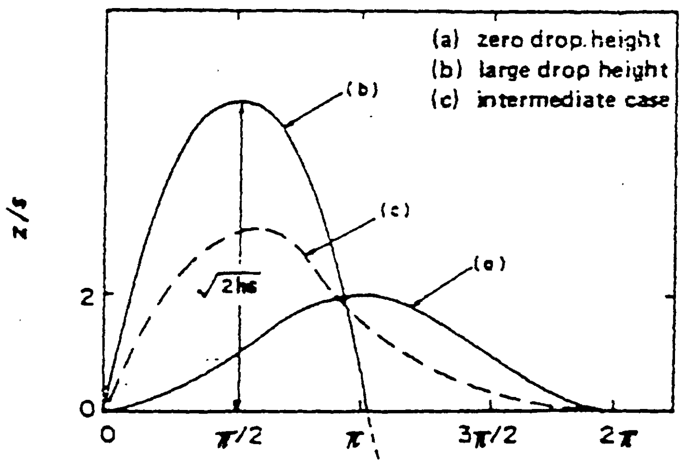

FIG 2.2 Three compression time relations. [41]

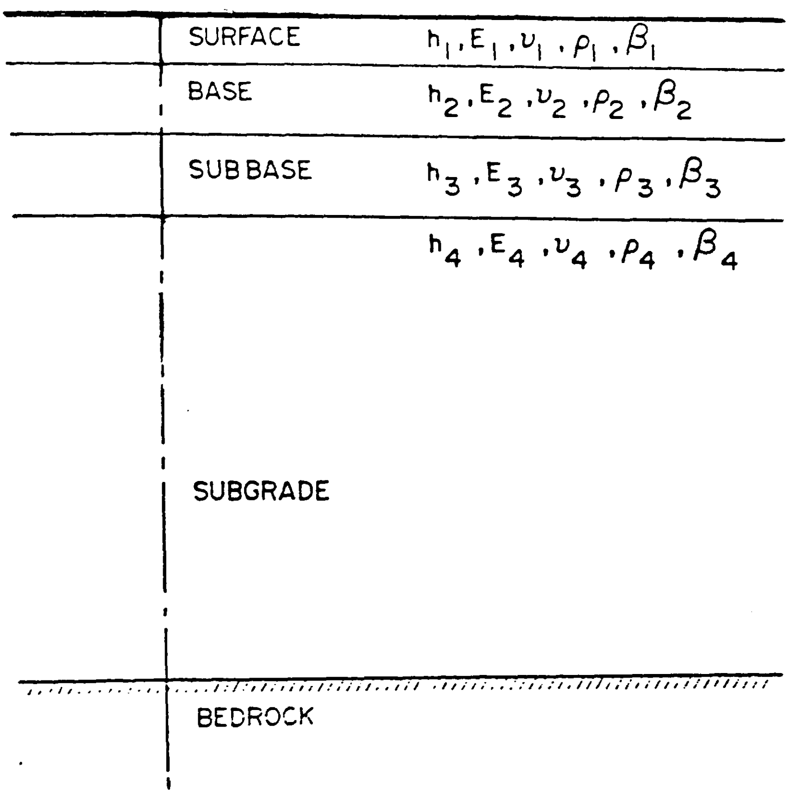

Fig.2.3 Multi-Layered Pavement System [31]

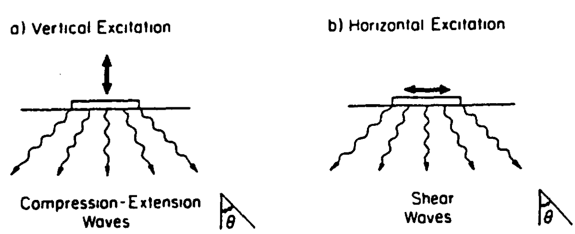

FIG. 2.4 Wave Propagation and Radiation Damping in Translational Modes [30, 38]

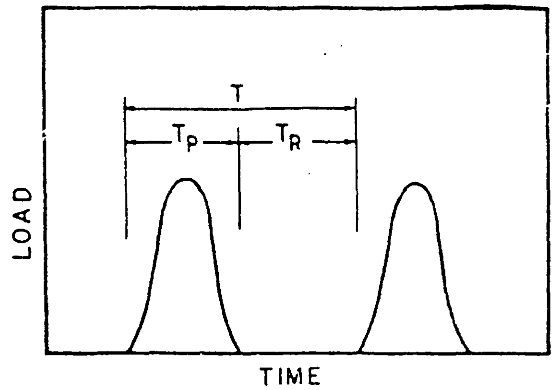

FIG. 2.5 Assumed Periodicity of FWD Impulses [41]

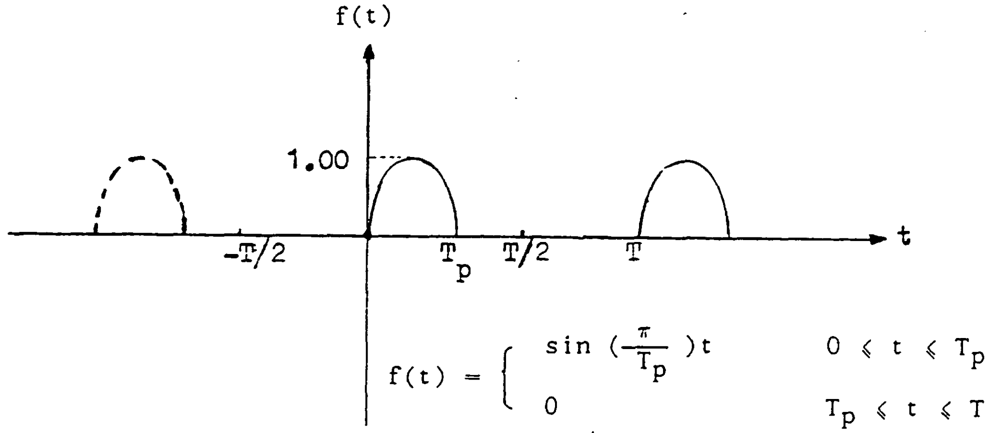

(FIG. 2.6) FOURIER SERIES REPRESENTATION OF A PULSE LOAD

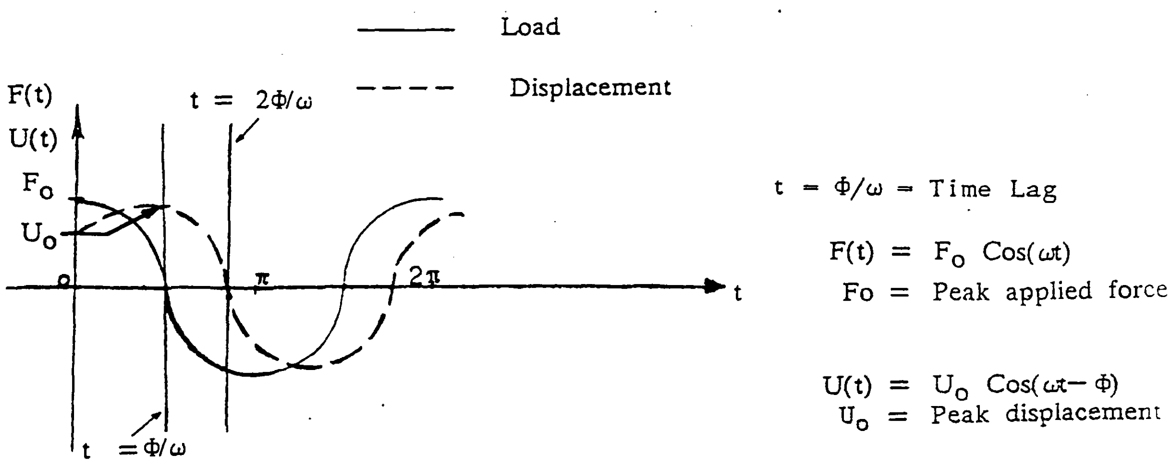

(FIG. 2.7) LOADING AND DISPLACEMENT

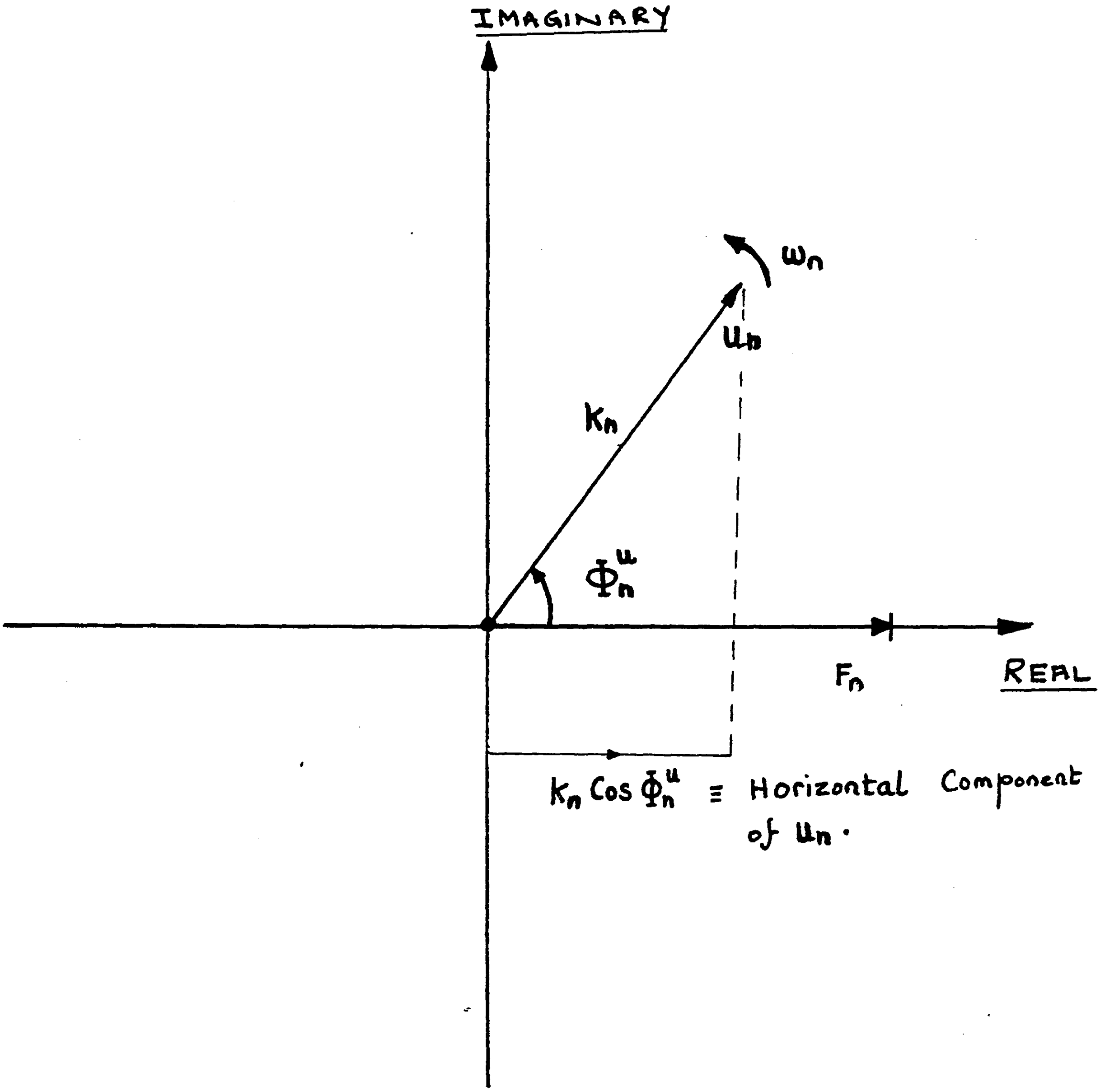

(FIG. 2.8) Loading and displacement amplitudes in the Complex Plane.

CHAPTER THREE NUMERICAL IMPLEMENTATION

3.1 INTRODUCTION

In this Chapter, the numerical modelling of pavements subjected to impulsive loading is presented. The Fourier series representation of transient (pulse) loads is discussed in detail and the accuracy of the computer program PULSE described in Chapter Two is then examined by means of a convergence study.

3.2 NUMERICAL MODELLING

3.2.1 Pavement representation

In this thesis, the pavement structure and subgrade is idealised as a layered visco-elastic continuum overlying bedrock at finite depth. Each layer of the multi-layered pavement structure is characterised by its mass density (p), Young's modulus (E), Poisson's ratio (v), material damping (β), and thickness (h), (Fig. 3.1). The materials are assumed to be linear and isotropic and no-slip conditions are assumed to exist at the layer interfaces.

3.2.2 Loading and displacements

A pulse (of unit pressure) was assumed to be applied to the pavement surface through a 300 mm diameter load platen. This results in a progressive deformation of the pavement over a relatively short period of time. These deflections were then computed at seven equally spaced transducer locations as shown in Fig. 3.2. In order to obtain more information on the deflection beneath the loaded area, the displacement at mid-radius of the load platen was also computed.

3.2.3 Fourier series expansion of loading impulse

The response of a linear elasto-dynamic system to transient loading can be obtained by superposition of sufficient harmonic terms of the appropriate Fourier series. The Fourier series expansion of the FWD (half-sine) pulse loading F(t) can be written (see Appendix -A-) as:

$$F(t) = \frac{2\,T_p}{\pi T} + \sum_{n=1}^{\infty} \frac{2A}{T} \left[\frac{\cos\,(B\,T_p) + 1}{A^2 - B^2} \right] \cos(Bt)$$

$$+ \sum_{n=1}^{\infty} \frac{2A}{T} \left[\frac{\sin\,(B\,T_p)}{A^2 - B^2} \right] \sin\,(Bt) \qquad \textbf{(3.1)}$$

where Tp = Impulse duration

T = Time period (typically 3 to 4 times Tp)

$A = \pi / Tp$

$B = 2\pi n / T$

t = time

Details of the calculations of the Fourier coefficients are given in Appendix -A-. Using the complex Exponential form, the Fourier series can be more conveniently represented as:

$$F(t) = \mathrm{Re}\left\{ \sum_{n=-\infty}^{+\infty} \frac{A}{T(A^2 + B^2)} \left[e^{-BT_p} + 1 \right] e^{Bt} \right\} \qquad (3.2)$$

where $A = \pi / Tp$

$B = 2\pi in / T$

$i = \sqrt{-1}$

Full details of the exponential form of the Fourier series are given in Appendix -B-. The exponential form for the Fourier series in Equation (3.2) has certain computational advantages compared to the equivalent trigonometric series of Equation (3.1). Fig. 3.3 shows an idealised impulse loading of an average duration, Tp, of 40 msec. The data were taken from reference number [42]. Table 3.1 gives the Fourier series representation of the loading impulse [calculated from Equation (3.1)] for a finite number of terms (N) of the expansion; here N takes the successive values of 2, 4, 8 and 16. Fig. 3.4 depicts these Fourier series representations. From Fig. 3.4 it is apparent that as the number of terms in the series increases, a more accurate result is obtained. These results indicate that about ten terms is sufficient to model the pulse load reasonably accurately.

3.2.4 Input parameters

The input required by the computer program PULSE includes;

(i) the number of pavement layers

and their properties, namely, density (P), thickness (h), Young's modulus (E), Poisson's ratio (v) and damping (β). In addition, the number of artificial sub-layers of each pavement layer must be specified,

(ii) the disk radius, the radial locations of the geophones and the applied pressure (kPa), and,

(iii) the number of terms in the Fourier series expansion, the loading period, T (divided into pulse width, Tp, and a nominal "rest phase", T_R). In addition, the user must specify the times for which deflection values are to be computed.

3.3 VALIDATION OF THE COMPUTER PROGRAM 'PULSE'

The validity of the computer program PULSE described in Chapter Two was investigated for a number of test cases. The results obtained from this study are presented in the sequel.

3.3.1 Harmonic loading

(i) A homogeneous soil of 10 m depth overlying bedrock was subjected to a 1.0 KPa harmonic load through a 2 m disk radius. Soil density, Young's modulus and Poisson's ratio were 2000 Kg/m3, 100 MPa and 0.30, respectively. Figs. 3.5.a and 3.5.b show the surface displacement versus loading frequency. Resonance occurred at a frequency of about 6 Hz with 5% damping. The deflection (29.5 * 10 E -9 m) obtained under static loading conditions was compared with that for the surface displacement (u) of a statically loaded elastic semi-infinite solid;

$$u = [\, 2\, q\, (\, 1 - v^2\,)\, a\,] \,/\, E \qquad (3.3)$$

where u = surface displacement

q = applied pressure

a = disk radius

v = Poisson's ratio

E = Young's modulus

Substituting the above soil properties and applied loading into Equation (3.3), we obtain, u = 36.4 * 10 E -9 m. The difference (of about 18%) between the two results is attributed to the finite depth of the soil layer, (h/a = 5). These results also confirmed that about thirty sub-layers is sufficient to obtain solutions accurate to better than 5%.

(ii) A four-layer flexible pavement was subjected to harmonic loading through a disk of 0.15 m radius. Mamlouk and Davies [31] found that in multilayer pavements, about 30 sublayers were necessary to obtain good accuracy. Fig. 3.6 is a plot of the predicted surface displacement versus loading frequency in the vicinity (at radii 0.0 and 0.15 m, respectively) of the Road Rater device, using the same data by Mamlouk and Davies (Table 3.2). These results were in agreement with those obtained by Mamlouk and Davies and confirm that the computer program has been implemented correctly.

3.3.2 Impulse loading

(i) The displacement response of a typical three-layer flexible pavement (Table 3.3) to falling weight deflectometer loading is shown in Fig. 3.7. The data was taken from earlier work carried out by Sebaaly et al [42]. The results are in close agreement with those obtained by Sebaaly et al. Fig. 3.7 also shows that, due to the inertia of the pavement [31,41,42], the displacement wave lags the loading impulse by approximately 6 msec although its shape closely reflects the half-sine loading curve. The frequency content of the FWD load impulse used in the analysis and their corresponding amplitudes are given in Figs. 3.8.a and 3.8.b.

(ii) The results of the numerical model obtained (i.e. static deflections of pavements subjected to FWD loading) were compared with those of Sebaaly et al [42]. The comparison was carried out for typical in-service three-layer flexible pavement sections, namely, Bement, Monticello and Sherrard. Each section consists of a surface layer and a base course above the subgrade. Fig. 3.9 shows the deflections obtained using the static (zero frequency) analysis for the above sections. The results indicated that in all three sections, the static deflection values were within ± 3% of the deflection values obtained by Sebaaly et al.

3.3.3 Concluding remarks

The results given in this section confirm that the computer programme PULSE is capable of reproducing essential features of pavement response to dynamic loading.

3.4 CONVERGENCE STUDIES

In this section, a typical four-layer flexible pavement [31] with properties shown in Table 3.4 was used for convergence studies purposes.

3.4.1 Pavement sub-layers

A potential source of error in the pavement analysis is the assumption of linearity in displacements within each layer in the direction of layering. This being so, a high degree of accuracy can only be obtained if each pavement layer is divided into several sub-layers. This, of course, has the disadvantage of increasing the computational time (cost) as the number of sub-layers is increased. The discretisation scheme adopted for the purposes of this study is shown in Table 3.5. Because the stresses developed by wheel loads are attenuated at greater depths, the most efficient means of sub-layering the subgrade is to increase the sub-layer thicknesses at deeper levels. For this purpose, a simple geometric progression was utilised to increment sub-layer thicknesses within the subgrade.

Fig. 3.10 shows the variation in peak displacement with respect to the increase in the number of sub-layers. The parabolic shape of the computational time curve indicates a quadratic relationship between the number of sub-layers and total computational time.

3.4.2 Layer configuration

To investigate the precision of the computed deflections, the effect of varying the configuration of the artificial sub-layers was examined. The pavement properties are listed in Table 3.6. Table 3.7 shows the results obtained for deflections directly beneath the (1 KPa) FWD load and at radii of 900 mm and 1800 mm (D900 and D1800, respectively). From Table 3.7, it is apparent that these are negligible differences (less than 1%) in the deflection values. This indicates that different sub-layer configurations have little effect on surface deflections. It was noted earlier that pavements with 25 sub-layers provide reasonable accuracy in comparison with those having 30 sub-layers, (Fig. 3.10).

3.4.3 Number of terms in the Fourier series loading expansion

The effect of an increase in the number of terms in the Fourier series (see Appendix -A-) on the peak centroidal displacement is illustrated in Fig. 3.11. Clearly, here there is a linear relationship between the number of terms and the computation time. Figs. 3.12 and 3.13 show the variation in the amplitudes of the Fourier coefficients a_n and b_n as the number of terms in the Fourier series loading expression increases (n= 1,2,..16).

Fig. 3.12 shows the negligible contribution of the Fourier coefficient beyond the tenth term approximately (i.e. the higher harmonics) to the series sum. This fact is illustrated in a different form in Fig. 3.13 in which the coefficient modulus $Fn[(a_n^2 + b_n^2)^{1/2}]$ diminishes in spiral form as N increases. Fig. 3.14 depicts the amplitudes and phase angles $[\mathrm{Tan}^{-1}(b_n/a_n)]$ of each term of the series.

3.4.4 Loading rate

The effect of changes in FWD loading rate on pavement response is illustrated in Fig. 3.15. The pavement (with properties shown in Table 3.4) was subjected to a 1.0 KPa FWD load. Centroidal displacements are plotted against the ratio of impulse width Tp to the nominal period T. In one case, a constant loading period of 100 msec was assumed while the pulse width was varied while in the second case a constant pulse width of 40 msec was assumed while the loading period was varied. From the displacement curves, it is apparent that varying the pulse width has much greater influence on the peak surface displacement than varying the nominal period T. The peak surface displacements increase by about 8% for every 10 msec increase in the pulse duration whilst the peak surface displacements increase by less than 1% for every 20 msec increase in the loading period (T).

In a separate study, various pavements (Table 3.8 - 3.11) were subjected to impulse loads, with pulse widths of 20, 30 and 40 msec, respectively. Figs. 3.16.a - 3.19.c show a series of dynamic and static deflection basins as well as magnification factors for these pavements. It is evident from these figures that for flexible pavements, displacements increase by approximately 10-15% with every 10 msec increase in the pulse duration, (Tp) but somewhat less for rigid pavements.

3.4.5 <u>Quiescent (rest) period</u>

The state of pavements during the rest period was investigated using the data listed in Tables 3.8 and 3.9. Fig. 3.20.a and 3.20.b show pavement surface displacements versus time and distance from the centroid for a four-layer flexible pavement (subgrade stiffness = 100 MPa). Similarly, Figs. 3.21.a - 3.21.b and Figs. 3.22.a - 3.23.b show such variations for a three-layer flexible pavement (subgrade stiffnesses = 50 and 30 MPa, respectively). A 6 m thick subgrade was assumed in this study. These show that sufficient time must be allowed for the pavement surface to recover from the FWD blow, especially at points furthest from the centroid. The time taken for a quiescent state to be reached is primarily a function of subgrade thickness and stiffness. Figs. 3.22.a - 3.23.b show the effect of increasing the nominal period (for constant pulse duration, Tp) on the state of pavement during the rest period. Sufficiently long rest periods enable pavements to recover fully and reach a quiescent state before any subsequent blow is imparted by the FWD.

3.4.6 Disk Radius

To investigate the effect of different disk (load platen) radii on the peak centroidal (surface) displacement, a typical four-layer flexible pavement (Table 3.4) was subjected to 500 KPa and 1000 KPa FWD load, respectively. The load was applied via 0.15 m, 0.225 m and 0.30 m radius disks, respectively. From Fig. 3.24 it is apparent that the resulting displacements for both static and dynamic loadings are not directly proportional to the disk radii. That is doubling the disk radius resulted in a four-fold increase in the loading area thus, resulting in an increase in the total displacement by a factor of four. Figs. 3.25.a and 3.25.b illustrate the possible load distribution for two different disk radii under static (dynamic) loading conditions.

3.5 DISCUSSION OF RESULTS

3.5.1 Effect of number of pavement sub-layers

A pulse duration, Tp of 40 msec, a period, T of 220 msec together with ten terms in the Fourier series was used (and kept constant throughout) to examine the effect of the number of sub-layers on the FWD response. From Fig. 3.10 it can be seen that reasonable accuracy is obtained when the pavement layers are divided into approximately 25 sub-layers.

3.5.2 Effect of number of terms in the Fourier series loading expansion

A pulse duration of 40 msec, a period of 220 msec and 25 sub-layers were used (and kept constant throughout) to study the effect of the increase in the number of Fourier series terms on the peak magnitude of the FWD pulse. Figs. 3.11 - 3.13 indicate the adequacy of ten terms of the series for obtaining a reasonably good degree of accuracy. Table 3.12 shows the result of the Fourier series representation of pulse loading for ten terms.

A further investigation into the effect of number of terms in the Fourier series for longer nominal loading periods, T is illustrated in Fig. 3.26. Peak load magnitudes deviate excessively from the true solution (indicated by unity on the vertical scale) when the nominal loading period exceeds approximately 400 msec, (i.e. a period / pulse ratio of about 10). Thus, for longer loading periods, higher values of N are required in order to preserve accuracy. It is noteworthy that even for low values of the period / pulse ratio considerable fluctuations may be observed in Fig. 3.26. These are due to analytical singularities which occur when the loading period is an even multiple of the impulse width (see Appendix -A-). These conditions can of course be easily circumvented by specifying odd multiples.

3.5.3 Effect of loading rate

Fig. 3.15 shows a rapid rise in peak displacement as the pulse duration increases from 20 msec to 40 msec while the nominal period, T (100 msec) remains constant. The peak displacement, however, tends to decrease gradually with a decrease in period, T. The effect of the pulse width and the period were further studied in Figs. 3.27.a and 3.27.b, where it becomes apparent that the occurrence of resonance in the subgrade layer is independent of both the applied pulse, Tp and the loading period, T. The occurrence of resonance in the subgrade layer is discussed in detail in Chapter Four. From this study, it was concluded that a pulse duration, Tp of 40 msec and a loading period, T of 140 msec (i.e. Tp/T = 0.285 in Fig. 3.15) were suitable values for future analysis, in other words it was found that a rest duration, T_R of 100 msec to be sufficient to allow pavements to recover from FWD blows.

3.6 CONCLUSIONS

From the studies carried out in this Chapter, it is concluded that a Fourier series representation of FWD loading is a convenient way to model the desired shape, magnitude and duration of the impulsive loading.

A study of the parameters which have a major influence on the convergence of the solution process has been conducted and the optimum values of pavement sub-layers, Fourier series terms and nominal loading period have been determined. Consequently, twenty five pavement sub-layers, ten Fourier series terms and pulse durations and loading periods of 40 msec and 140 msec, respectively have been adopted as standard values in the parametric studies carried out in the following Chapter.

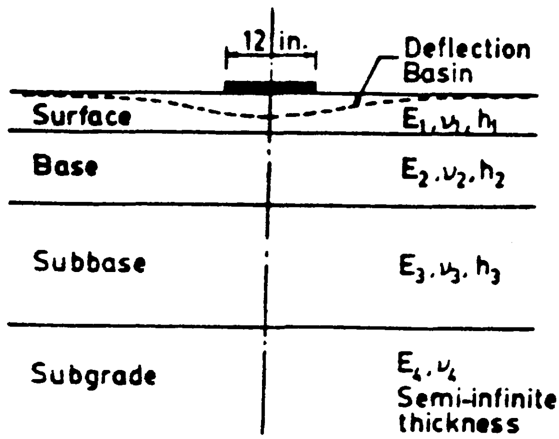

FIG. 3.1 *Typical four-layer pavement system subjected to circular load and the corresponding deflection basin.* [25]

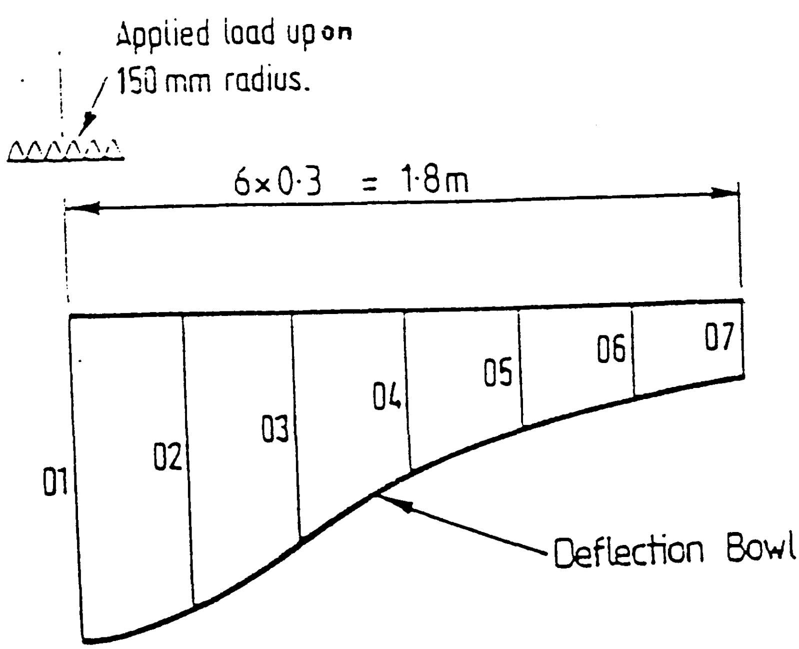

FIG. 3.2 Measurement of the deflection bowl [5]

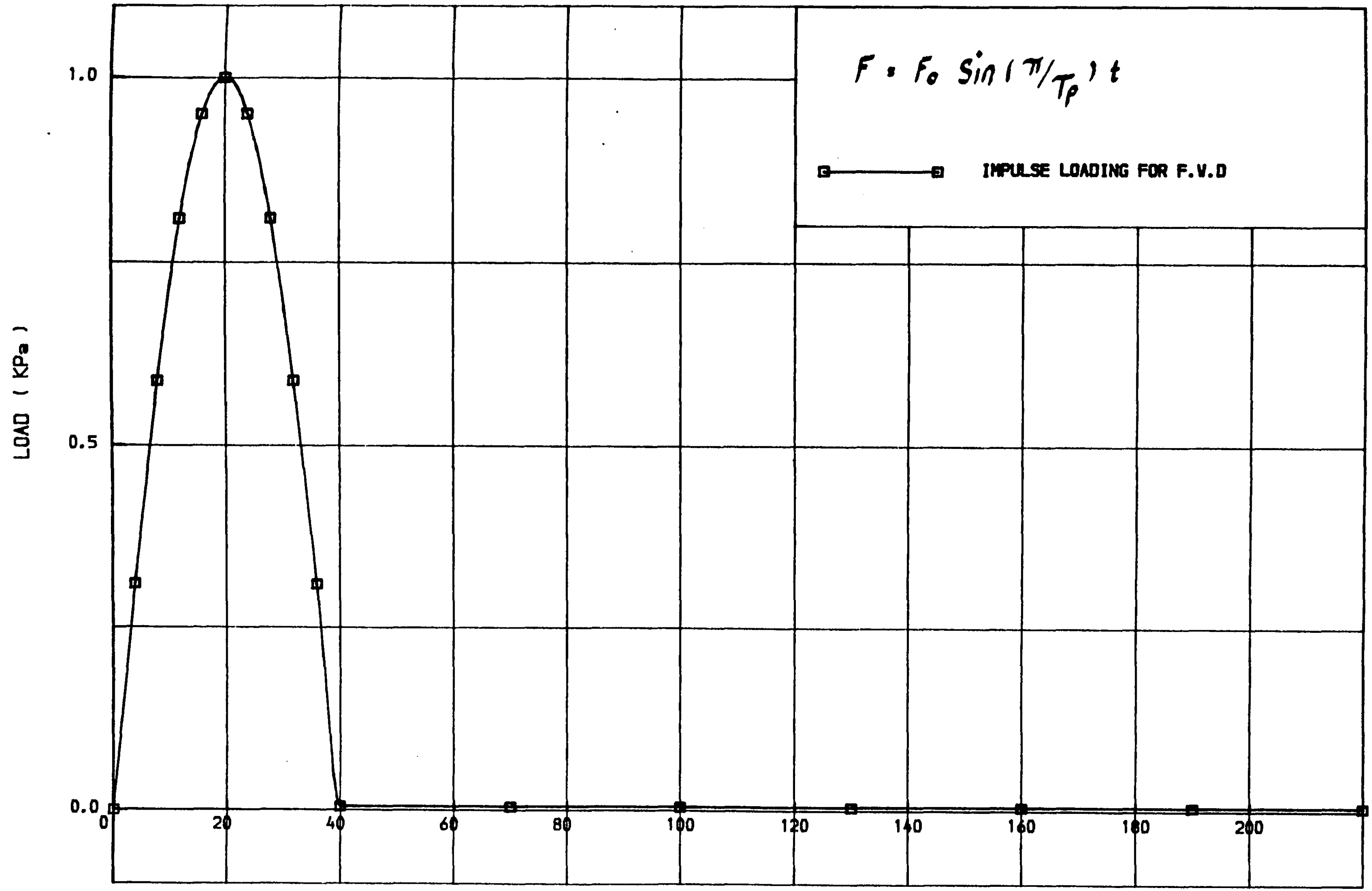

FIG. 3.3 An idealized impulse loading

PERIOD = PULSE DURATION + REST DURATION

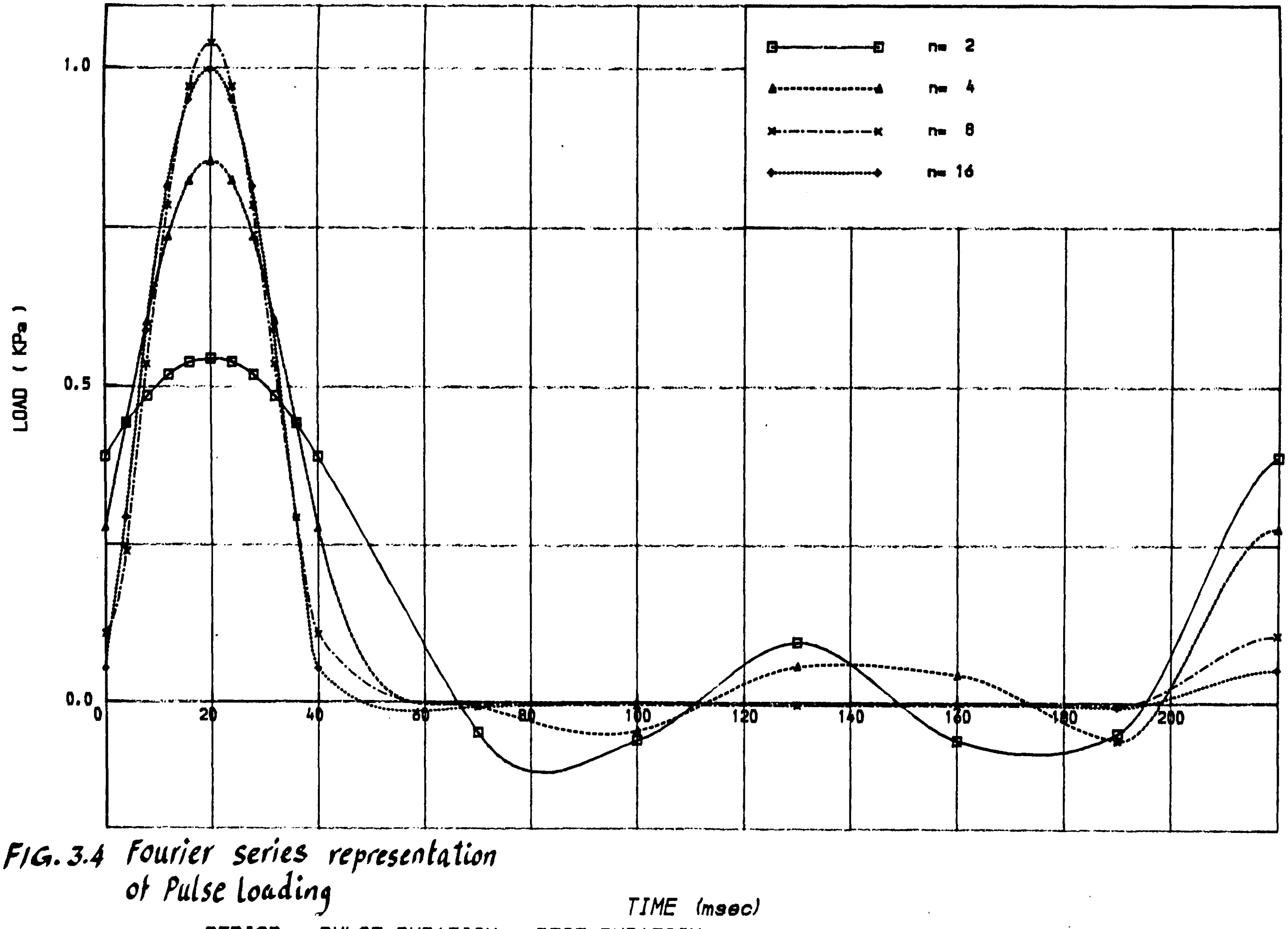

FIG. 3.4 Fourier series representation of Pulse Loading

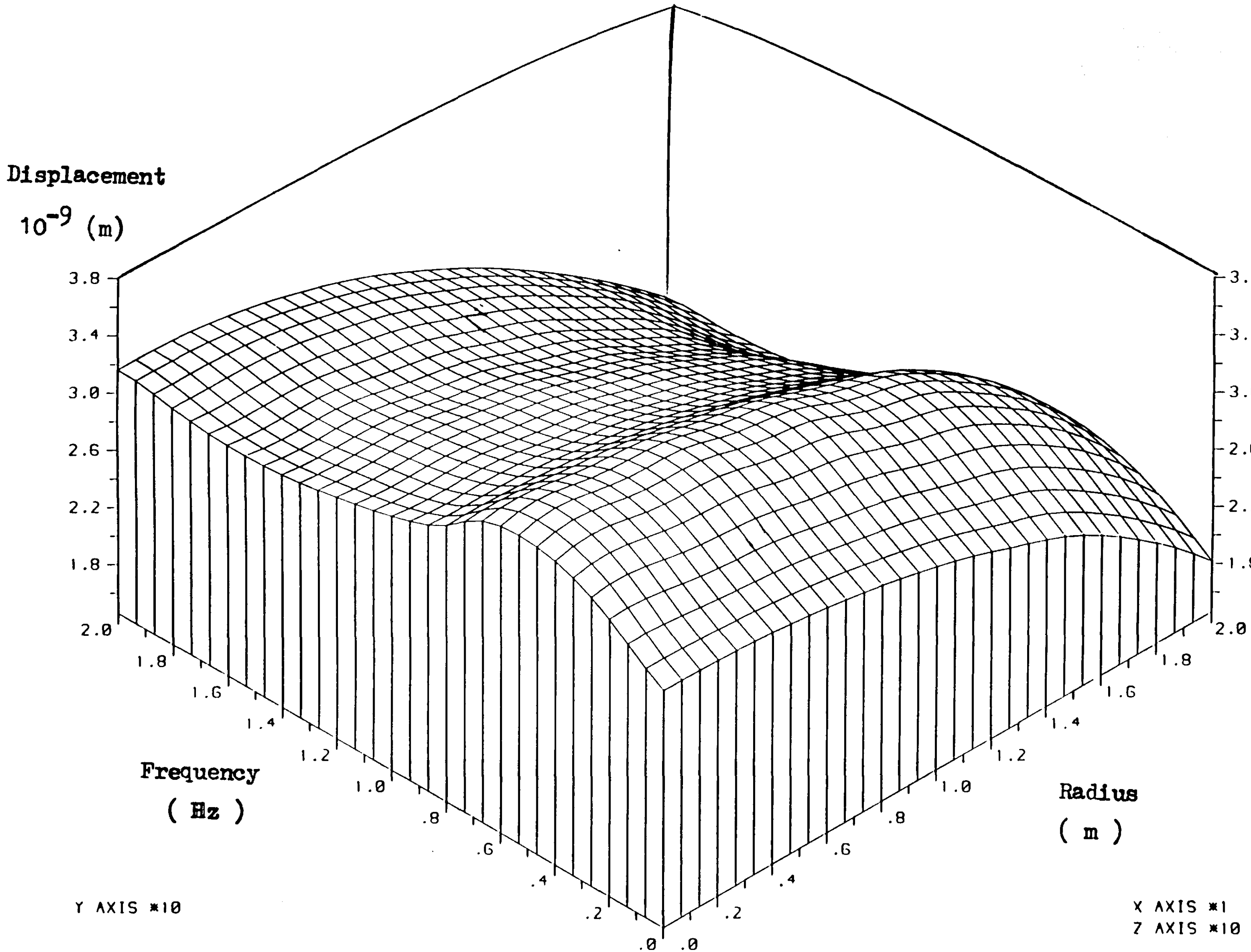

(FIG.3.5.a) ISOMETRIC VIEW OF DISPLACEMENT (m) Vs FREQUENCY (Hz)and DISTANCE (m)

CONTOUR OF DISPLACEMENT FOR A HOMOGENEOUS SOIL LAYER

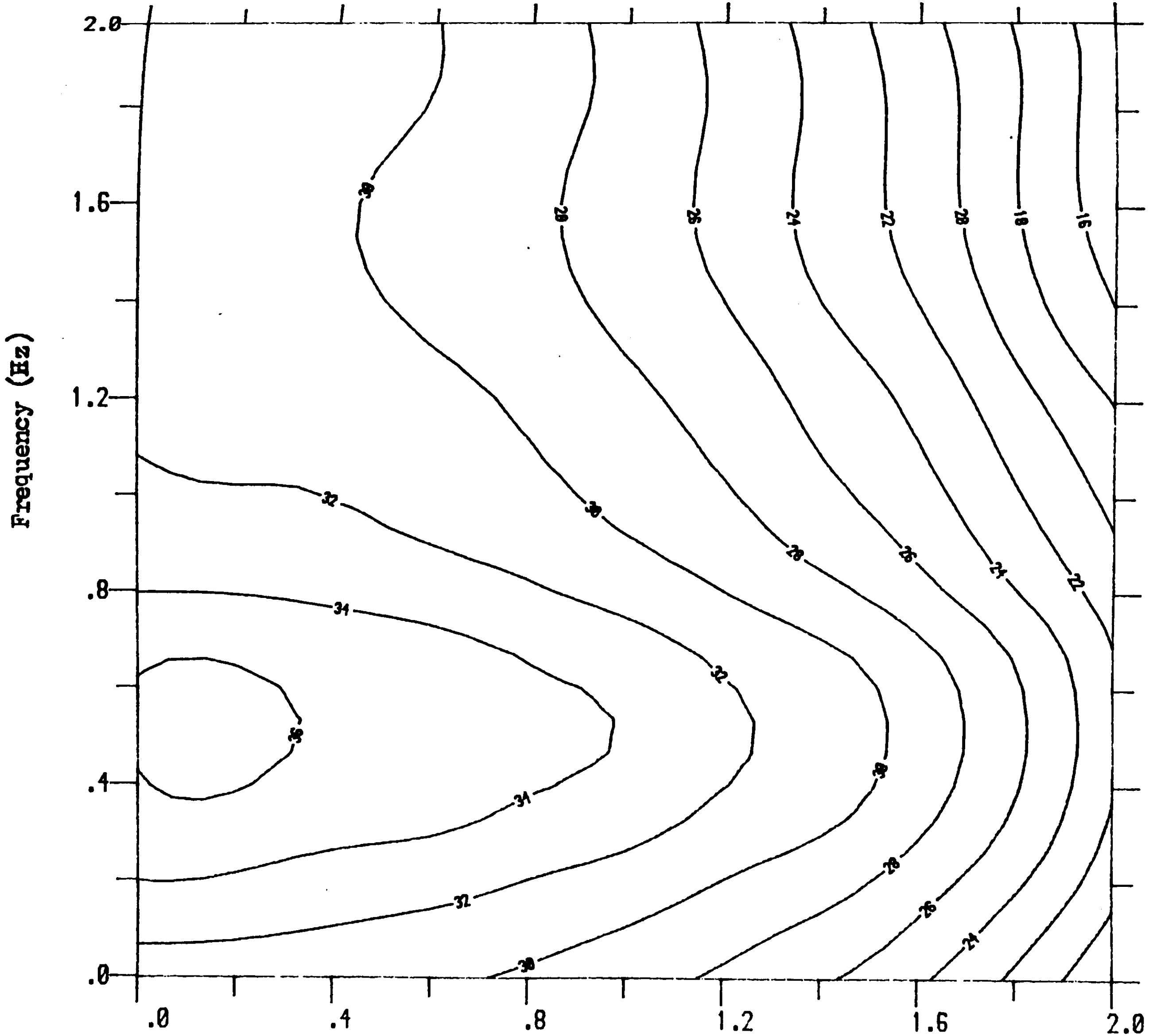

(FIG. 3.5.b)

X AXIS *1
Y AXIS *10

Radius (m)

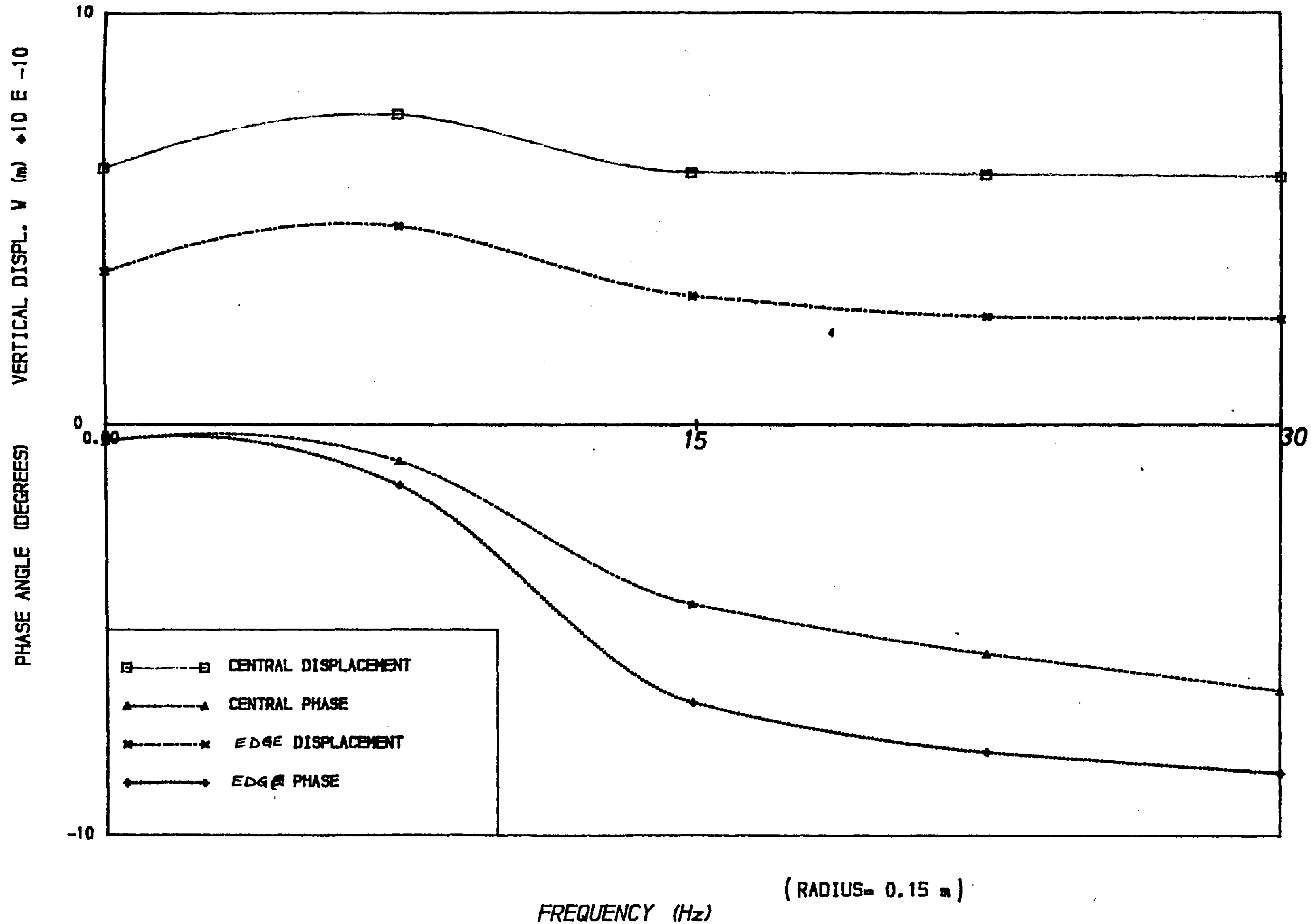

(FIG. 3.6) Surface Displacement versus Frequency of Excitation

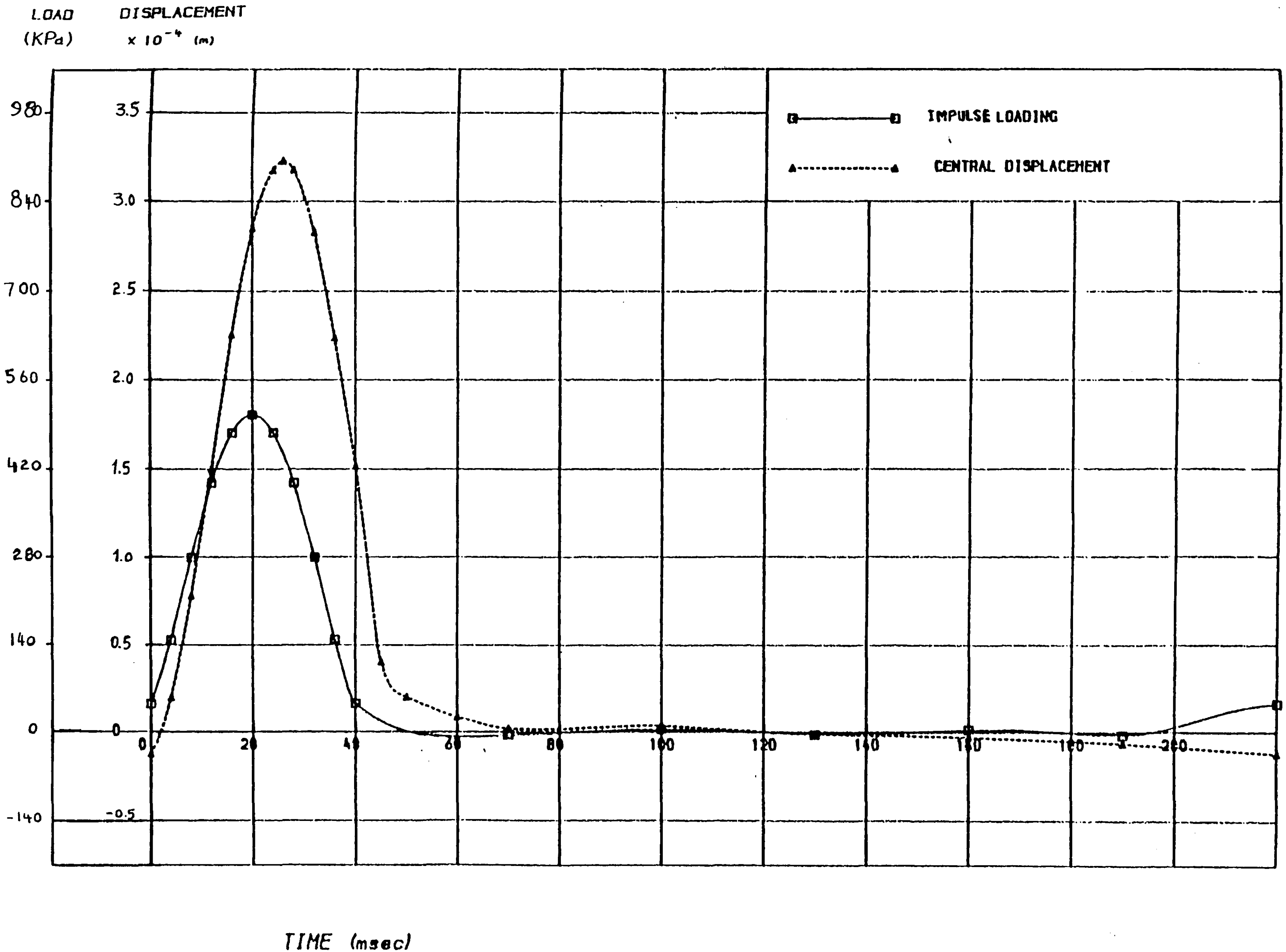

(FIG. 3.7) FWD load impulse and pavement displacement response at center of baseplate.

Frequency (Hz)	Relative Amplitude	Cumulative Amplitude (percent)
0	51	9
4.5	100	26.8
9.1	94	43.5
13.6	84	56.4
18.2	72	71.2
22.7	58	81.5
27.3	44	89.3
31.8	25	93.8
36.4	20	97.3
40.9	11	99.3
45.5	4	100.0

(FIG. 3.8.a) Frequency Content of FWD Load Impulse [42].

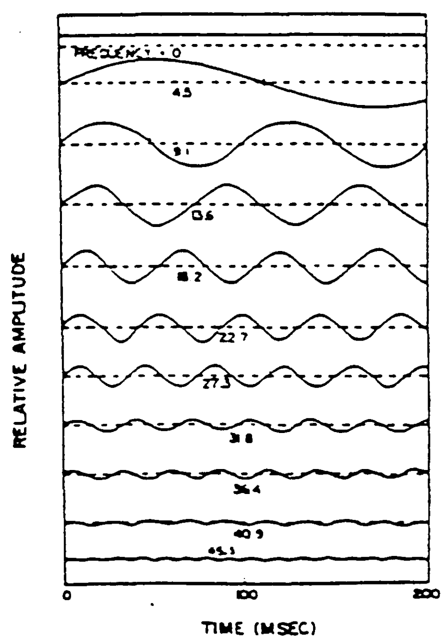

(FIG. 3.8.b) Equivalent Theoretical Harmonic Component of FWD impulse [42].

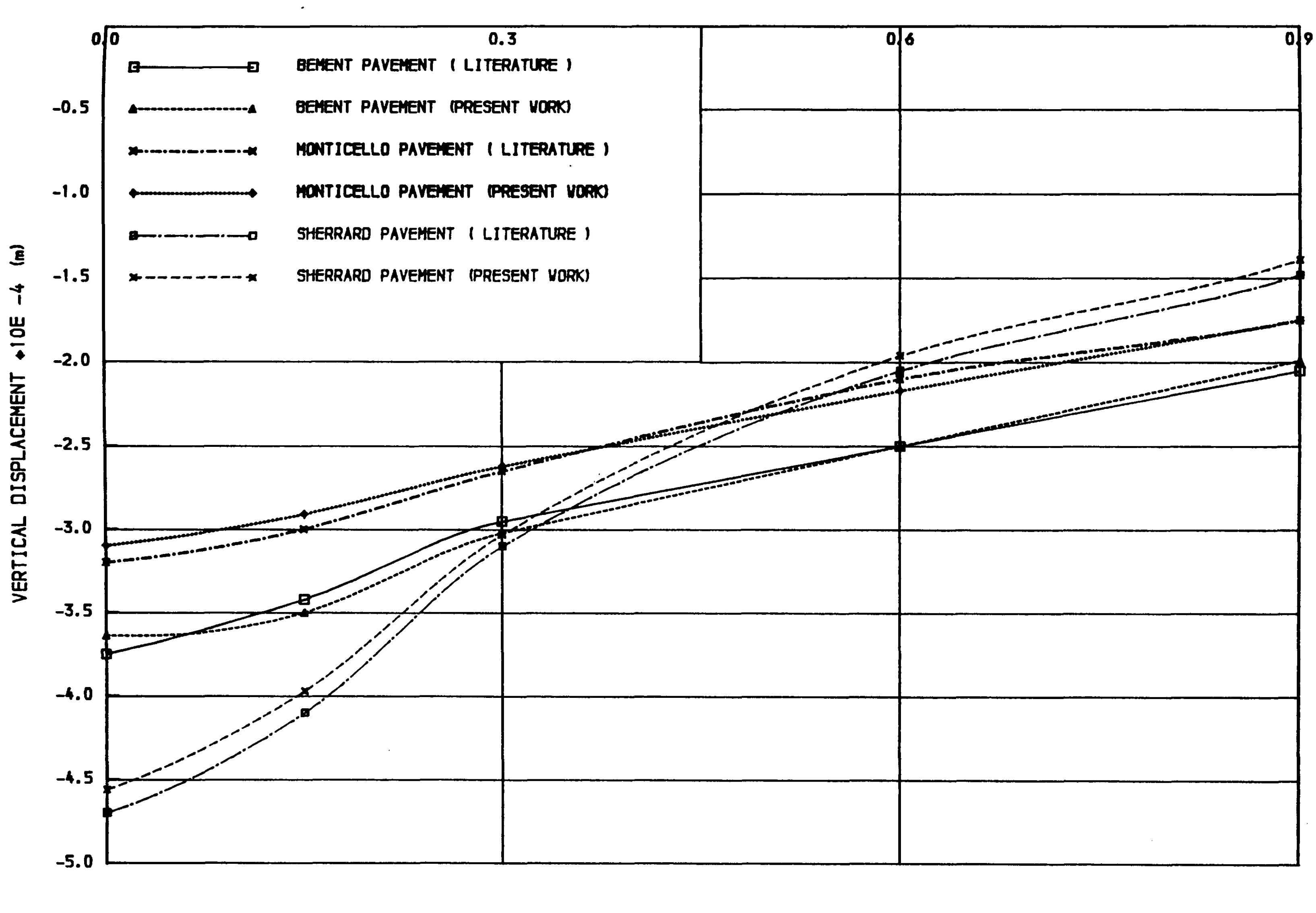

(FIG. 3.9) DEFLECTION BASINS (STATIC ANALYSIS)

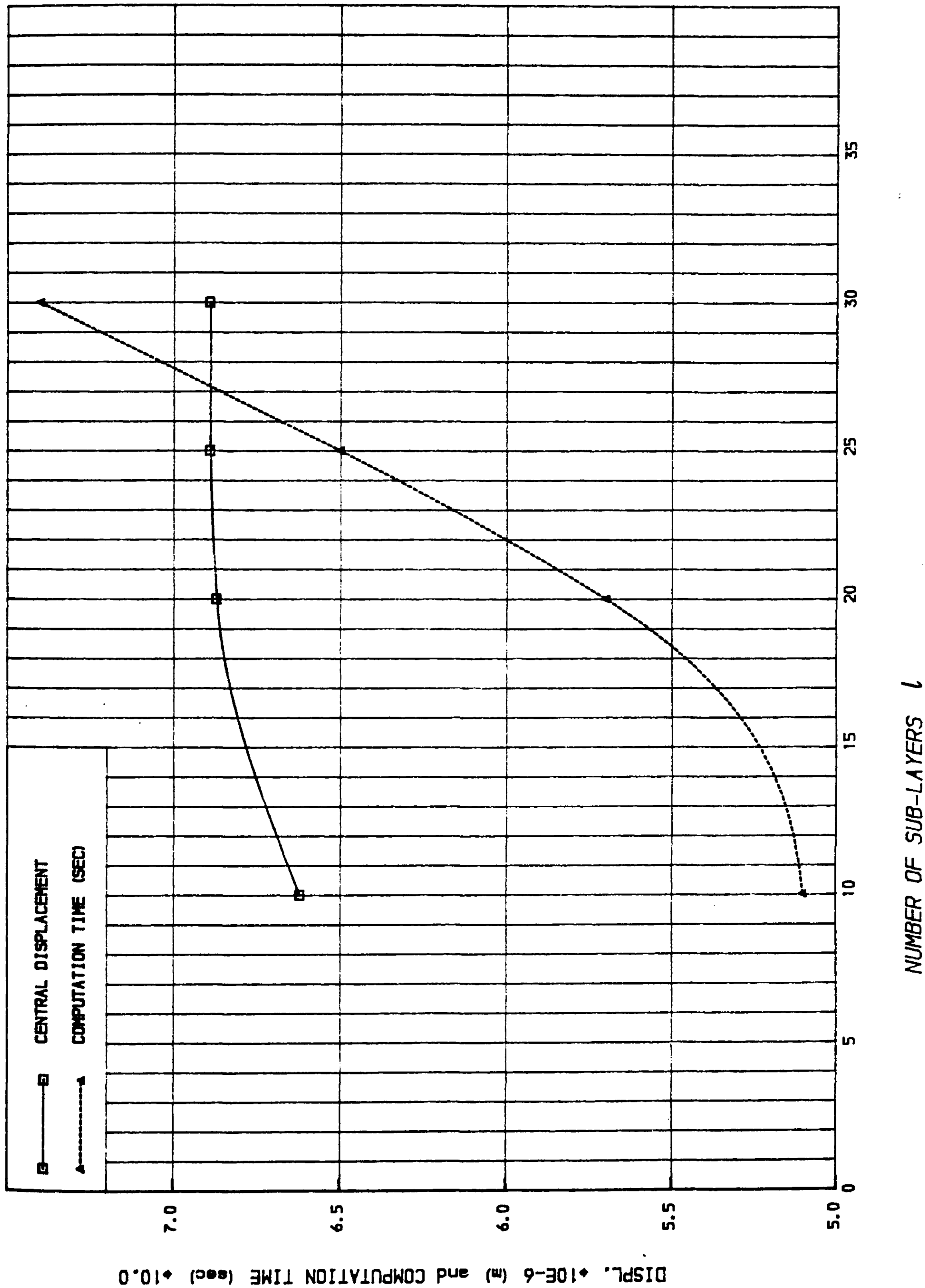

(FIG. 3.10) DISPL. AND TIME VARIATION w.r.t l

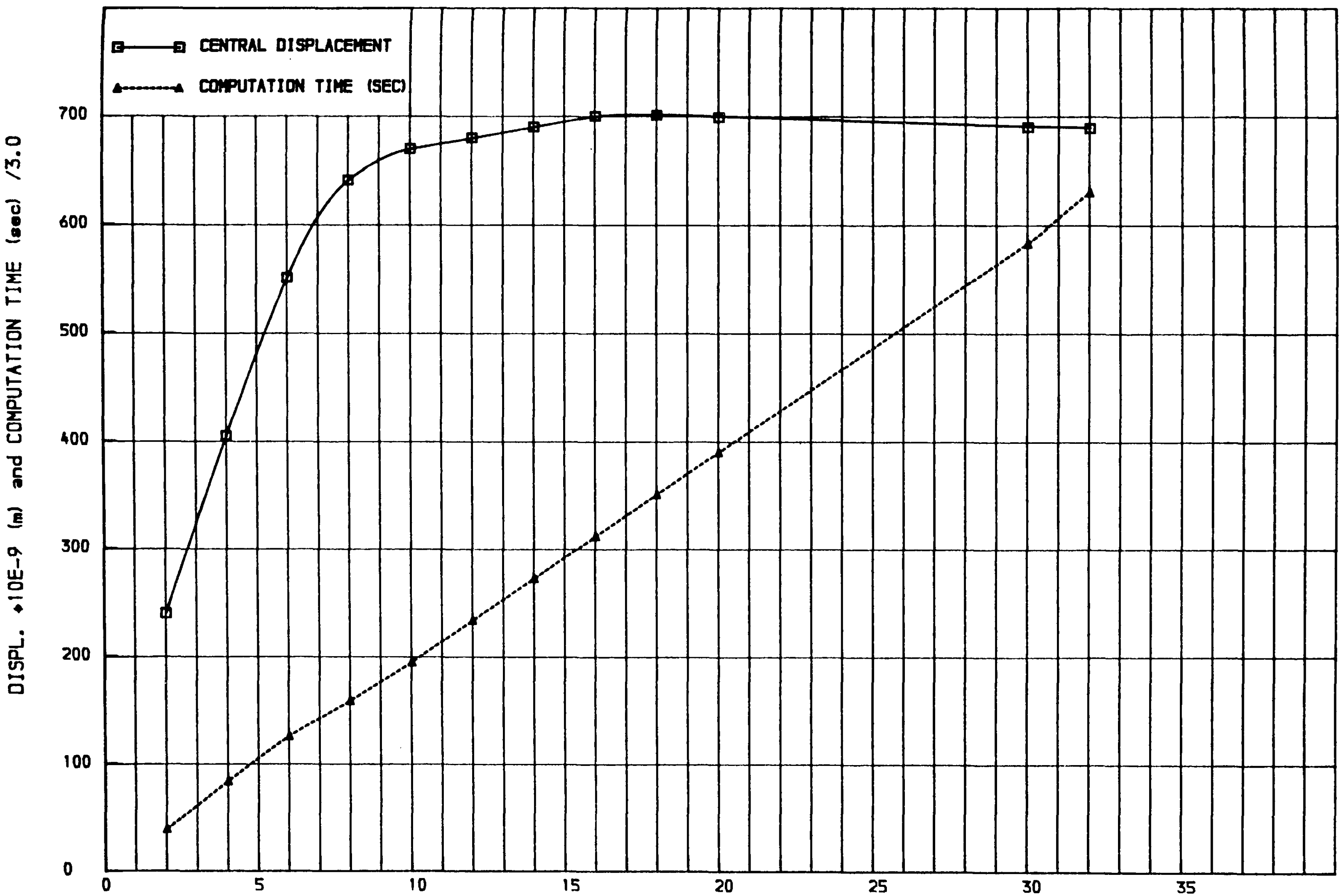

(FIG. 3.11) DISPL. AND TIME VARIATION w.r.t 'n'

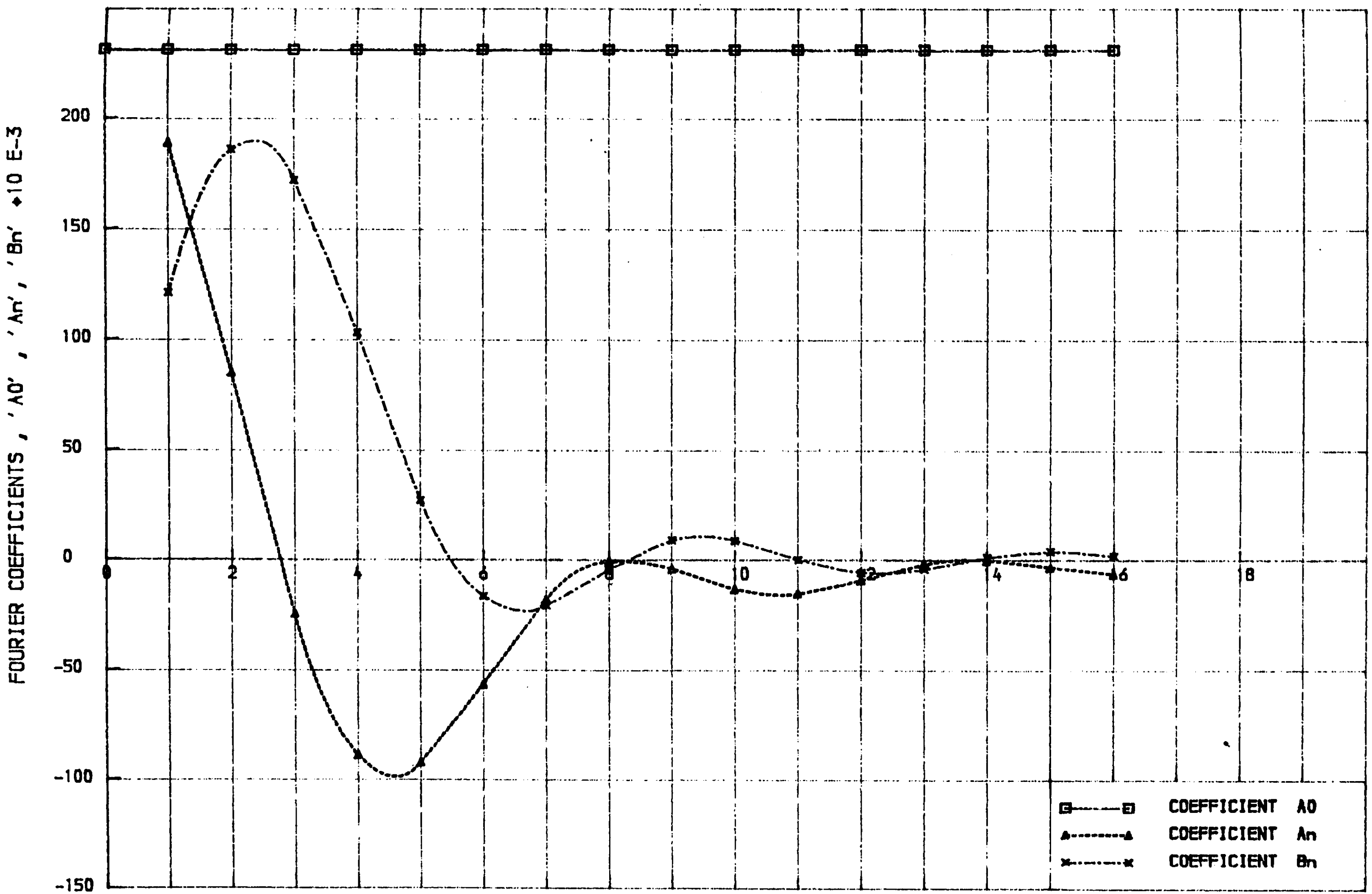

(FIG. 3.12) 'An' AND 'Bn' VARIATION w.r.t 'n'

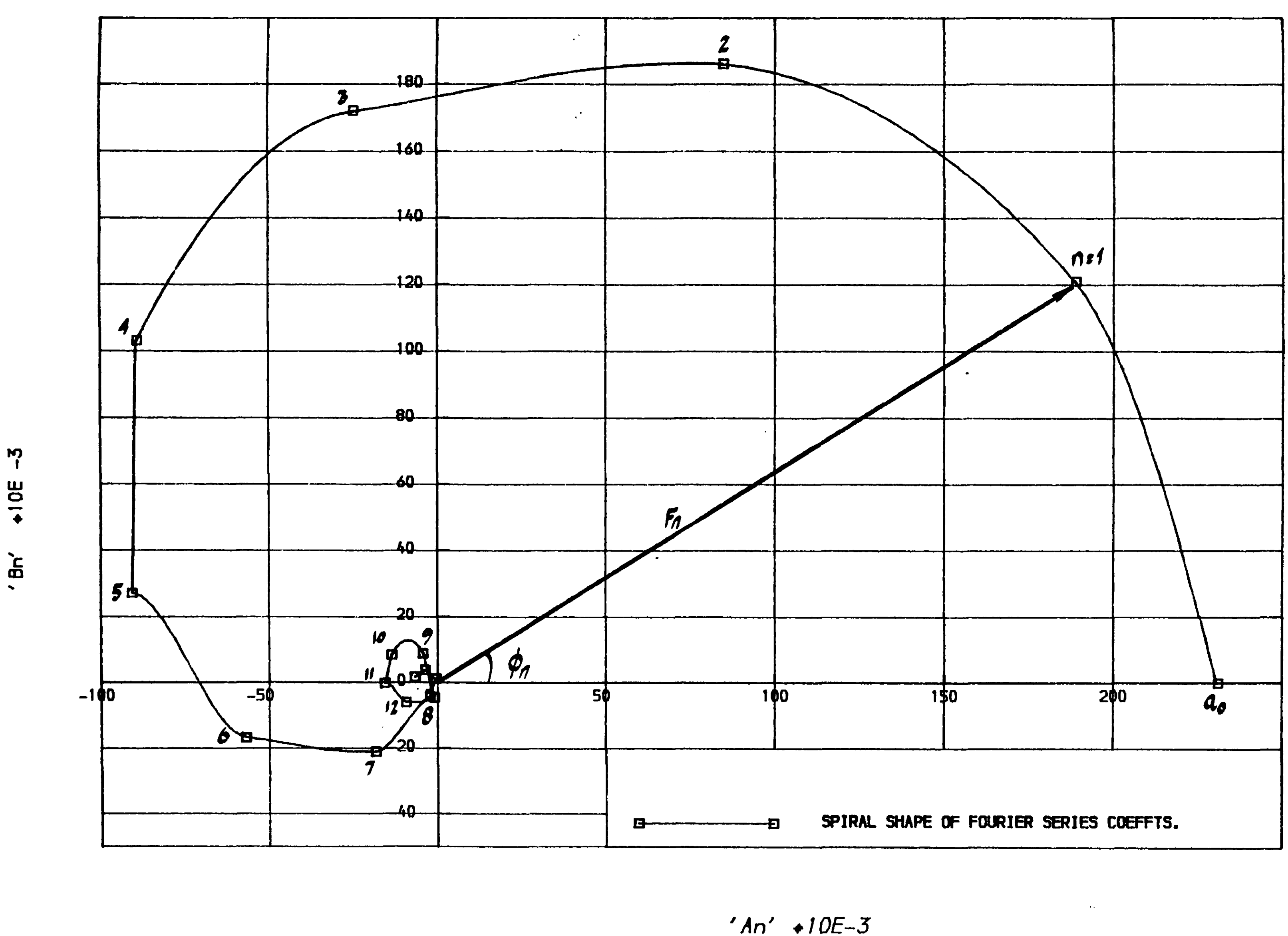

(FIG. 3.13) 'An' AND 'Bn' VARIATION w.r.t 'n'

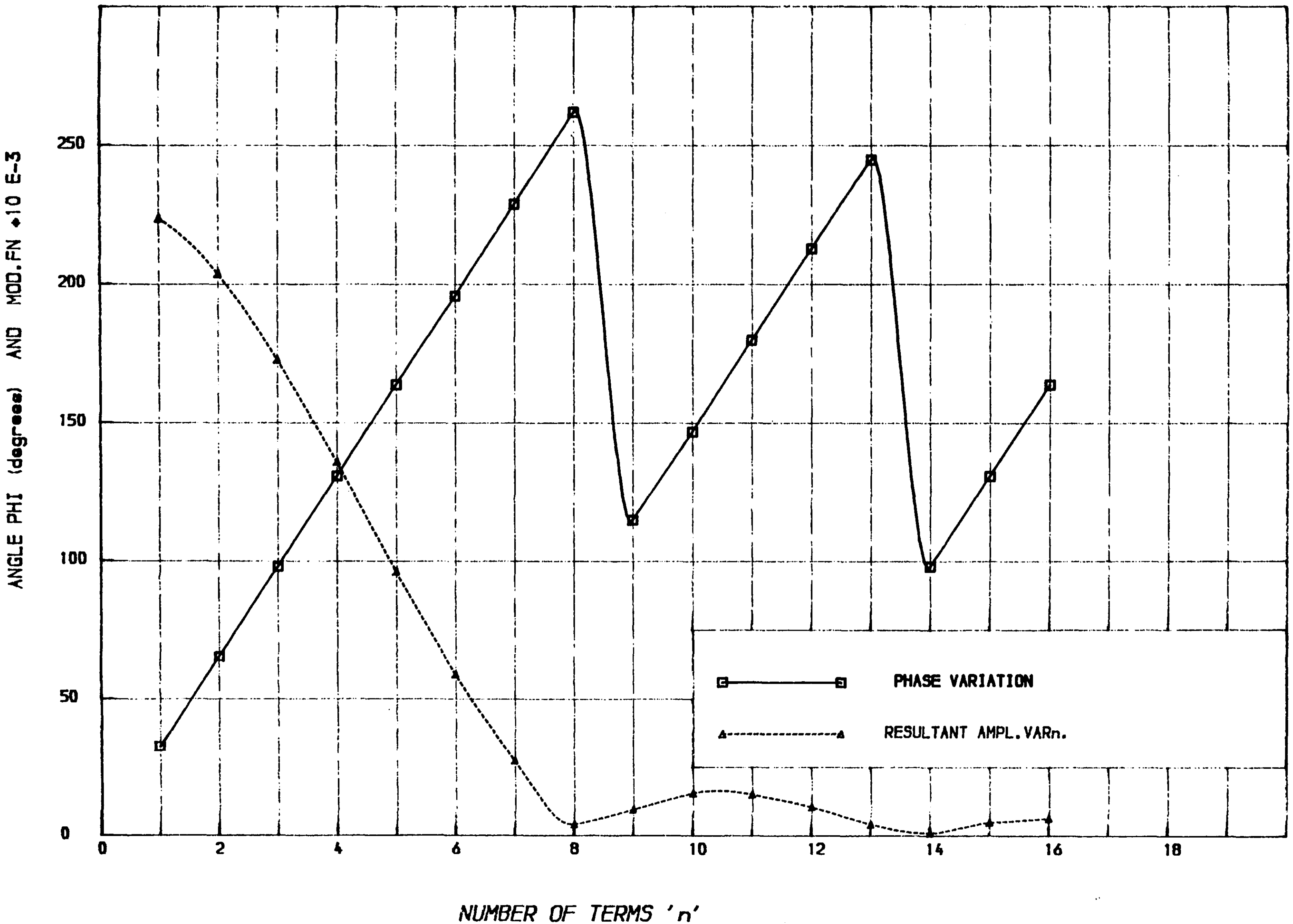

(FIG. 3.14) ' ANGLE PHI' AND 'MODULUS FUNCTION' VARIATION w.r.t 'n'

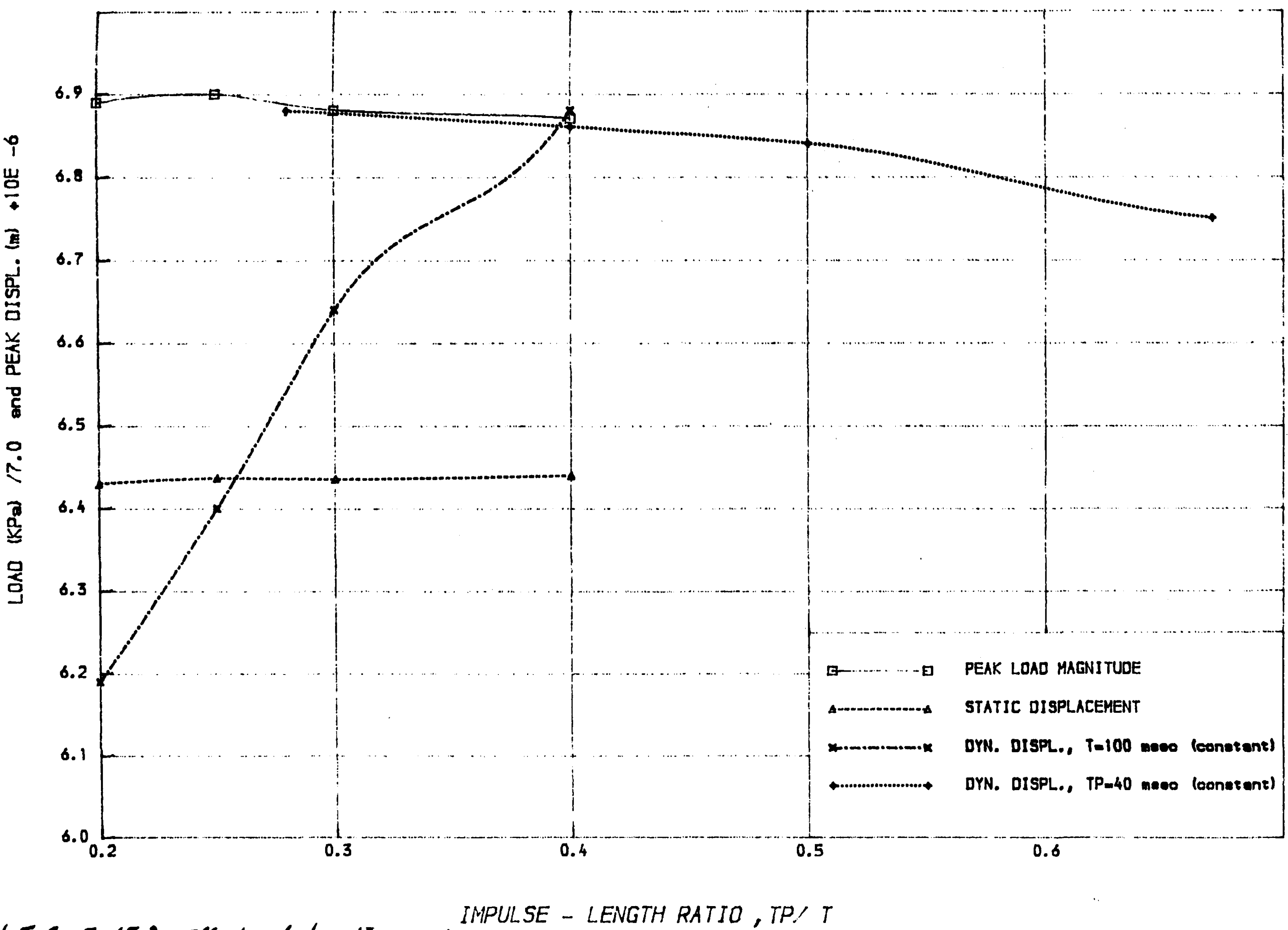

(FIG. 3.15) **Effect of loading rate on the Pavement response**

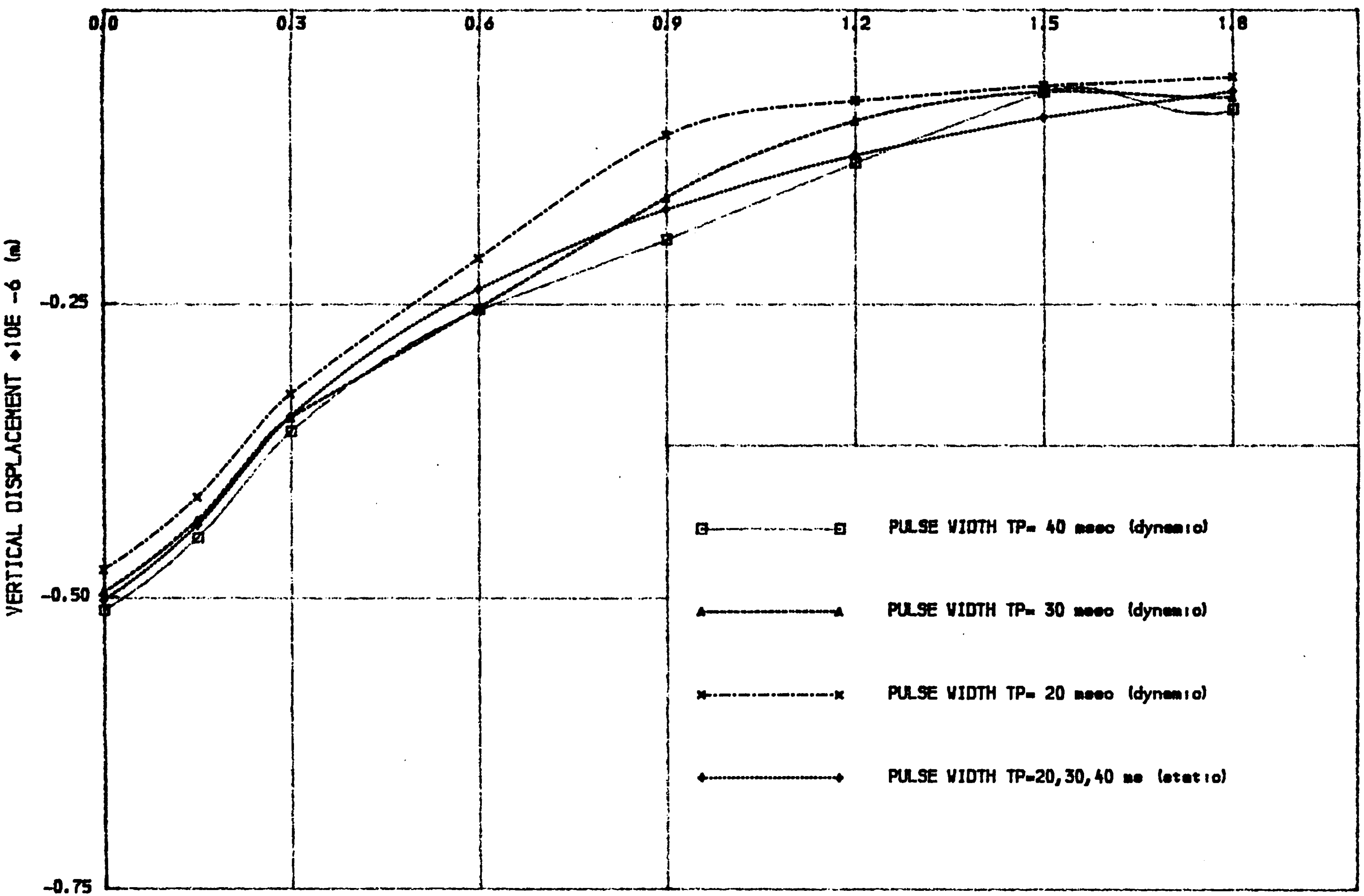

(FIG. 3.16a)

FOUR LAYER FLEXIBLE PAVEMENT

PERIOD T= 140 msec (CONSTANT)
DEFLECTION BASINS (PULSE WIDTH ANALYSIS)

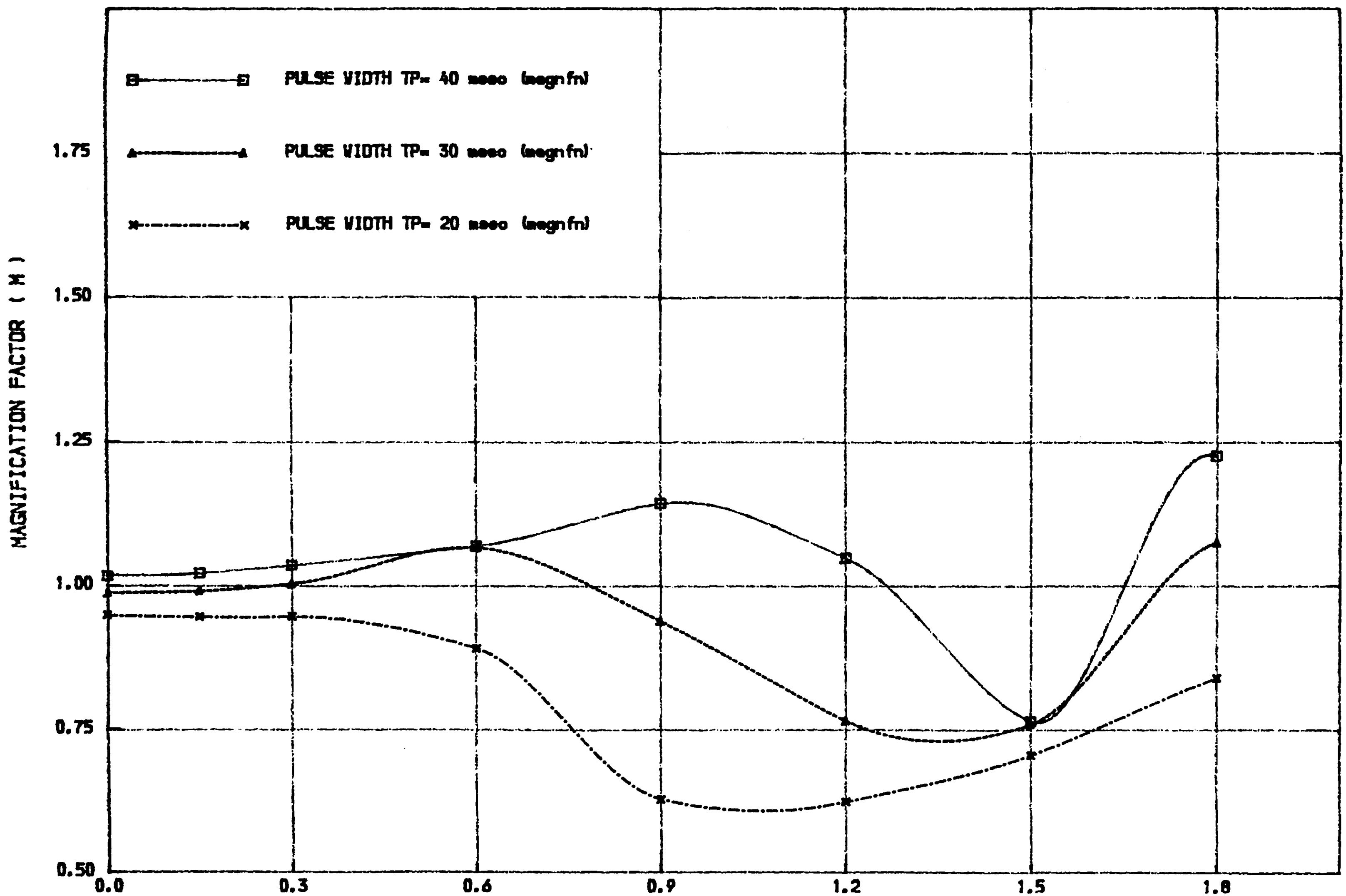

(FIG.3.16.b) *RERIOD T= 140 msec (PULSE VIDTH ANALYSIS)* *RADIUS* (m) **FOUR LAYER FLEXIBLE PAVEMENT**

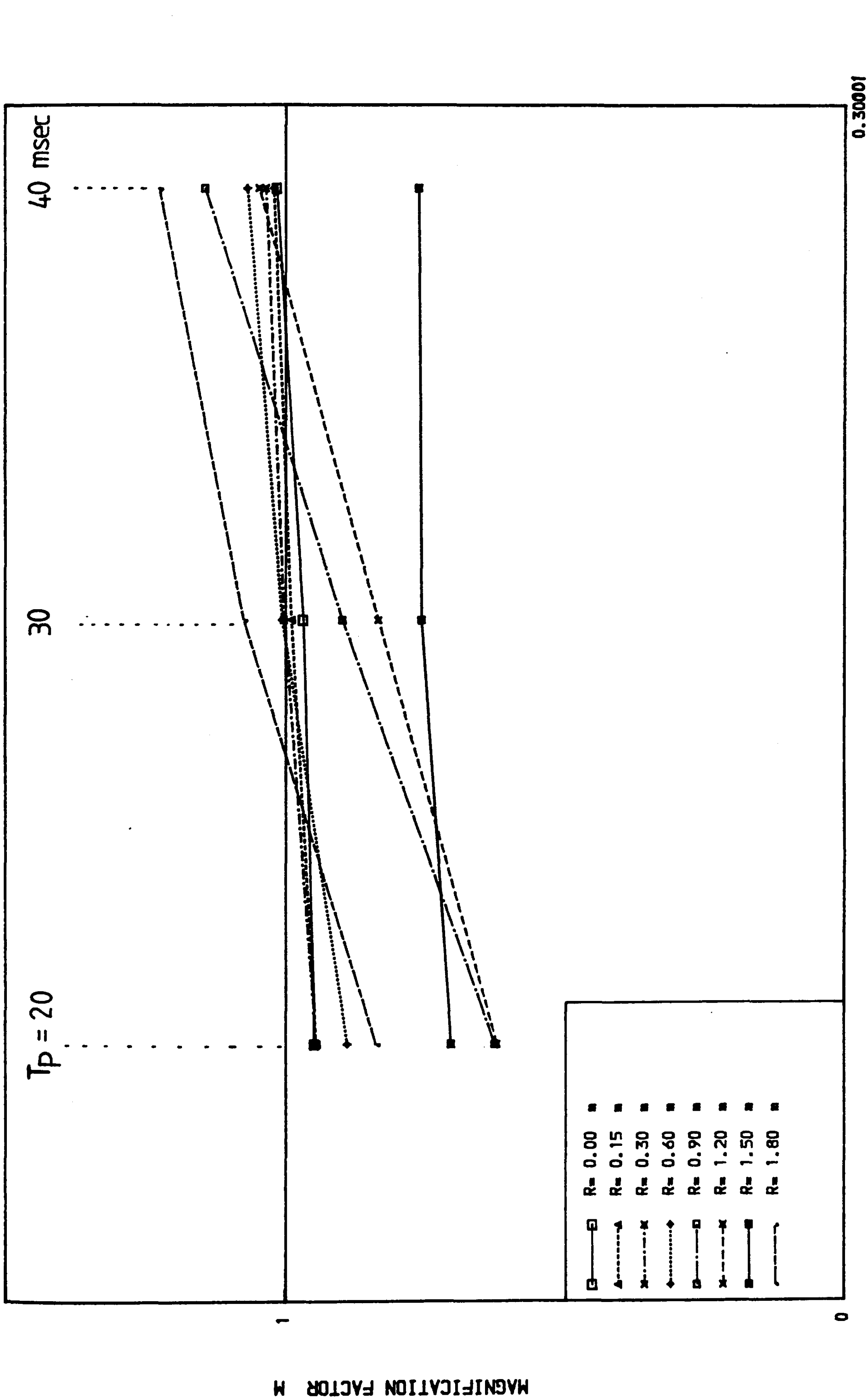

FOUR- LAYER FLEXIBLE PAVEMENT

T = 140 msec

T_P / T ratio
(PULSE WIDTH ANALYSIS)

(FIG.3.16.c)

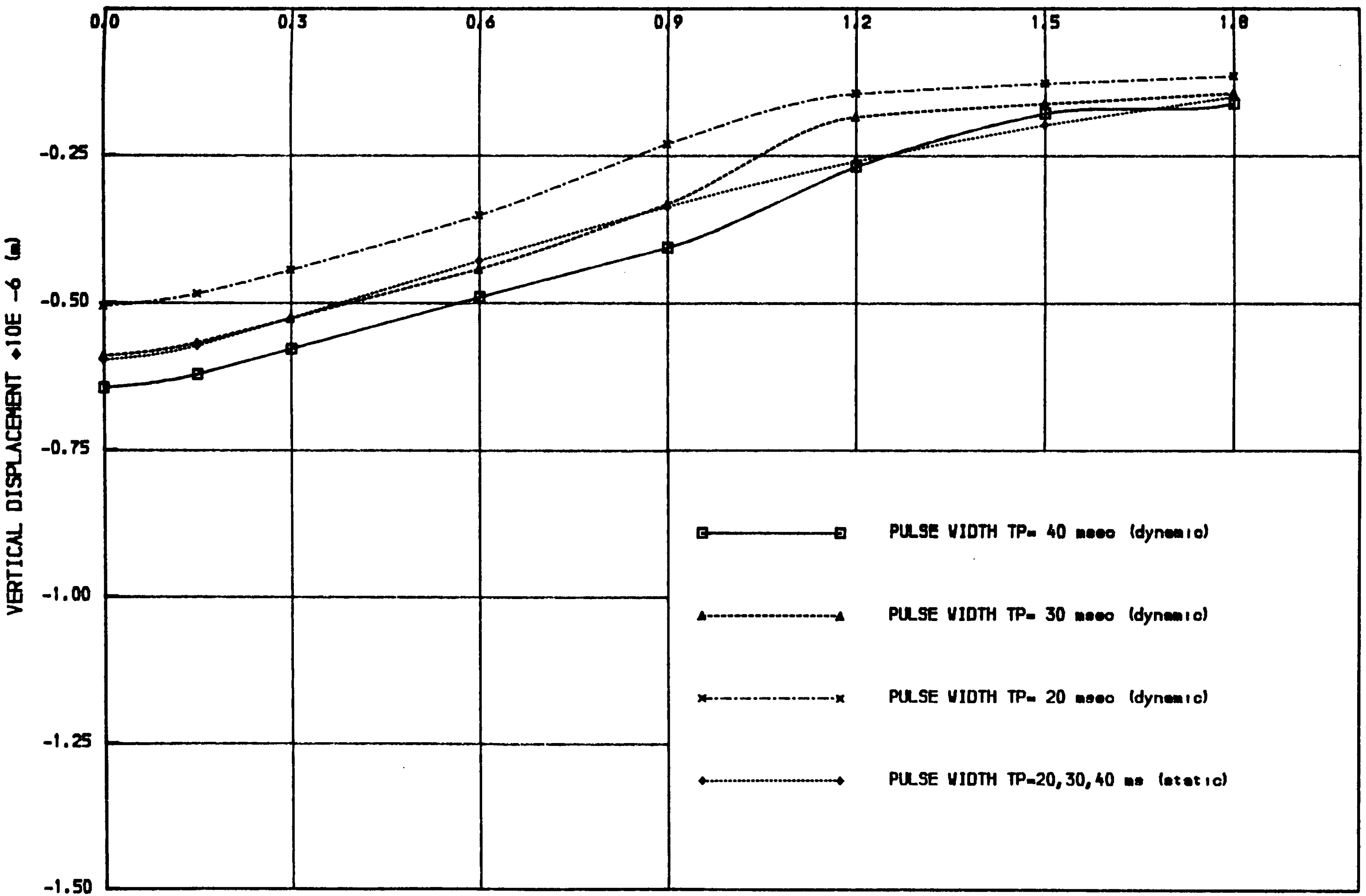

(FIG.3.17.a)

THREE-LAYER SYSTEM **FLEXIBLE**

RADIUS (m)

PERIOD T= 140 msec (CONSTANT)

DEFLECTION BASINS (PULSE VIDTH ANALYSIS)

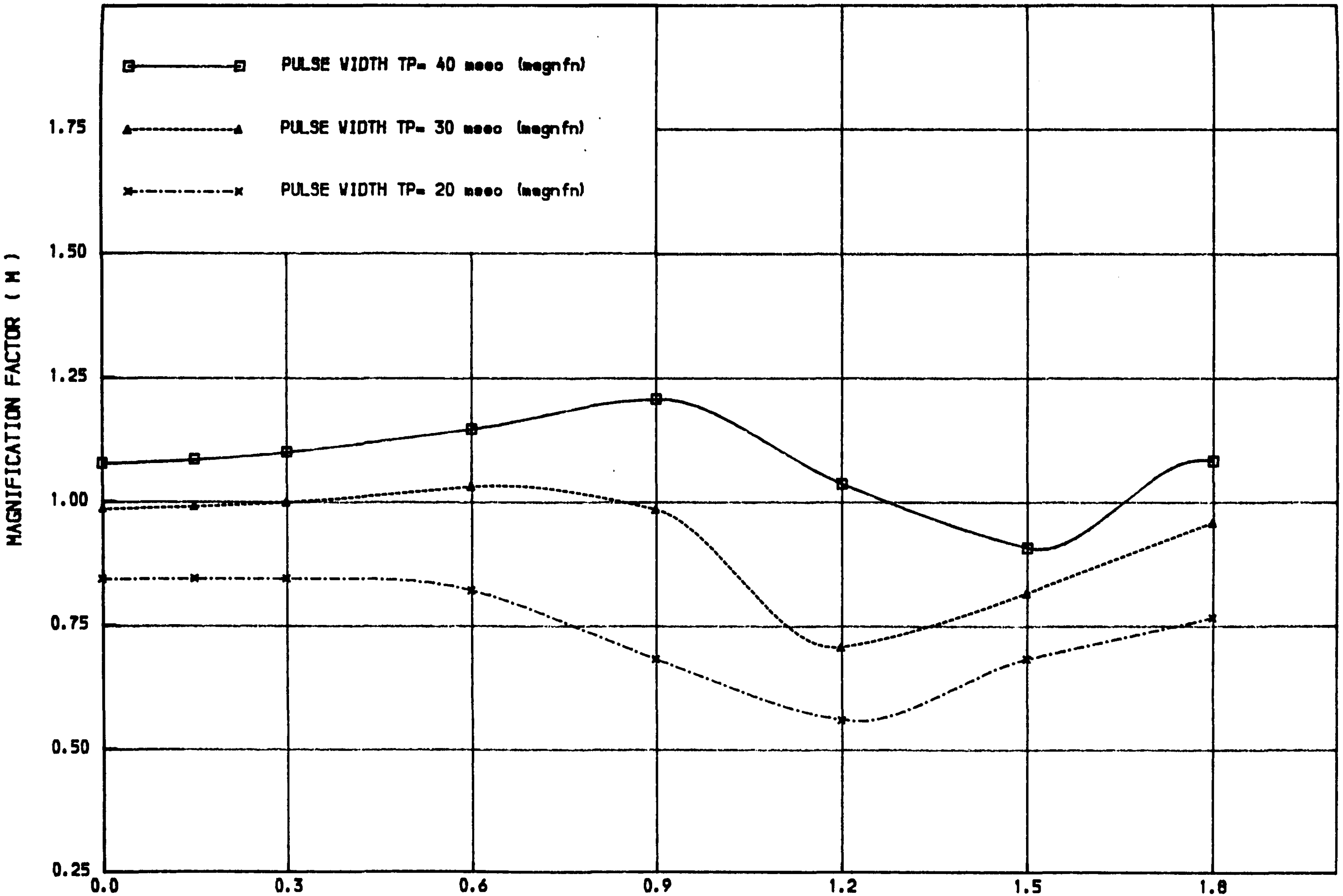

(FIG.3.17.b) RERIOD T= 140 msec
(PULSE VIDTH ANALYSIS)

THREE-LAYER SYSTEM **FLEXIBLE**

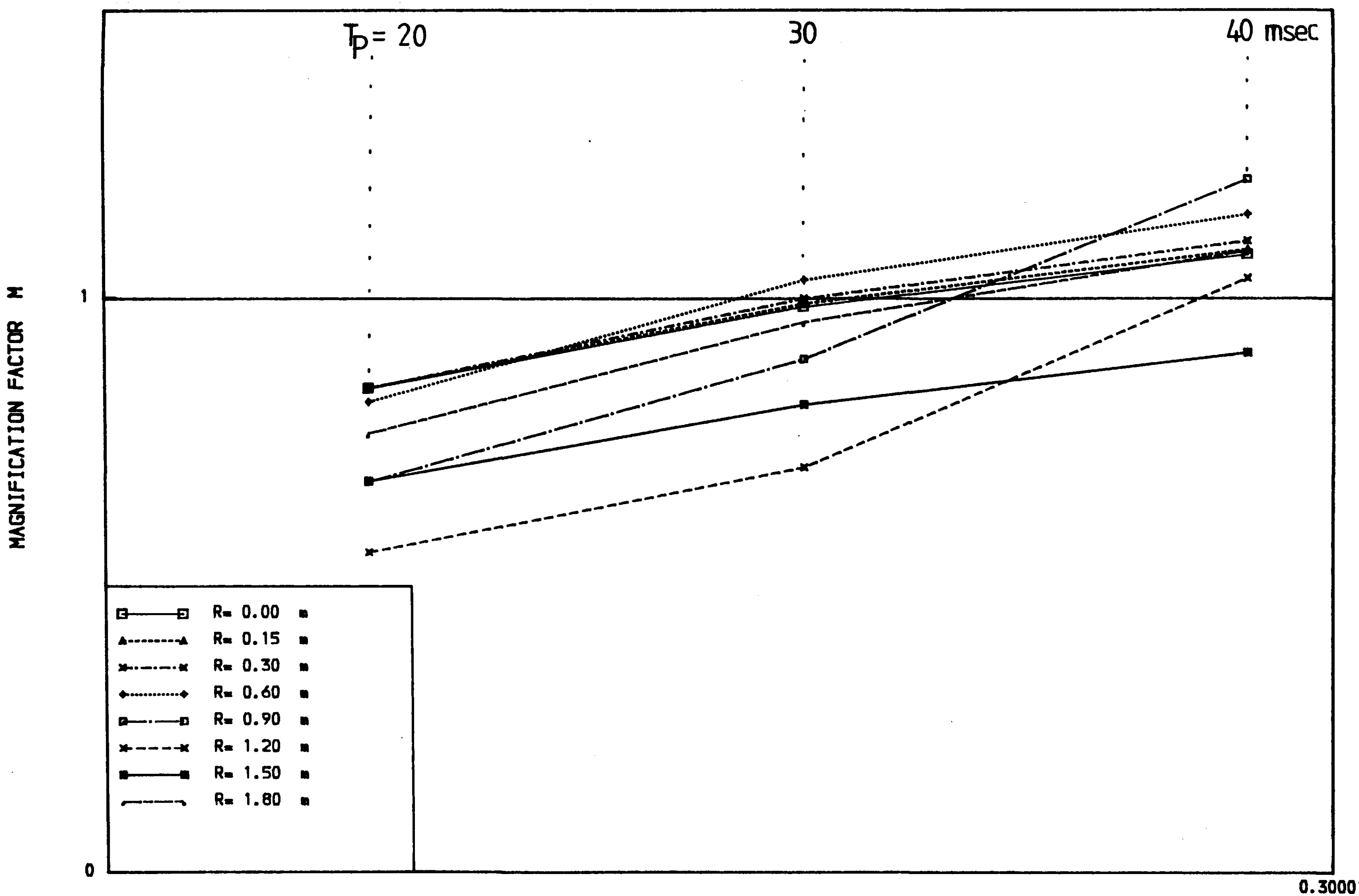

THREE- LAYER FLEXIBLE PAVEMENT

T = 140 msec

Tp / T ratio

(PULSE VIDTH ANALYSIS)

(FIG. 3.17.c)

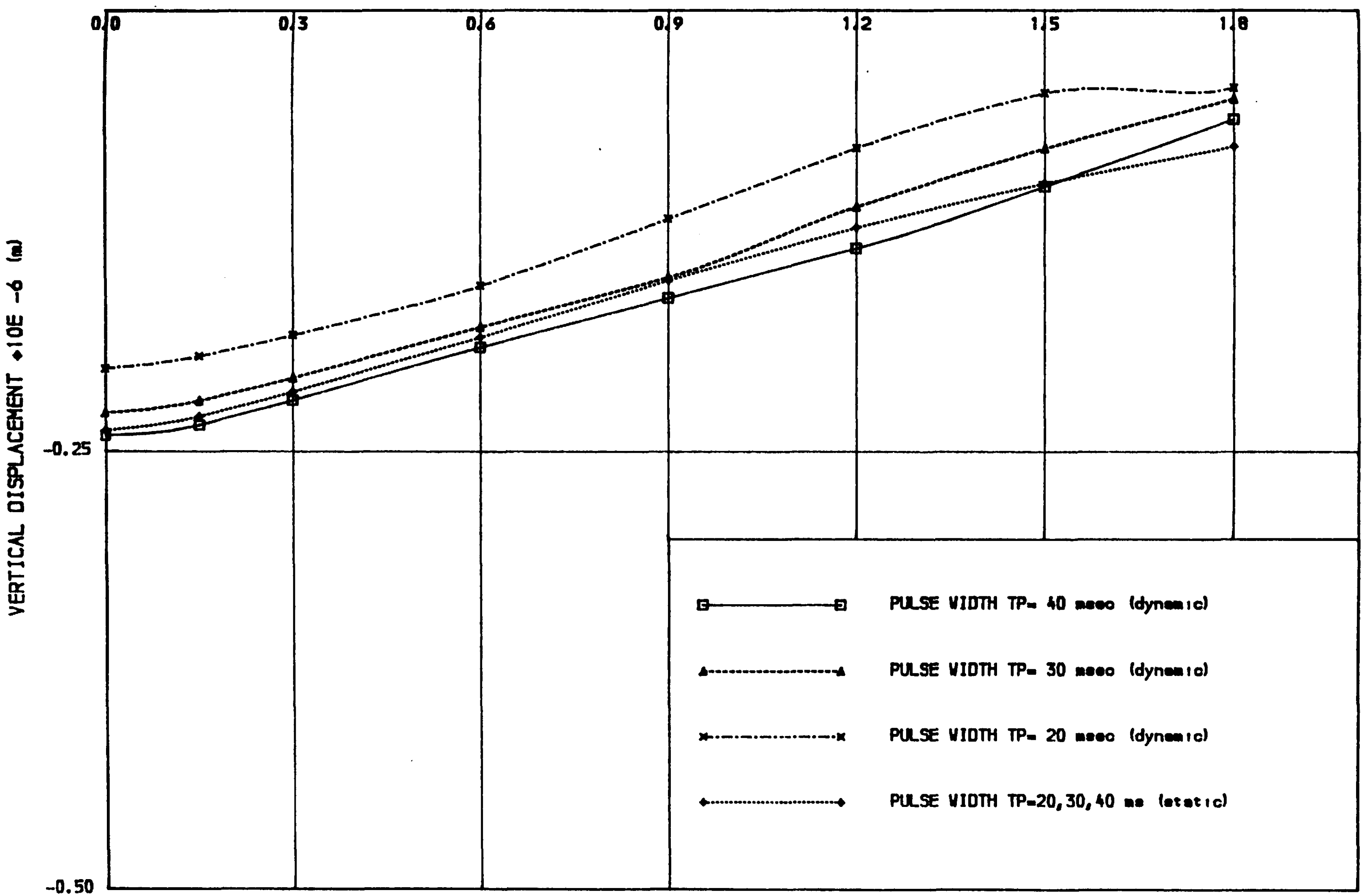

(FIG. 3.18.a)

RIGID PAVEMENT *** THREE-LAYER SYSTEM
RADIUS (m)

PERICD T= 140 msec (CONSTANT)
DEFLECTION BASINS (PULSE VIDTH ANALYSIS)

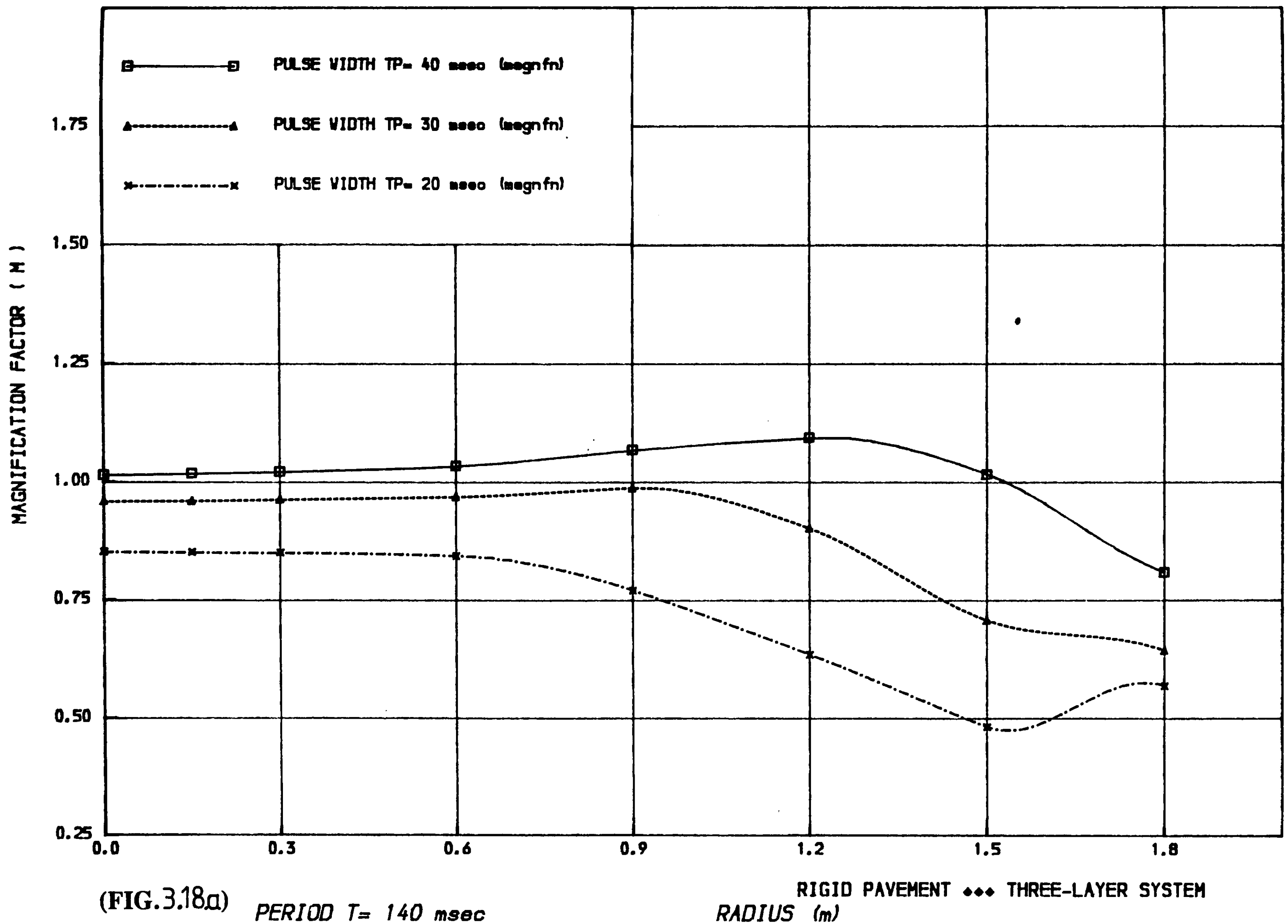

(FIG.3.18a) PERIOD T= 140 msec
(PULSE VIDTH ANALYSIS)

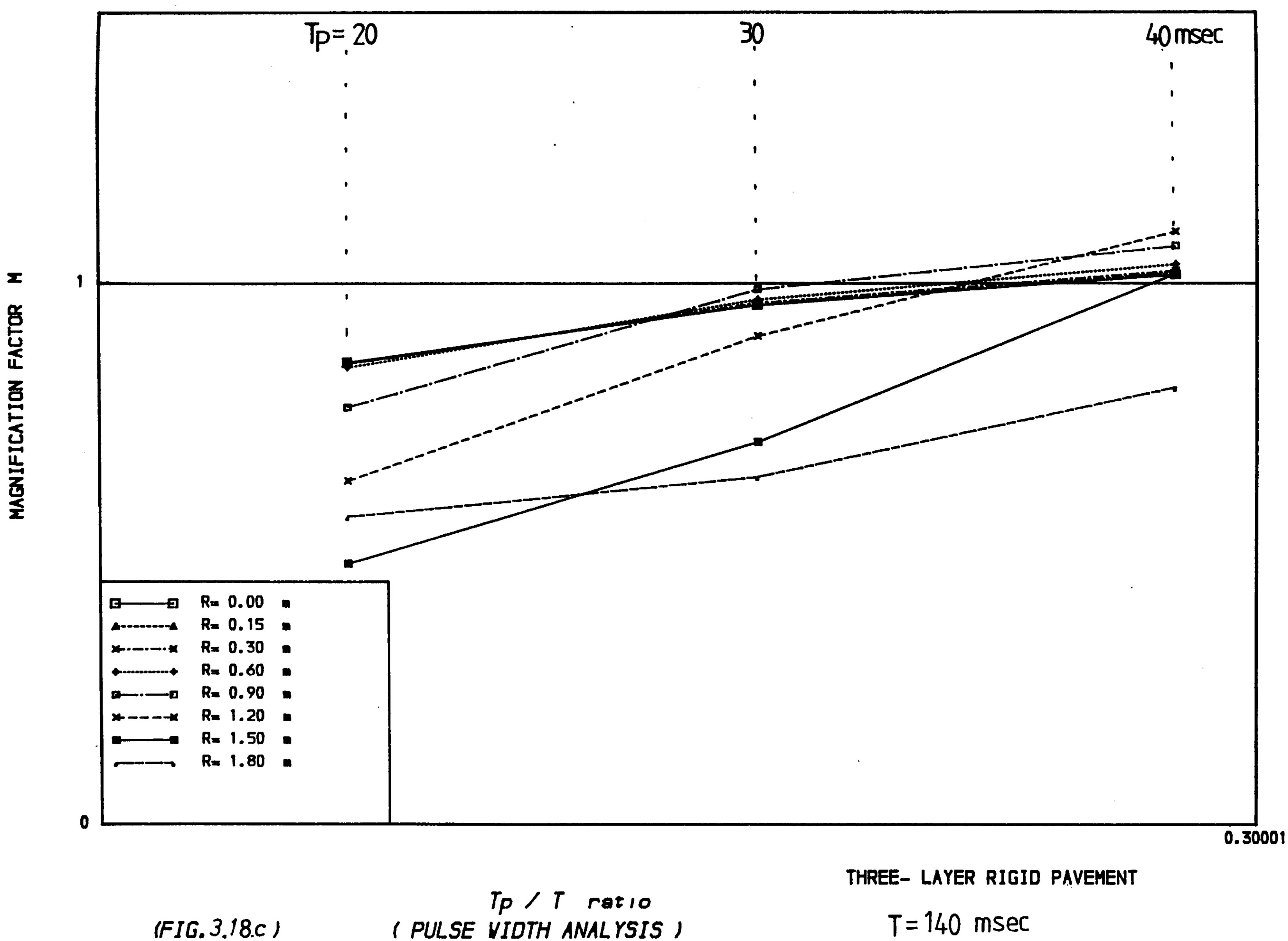

THREE- LAYER RIGID PAVEMENT

T= 140 msec

(FIG. 3.18.c)

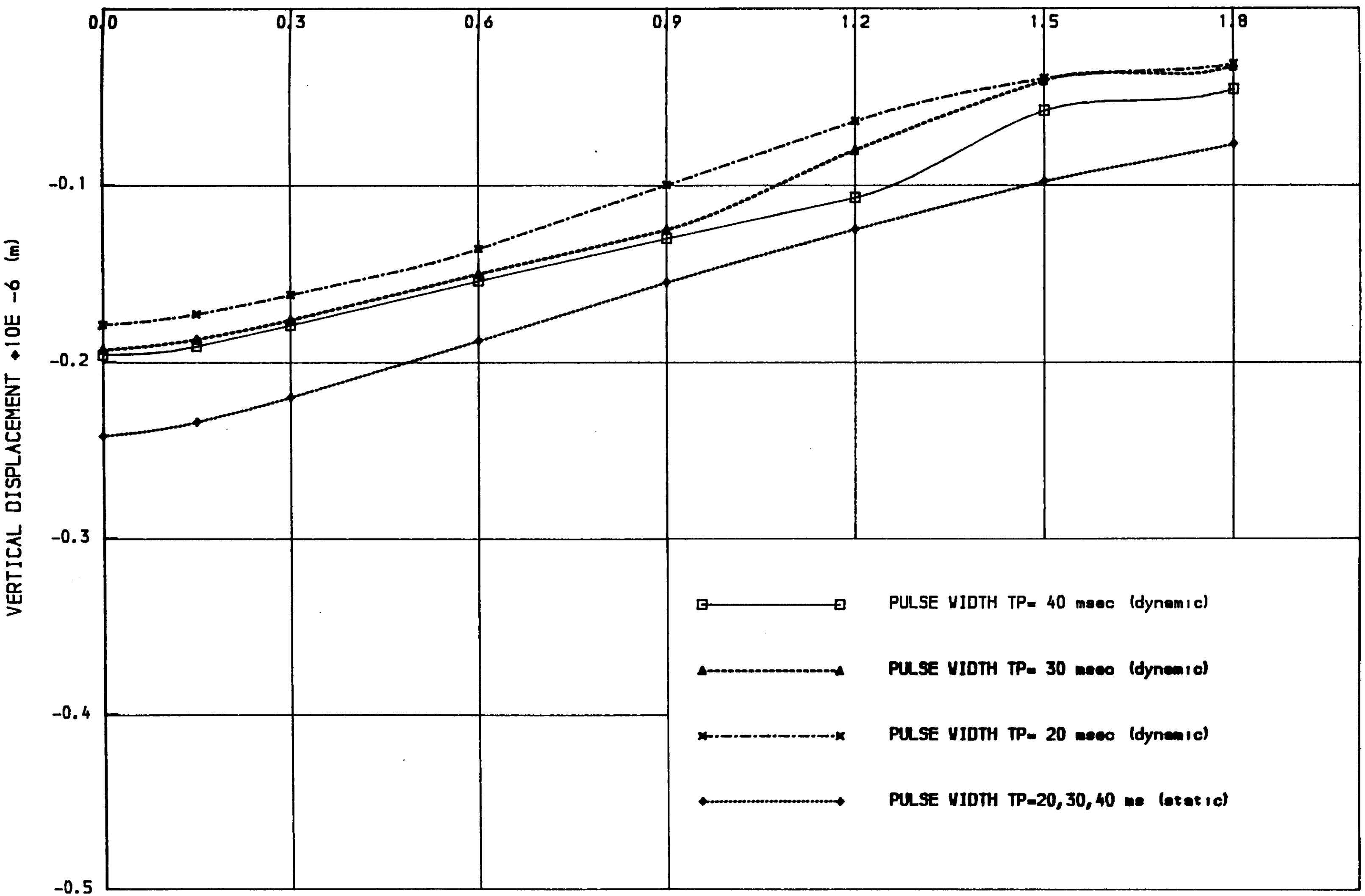

(FIG.3.19.a)

RIGID AIRPORT RUNWAY ◆◆◆ TWO-LAYER SYSTEM

PERIOD T= 140 msec (CONSTANT) *RADIUS (m)*

DEFLECTION BASINS (PULSE WIDTH ANALYSIS)

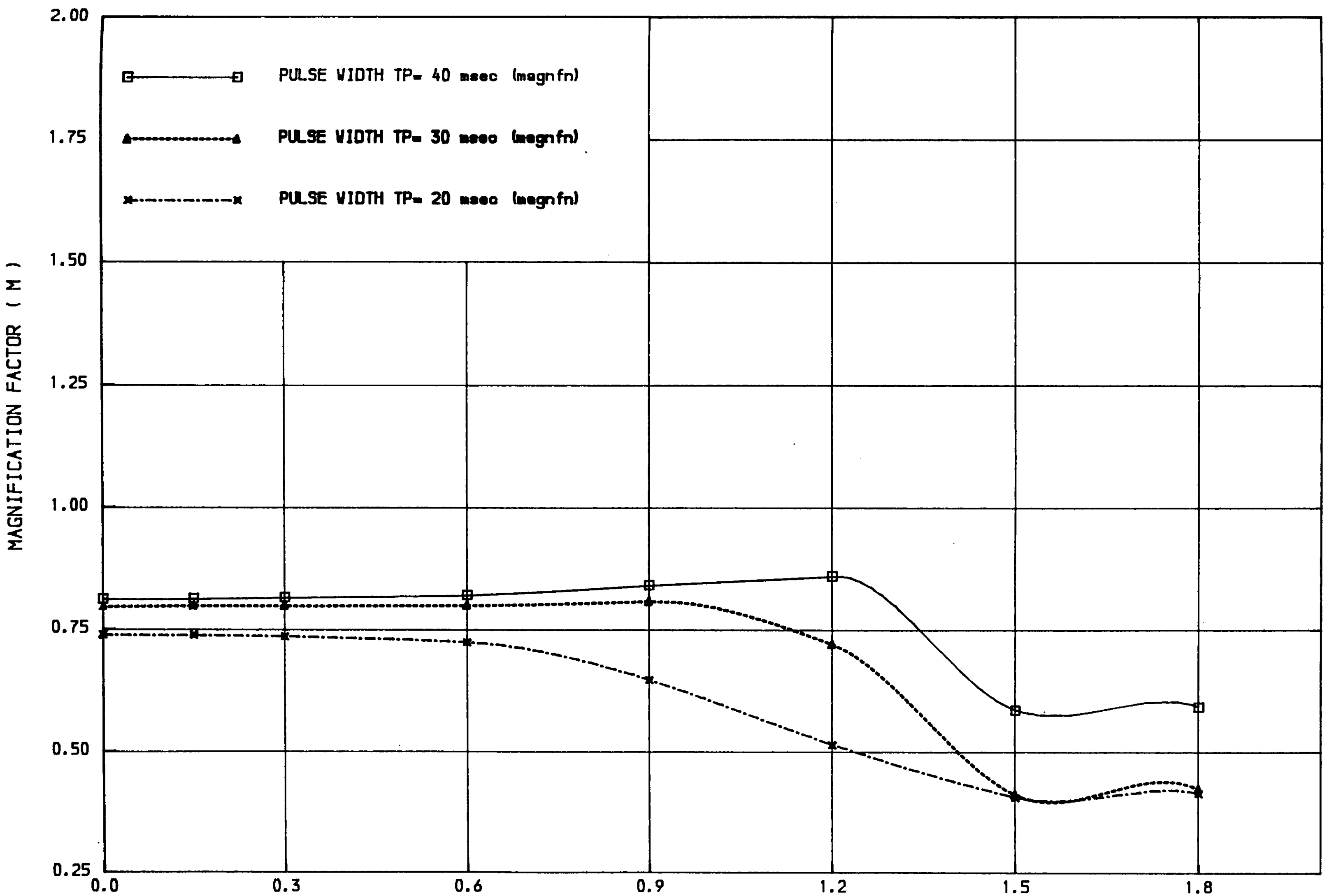

(FIG.3.19b) PERIOD T= 140 msec (PULSE VIDTH ANALYSIS)

RIGID AIRPORT RUNWAY ◆◆◆ TWO-LAYER SYSTEM

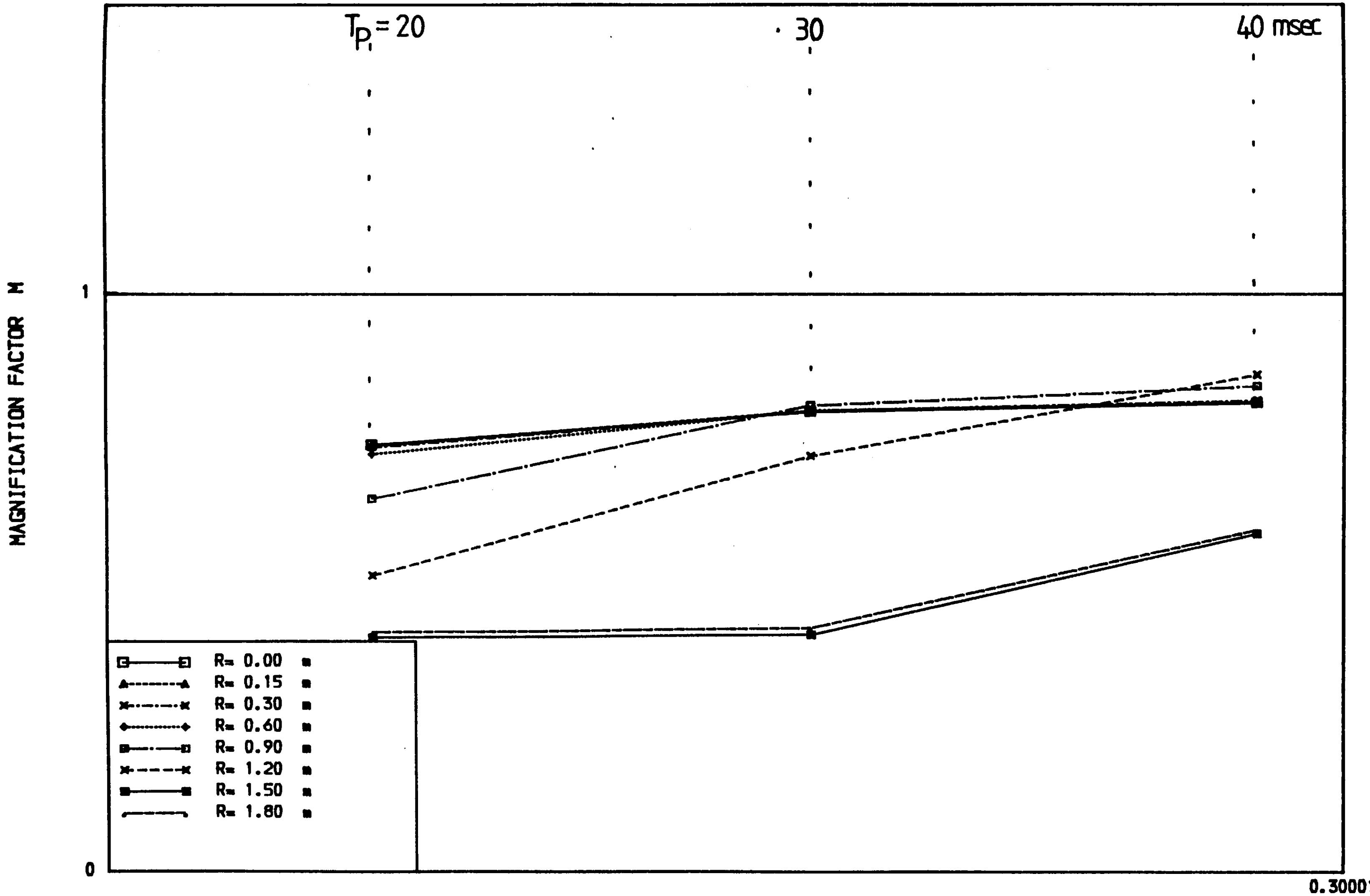

AIRPORT RUNWAYS (TWO- LAYER SYSTEM)

Tp / T ratio

(FIG. 3.19.c) (PULSE WIDTH ANALYSIS) T = 140 msec

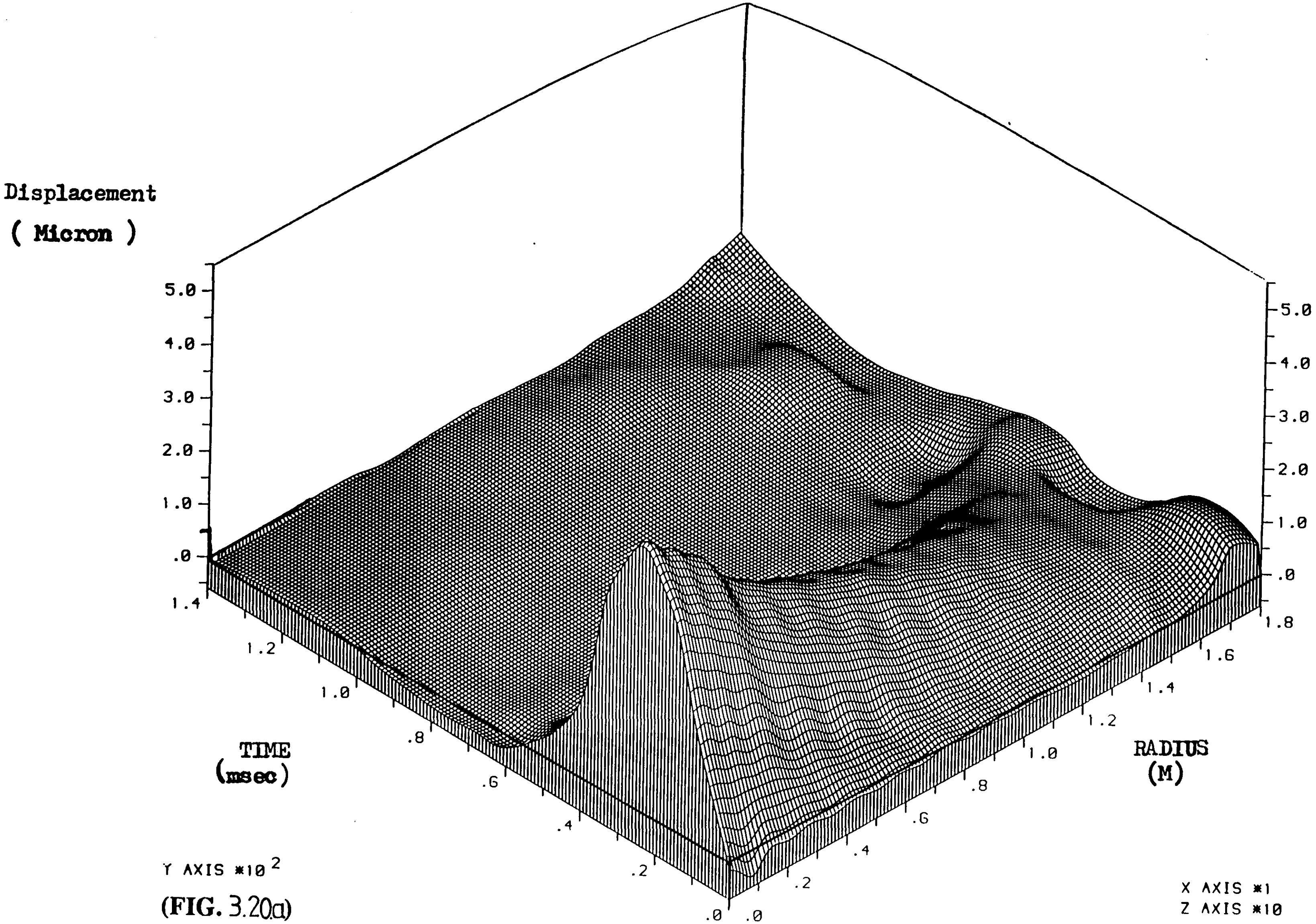

(FIG. 3.20a)

ISOMETRIC VIEW OF DISPL.*10E -8 (M) Vs RADIUS (M) & TIME (msec)

FOUR LAYER FLEXIBLE PAVEMENT

(Subgrade Stiffness= 100 MPa)

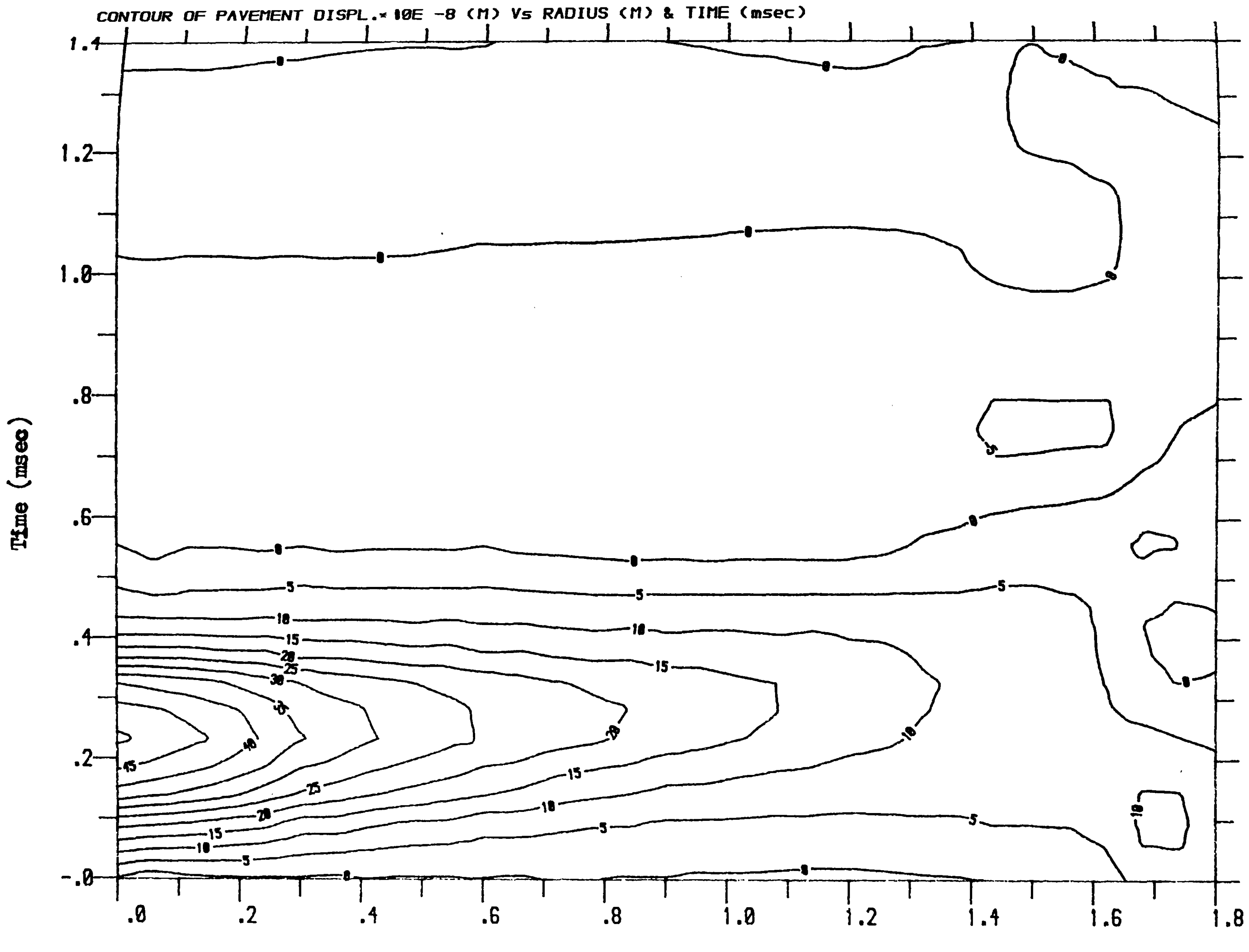

(FIG. 3.20b)

FOUR LAYER FLEXIBLE PAVEMENT

Subgrade Stiffness = 100 MPa

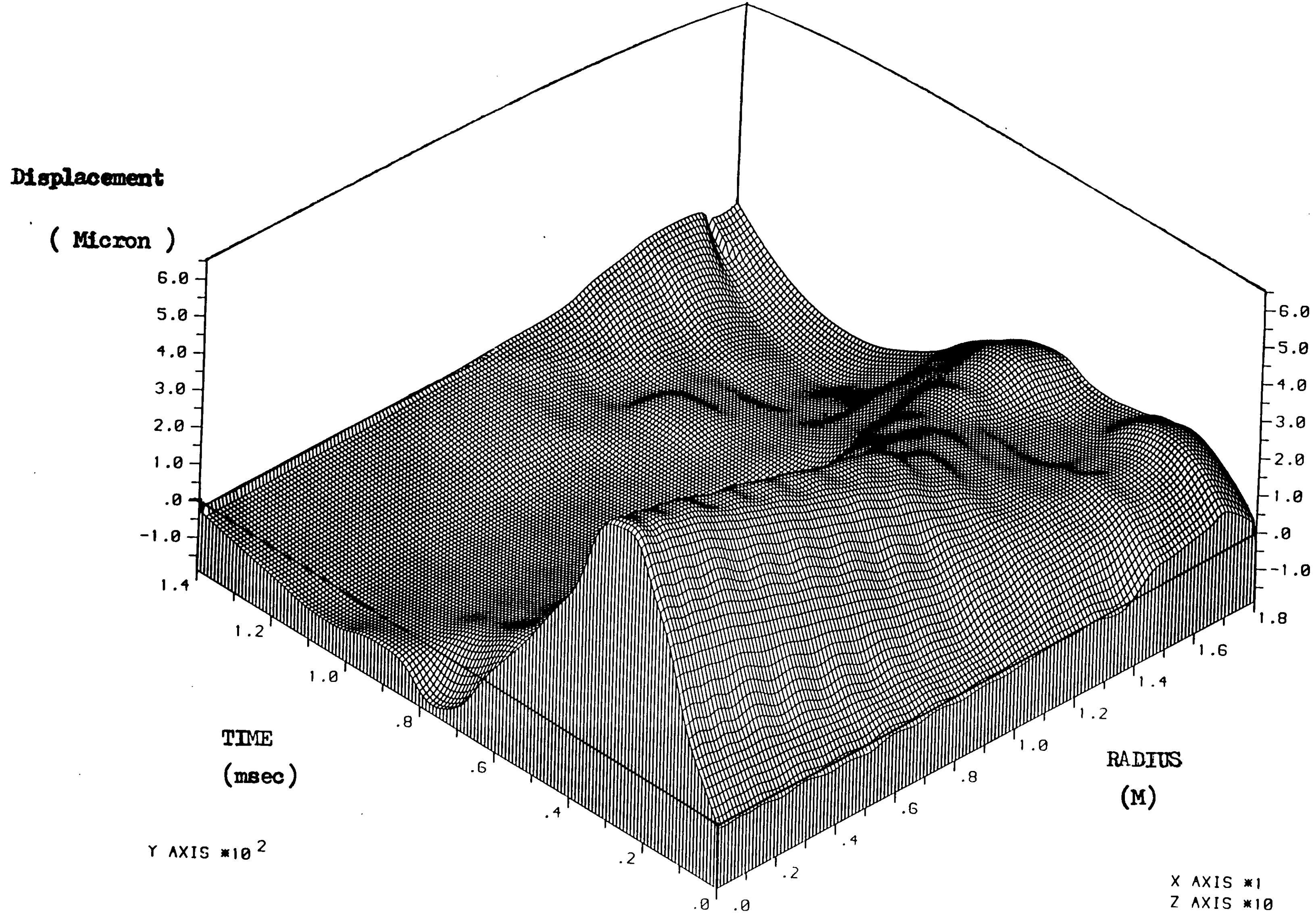

(FIG.3.21a) ISOMETRIC VIEW OF DISPL.* 10E -8 (M) Vs RADIUS (M) & TIME (msec)

THREE LAYER FLEXIBLE PAVEMENT

(subgrade stiffness= 50 MPa)

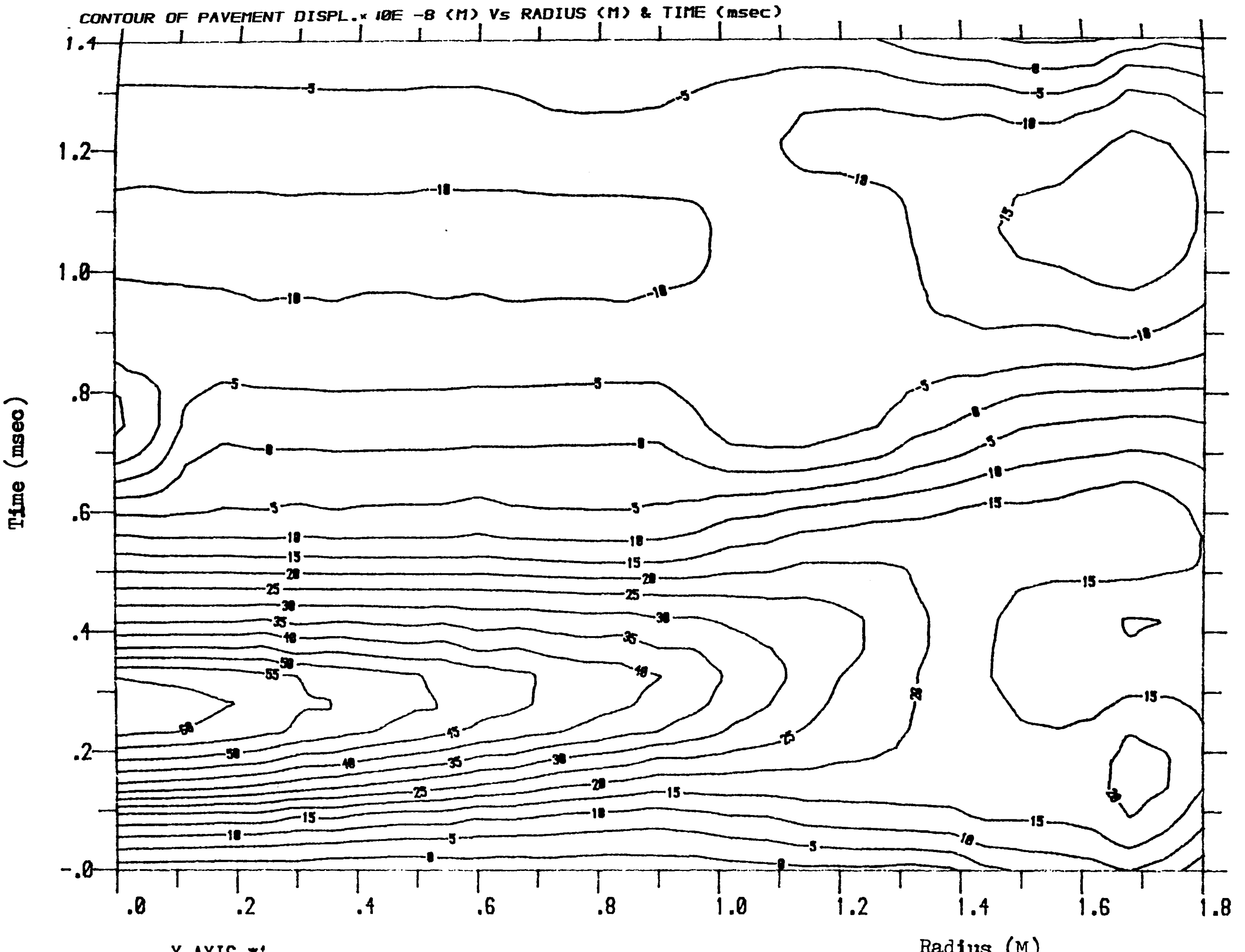

(FIG.3.21.b) X AXIS *1 Y AXIS *10^2 **THREE LAYER FLEXIBLE PAVEMENT**

(subgrade stiffness= 50 MPa)

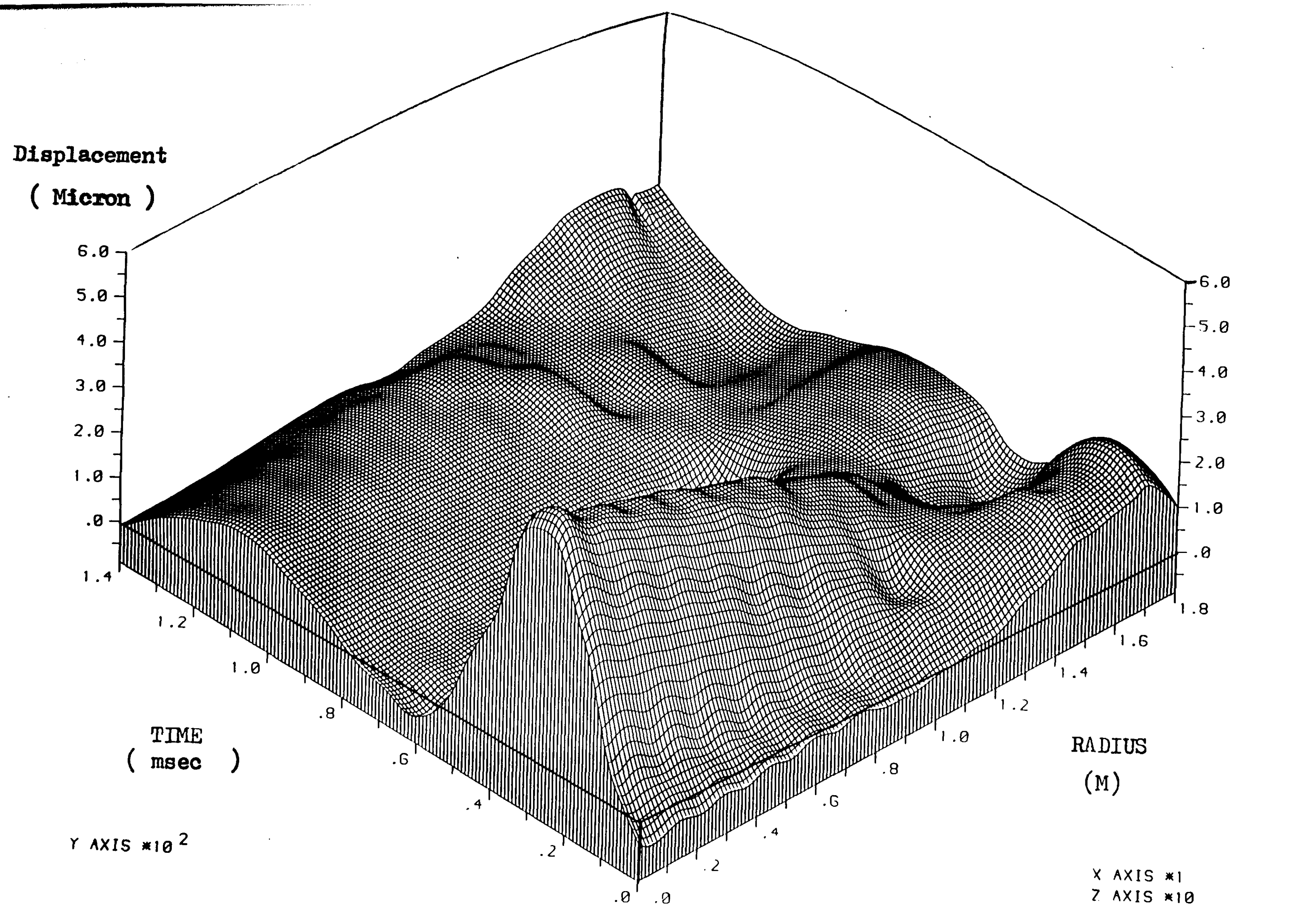

(FIG. 3.22a) ISOMETRIC VIEW OF DISPL. *10E -8 (M) Vs RADIUS (M) & TIME (msec)

THREE LAYER FLEXIBLE PAVEMENT

(Subgrade Stiffness = 30 MPa)

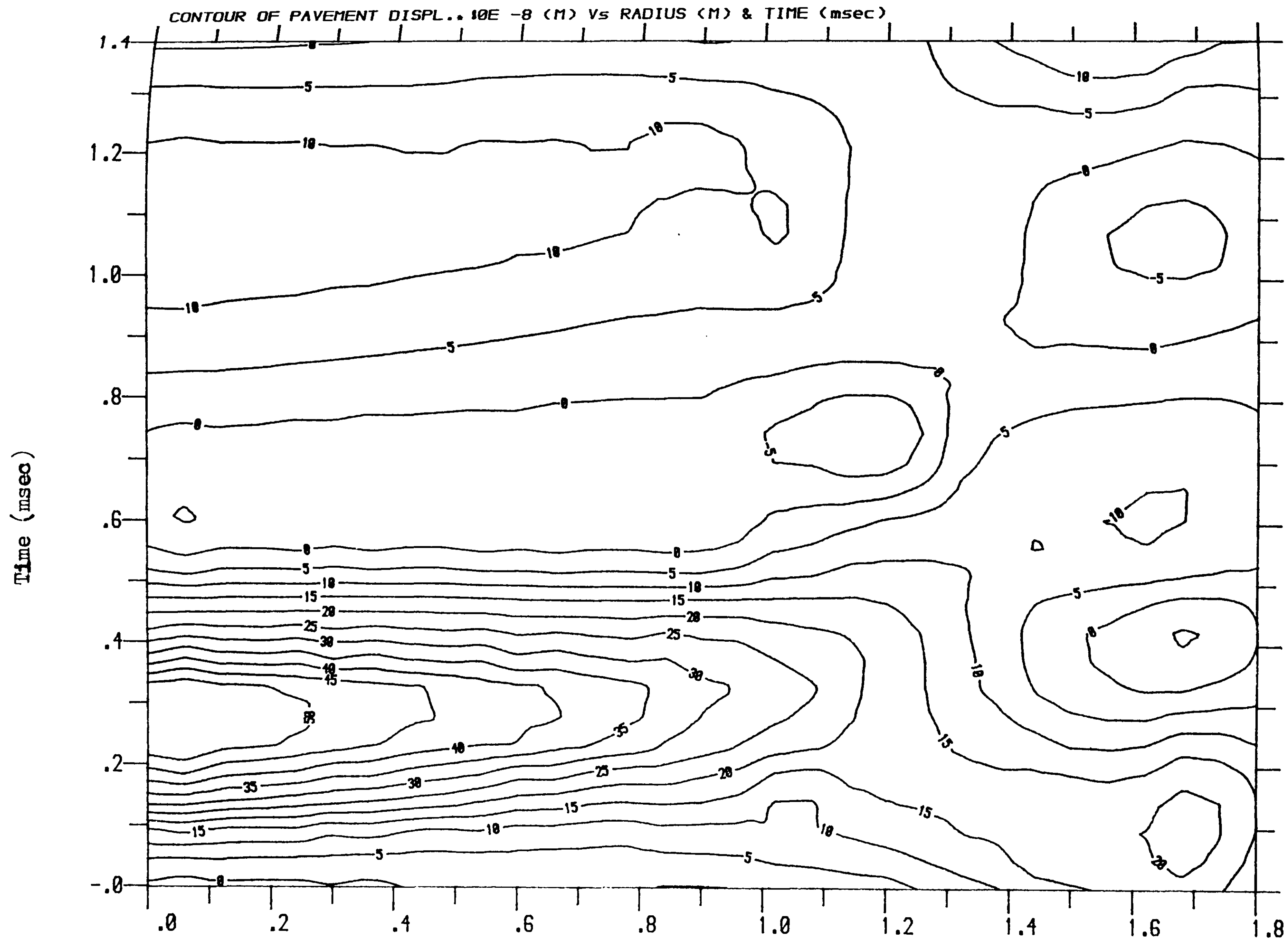

(FIG. 3.22b) X AXIS *1
Y AXIS *10^2

THREE LAYER FLEXIBLE PAVEMENT

(Subgrade Stiffness = 30 MPa)

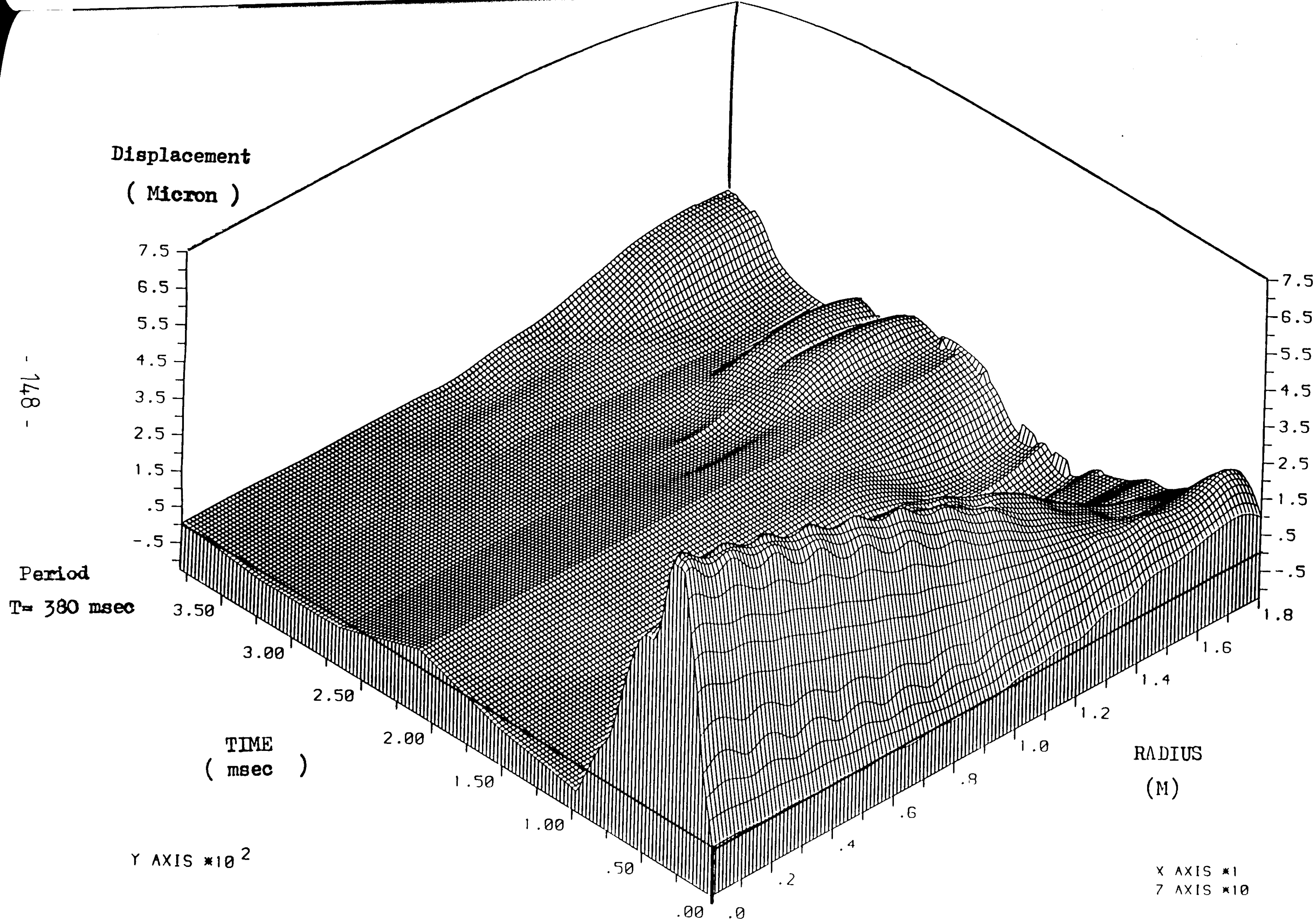

(FIG. 3.23a) ISOMETRIC VIEW OF DISPL.* 10E -8 (M) Vs RADIUS (M) & TIME (msec)

THREE LAYER FLEXIBLE PAVEMENT

(Subgrade Stiffness = 30 MPa)

CONTOUR OF PAVEMENT DISPL.* 10E -8 (M) Vs RADIUS (M) & TIME (msec)

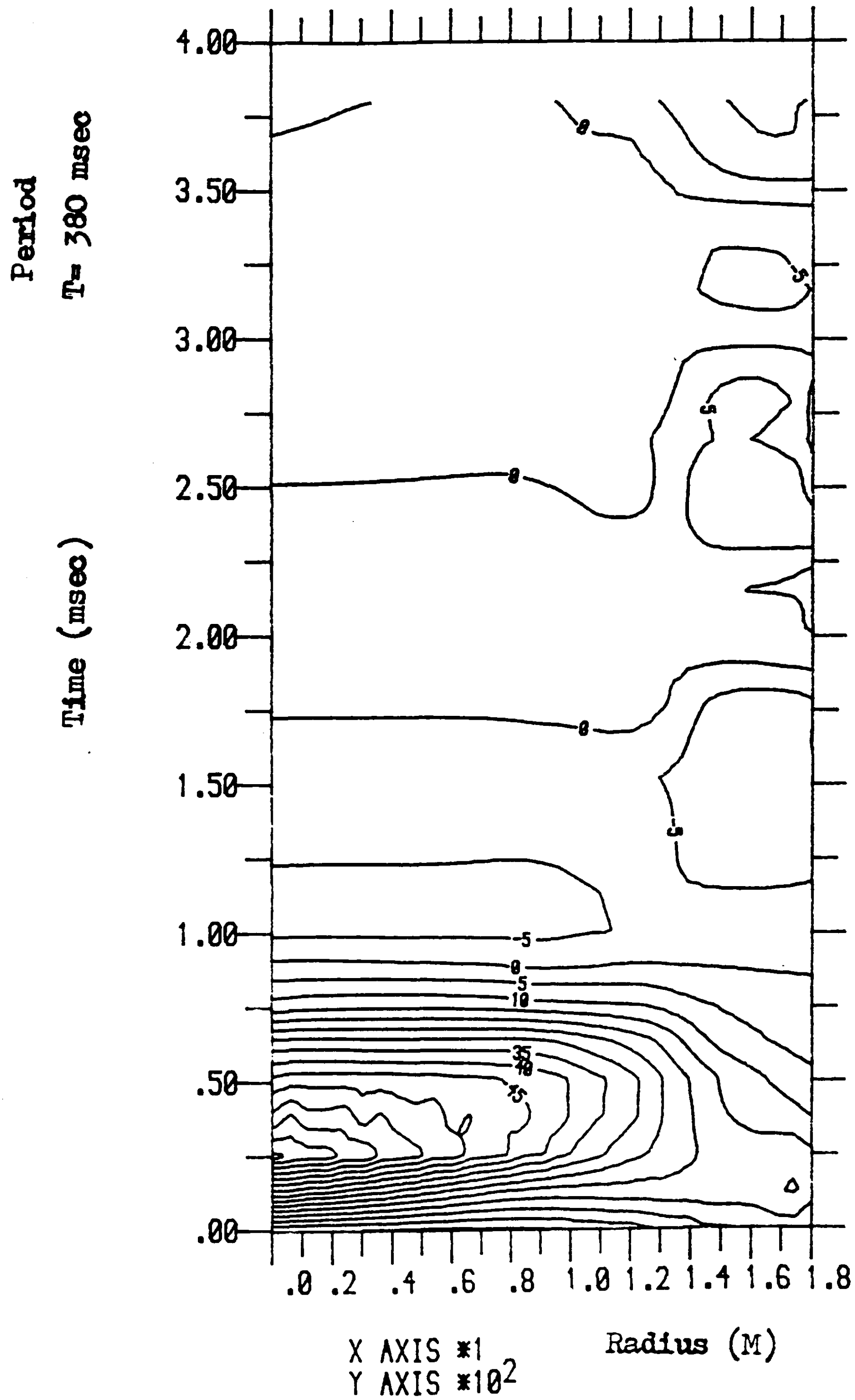

(FIG. 3.23.b) THREE LAYER FLEXIBLE PAVEMENT

(Subgrade Stiffness = 30 MPa)

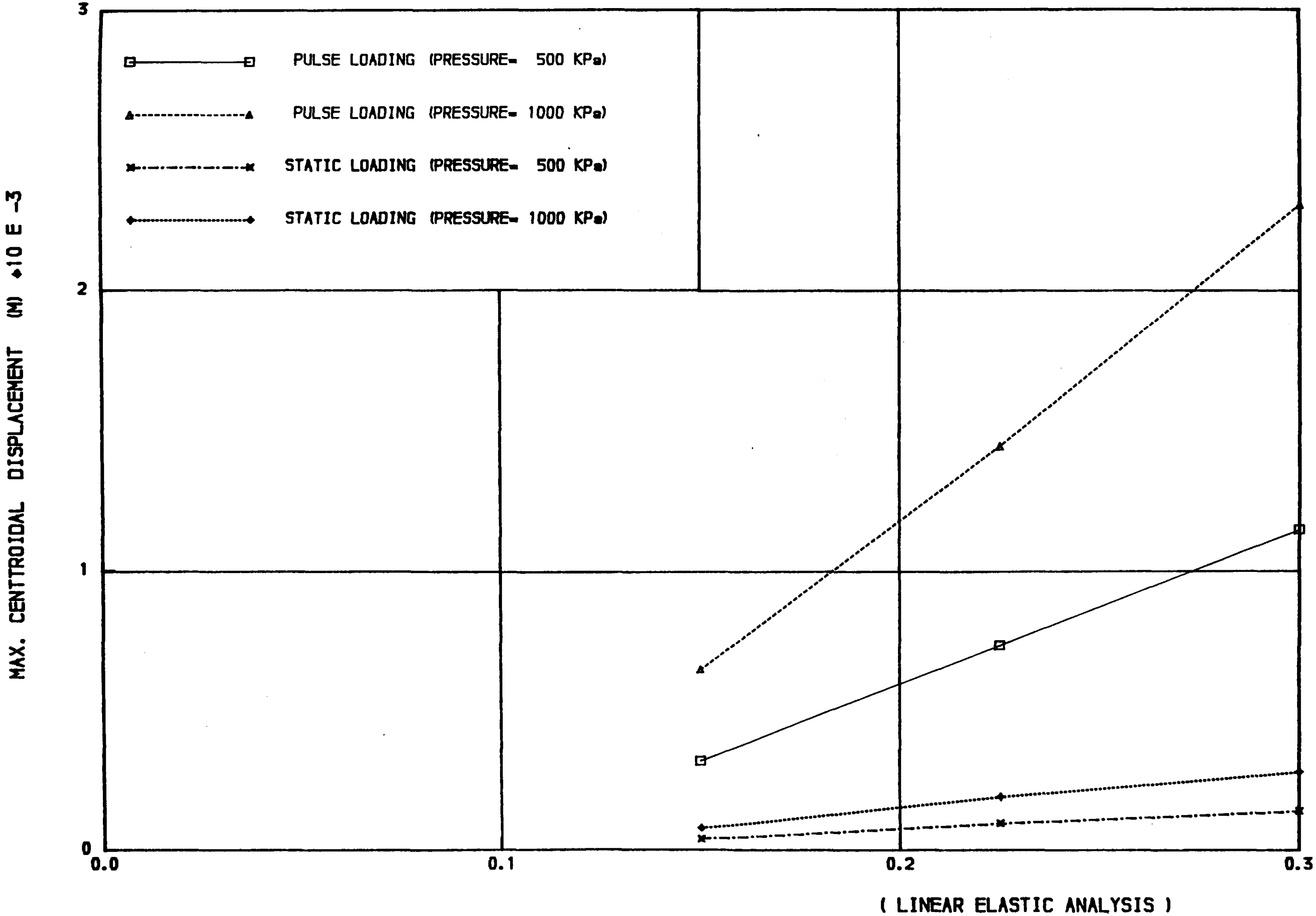

(FIG. 3.24) EFFECT OF CHANGE IN DISK RADIUS

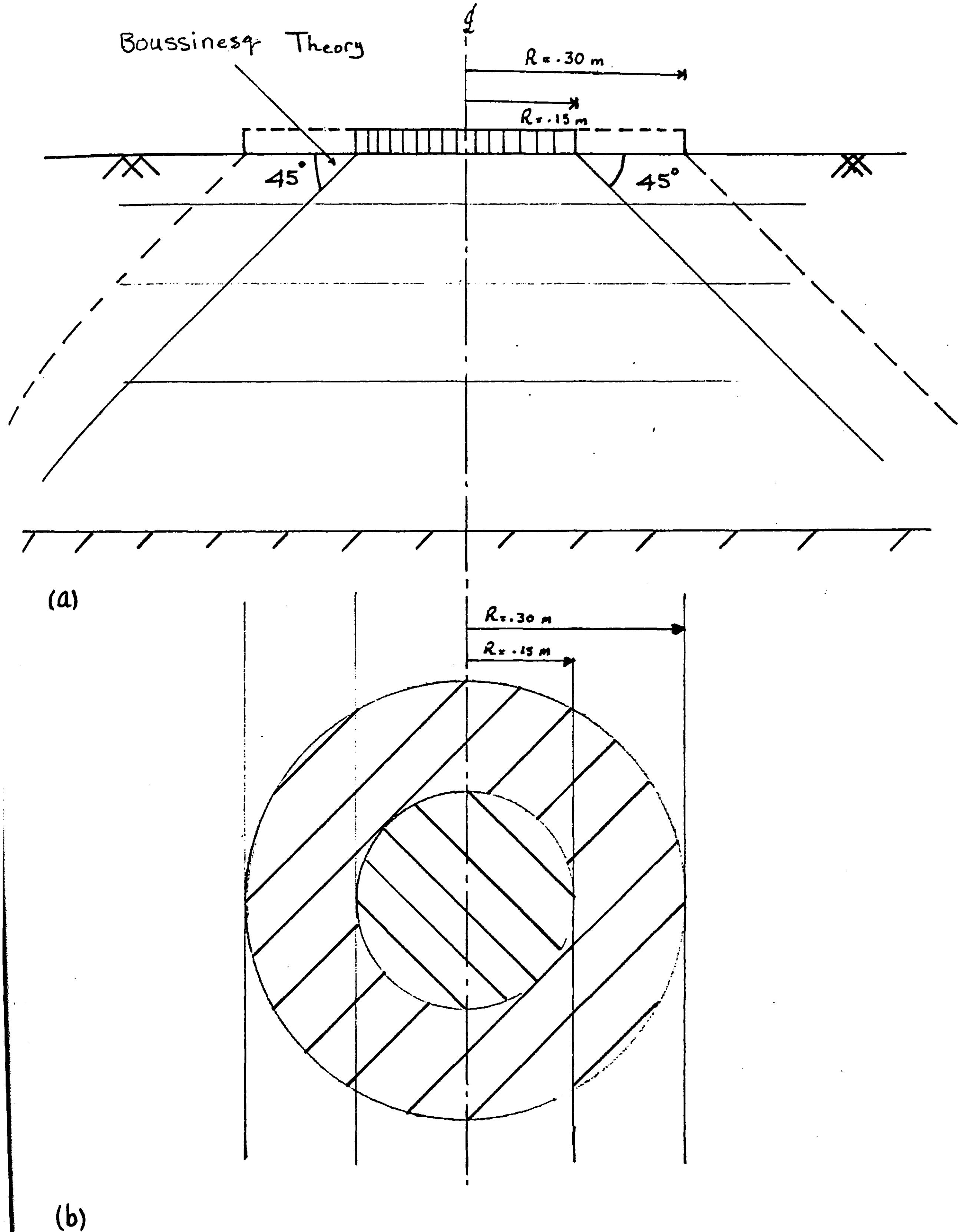

(Fig. 3.25) Effect of change in radius

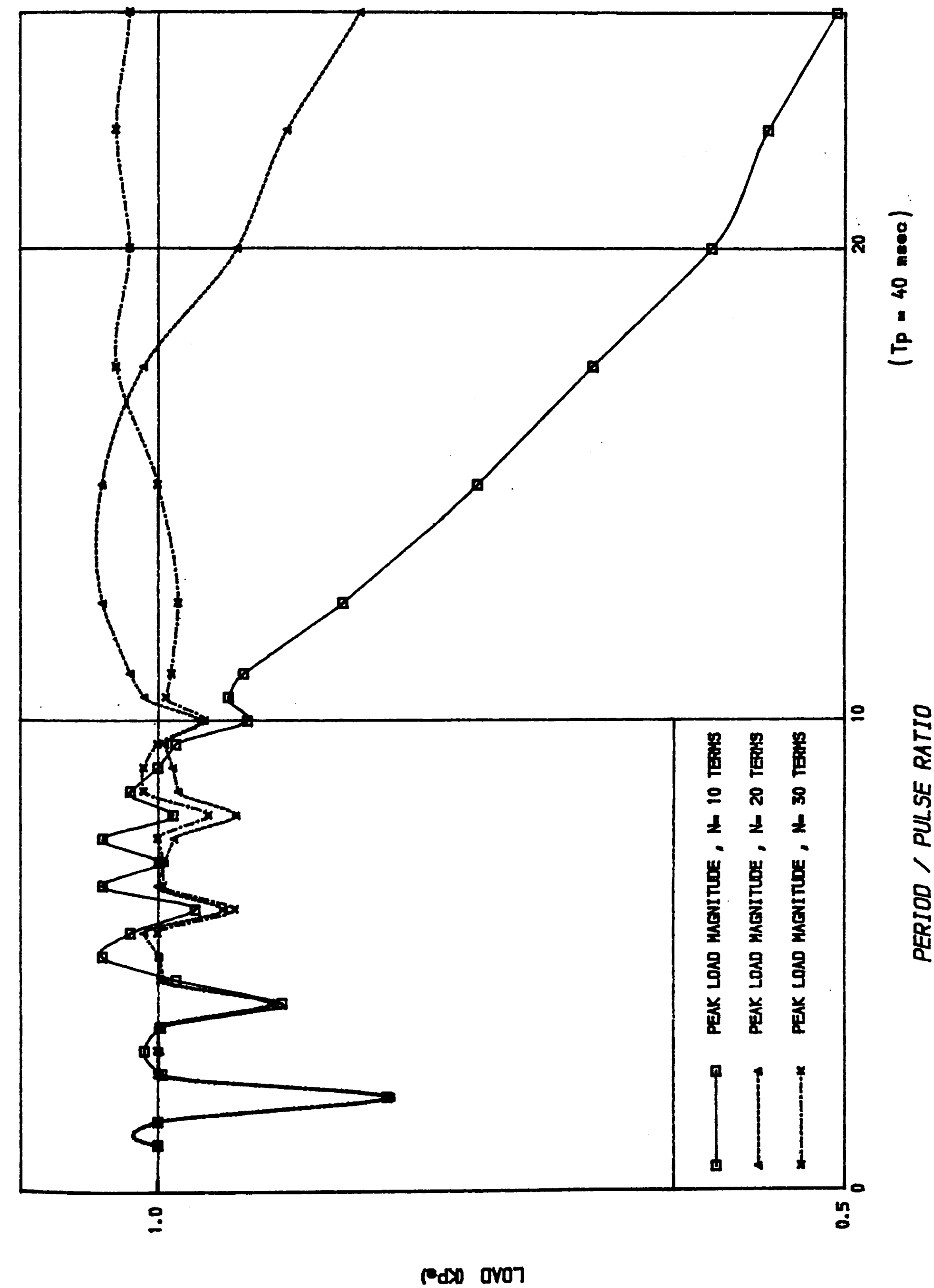
LOAD (KPa)
1.0
0.5
0
10
20
(Tp = 40 msec)
PERIOD / PULSE RATIO
PEAK LOAD MAGNITUDE , N= 10 TERMS
PEAK LOAD MAGNITUDE , N= 20 TERMS
PEAK LOAD MAGNITUDE , N= 30 TERMS

(FIG.3.26)

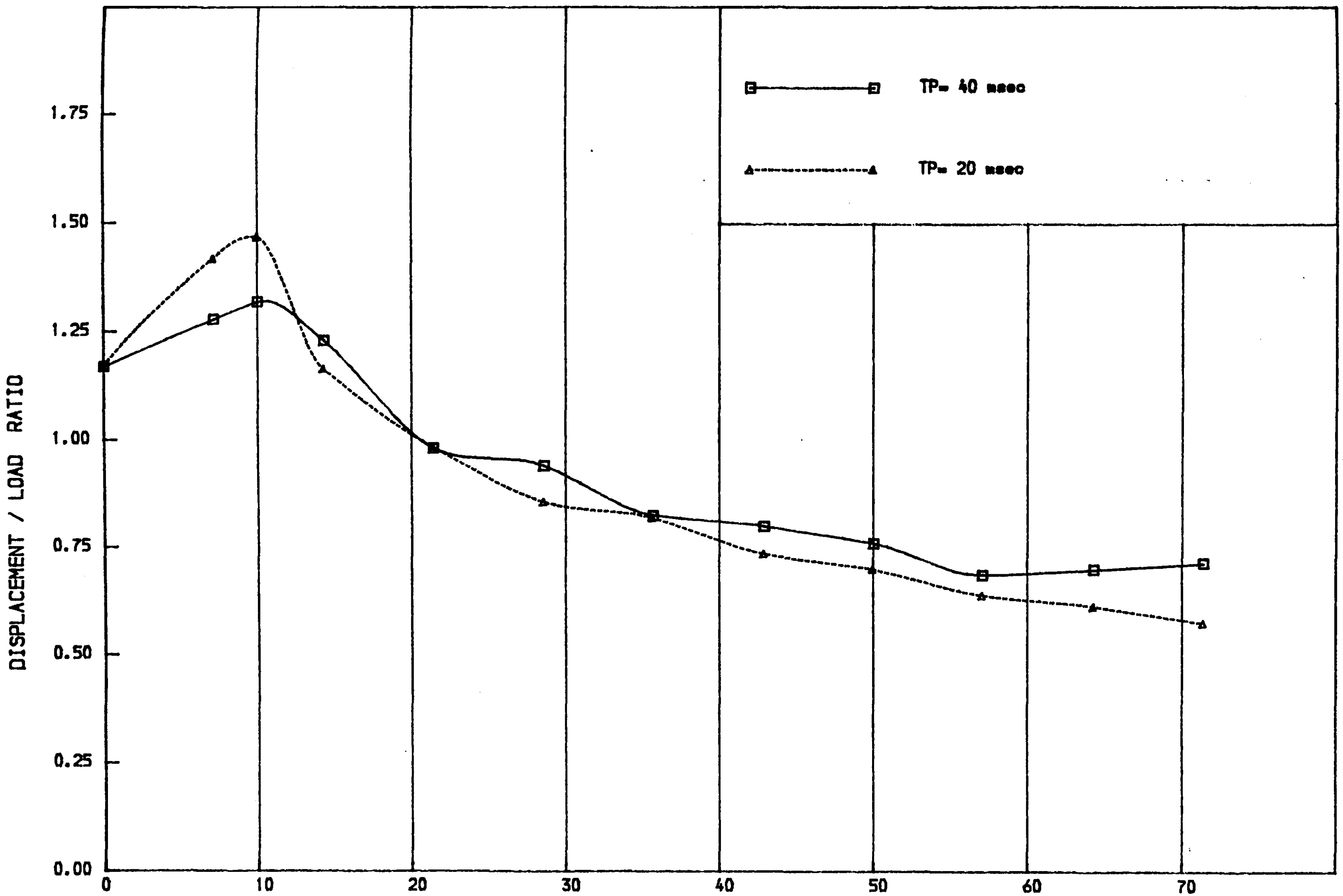

(FIG. 3.27a)

FREQUENCY (HZ)

SUBGRADE THICKNESS= 3.800 m

T= 140 msec

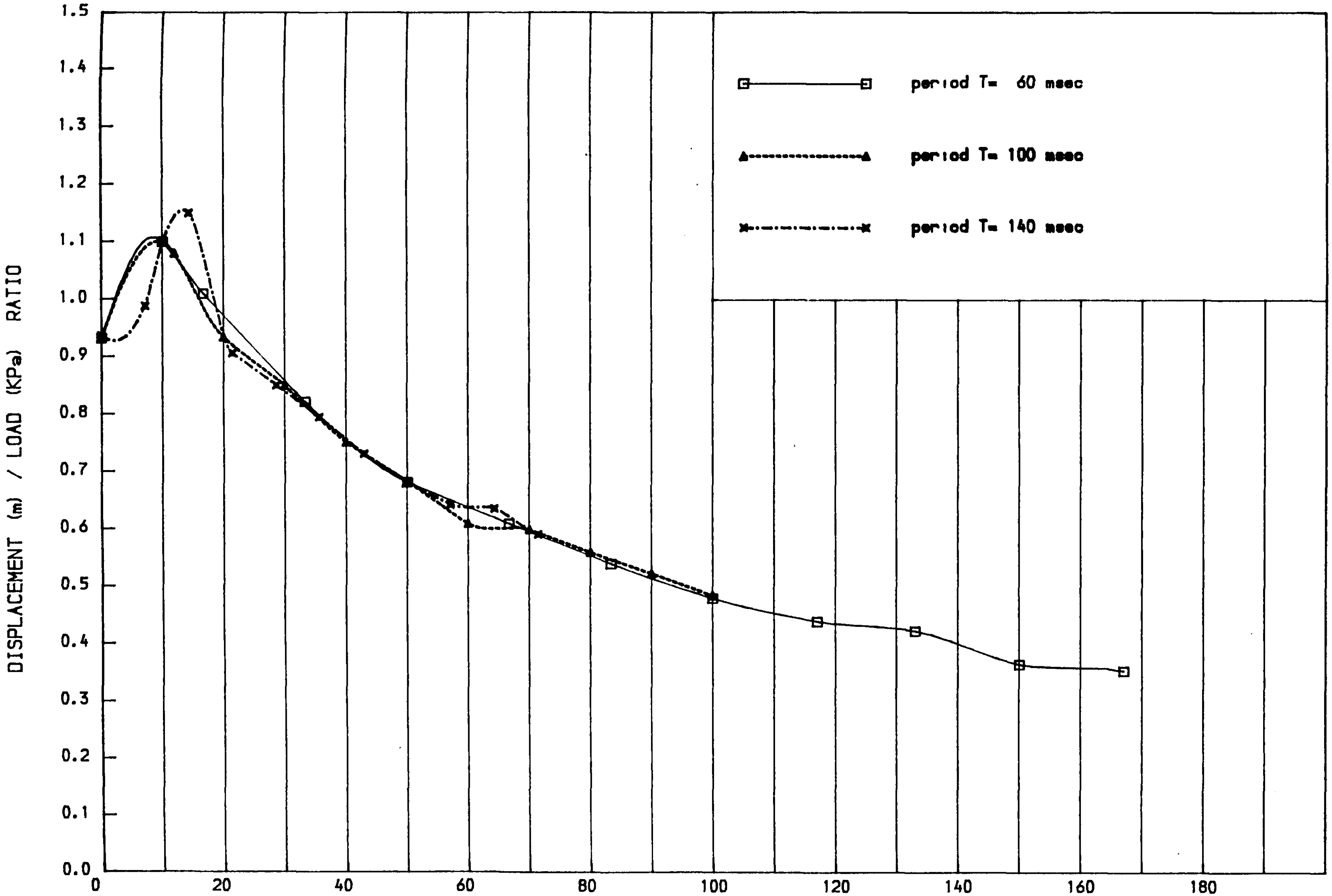

(FIG. 3.27.b)

TP= 40 msec (constant)

FREQUENCY (HZ)

SUBGRADE THICKNESS= 3.800 m

TIME	FUNCTION	FUNCTION VALUES			
sec.	$\sin(\pi/T_p)t$	N= 2	N= 4	N= 8	N= 16
0.00E+00	0.00E+00	3.89E−01	2.76E−01	1.08E−01	5.38E−02
4.00E−03	3.09E−01	4.42E−01	4.42E−01	2.93E−01	2.93E−01
8.00E−03	5.88E−01	4.85E−01	6.02E−01	5.36E−01	5.88E−01
1.20E−02	8.09E−01	5.18E−01	7.35E−01	7.85E−01	8.14E−01
1.60E−02	9.51E−01	5.38E−01	8.23E−01	9.71E−01	9.50E−01
2.00E−02	1.00E+00	5.44E−01	8.54E−01	1.04E+00	9.98E−01
2.40E−02	9.51E−01	5.38E−01	8.23E−01	9.71E−01	9.50E−01
2.80E−02	8.09E−01	5.18E−01	7.35E−01	7.85E−01	8.14E−01
3.20E−02	5.88E−01	4.85E−01	6.02E−01	5.36E−01	5.88E−01
3.60E−02	3.09E−01	4.42E−01	4.42E−01	2.93E−01	2.93E−01
4.00E−02	5.40E−06	3.89E−01	2.76E−01	1.08E−01	5.38E−02
7.00E−02	0.00E+00	−4.82E−02	−5.88E−03	−2.92E−03	−5.82E−03
1.00E−01	0.00E+00	−6.03E−02	−4.48E−02	−3.11E−03	−1.32E−04
1.30E−01	0.00E+00	9.55E−02	5.80E−02	−2.49E−03	3.44E−03
1.60E−01	0.00E+00	−6.03E−02	−4.48E−02	−3.11E−03	−1.32E−04
1.90E−01	0.00E+00	−4.82E−02	−5.88E−03	−2.92E−03	−5.82E−03
2.20E−01	0.00E+00	3.89E−01	2.76E−01	1.08E−01	5.38E−02

Table 3.1 - Fourier series Representation of Pulse Loading

Layer	Thickness h (mm)	Young's modulus E (MPa)	Mass density p (Kg/m3)	Poisson's ratio v	Damping β (%)
Surface	51	3 500	2 400	0.35	5
Base	153	700	2 320	0.40	5
Subbase	306	150	2 160	0.40	5
Subgrade	3 825	55	1 920	0.45	5

Table 3.2 Properties of a typical Four-layer flexible pavement [31].

Layer	Thickness h (mm)	Stiffness E (MPa)	Density p(Kg/m3)	Poisson's ratio v	Damping β (%)
Surface	100	1 200	2 300	0.35	5
Base	150	12 000	2 250	0.40	5
Subgrade	18 000	50	1 850	0.45	5

Table 3.3 Three-layer flexible pavement properties (Bement section) [42].

Layer	Thickness h (mm)	Young's modulus E (MPa)	Mass density p (Kg/m3)	Poisson's ratio v	Damping β (%)
Surface	51	3 500	2 400	0.35	5
Base	153	700	2 320	0.40	5
Subbase	306	150	2 160	0.40	5
Subgrade	3 825	55	1 920	0.45	5

Table 3.4 Properties of a typical Four-layer flexible pavement [31].

Scheme number	Subgrade sub-layers	Pavement sub-layers	Total sub-layers
1	3	7	10
2	5	10	15
3	8	12	20
4	10	15	25
5	12	18	30

Table 3.5 Pavement layer discretisation scheme

Layer	Thickness	Young's modulus	Mass density	Poisson's ratio	Damping
	h (mm)	E (MPa)	p (Kg/m3)	v	β (%)
Surface	200	40 000	2 400	0.20	5
Base	150	200	2 100	0.40	5
Subgrade	6 000	100	1 900	0.45	5

Table 3.6 Three-layer flexible pavement

Pavement layer	Number of artificial sublayers				
Surface	5	5	10	10	10
Base	5	10	5	5	10
Subgrade	15	10	10	15	10
TOTAL	25	25	25	30	30
D0 (microns)	0.717	0.717	0.717	0.718	0.718
D900 (microns)	0.430	0.430	0.430	0.432	0.431
D1800 (microns)	0.115	0.114	0.114	0.116	0.115

Table 3.7 Deflections at 0, 900 and 1800 mm from the centroid

Layer	Thickness h (mm)	Young's modulus E (MPa)	Mass density ρ (Kg/m3)	Poisson's ratio ν	Damping β (%)
Surface	100	4 000	2 400	0.35	5
Roadbase	200	1 000	2 300	0.40	5
Subbase	300	200	2 100	0.40	5
Subgrade	6 000	100	1 900	0.45	5

Table 3.8 Properties of a typical Four-layer flexible pavement.

Layer	Thickness h (mm)	Young's modulus E (MPa)	Mass density ρ (Kg/m3)	Poisson's ratio ν	Damping β (%)
Surface	200	10 000	2 400	0.30	5
Base	200	100	2 100	0.40	5
Subgrade	6 000	50	1 900	0.45	5

Table 3.9 Properties of a typical Three-layer flexible pavement.

Layer	Thickness	Young's modulus	Mass density	Poisson's ratio	Damping
	h (mm)	E (MPa)	p (Kg/m3)	v	β (%)
Surface	200	40 000	2 400	0.20	5
Base	150	200	2 100	0.40	5
Subgrade	6 000	100	1 900	0.45	5

Table 3.10 Properties of a typical Three-layer rigid pavement.

Layer	Thickness	Young's modulus	Mass density	Poisson's ratio	Damping
	h (mm)	E (MPa)	p (Kg/m3)	v	β (%)
Slab	200	40 000	2 200	0.20	5
Subgrade	6 000	100	1 900	0.45	5

Table 3.11 Properties of a typical Two-layer rigid pavement.

MAX. VALUE OF N USED IN THE TERMS OF THE F.S. 10

PULSE DURATION TP= 0.040 SEC
REST DURATION TR= 0.180 SEC

NO. OF INTERVALS IN THE PULSE PHASE 10
NO. OF INTERVALS IN THE RESTING PHASE 6

PEAK PRESSURE DUE TO THE PULSE= 1.00

TIME	FUNCTION	FUNCTION VALUES	COMPLEX FUNCTION (REAL)	COMPLEX FUNCTION (IMAG)
0.00E+ 00	0.00E+ 00	1.87E− 02	1.87E− 02	− 5.62E− 01
4.00E− 03	3.09E− 01	3.12E− 01	3.12E− 01	− 7.04E− 01
8.00E− 03	5.88E− 01	5.89E− 01	5.89E− 01	− 6.51E− 01
1.20E− 02	8.09E− 01	8.09E− 01	8.09E− 01	− 4.92E− 01
1.60E− 02	9.51E− 01	9.50E− 01	9.50E− 01	− 2.64E− 01
2.00E− 02	1.00E+ 00	9.99E− 01	9.99E− 01	1.27E− 06
2.40E− 02	9.51E− 01	9.50E− 01	9.50E− 01	2.64E− 01
2.80E− 02	8.09E− 01	8.09E− 01	8.09E− 01	4.92E− 01
3.20E− 02	5.88E− 01	5.89E− 01	5.89E− 01	6.51E− 01
3.60E− 02	3.09E− 01	3.12E− 01	3.12E− 01	7.04E− 01
4.00E− 02	2.65E− 06	1.87E− 02	1.87E− 02	5.62E− 01
7.00E− 02	0.00E+ 00	2.91E− 04	2.91E− 04	1.82E− 01
1.00E− 01	0.00E+ 00	− 3.97E− 04	− 3.96E− 04	1.87E− 02
1.30E− 01	0.00E+ 00	4.22E− 04	4.22E− 04	6.29E− 07
1.60E− 01	0.00E+ 00	− 3.97E− 04	− 3.97E− 04	1.87E− 02
1.90E− 01	0.00E+ 00	2.91E− 04	2.90E− 04	− 1.82E− 01
2.20E− 01	0.00E+ 00	1.87E− 02	1.87E− 02	− 5.62E− 01

Table 3.12 Fourier series representation of pulse loading for N = 10

CHAPTER FOUR RESULTS

4.1 INTRODUCTION

In this chapter, the effects of changes in pavement layer stiffnesses and thicknesses on pavement response to Falling Weight Deflectometer testing are investigated. The study encompasses two types of pavement (Flexible and Rigid) consisting of various numbers of layers. A large number of dynamic and static deflection basins as well as their corresponding magnification factors are presented. The results of these parametric studies are used to develop design charts.

4.2 PARAMETRIC STUDIES

4.2.1 The study of major pavement parameters

In this study, the two major pavement parameters, namely, elastic modulus (E) and layer thickness (h) are investigated. Figs. 4.1.a-4.1.d show typical stiffness profiles, in a qualitative sense, for flexible pavements while Figs. 4.1.e and 4.1.f depict layer profiles for rigid pavements.

The layer stiffnesses and thicknesses used in the parametric study are presented in Tables 4.1.a-4.4.b. The displacement responses of typical Four-Layer Flexible Pavements (4LFP) with various layer stiffnesses and thicknesses to (1.0 KPa) FWD loading are shown in Figs. 4.2.a-4.5.b (stiffness variations) and Figs. 4.6.a-4.9.b (thickness variations). Similar results are also presented for Three-Layer Flexible Pavements (3LFP), (Figs. 4.10.a-4.15.b) ; Three-Layer Rigid Pavements (3LRP), (Figs. 4.16.a-4.21.b) and Two-Layer Rigid Pavements (2LRP), (Figs. 4.22.a-4.25.b).

In the layer stiffness analyses of the above pavements, the effect of changes in the stiffnesses of individual layers on the (surface) displacement response were investigated. That is, the stiffnesses Ei (where i represents the layer number and ranges from 1 to 4) of each individual layer is both doubled (100%) and halved (50%), (Table 4.1.a-4.4.a), (100% and 50% represent a very sound and a deteriorated pavement layer, respectively). For each case, two deflection bowls (dynamic and static deflections at various radial points) as well as the corresponding magnification factors M (Dynamic deflection / Static deflection) are shown.

Fig. 4.2.a. shows the result of an analysis of the effects of changes in the stiffness of the surface layer (E1) on the response of the 4LFP. It can be seen that for all values of surface moduli (E1), dynamic deflections are greater than their static counterparts by approximately 5% at the centroid and up to 25% at points remote from the loaded area (with the exception of D1500, the deflection at 1500 mm from the centroid). This result is clearly depicted in Fig. 4.2.b, where the magnification factor M is plotted as a function of radius. From Fig. 4.2.a it is apparent that for a 50% reduction in the surface stiffness, about 10% increase in both dynamic and static deflections is produced in the vicinity of the loaded region. The significant changes in the dynamic and static deflections (due to changes in the surface stiffness) in the loaded region, suggest that surface stiffness controls the surface deflections over a distance of about 300 mm from the centroid.

Similarly, in the roadbase stiffness (E2) analysis of 4LFP, (Figs. 4.3.a-4.3.b) the dynamic deflections are greater than the static by about 5-25% over a distance of 1800 mm from the centroid (with the exception of D1500). For a 50% reduction in the roadbase stiffness, a 20-30% increase in both dynamic and static deflections takes place. From this analysis, it is evident that roadbase stiffness controls the surface deflection over a wider span (0 - 600 mm).

Similar features are observed for (4LFP) subbase stiffness (E3) analysis, (Figs. 4.4.a-4.4.b).

The layer which contributes most significantly to the surface deflection is the subgrade layer [5]. Fig. 4.5.a illustrates the computed deflection bowls for various (4FLP) subgrade stiffnesses. It can be seen that changes in the subgrade stiffness result in significant changes to the whole dynamic (static) deflection bowl. Quantitatively, a 50% reduction in the subgrade stiffness results in a 25-30% increase in the deflections (0-1800 mm) which suggests that in the development of any pavement evaluation method, the elastic characteristics of the subgrade (i.e. its stiffness) must be accurately modelled.

In the layer thickness analyses of these pavements, the thicknesses of the individual layers hi (i = 1 - 4) are also doubled and halved (Table 4.1.b-4.4.b) and the effect of such changes on the shape of the dynamic (static) surface displacements (deflection bowls) are investigated. For each case, magnification factors are also plotted.

In the analysis of the 4LFP, changes in the dynamic (static) surface displacements resulting from changes in the surface thickness (h1) occur over greater radial distances (approximately 0-900 mm from the centroid),

(Fig. 4.6.a). Dynamic deflections are again greater than those of the static by about 5-25% (Fig. 4.6.b). Similar features are also observed for variation in the roadbase thickness (h2), (Figs. 4.7.a-4.7.b). Changes in the subbase and subgrade thicknesses (h3 and h4, respectively) have very little influence on the magnitude of the deflection bowls. Nonetheless, the dynamic deflections exceed those of the static by about 10-30% (Figs. 4.8.a-4.9.b).

Tables 4.5.a-4.8.b illustrate the effect of changes in both stiffness and thickness on the overall displacement response while Figs. 4.26.a-4.27.d show the effect of changes in both stiffness and thickness on the peak centroidal displacement (only) for various types of pavement (4LFP, 3LFP, 3LRP and 2LRP).

From Figs. 4.26.a- 4.26.d and Figs. 4.27.a- 4.27.d, it is apparent that, in most cases, changes in both stiffnesses and thicknesses of the intermediate layers (roadbase and subbase) with the exception of 4LFP have almost negligible influence on the centroidal deflection Do. Thus, more attention was devoted to the effect of changes in surface and subgrade stiffnesses and thicknesses on the FWD response. This is described in Section 4.3. 'Design charts'.

4.3.2 The study of minor pavement parameters

1/ Poisson's ratio (v) - In the analysis and prediction of pavement response to loading, this quantity exerts far less influence on the overall results than the corresponding variations in layer stiffnesses [25,42]. Therefore, typical Poisson's ratio values may be assumed for various pavement materials without introducing excessive error. In this study, Poisson's ratios in the range of 0.2-0.45 were assumed for the individual layers of various pavements.

2/ Mass density (p) - During some preliminary investigation into the effect of various pavement parameters on the displacement response, the influence of the mass density (within the practical bounds) on the overall results was found to be negligible, especially at low loading frequencies. For the purpose of this study, the mass densities of the surface, roadbase, subbase and subgrade layers were assumed to be 2400, 2300, 2100 and 1900 Kg/m3, respectively [31].

3/ Temperature (T) - Temperature variations in pavements can easily be accommodated in the computer program PULSE by specifying pavement layer stiffnesses appropriate to the ambient temperatures. In general, pavement layer stiffness values could be expressed as a function of temperature. In the previous Section, the values of Young's moduli corresponded to temperatures ranging from 5-20 Degrees C [9,11,39,44,53].

4.2.3 Discussion

The deflections at remote points from the loaded area are primarily governed by the stiffnesses of the deeper layers. There are some ranges of depth to bedrock for which the difference in dynamic effects at various points (in this study, at 1500 mm from the centroid) may lead to an erroneous estimate (by -40%) of the elastic moduli. Figs. 4.28.a-4.29.b show the deflection basin's history as well as the evolution of these distortions. Moreover, the phase difference between load and pavement response is larger at greater distances from the centre of the base plate (Fig. 4.30).

The ratio (M) of dynamic to static deflection versus radial distance shown in the preceding section for pavements subjected to impulse loadings of 40 msec show that the dynamic deflections initially increase smoothly with increase in distance from the loading area but thereafter decay and in many cases form a trough at 1500 mm radius. It is unclear whether this phenomenon is a faithful reflection of reality or some peculiarity arising out of the numerical modelling. Some studies on this point have shown that the phenomenon is remarkably persistent but there has been insufficient time to provide a definitive answer to date and further work in this area is needed.

Clearly, the deflection ratios are not the same at all radial locations. Figs. 4.31.a and 4.31.b show that for a typical three layer flexible pavement, the deflection ratios tend to increase with increase in distance away from the load and decrease with increase in the loading frequency.

4.3 DESIGN CHARTS

Deflection interpretation charts were derived from a comprehensive parametric study which involved the investigation of the effect of variations in pavement layer stiffnesses and thicknesses on pavement response to FWD loading. Several combinations of material stiffnesses and layer thicknesses for various types of pavements were analysed for this purpose. Tables 4.9.a - 4.12.b give details of the parameters used in this study, from which a series of charts for dynamic and static pavement response to the FWD were plotted and are described in the sequel.

4.3.1 Stiffness and thickness charts

4.3.1.1 Surface stiffness - Subgrade stiffness charts

From the study of the deflection basins described earlier, it is apparent that the deflection at a radial distance of 1800 mm (D1800) is largely influenced by the subgrade stiffness while the surface stiffness can be approximately characterised by the slope of the deflection basin, (i.e. quantified by the deflection difference (D0 - D900) [5]). Figs. 4.32.a and 4.32.b represent the surface deflection (D0 - D900) versus subgrade deflection (D1800) for various combinations of surface and subgrade stiffnesses of four-layer flexible pavements subjected to static and FWD loading, respectively. Figs. 4.33.a - 4.35.b show similar charts for three-layer flexible pavements, three-layer rigid pavements and two-layer rigid pavements, respectively.

4.3.1.2 Surface thickness - Subgrade stiffness charts

It was noted earlier that variations in subgrade thicknesses (of practical dimensions) had little influence on the shape and magnitude of deflection bowls. This being so, 'Thickness Charts' were produced for various surface thicknesses and subgrade stiffnesses. Figs. 4.36.a and 4.36.b present surface deflection (D0 - D900) versus subgrade deflection (D1800) for various combinations of surface thicknesses and subgrade stiffnesses of four-layer flexible pavements. Figs. 4.37.a - 4.39.b show such variations for three-layer flexible pavements, three-layer rigid pavements and two-layer rigid pavements, respectively.

4.3.2 Interpretation of charts

4.3.2.1 Chart features

Before analysing the stiffness and thickness charts in more detail, it is worth highlighting some features related to these charts. For constant subgrade stiffnesses, dynamic deflections (D0 - D900) for surface stiffnesses and thicknesses are less than those for static loading. For very stiff surface layers (E1) however, static and dynamic deflections (D0 - D900), (Fig. 4.40.a) coincide.

The latter statement is also valid for very thick surface layers (h1), (Fig. 4.40.b). Under such conditions, the magnification factor M at the vicinity of the loaded area (see also earlier deflection bowls) is expected to approach unity. Another feature of both stiffness and thickness charts is the resulting adverse effect on the dynamic deflections (D1800) when subgrade stiffness values approach the 'soft' range. That is, dynamic deflections (D1800) are greater than those for static loading for subgrade stiffnesses greater than 30 MPa (100 MPa) for flexible (rigid) pavements (Fig. 4.40.c). Conversely, dynamic deflections (D1800) are less than those for static loading for subgrade stiffnesses less than or equal to these values. This indicates that for low subgrade stiffnesses, magnification factors at 1800 mm from the centroid are less than unity. It also confirms the earlier deduction that the deflections at remote points from the centroid are generally governed by the stiffnesses of the deeper layers, particularly the subgrade.

4.3.2.2 Chart analysis

The stiffness and thickness charts may be analysed in two ways;

(a) Static and dynamic (stiffness and thickness) charts are compared by superposing the static charts on their dynamic counterparts,

(b) The effects of a typical error in FWD displacement measurements (e.g. by 10%) on both static and dynamic charts are examined.

To carry out the above analyses, it was necessary to study a limited number of points (five) on the charts (defined in Table 4.13).

4.3.2.3 Comparison of static and dynamic charts

Tables 4.14.a-4.17.b show the percentage difference obtained from the comparison of static and dynamic charts shown in Figs. 4.32-4.35 (stiffness charts) and Figs. 4.36-4.39 (thickness charts). E1, E2, E3 and E4 represent surface, base, subbase and subgrade stiffnesses, respectively and h1 is the surface thickness. Fig. 4.41 shows the percentage error in over/underestimation of surface and subgrade stiffnesses, (for four different pavements under study) whilst Fig. 4.42 shows the percentage error in surface thicknesses and subgrade stiffnesses for each of the five specified locations on the charts. It is interesting to observe from these two charts that almost all the computed errors are less than 30%. Table 4.18 shows that for all four types of pavements, surface stiffnesses are overestimated while subgrade stiffnesses are underestimated (with the exception of location 2). Location 2 represents a region of low stiffness (soft) for both surface and subgrade layers. Further careful investigation revealed the occurrence of convergence failure at low frequencies (5-15 Hz) for pavements with soft surfaces and soft subgrades and, therefore, the results for this location should be treated with caution. Table 4.19 also shows a similar trend; overestimation of surface thicknesses and underestimation of subgrade stiffnesses (with the exception of location 4). Location 4 represents a region of thick surface and soft subgrade layers. In this case, the peak displacements lagged the load by more than 20 msec, perhaps resulting in erroneous results since a relatively short quiescent period (100 msec) had been specified in this work. In any case, the study revealed that the response of pavements to dynamic loading is significantly different from their response to static loading. The results show that, in general, static analysis of the FWD overestimates the stiffnesses and thicknesses of surface layers and underestimates the stiffnesses of subgrade layers (for all four types of pavements studied) by approximately 20-30%.

4.3.2.4 Chart sensitivity

The effects of a typical 10% error in the FWD displacement measurements (D0, D900 and D1800) on pavement properties (stiffnesses and thicknesses) have been investigated in order to shed light on the effectiveness of back-analysis procedures. Figs. 4.32.a-4.39.b show the subsequent locations (1 - 5, shown by oblique arrows) of (D0 - D900) and D1800 after the occurrence of 10% (prescribed) error. The 'apparent' stiffness (thickness) values for various types of pavements are then compared with the 'true' stiffness (thickness) values. Tables 4.20.a-4.23.b show the percentage error in surface and subgrade stiffnesses as well as surface thicknesses and subgrade stiffnesses (for all types of pavements) incurred by 10% deviation in FWD deflection [(D0 - D900) and D1800] measurements. E'1, E'2, E'3 and E'4 are the surface, base, subbase and subgrade stiffnessses respectively, resulting from the above deviation and h'1 is the corresponding surface thickness. The results of the analyses are depicted in Figs. 4.43-4.46 (obtained from stiffness charts) and Figs. 4.47-4.50 (obtained from thickness charts).

From Tables 4.20.a-4.23.b it is apparent that a 10% error in FWD deflection measurements will result in percentage errors in surface stiffnesses (on both static and dynamic charts) in the range of 10-40% for flexible pavements and 0-20% for rigid pavements. Also a 10% error in FWD deflection measurements will result in percentage errors in subgrade stiffnesses (on both static and dynamic charts) in the range of 5-30% for both flexible and rigid pavements. Similarly, a 10% error in the FWD measurements will result in percentage errors in surface thicknesses and subgrade stiffnesses in the range of 0-30% for both flexible and rigid pavements. The results of the analyses are depicted in Figs. 4.43- 4.46 (obtained from stiffness charts) and Figs. 4.47-4.50 (obtained from thickness charts). For all the above cases, region 3 (stiff thick surface layers and stiff subgrades) was found to produce the least percentage error.

4.3.2.5 Deflection interpretation chart

The response of pavements to test loads has been characterised in terms of shapes of their deflection bowls [5,8,22]. One parameter used for this purpose is the ratio (Qr) between the deflection (Dr) in microns at a distance r in mm from the load to the deflection (Do) under the centre of the load (the ratio Qr is chosen instead of the radius of curvature because Qr can be measured more easily), Fig. 4.51.a. The distance r, which depends upon the type of pavement, is chosen such that Qr is about 0.50-0.60. Fig. 4.51.b shows the deflection interpretation chart for a typical three-layer flexible pavement (data obtained from Tables 4.2.a and 4.2.b) which illustrates the relationship between surface stiffness (E1) in MPa, surface deflection (Do), Q600 and surface thickness (h1) for predetermined values of base thickness (h2), subgrade stiffness (E3) and applied load, P (KPa). Similar charts (based on static analyses only) with the wider range of h1, E1 and Qr have been given in References 8, 9, 27 and 28. With Do and Q600 (the ratio of D600 to D0) measured, two unknown properties of the pavement (E1 and h1) can be determined if the base layer thickness (h2) and subgrade stiffness (E3) are known. The base stiffness (E2) can be obtained using the empirical relationship described by Dormon and Metcalf

[14] ;

$$E2 = K \cdot E3 \qquad (4.1)$$

where $$K = 0.206\,(h2)^{0.45} \qquad (4.2)$$

for $$2 < K < 4$$

with E2 and E3 in MPa and h2 in mm.

Fig. 4.51.b clearly shows that for all values of Q600, there is a distinct difference (10-20%) between the static and dynamic deflection profiles. When similar charts [8,9,27,28] are employed in the determination of structural properties of pavements (surface and base stiffnesses, in this case), the validity of (statically based) charts and the accuracy of the method of interpretation should be viewed with caution.

4.3.2.6 Concluding remarks

The results obtained in this section show that static analyses of the FWD overestimate the stiffnesses and thicknesses of the surface layers and underestimate the stiffnesses of the subgrade layers (for all four types of pavements studied) by approximately 20-30% in many cases.

A desk study carried out to investigate the effects of error in (Do - D900) and D1800 on pavement properties showed that small experimental errors can lead to large errors in the determination of pavement properties such as stiffness and thickness. The relatively large percentage error in the corresponding charts resulting from 10% deviation in the FWD deflection measurements is at variance with rather optimistic claims [25] that surface and subgrade stiffnesses can be determined using back-analysis procedures (described in detail in Chapter One) within 10% and 3%, respectively. The study also showed that for practical purposes, the 'optimum design region' i.e. location 3 (stiff thick surface layers and stiff subgrades)yield the lowest errors in the determination of pavement properties.

4.3.3 SUBGRADE ANALYSIS

4.3.3.1 Subgrade thickness

Fig. 4.52 shows the effect of changes in subgrade thickness on the dynamic response of pavements. The data employed were taken from Table 4.2.b (see Figs. 4.15.a and 4.15.b for the corresponding deflection basins and magnification factors, respectively). When subgrades are shallow, resonances occur and the dynamic deflections greatly exceed those obtained under static loading conditions. The fundamental frequency (i.e. the first harmonic mode) is almost inversely proportional to the depth of the subgrade, implying that resonance occurs primarily within the subgrade layer. The following semi-empirical equation appears to predict the resonant frequency reasonably well [12];

$$f = 0.4\ Cs\ /\ H \qquad (4.3)$$

where f = resonant frequency

Cs = shear wave velocity of the subgrade layer

H = subgrade thickness

Subgrade thicknesses of 3, 6 and 12 metres were used for this study and the frequencies at which resonance occurred were approximately 13, 6 and 3 Hz, respectively. The resonant response at the second harmonic is far less pronounced.

4.3.3.2 Subgrade stiffness

Figs. 4.53 - 4.57 illustrate the influence of subgrade stiffness on pavement response to FWD loading. This effect is shown for various values of surface layer stiffnesses but constant subgrade thicknesses. Data were taken from Table 4.10.a. It is apparent that subgrades with low stiffnesses (< 50 MPa) have low magnification factors, but magnification factors tend to increase as surface stiffnesses decreases. Using the data from Table 4.10.a, the effect of subgrade stiffness on the deflections of the outermost sensor (D1800) for various values of surface thicknesses (h1) was investigated (Fig. 4.58). The results revealed large differences between the deflections predicted by static and dynamic analyses, particularly for flexible subgrades. McCullough and Taute [32] produced comparable charts based on static analyses. Based on an extensive parametric study, they found that the subgrade stiffness could be determined accurately from the deflection of the outermost sensor alone. By reference to Fig. 4.58, it is evident that this static interpretation of deflection measurements would lead to an error of (approximately) 30-40% in the prediction of subgrade stiffnesses.

Evidently in order to predict surface deflections accurately, the elastic characteristics of subgrade in particular must be modelled as accurately as possible. Brown [5] modelled the subgrade by a series of sub-layers, each with different elastic stiffnesses appropriate to the effective overburden stresses and load induced stresses at the relevant depths. The stiffness profile is shown in Fig. 4.59. The subbase was assumed to be 200 mm thick and its Young's modulus was 100 MPa. Brown presented a series of charts to determine (by back-analysis) pavement stiffnesses from measured deflection bowls. The formation stiffness (E_f) was related to D1800 while the stiffness of the roadbase (E_b) was related to (D0 - D900). The flexural stiffness of the base was conveniently represented by the parameter $E_b * h_b^3$. Fig. 4.60 shows a relationship between the parameters $E_b * h_b^3$, D1800 and E_f. An initial seed value of E_b is used with the measured values of h_b (from coring) and D1800 to determine a first estimate of E_f from Fig. 4.60 . Fig. 4.61 is then entered with the value of (D0 - D900) to determine E_b. The procedure is repeated until convergence is achieved. These results are of course derived from a static analysis of the FWD tests.

Using the computer program PULSE these analyses have been repeated in order to evaluate the influence of pavement inertia on the results. The pavement shown in Fig. 4.59 was analysed as an example. Only formation stiffnesses (E_f) of 50 MPa for base thicknesses (h_b) of

200 mm and 500 mm were analysed. The results are presented in Figs. 4.60 and 4.61. In Fig. 4.60 the static deflections closely correlate with those for Brown's for both 200 mm and 500 mm thick bases. The static deflections for the corresponding thicknesses tend to diverge from those for Brown's as the base stiffness 'softens'. In other words, a 150% increase in the base thickness will result in a 5-10% decrease in the deflection (at radius 1800 mm) for low base stiffnesses. Although the percentage error incurred in the deflection (D1800) is not excessive, it reveals the dependence of the deflection profiles on the base thicknesses. Thus, care should be exercised when employing the developed charts for pavements with soft base layers. There is good correlation between the static results for (D0 - D900) obtained in this study and those for Brown's depicted in Fig. 4.61. Again the differences between dynamic and static profiles come into focus at low stiffness values of the base layer E_b indicating the influence of pavement inertia.

4.4 CONCLUSIONS

A comprehensive parametric study of major pavement parameters (stiffness and thickness) has been conducted in this chapter in which the effect of changes in pavement layer stiffnesses and thicknesses on pavement response to FWD testing have been examined. Investigation of design charts (developed from parametric studies) revealed that the response of pavements to dynamic loading is significantly different from their response to static loading. Static analyses of the FWD yield surface stiffness (thickness) values approximately 20-30% higher and subgrade stiffness values 20-30% lower than those obtained using the elasto-dynamic analyses; these differences are primarily due to the inertial forces in the pavement.

In the study of pavement subgrades, it was found that resonances arise principally in the subgrade and can be quite marked for shallow subgrades.

Structural stiffness of the layers:-

Flexible pavements -

i) Four layer system:-

a) Trunk Road

STIFF

VERY STIFF

SOFT

VERY SOFT

(Fig. 4.1.a)

b) Motorway Access

STIFF

MEDIUM

SOFT

VERY SOFT

(Fig. 4.1.b)

c) Most common four layer pavements for design purposes:-
In this system the modulus of elasticity decreases from top to bottom - values depend on the boundary conditions, e.g. [48]

E(MPa) SEMI-INFINITE		E(MPa) RIGID BOTTOM
37,250	VERY STIFF	34,000
3,400	STIFF	2,600
1,200	MEDIUM	350
250 ↓ ∞	SOFT	175

(Fig. 4.1.c)

ii) Three-layer system:-

WEARING (HRA) 40%

VERY STIFF (HRA) 60%

(SUBBASE) MEDIUM

SOFT
(SUBGRADE)

(Fig. 4.1.d) / / / / / /

Rigid Pavements:-

i) Three-layer system - Heavy duty roads and runways

SLAB ^^^^ EXTREMELY STIFF
^^^^

SUBBASE SOFT

SUBGRADE SOFT

(Fig. 4.1.e.) / / / / / /

ii) Two-layer system - Airport runways and taxiways (special case)

^^^^
^^^^
EXTREMELY STIFF

SOFT

(Fig. 4.1.f) / / / / / /

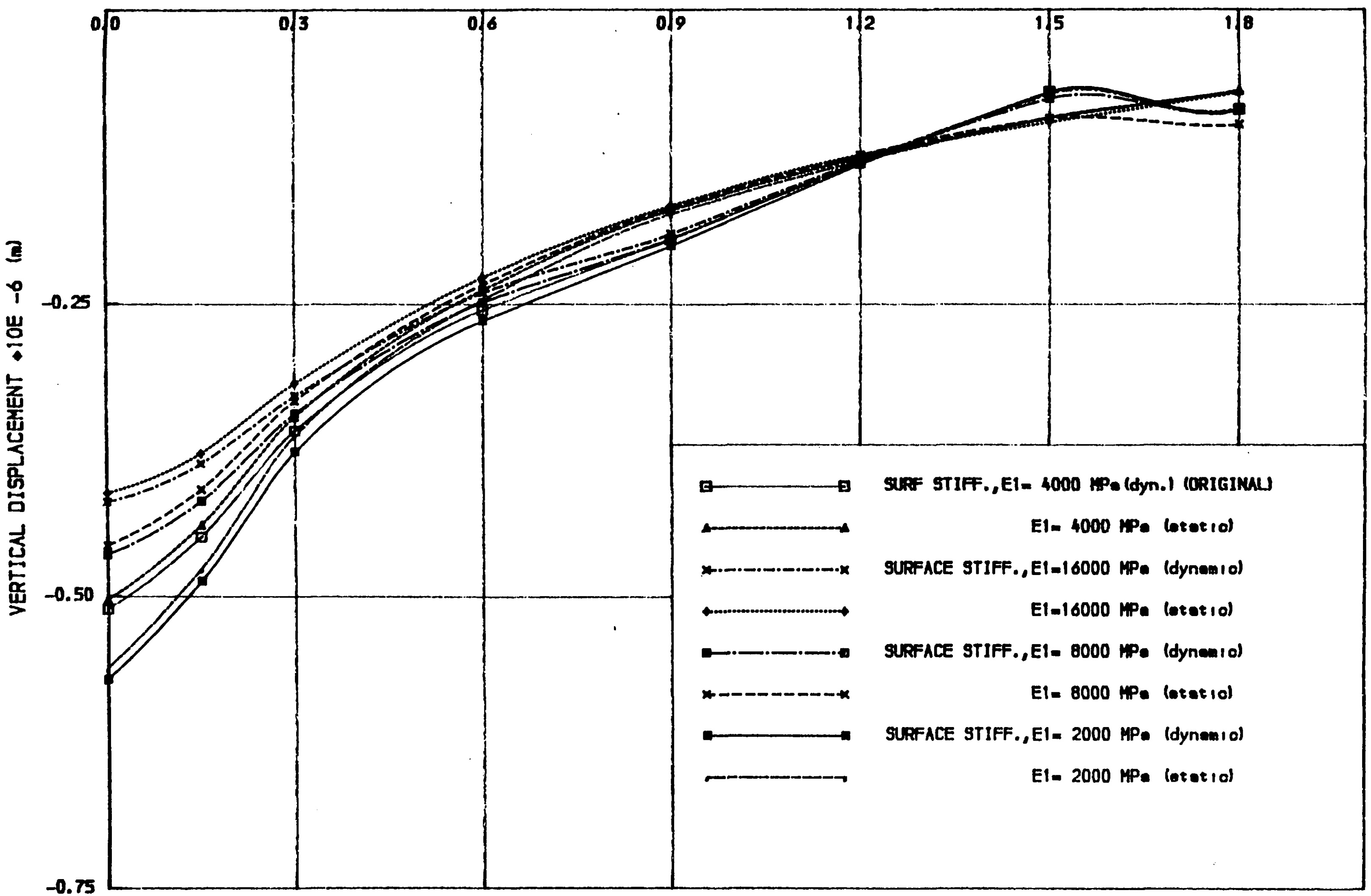

(FIG. 4.2.a)

FOUR LAYER FLEXIBLE PAVEMENT

RADIUS (m)

DEFLECTION BASINS (SURFACE STIFFNESS ANALYSIS)

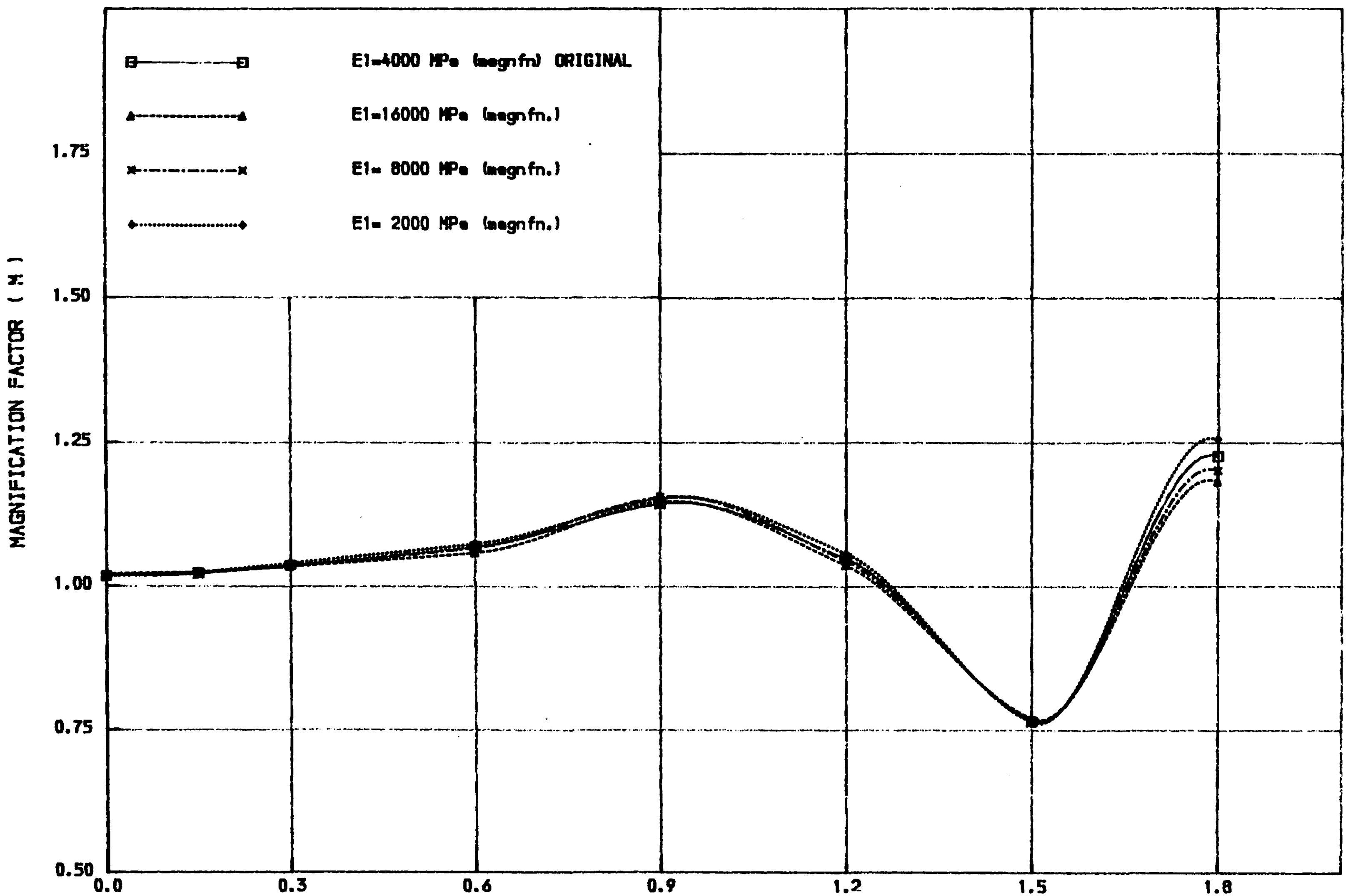

(FIG.4.2.b)

FOUR LAYER FLEXIBLE PAVEMENT

TP= 40 msec , RERIOD T= 140 msec

(SURFACE STIFFNESS ANALYSIS)

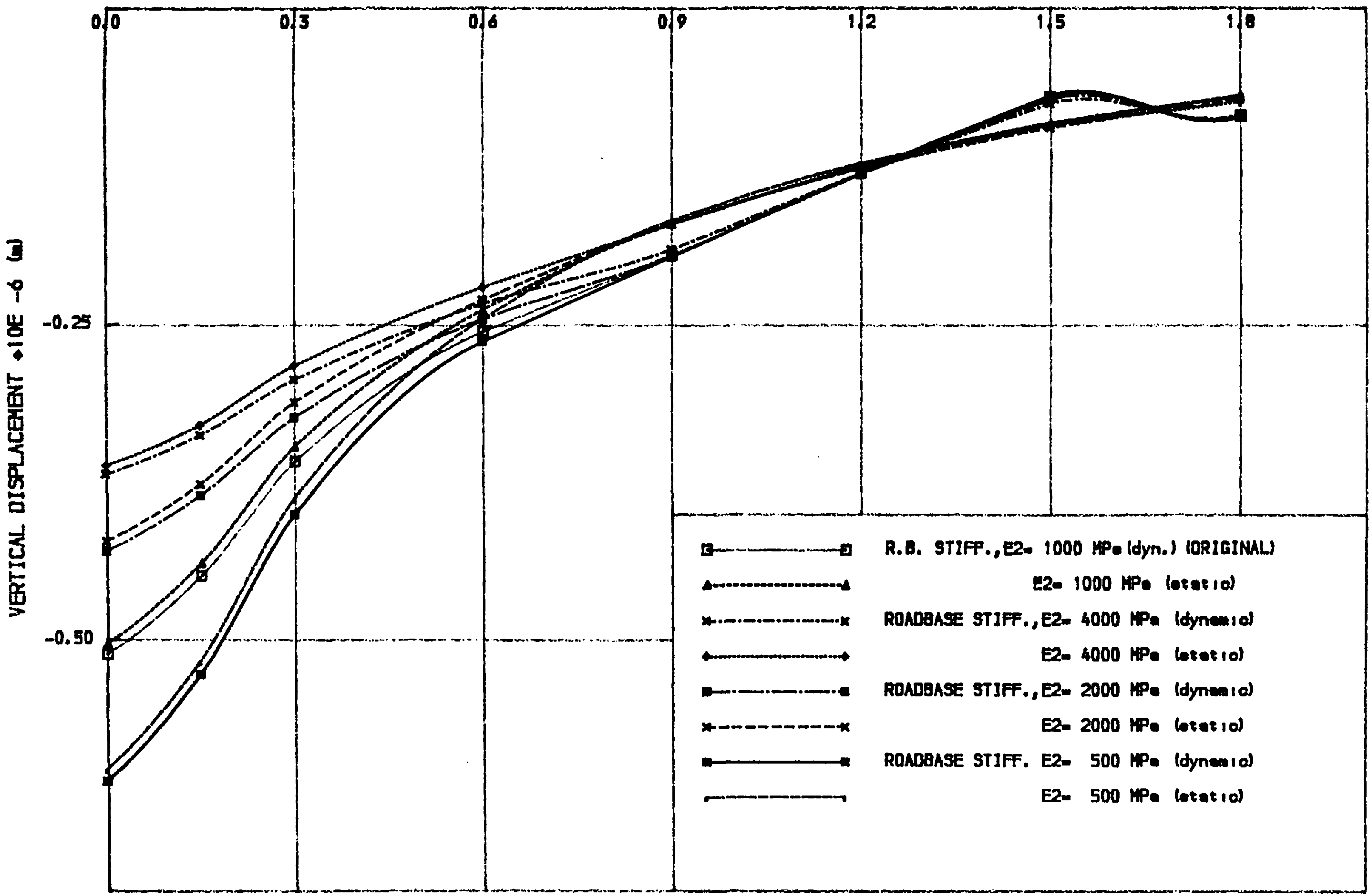

FOUR LAYER FLEXIBLE PAVEMENT

(FIG.4.3.a) DEFLECTION BASINS (ROADBASE STIFFNESS ANALYSIS)

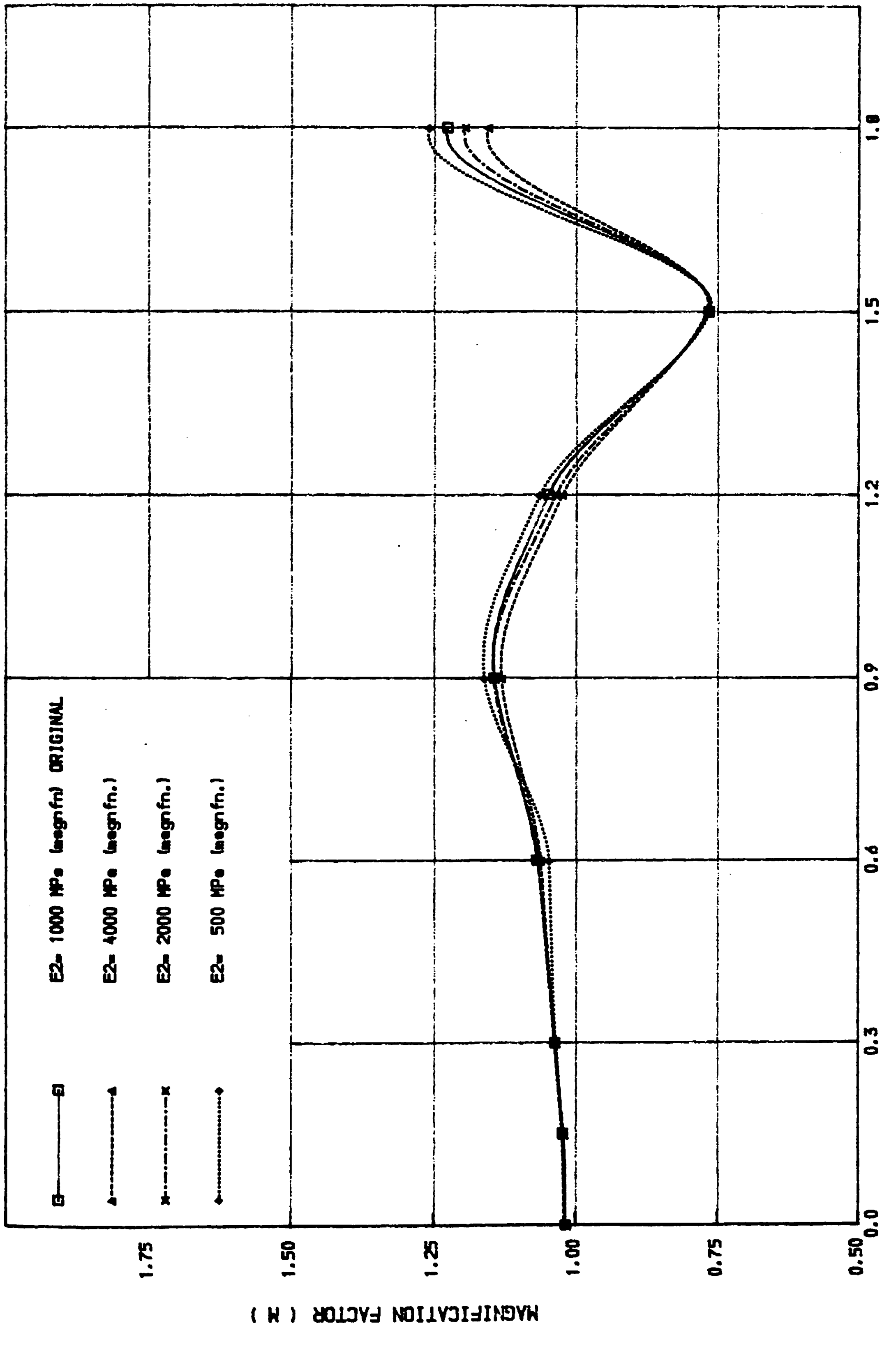

FOUR LAYER FLEXIBLE PAVEMENT

(FIG. 4.3.b) TP= 40 msec , RERIOD T= 140 msec
(ROADBASE STIFFNESS ANALYSIS)

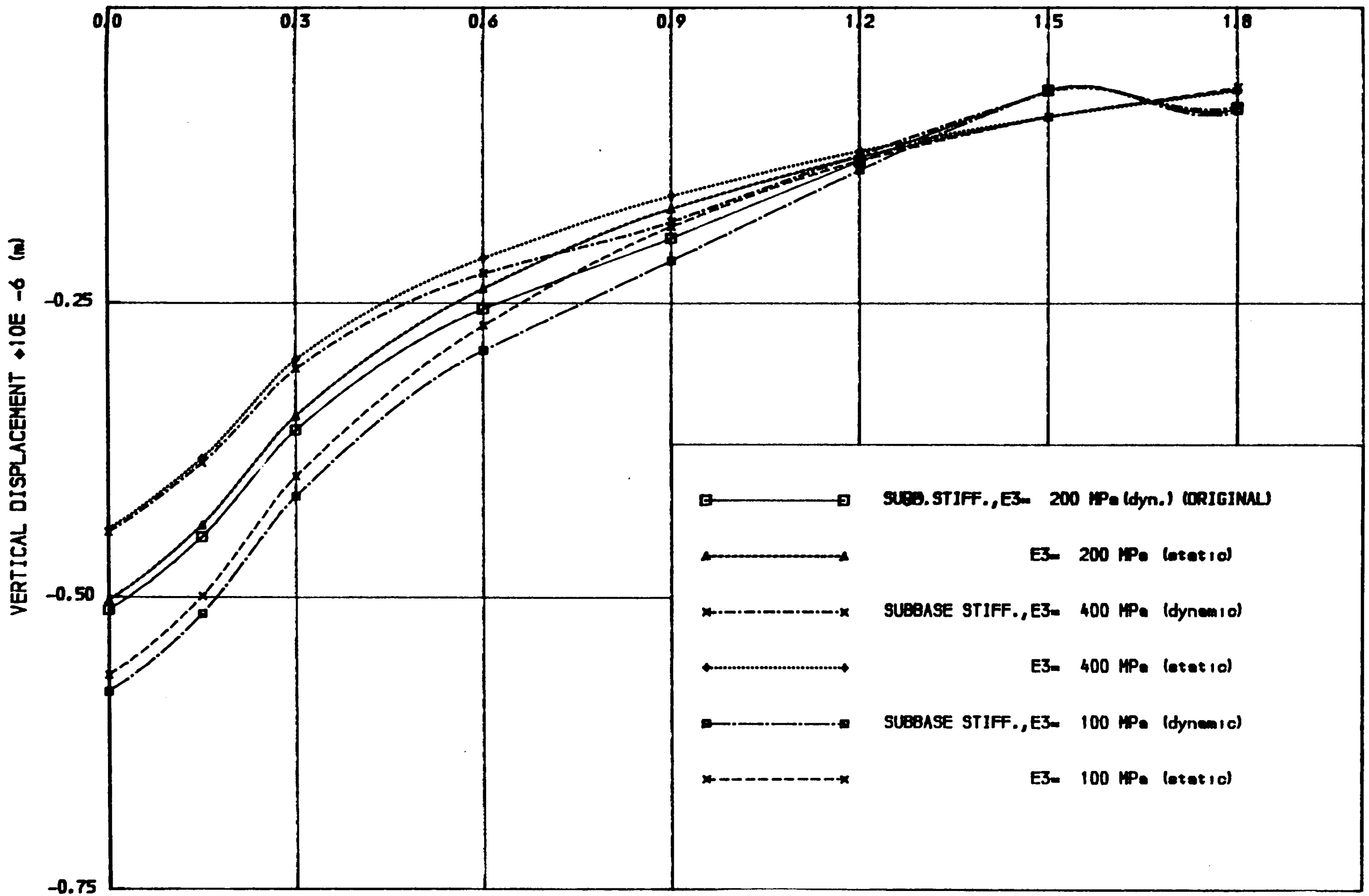

(FIG.4.4.a)

FOUR LAYER FLEXIBLE PAVEMENT

RADIUS (m)

DEFLECTION BASINS (SUBBASE STIFFNESS ANALYSIS)

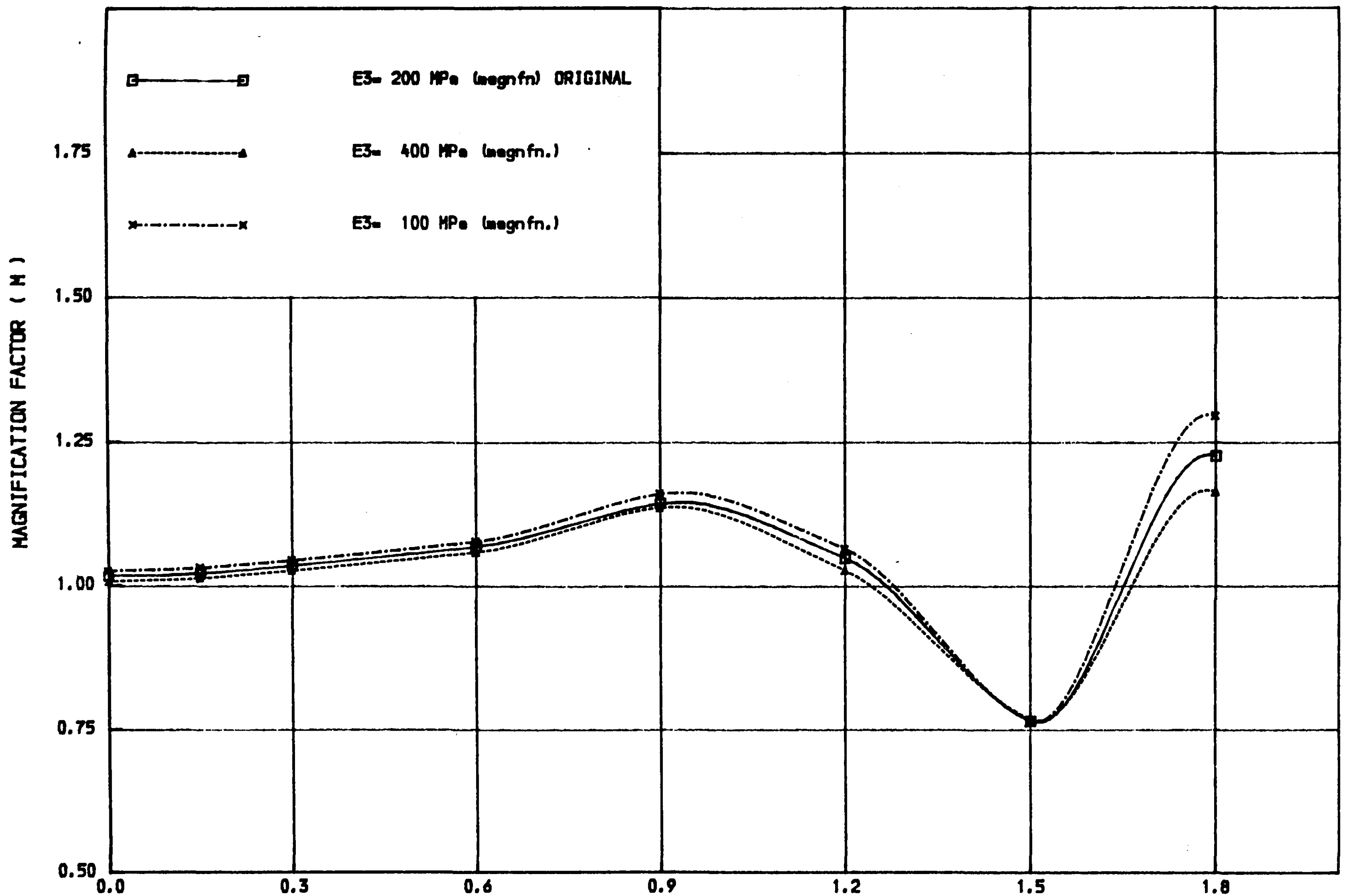

FOUR LAYER FLEXIBLE PAVEMENT

(FIG. 4.4.b) TP= 40 msec , RERIOD T= 140 msec RADIUS (m)
(SUBBASE STIFFNESS ANALYSIS)

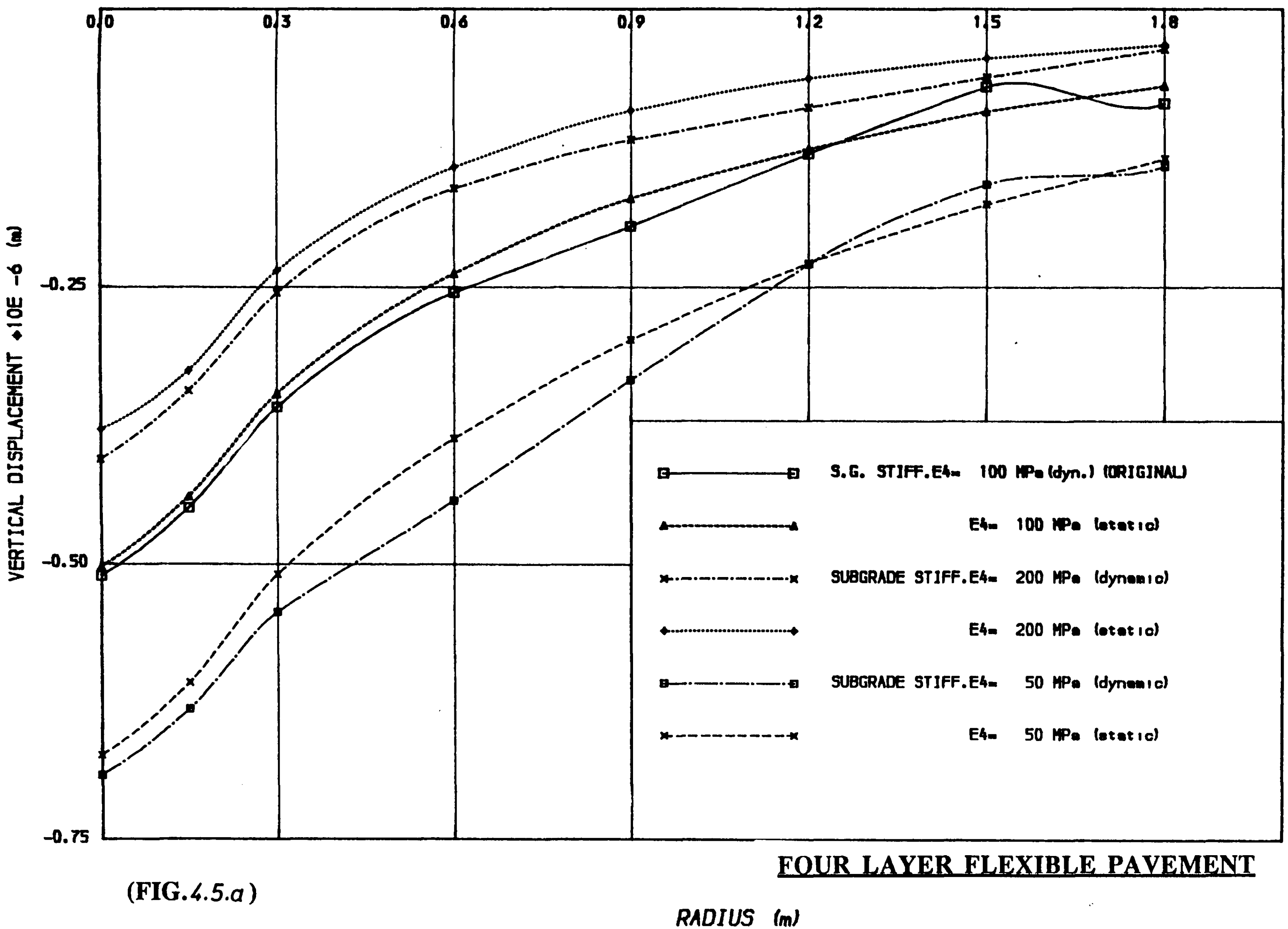

FOUR LAYER FLEXIBLE PAVEMENT

(FIG.4.5.a)

DEFLECTION BASINS (SUBGRADE STIFFNESS ANALYSIS)

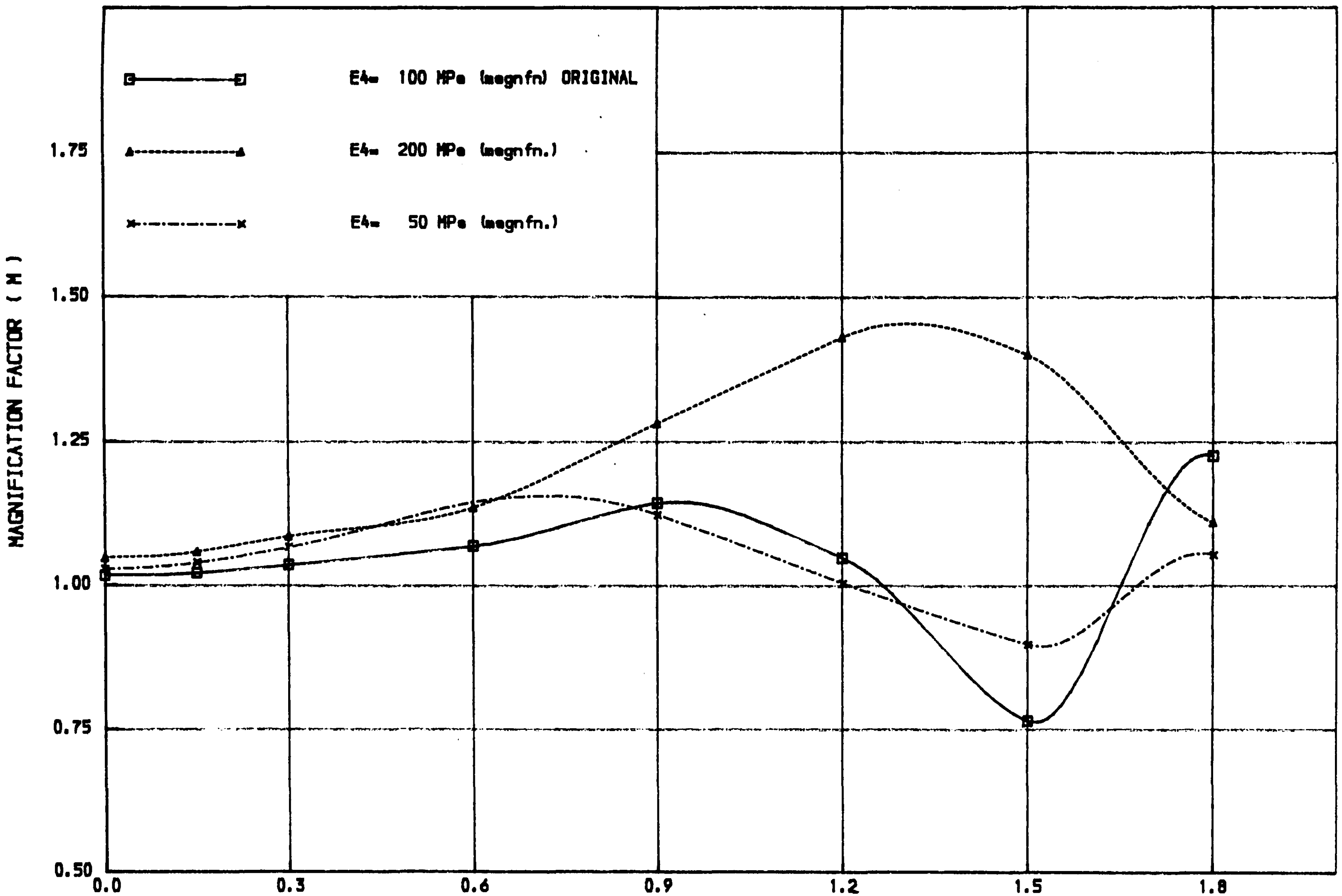

FOUR LAYER FLEXIBLE PAVEMENT

(FIG. 4.5.b) *TP= 40 msec , PERIOD T= 140 msec* *RADIUS (m)*

(SUBGRADE STIFFNESS ANALYSIS)

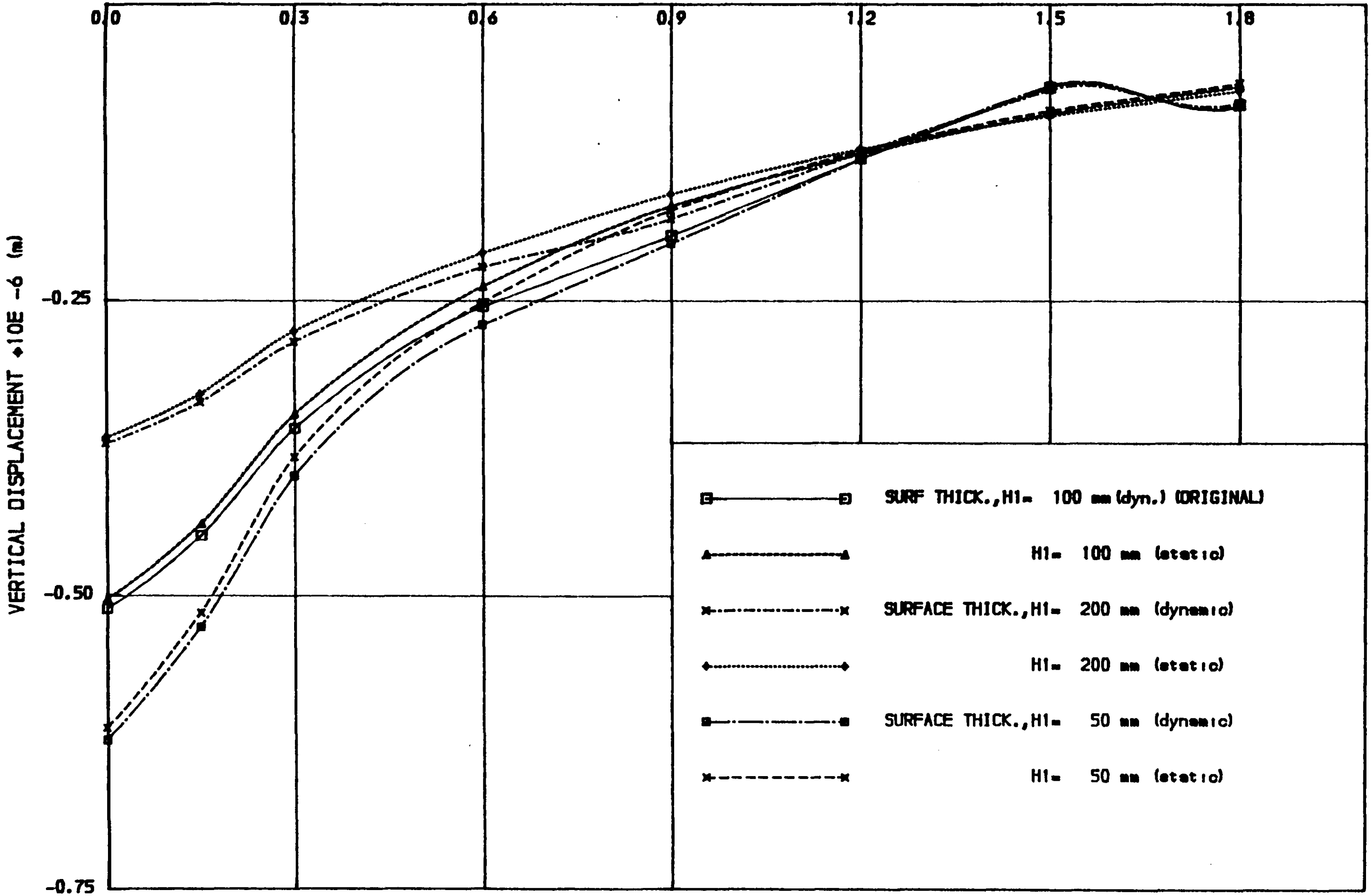

(FIG. 4.6.a)

FOUR LAYER FLEXIBLE PAVEMENT

RADIUS (m)

DEFLECTION BASINS (SURFACE THICKNESS ANALYSIS)

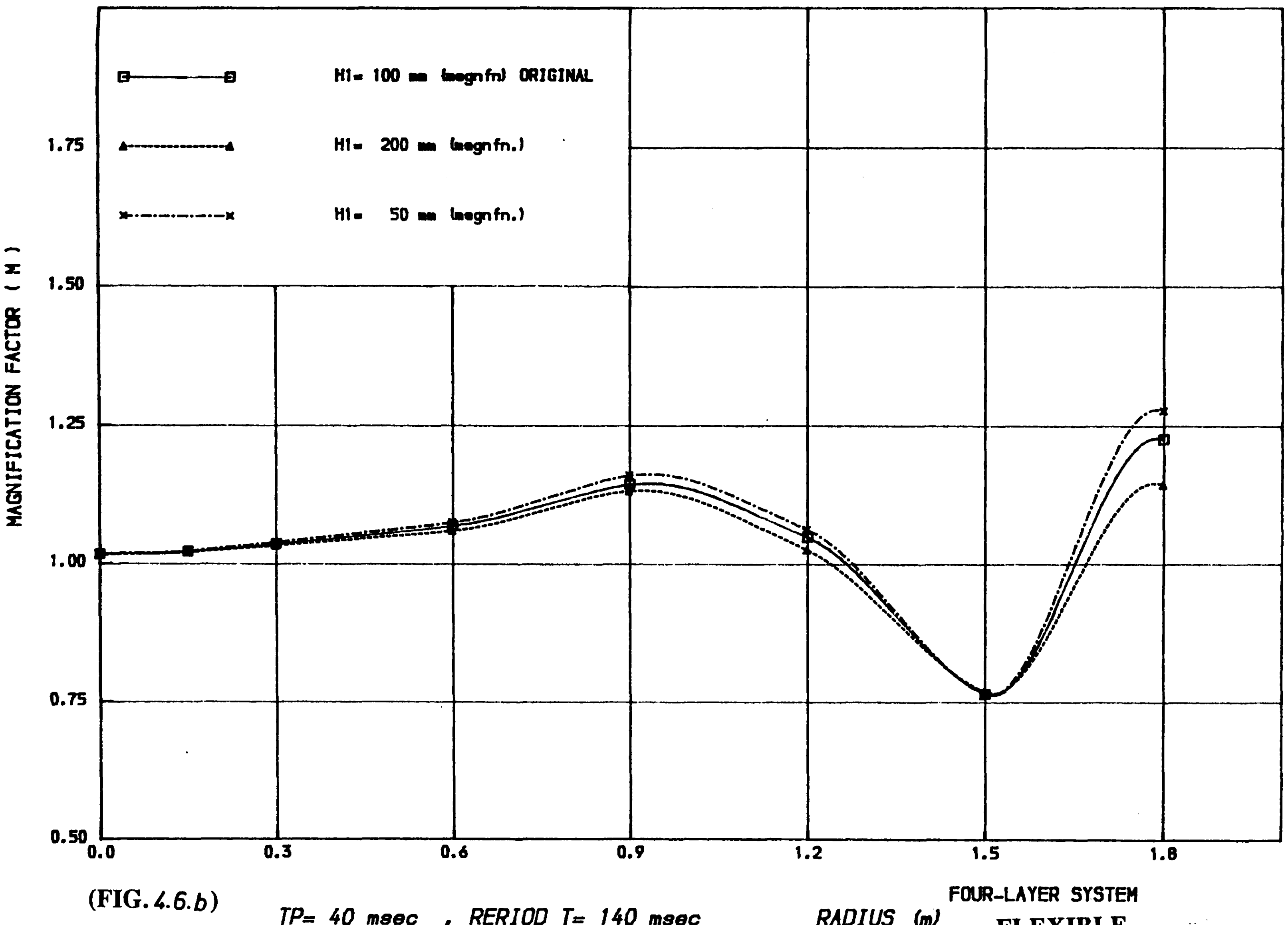

(FIG. 4.6.b) TP= 40 msec , RERIOD T= 140 msec
(SURFACE THICKNESS ANALYSIS)

FOUR-LAYER SYSTEM
FLEXIBLE

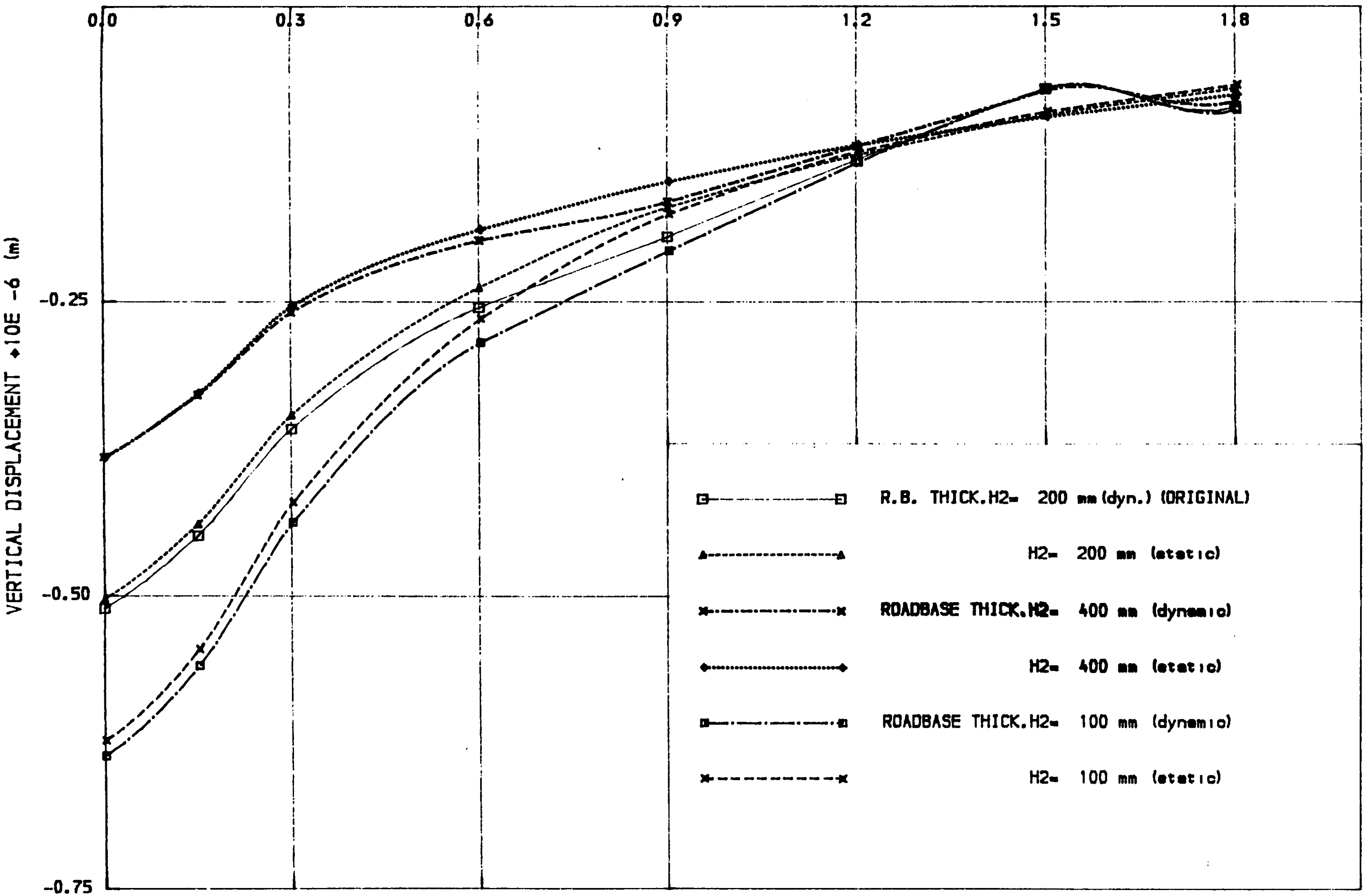

(FIG. 4.7.a)

RADIUS (m)

DEFLECTION BASINS (ROADBASE THICKNESS ANALYSIS)

FOUR-LAYER SYSTEM

FLEXIBLE

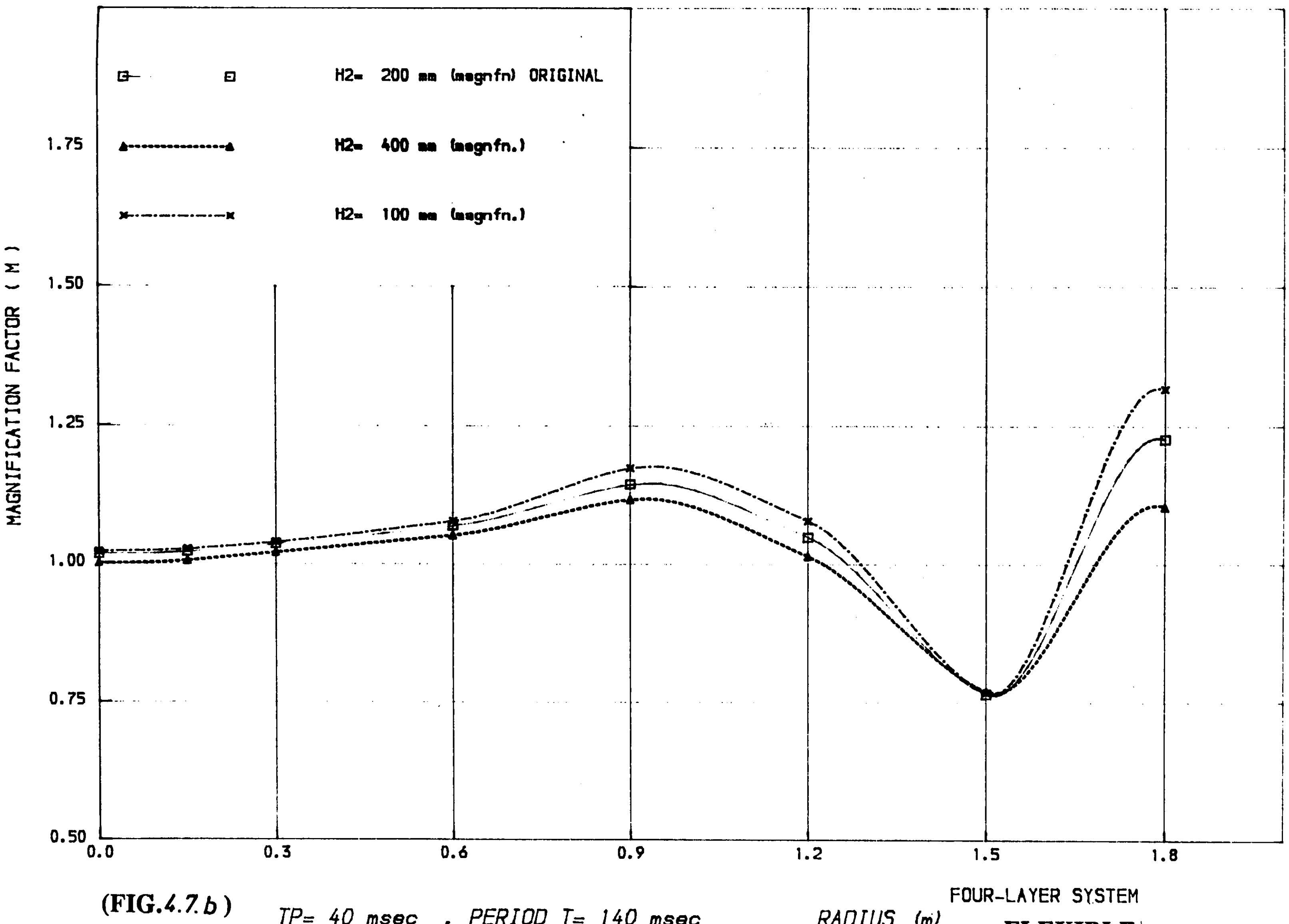

(FIG.4.7.b) TP= 40 msec , PERIOD T= 140 msec
(ROADBASE THICKNESS ANALYSIS)

FOUR-LAYER SYSTEM

FLEXIBLE

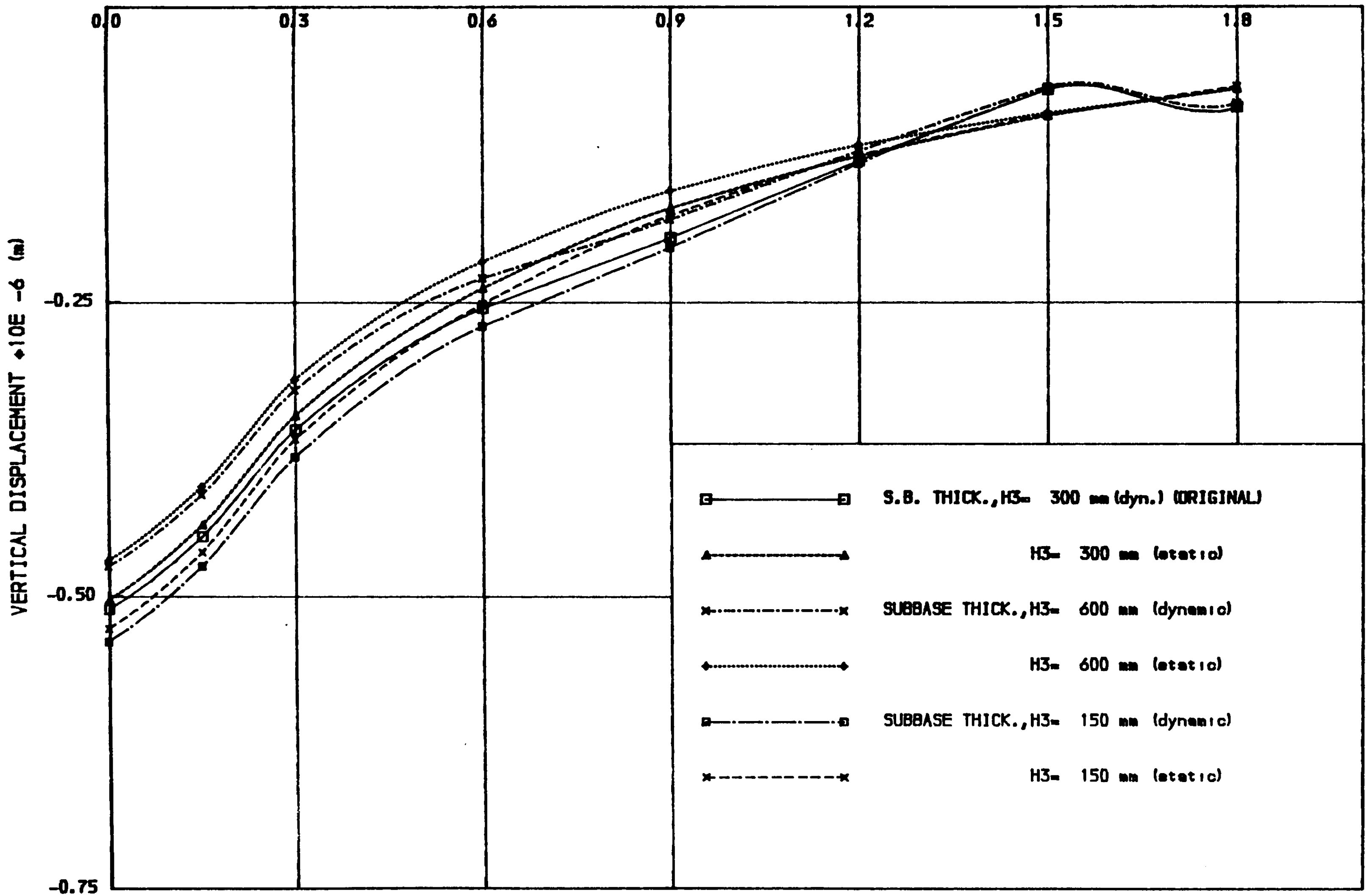

(FIG. 4.8.a)

FOUR-LAYER SYSTEM **FLEXIBLE**

RADIUS (m)

DEFLECTION BASINS (SUBBASE THICKNESS ANALYSIS)

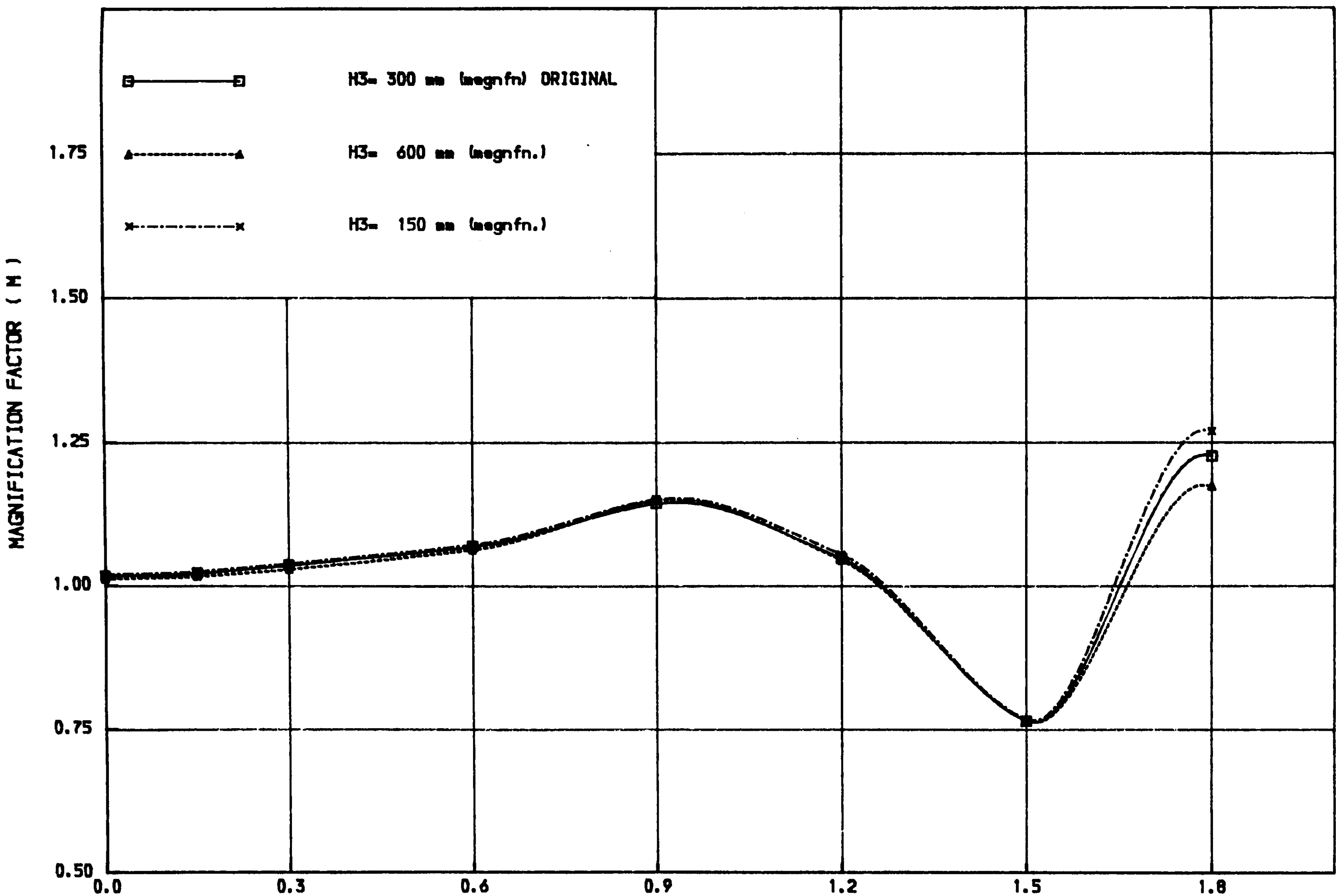

(FIG. 4.8.b)

TP= 40 msec , PERIOD T= 140 msec
(SUBBASE THICKNESS ANALYSIS)

FOUR-LAYER SYSTEM

FLEXIBLE

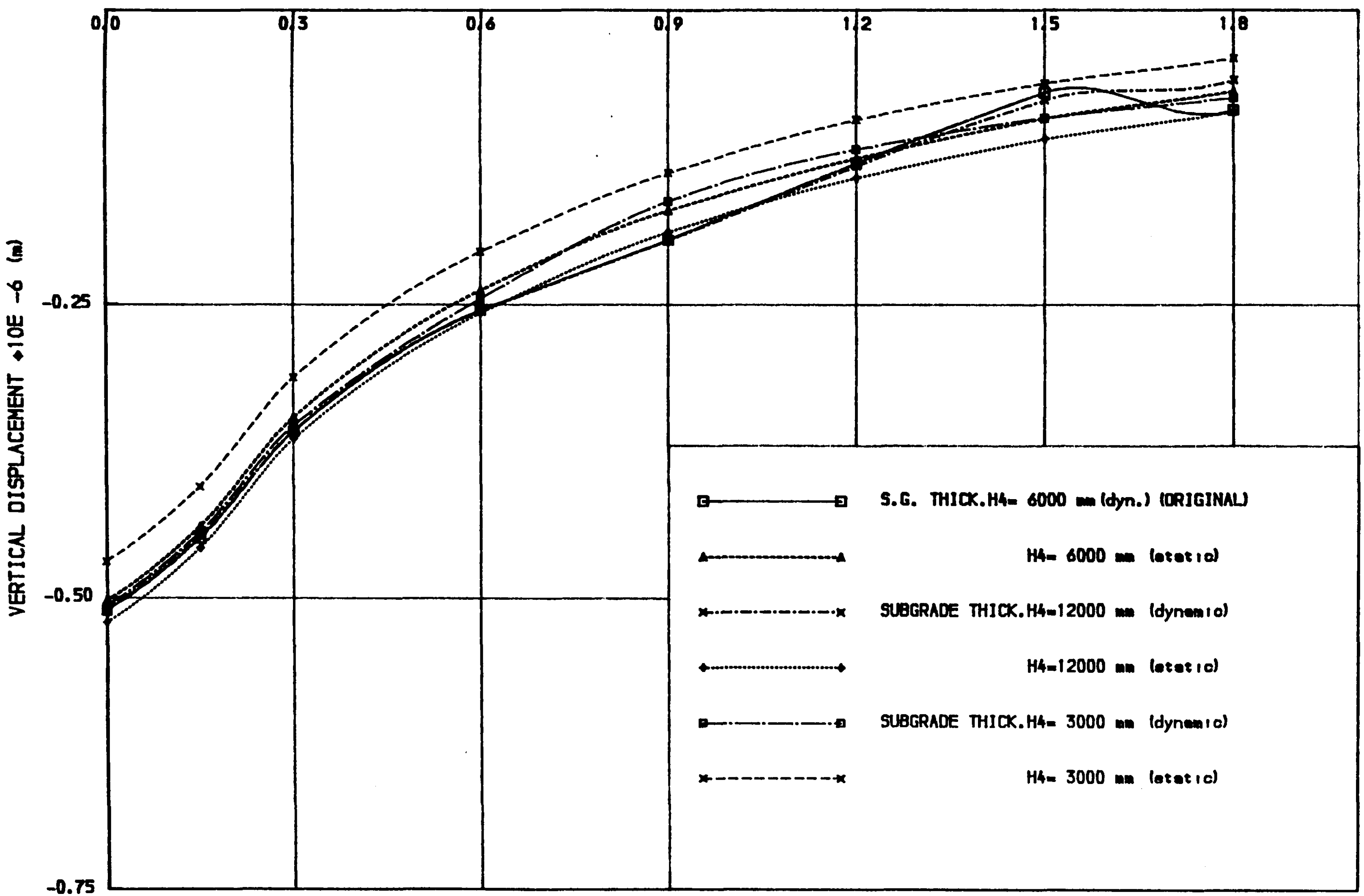

(FIG. 4.9.a)

DEFLECTION BASINS (SUBGRADE THICKNESS ANALYSIS)

FOUR-LAYER SYSTEM

FLEXIBLE

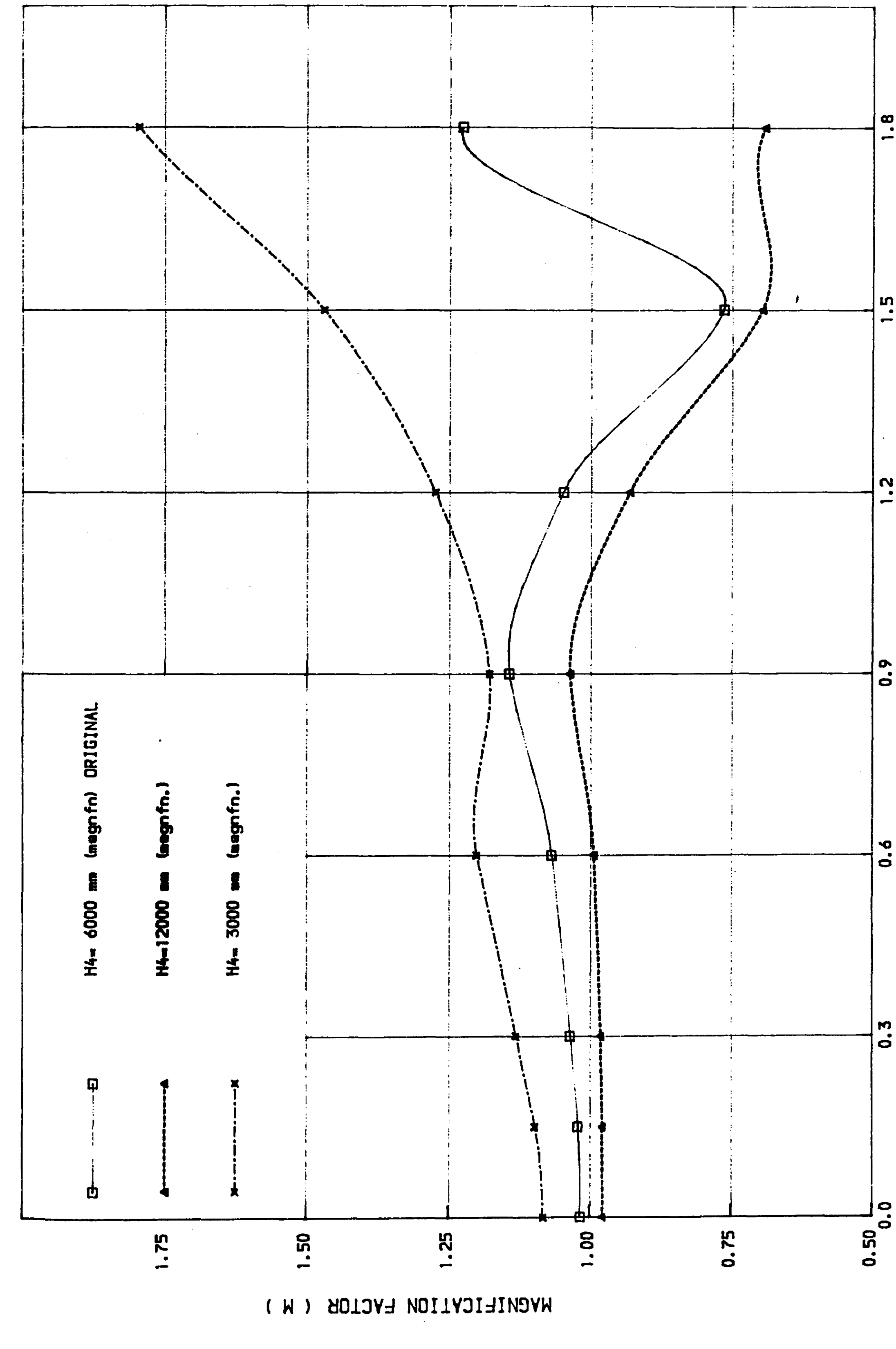

(FIG. 4.9.b) TP= 40 msec , PERIOD T= 140 msec
(SUBGRADE THICKNESS ANALYSIS)

FOUR-LAYER SYSTEM

FLEXIBLE

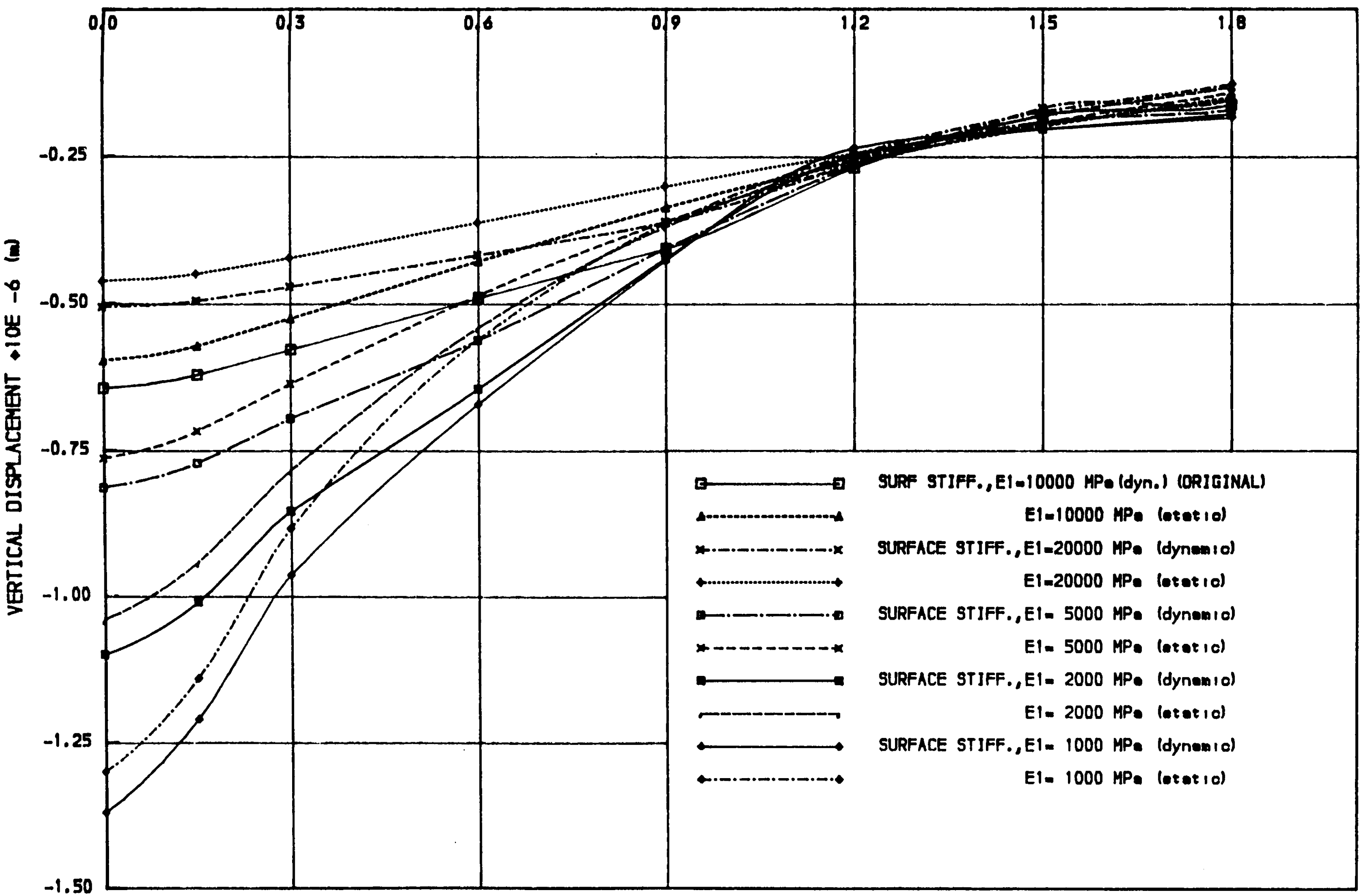

(FIG. 4.10a)

DEFLECTION BASINS (SURFACE STIFFNESS ANALYSIS)

THREE-LAYER SYSTEM

FLEXIBLE

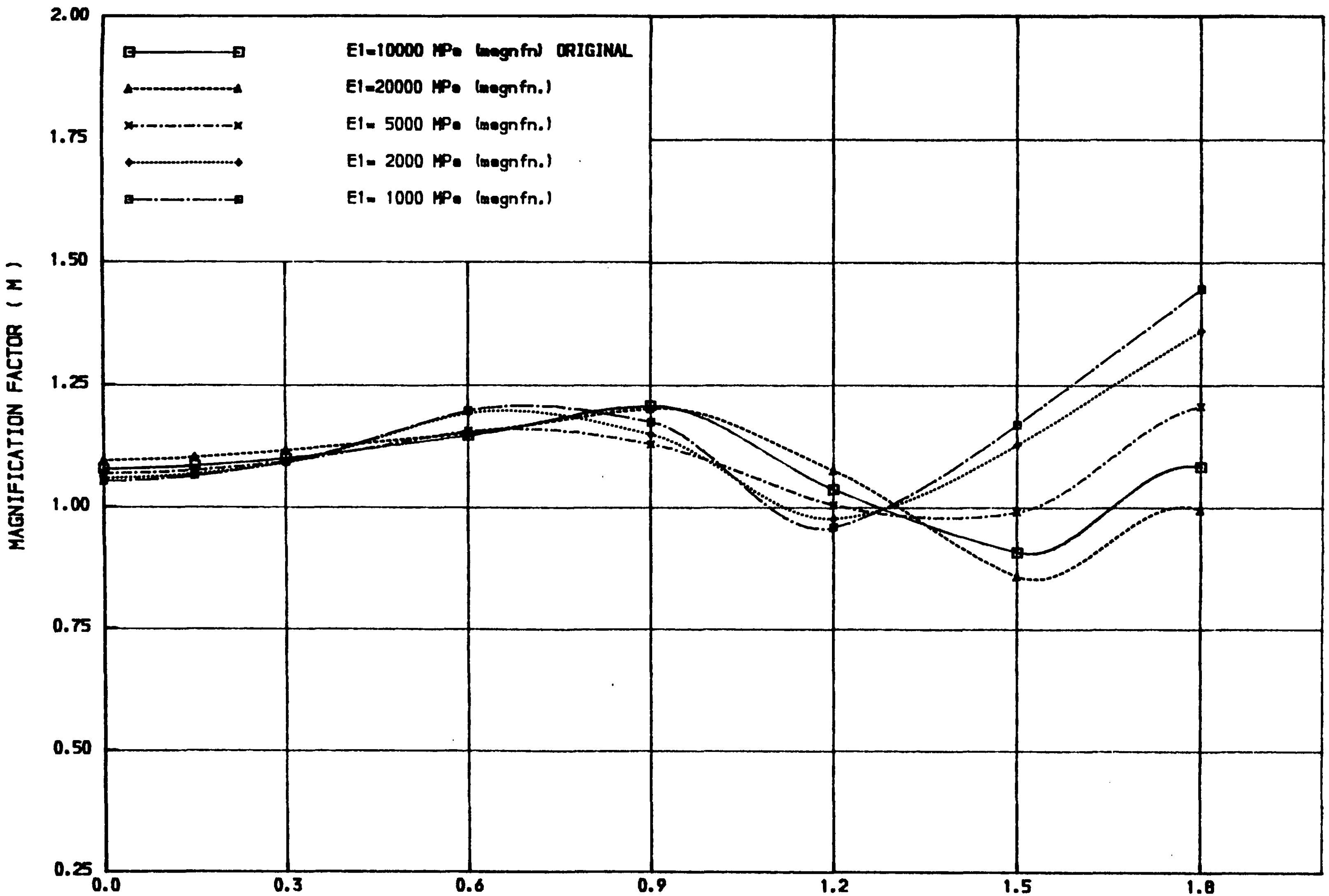

(FIG. 4.10.b)

THREE-LAYER SYSTEM **FLEXIBLE**

TP= 40 msec , PERIOD T= 140 msec
(SURFACE STIFFNESS ANALYSIS)

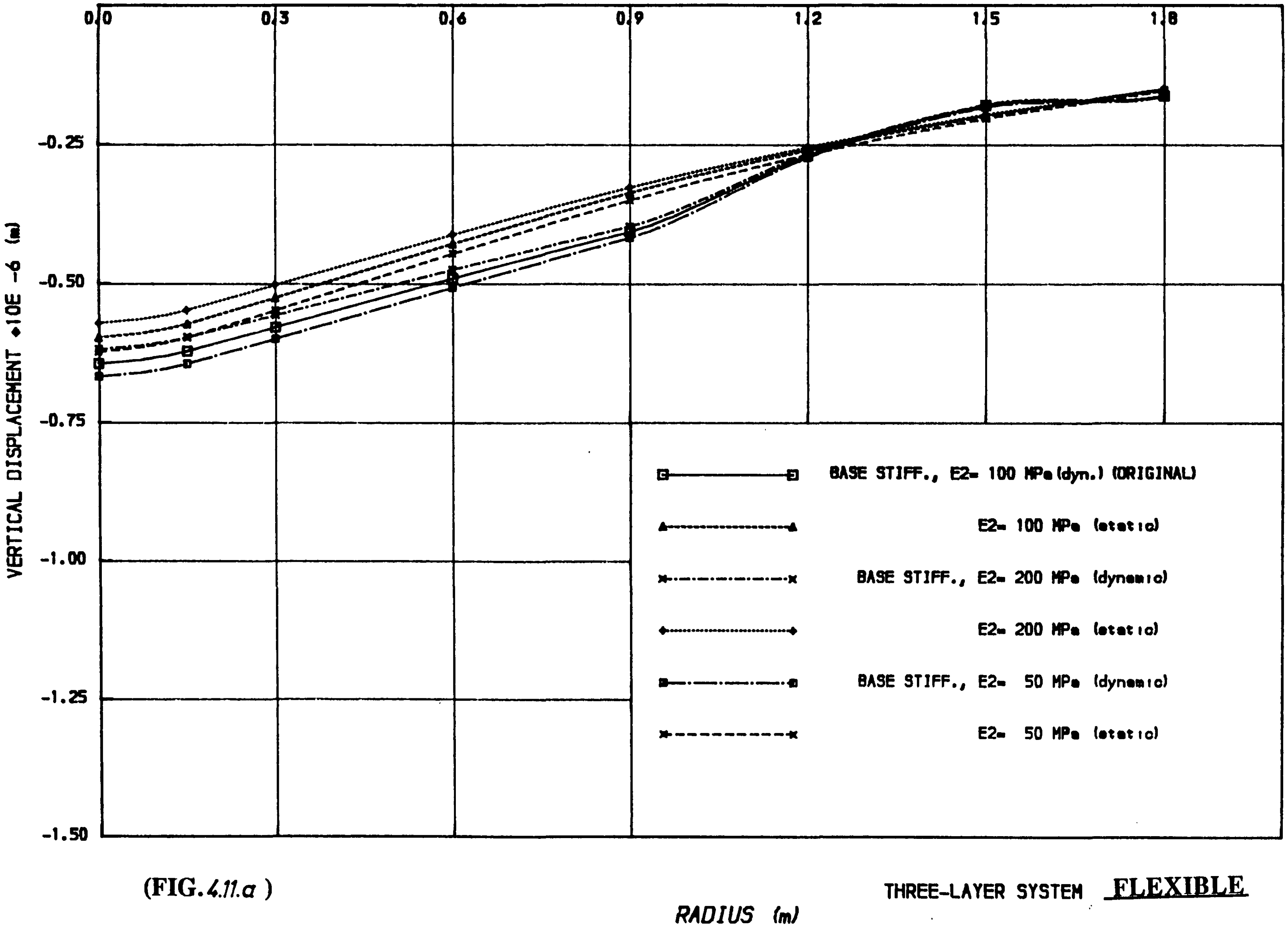

(FIG. 4.11.a)

THREE-LAYER SYSTEM **FLEXIBLE**

DEFLECTION BASINS (BASE STIFFNESS ANALYSIS)

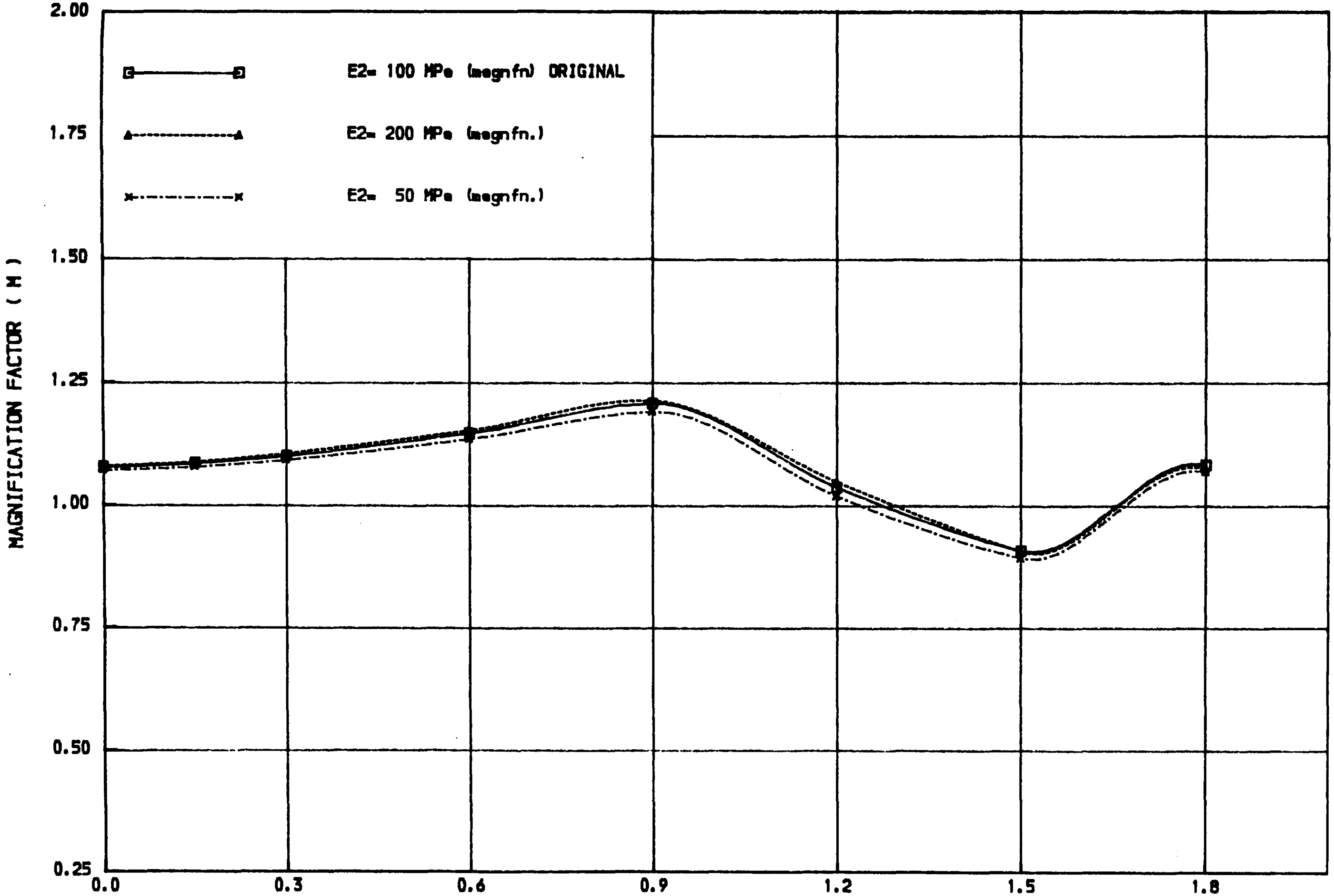

(FIG. 4.11.b) TP= 40 msec , PERIOD T= 140 msec
(BASE STIFFNESS ANALYSIS)

THREE-LAYER SYSTEM
FLEXIBLE

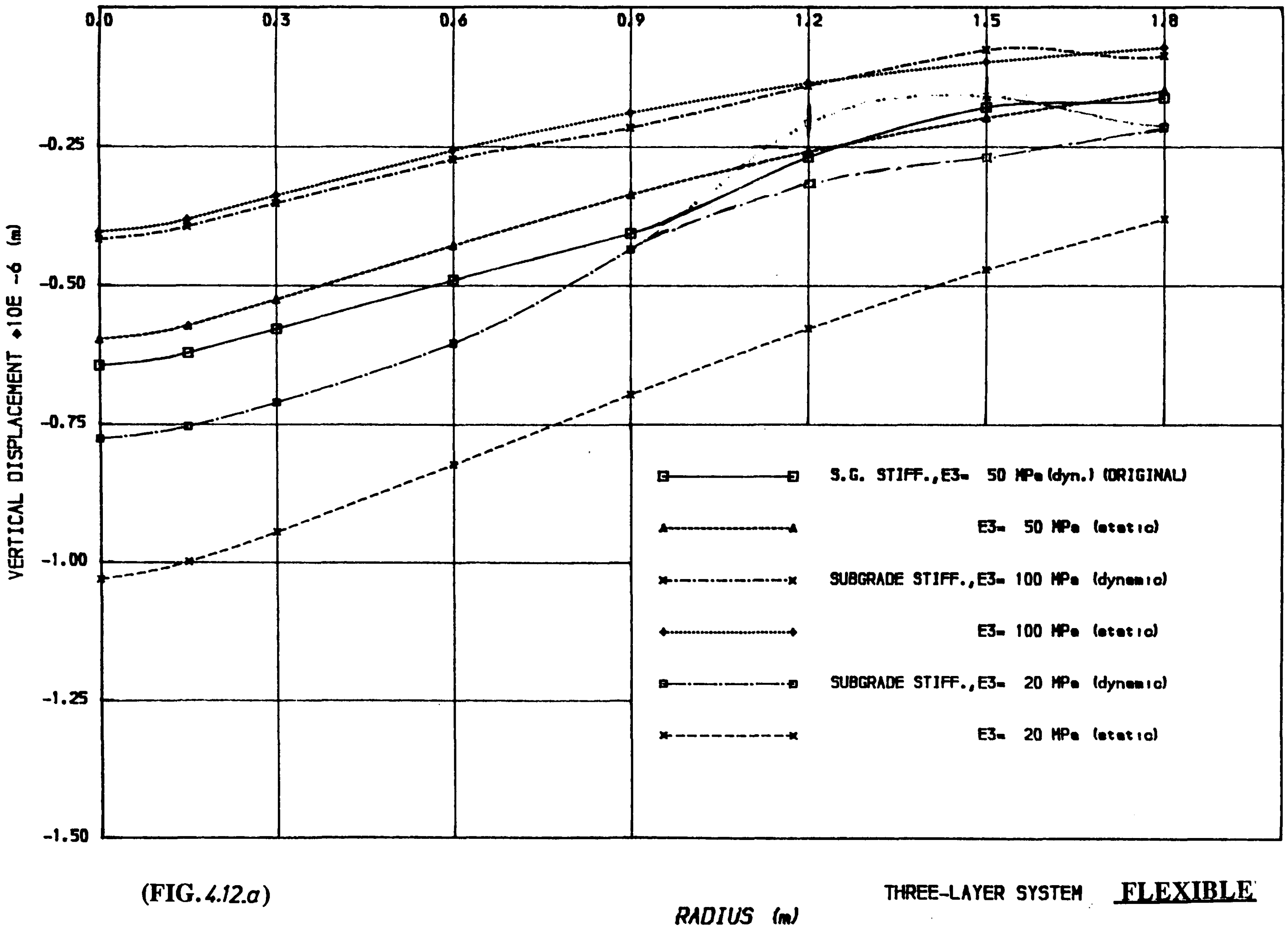

(FIG. 4.12.a) THREE-LAYER SYSTEM **FLEXIBLE**

DEFLECTION BASINS (SUBGRADE STIFFNESS ANALYSIS)

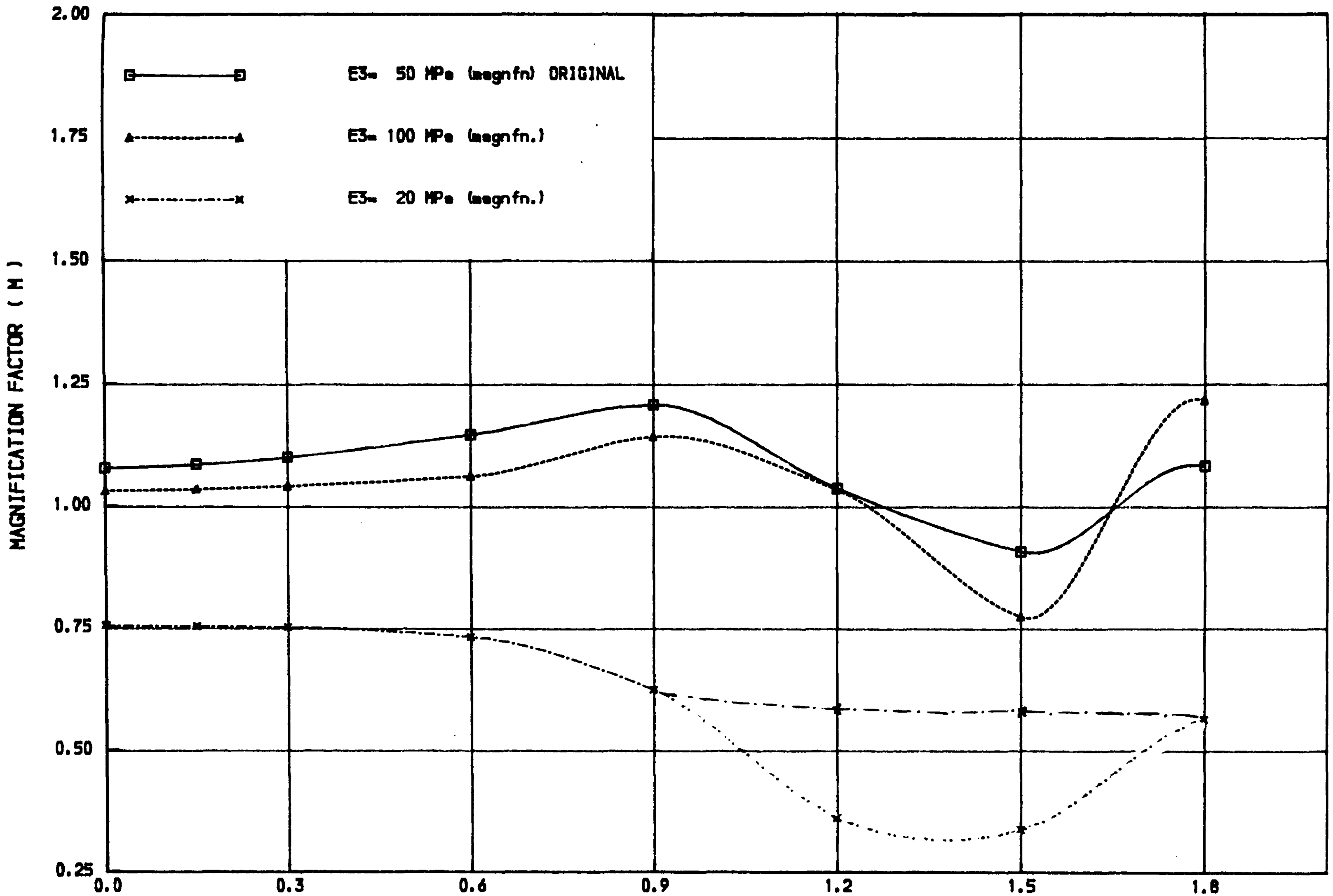

THREE-LAYER SYSTEM

(FIG. 4.12.b) TP= 40 msec , PERIOD T= 140 msec RADIUS (m)
(SUBGRADE STIFFNESS ANALYSIS)

FLEXIBLE

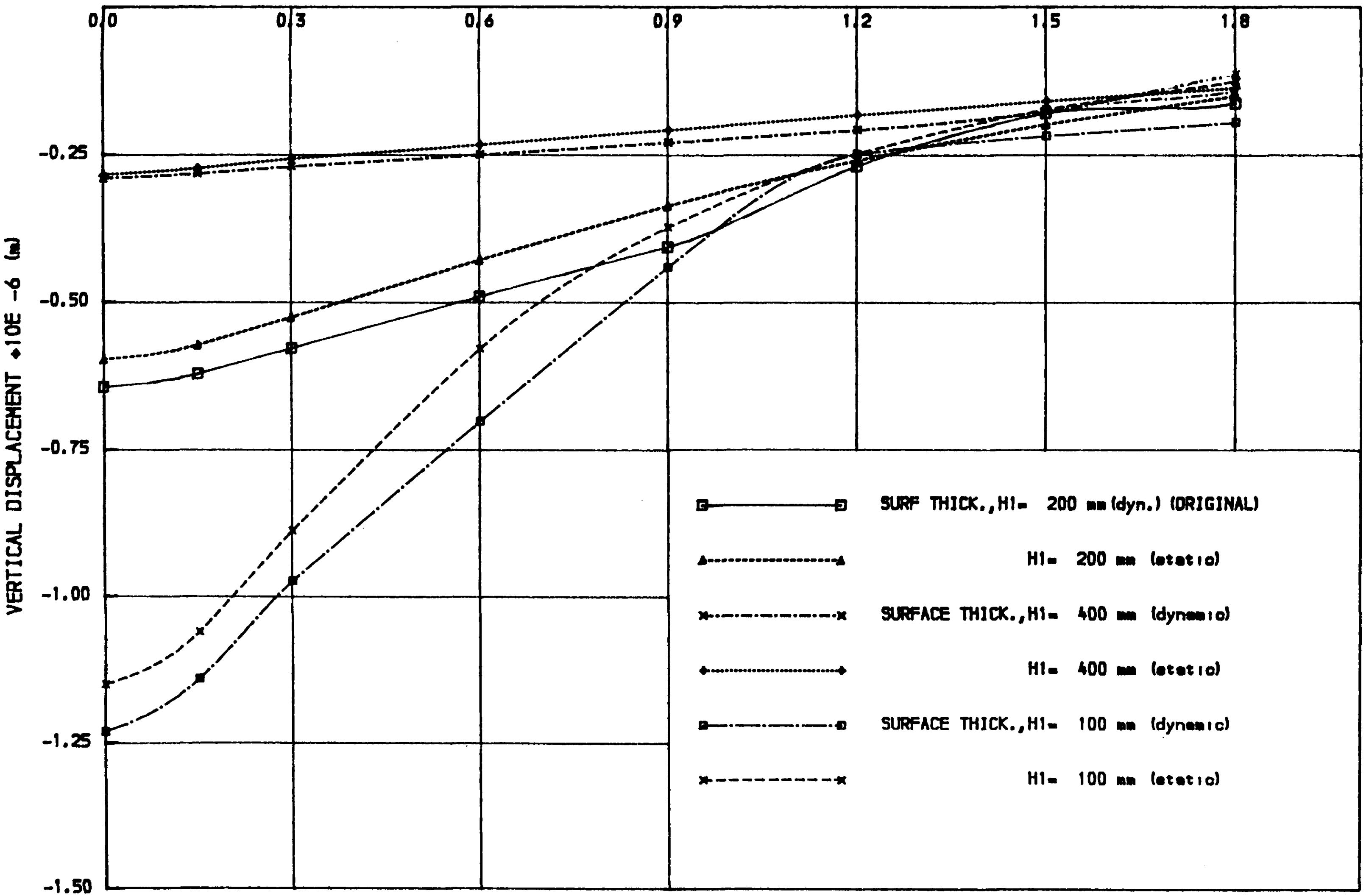

(FIG. 4.13.a)

THREE-LAYER SYSTEM **FLEXIBLE**

RADIUS (m)

DEFLECTION BASINS (SURFACE THICKNESS ANALYSIS)

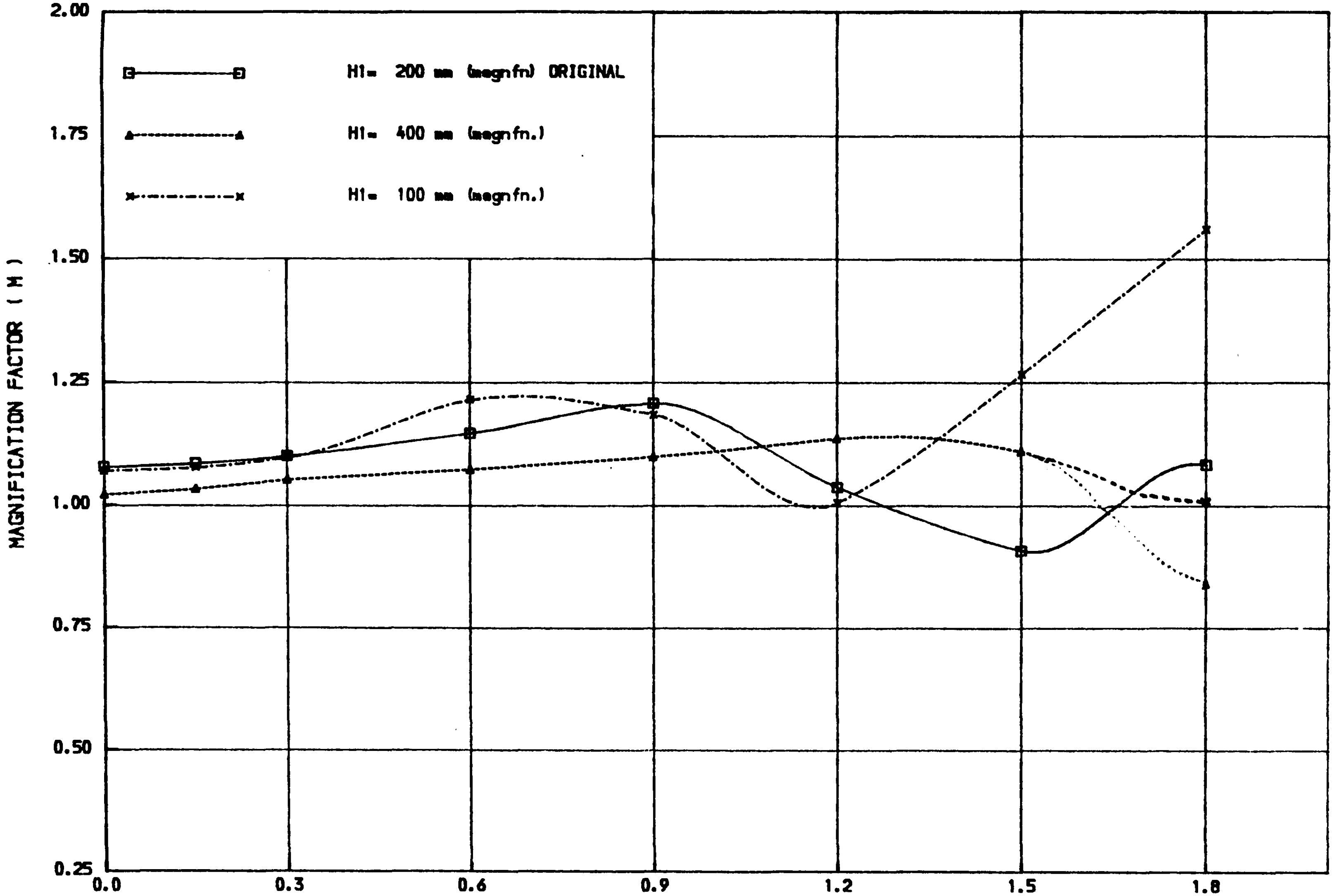

THREE-LAYER SYSTEM **FLEXIBLE**

(FIG.4.13.b) *TP= 40 msec , PERIOD T= 140 msec* *RADIUS (m)*

(SURFACE THICKNESS ANALYSIS)

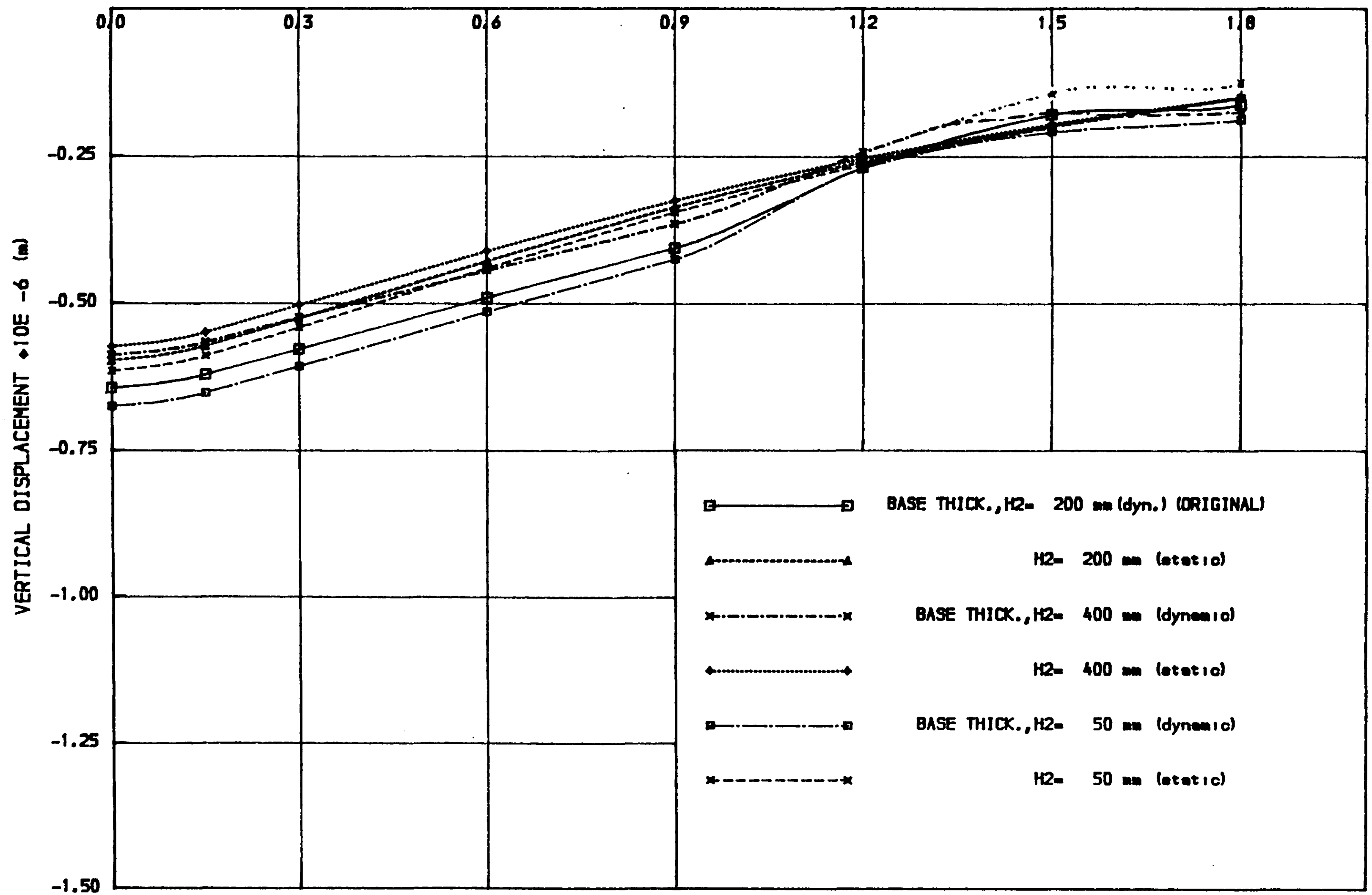

(FIG.4.14.a) THREE-LAYER SYSTEM **FLEXIBLE**

DEFLECTION BASINS (BASE THICKNESS ANALYSIS)

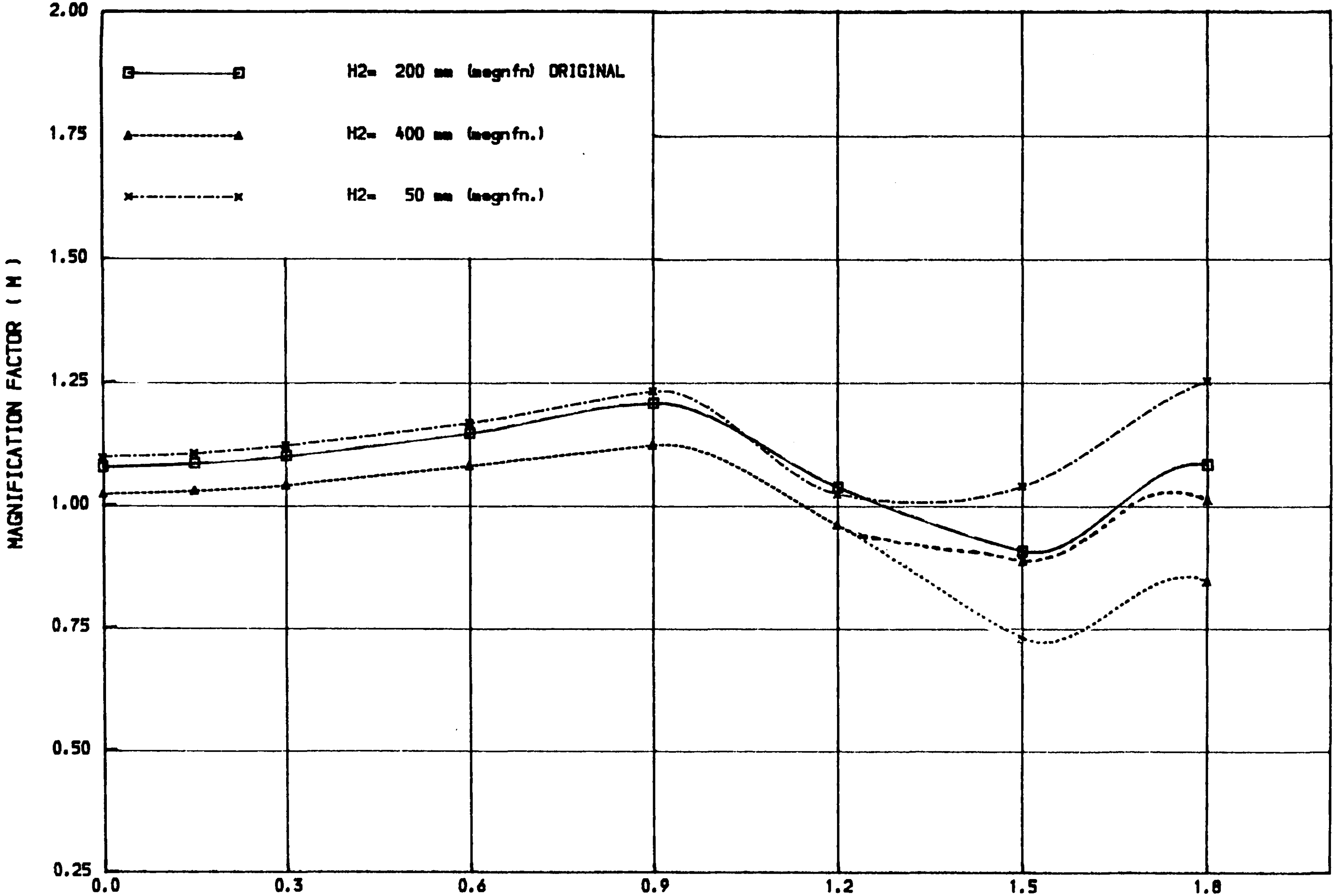

FLEXIBLE

(FIG. 4.14.b) TP= 40 msec , PERIOD T= 140 msec
(BASE THICKNESS ANALYSIS)

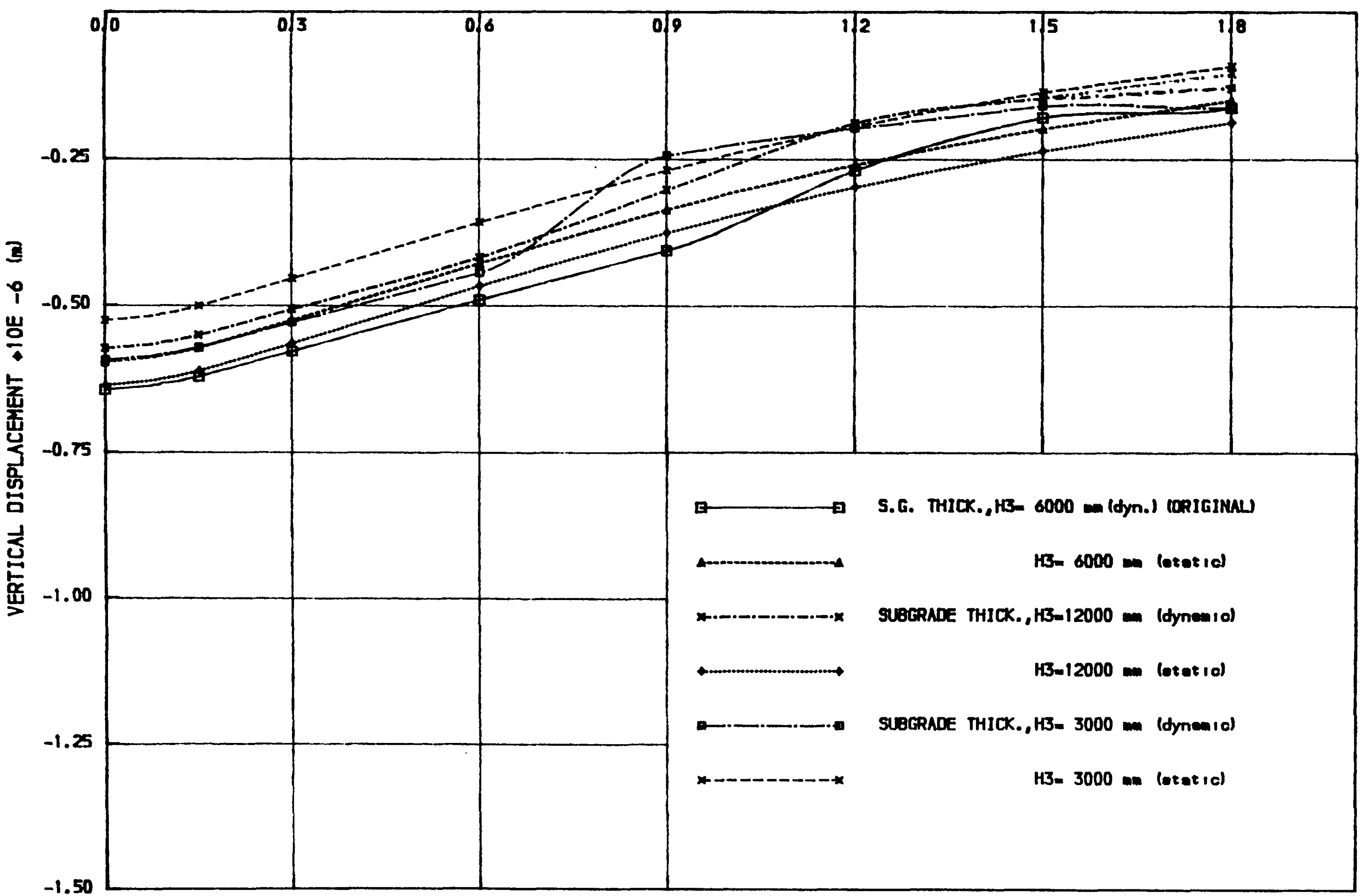

(FIG. 4.15a)

THREE-LAYER SYSTEM **FLEXIBLE**

DEFLECTION BASINS (SUBGRADE THICKNESS ANALYSIS)

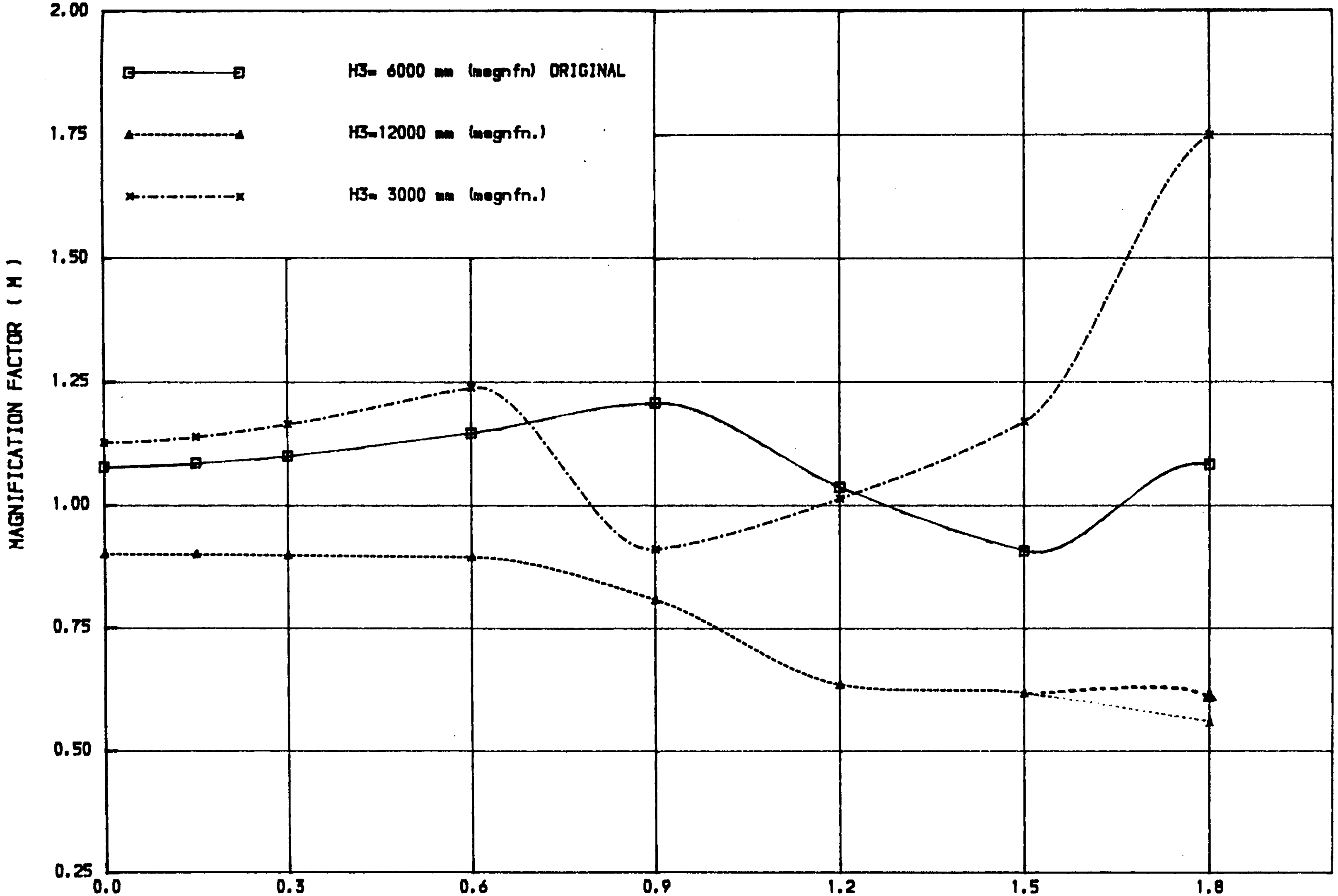

THREE-LAYER SYSTEM **FLEXIBLE**

(FIG.4.15.b) TP= 40 msec , PERIOD T= 140 msec
(SUBGRADE THICKNESS ANALYSIS)

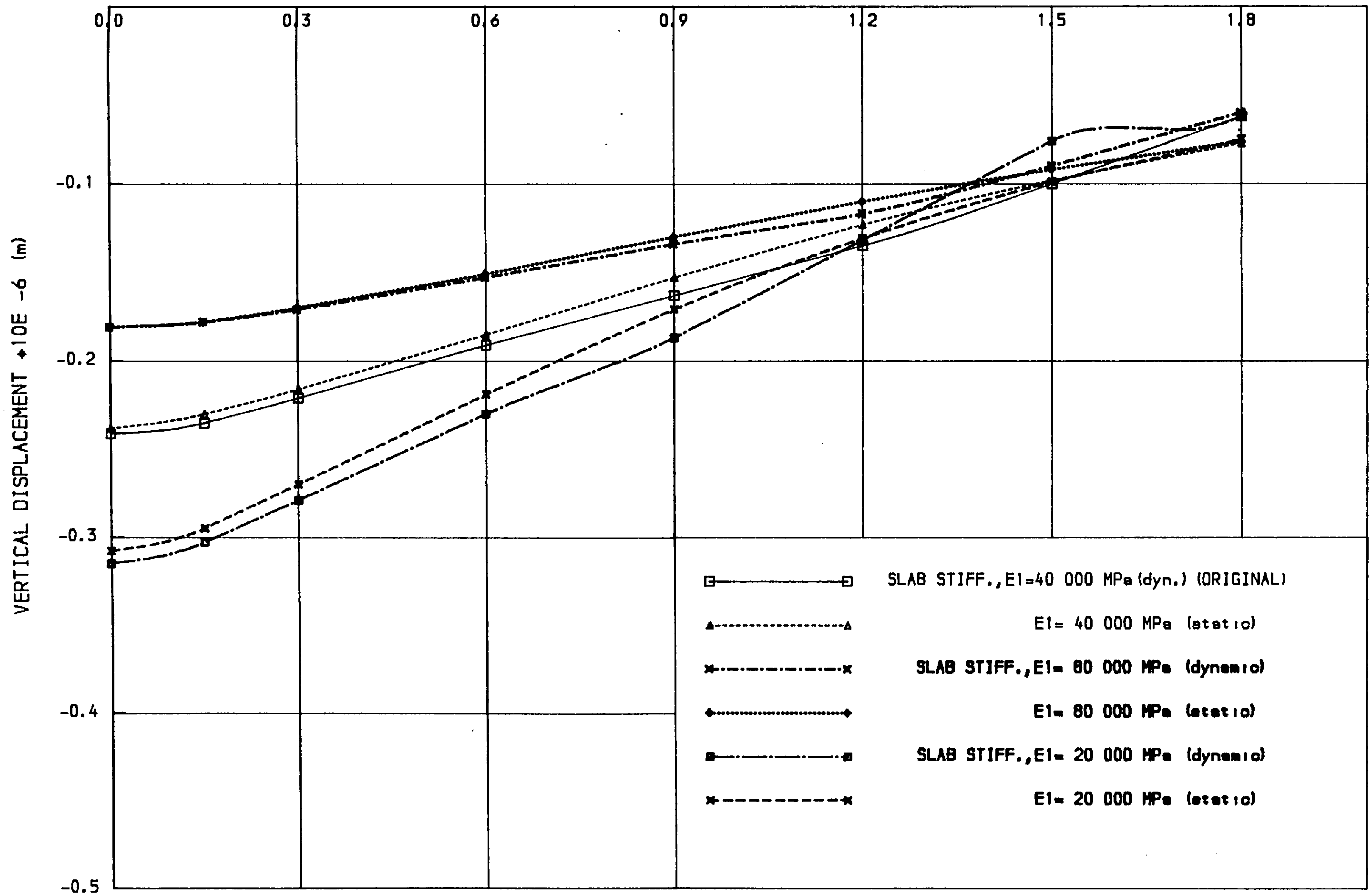

(FIG.4.16.a)

DEFLECTION BASINS (SLAB STIFFNESS ANALYSIS)

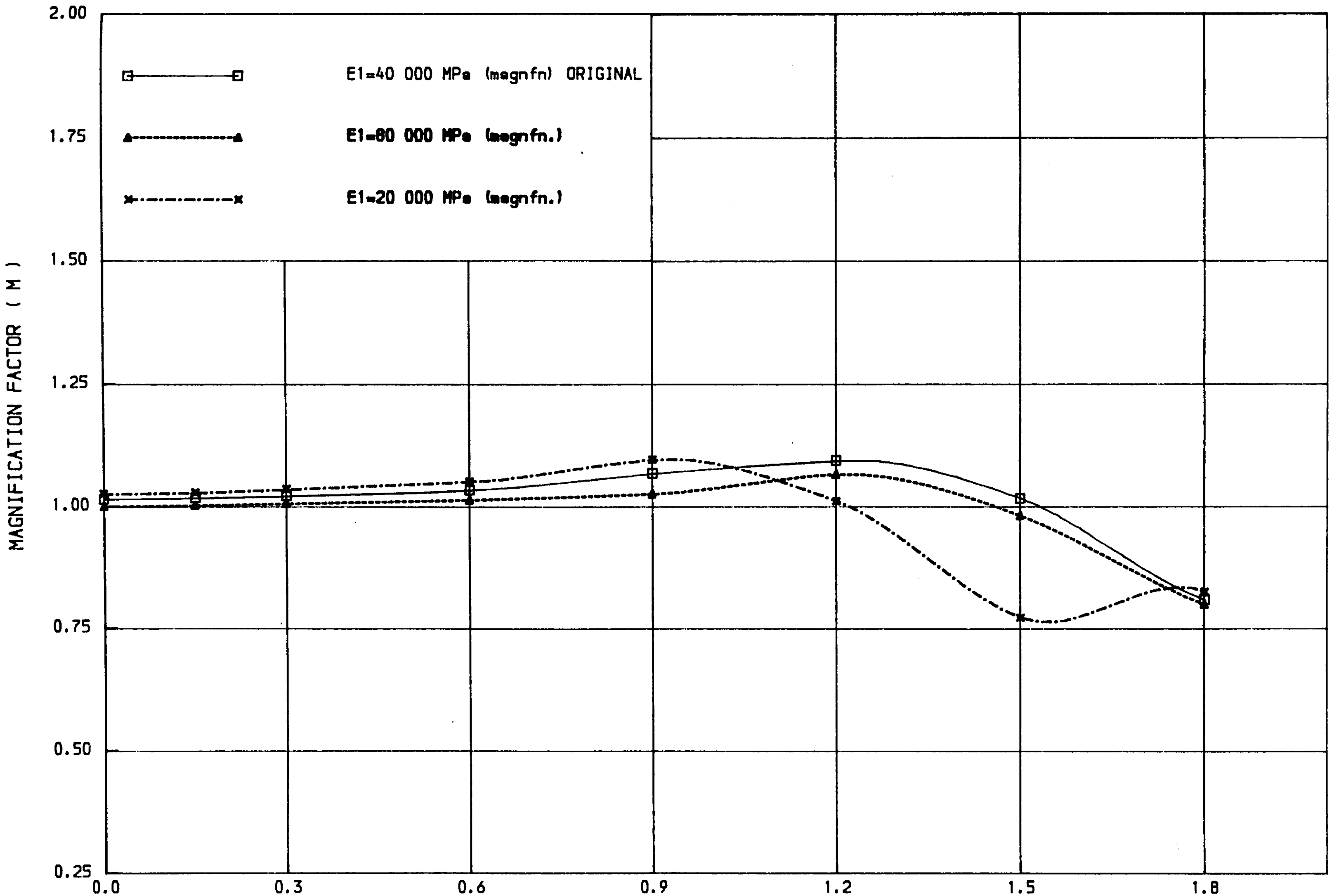

RIGID PAVEMENT ♦♦♦ THREE-LAYER SYSTEM

(FIG.4.16.b) *TP= 40 msec , PERIOD T= 140 msec*

(SLAB STIFFNESS ANALYSIS)

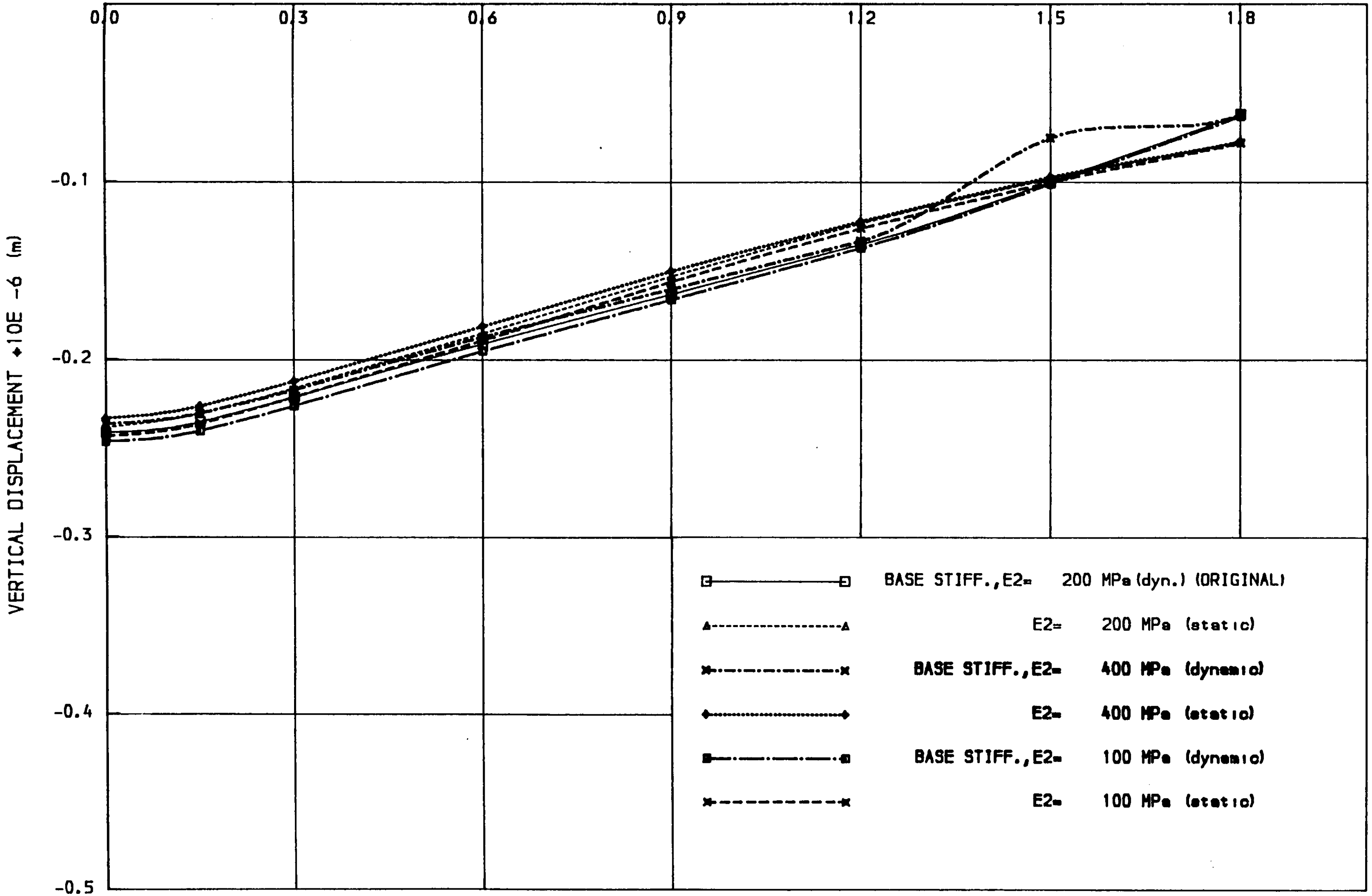

(FIG.4.17.a)

RIGID PAVEMENT *** THREE-LAYER SYSTEM

RADIUS (m)

DEFLECTION BASINS (BASE STIFFNESS ANALYSIS)

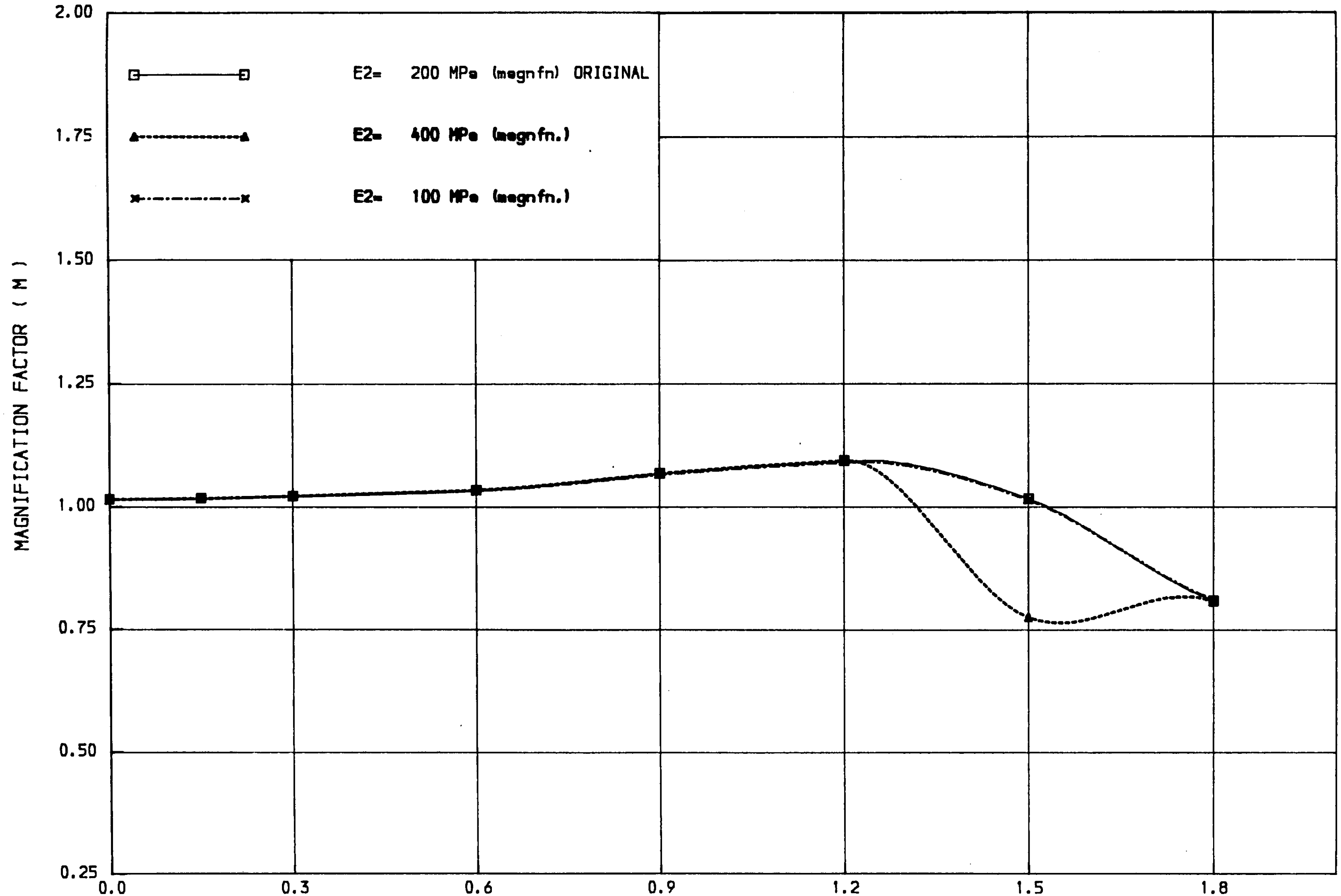

(FIG.4.17.b) *TP= 40 msec , PERIOD T= 140 msec*
(BASE STIFFNESS ANALYSIS)

RIGID PAVEMENT ♦♦♦ THREE-LAYER SYSTEM
RADIUS (m)

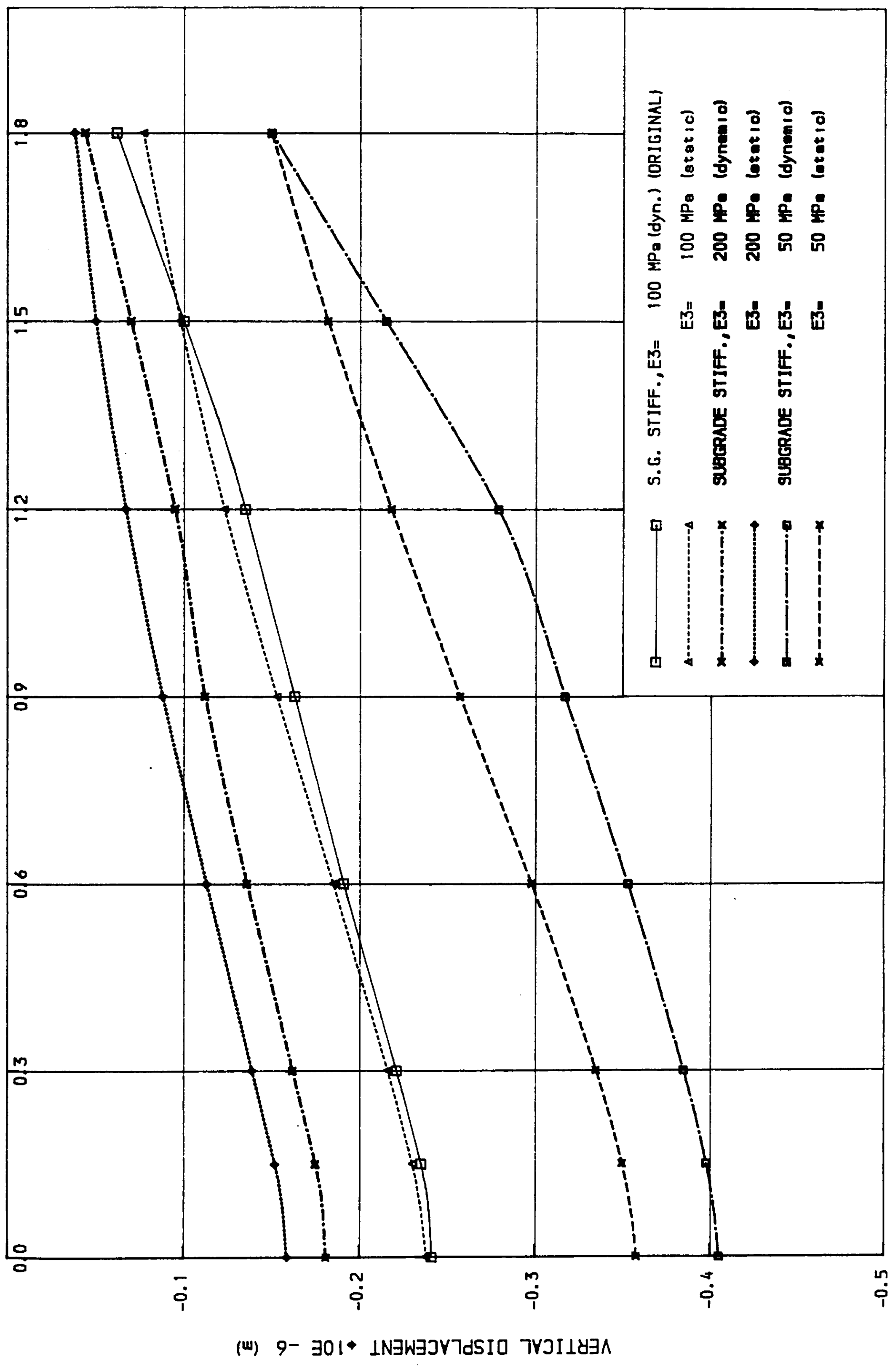

(FIG.4.18.a)

RADIUS (m)

RIGID PAVEMENT *** THREE-LAYER SYSTEM

DEFLECTION BASINS (SUBGRADE STIFFNESS ANALYSIS)

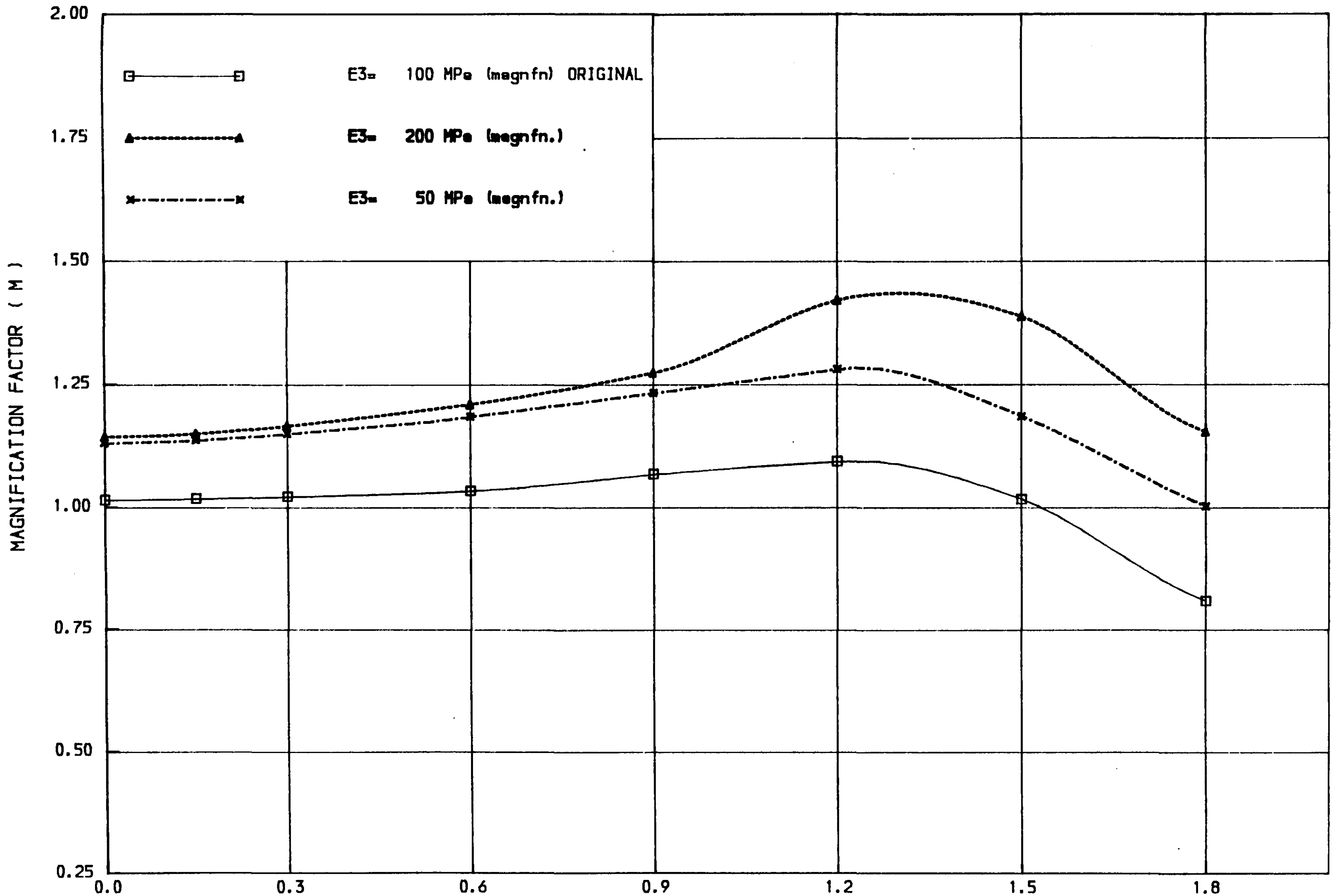

(FIG.4.18.b) *TP= 40 msec , PERIOD T= 140 msec*
(SUBGRADE STIFFNESS ANALYSIS)

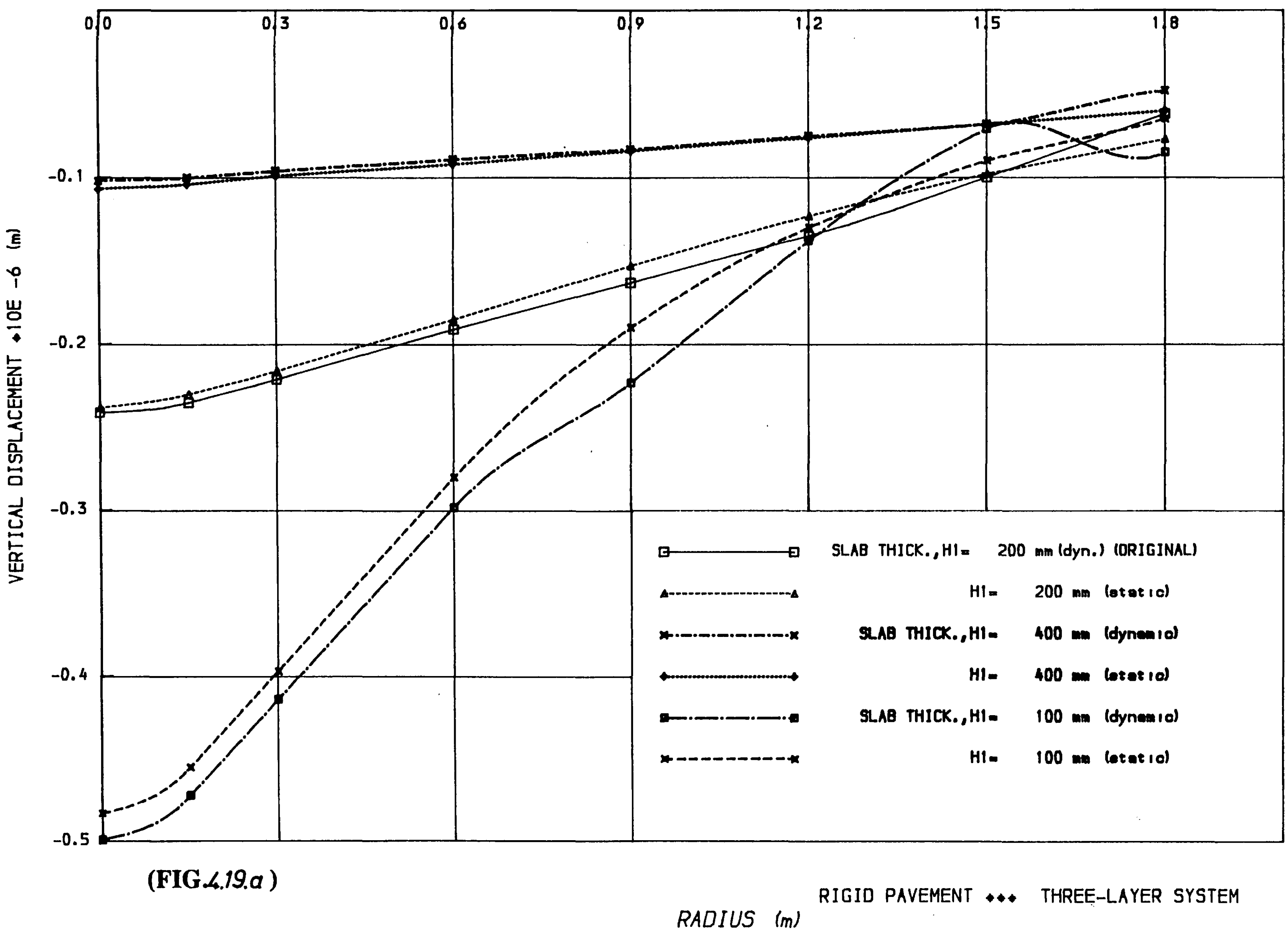

(FIG.4.19.a)

RIGID PAVEMENT *** THREE-LAYER SYSTEM

DEFLECTION BASINS (SLAB THICKNESS ANALYSIS)

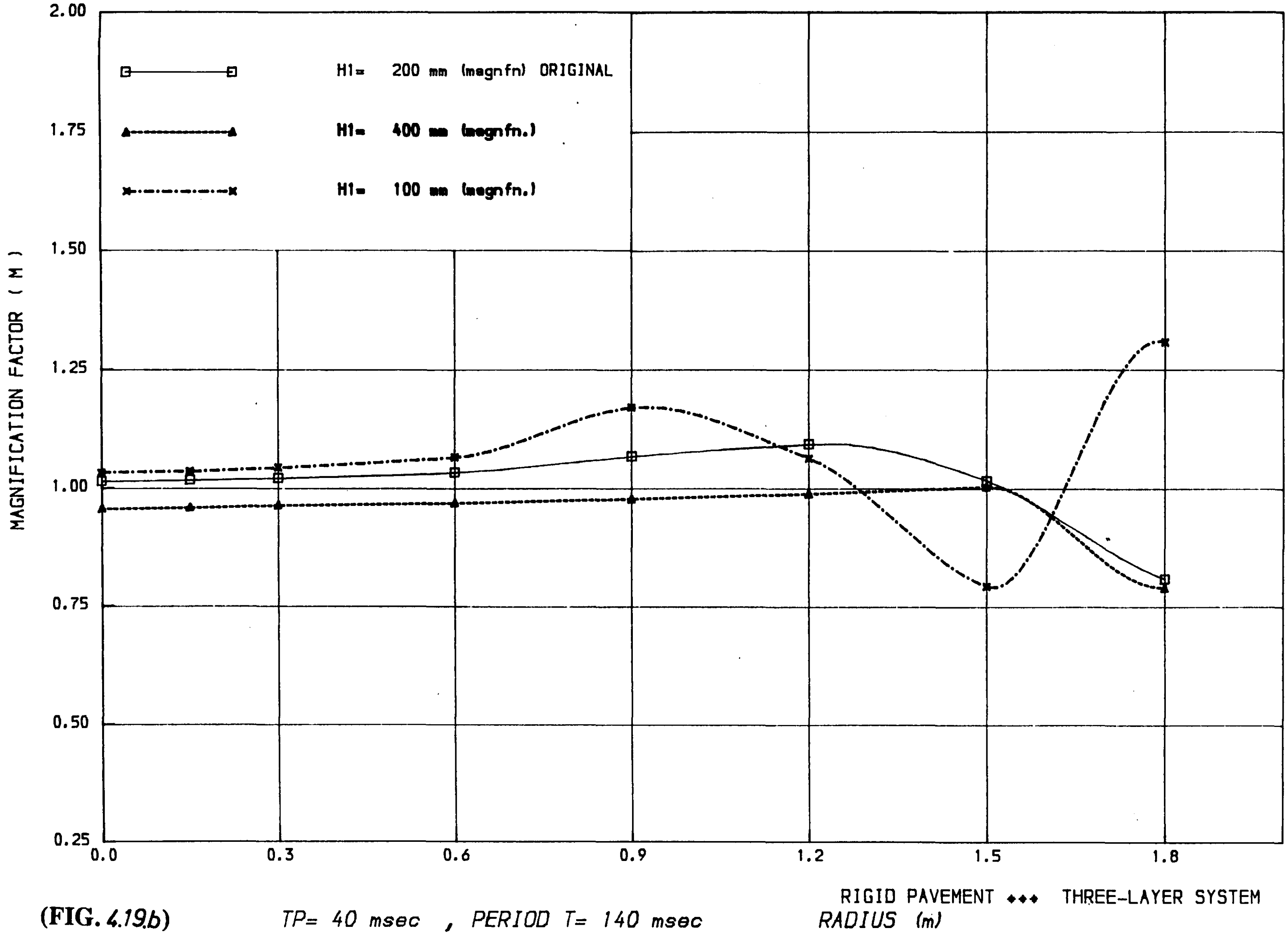

(FIG. 4.19b) TP= 40 msec , PERIOD T= 140 msec
(SLAB THICKNESS ANALYSIS)

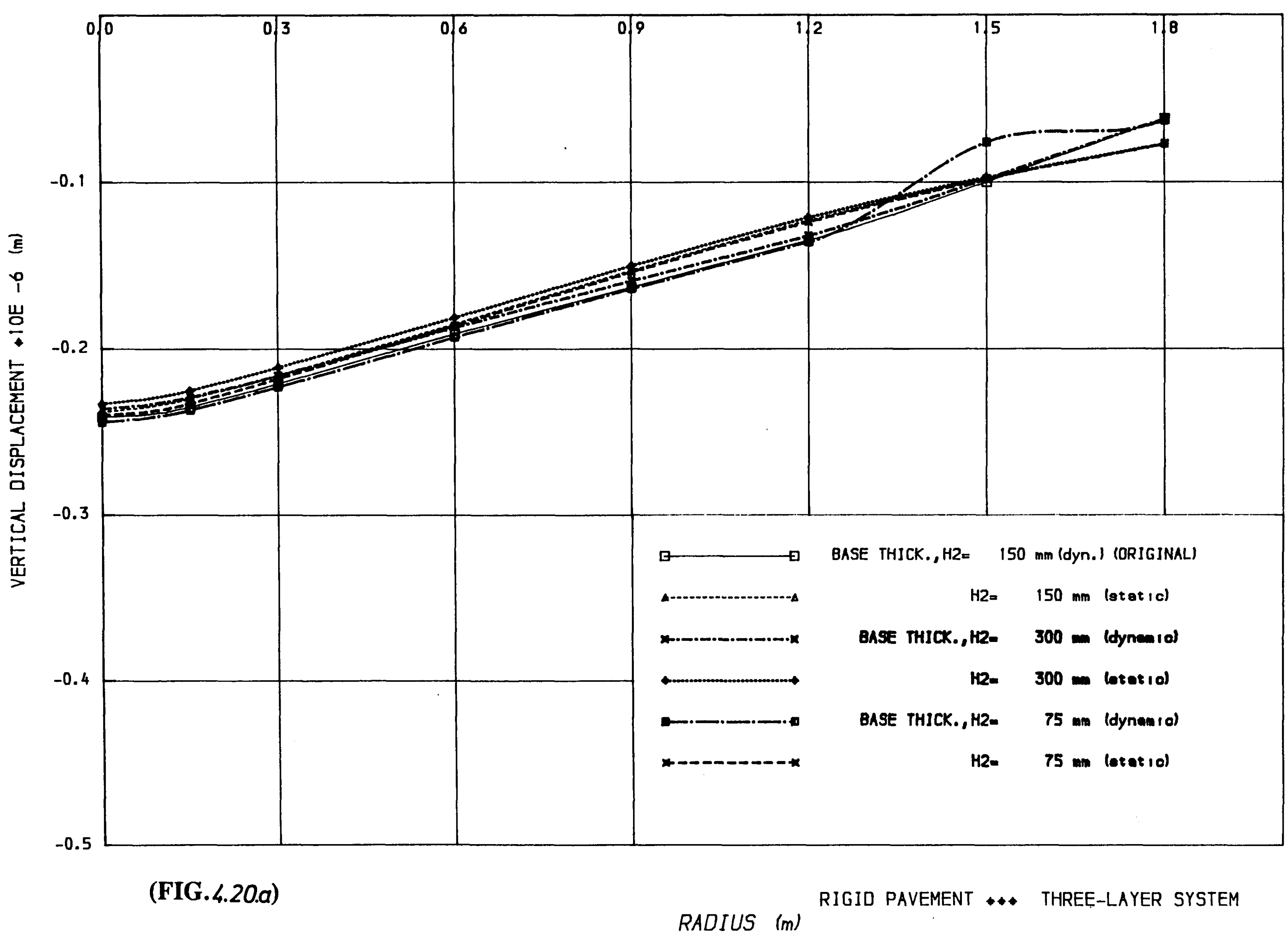

(FIG.4.20a)

DEFLECTION BASINS (BASE THICKNESS ANALYSIS)

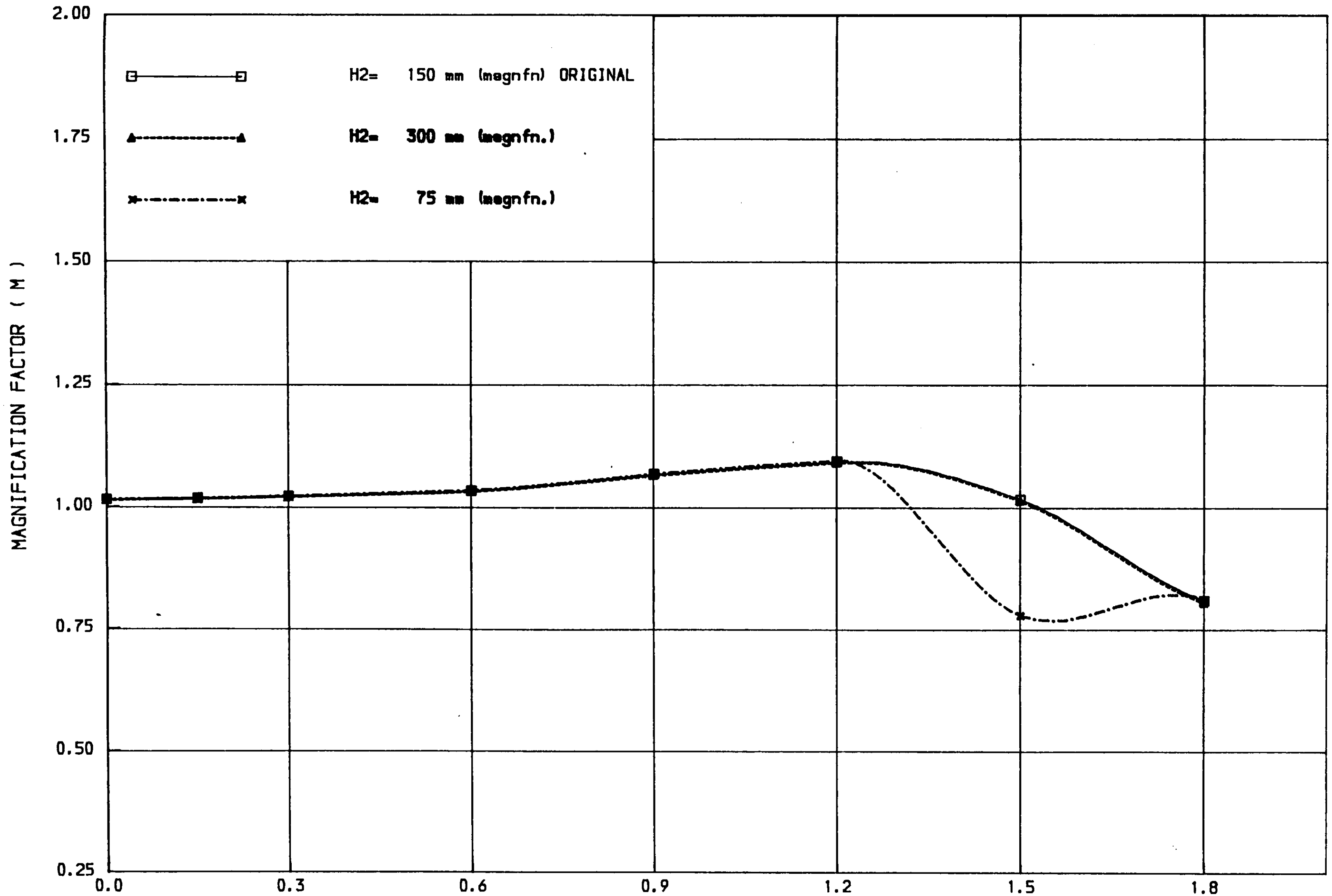

RIGID PAVEMENT +++ THREE-LAYER SYSTEM

RADIUS (m)

(FIG.4.20b) TP= 40 msec , PERIOD T= 140 msec

(BASE THICKNESS ANALYSIS)

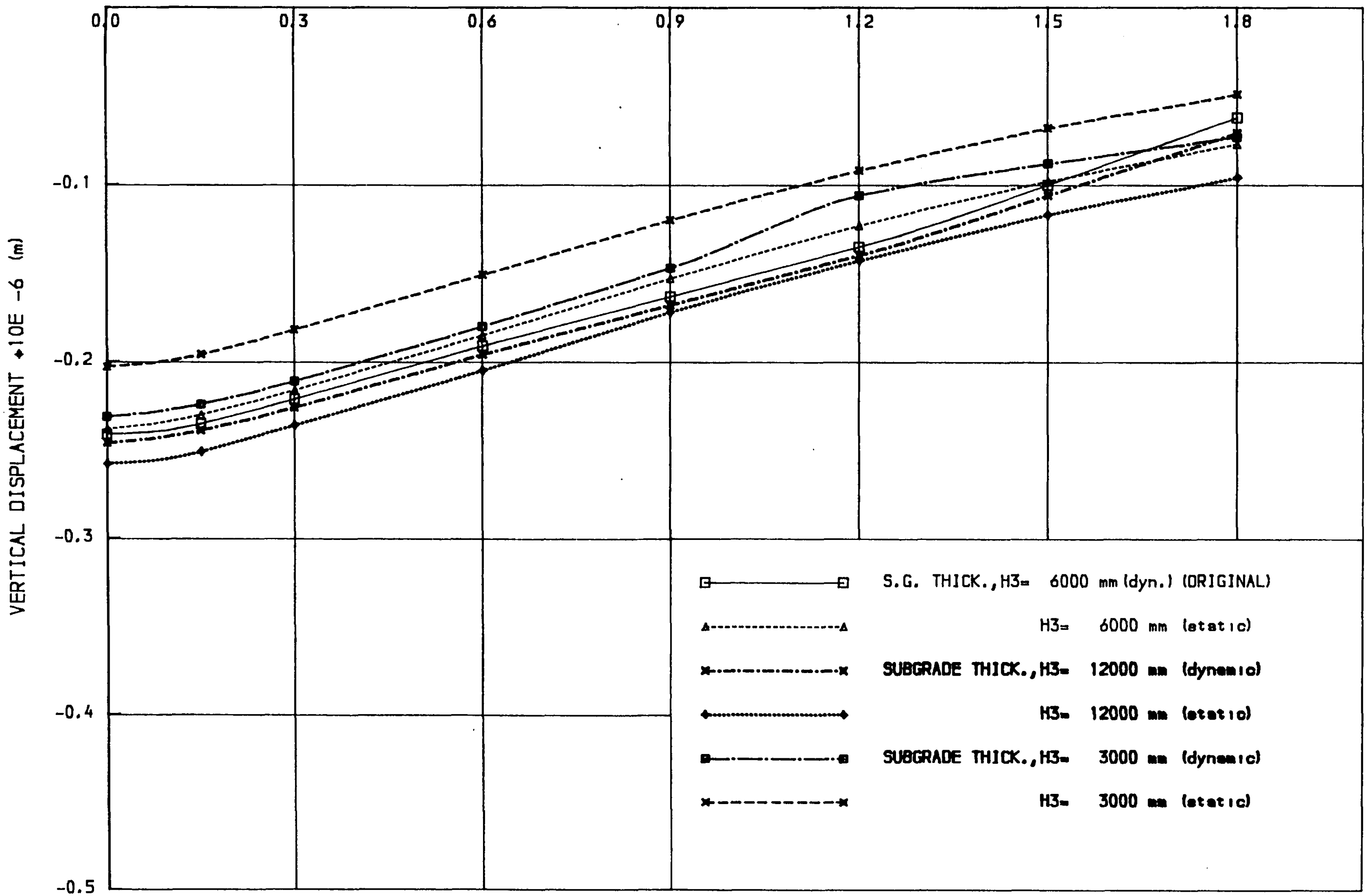

(FIG. 4.21a)

RIGID PAVEMENT *** THREE-LAYER SYSTEM

DEFLECTION BASINS (SUBGRADE THICKNESS ANALYSIS)

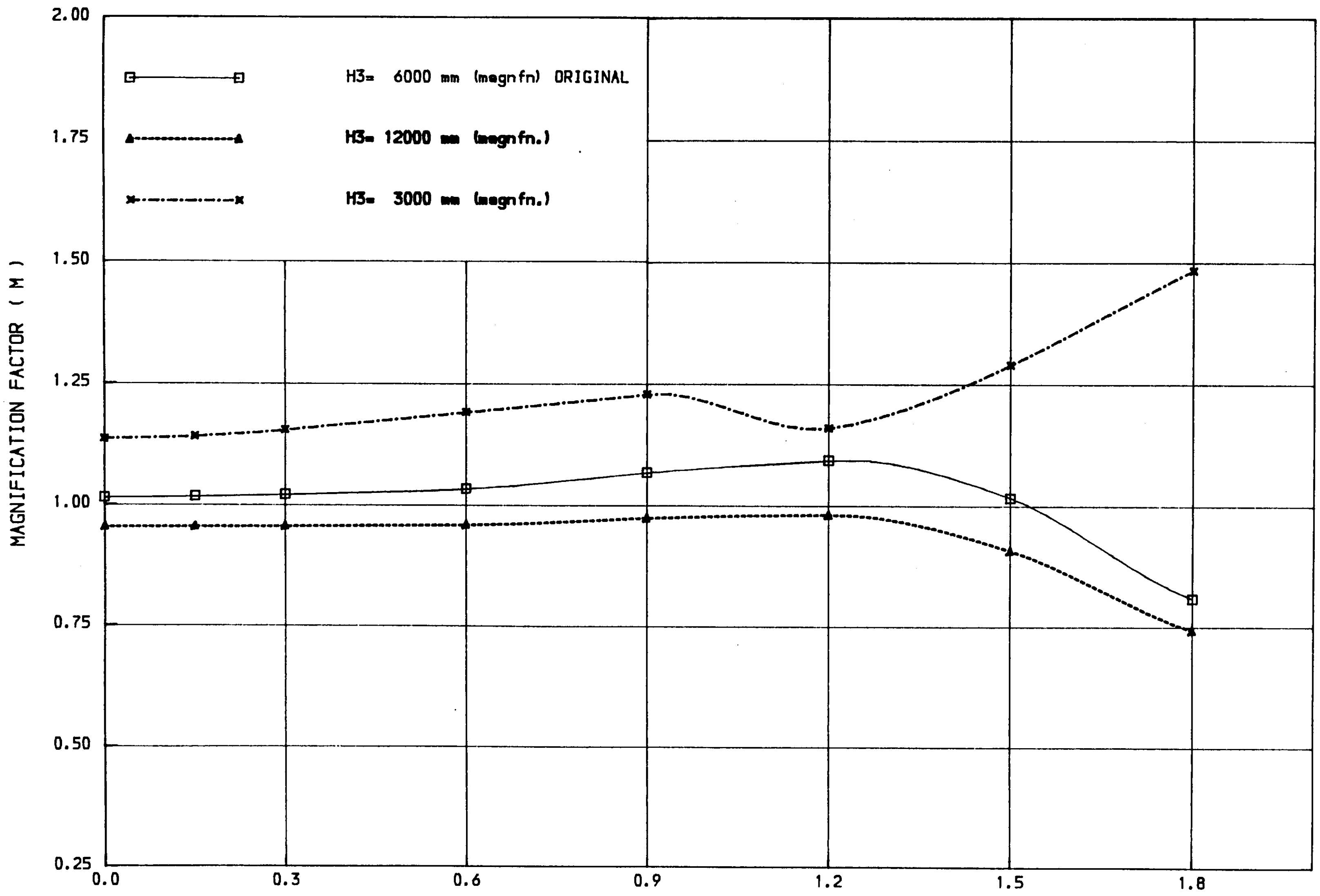

(FIG.4.21b) TP= 40 msec , PERIOD T= 140 msec
(SUBGRADE THICKNESS ANALYSIS)

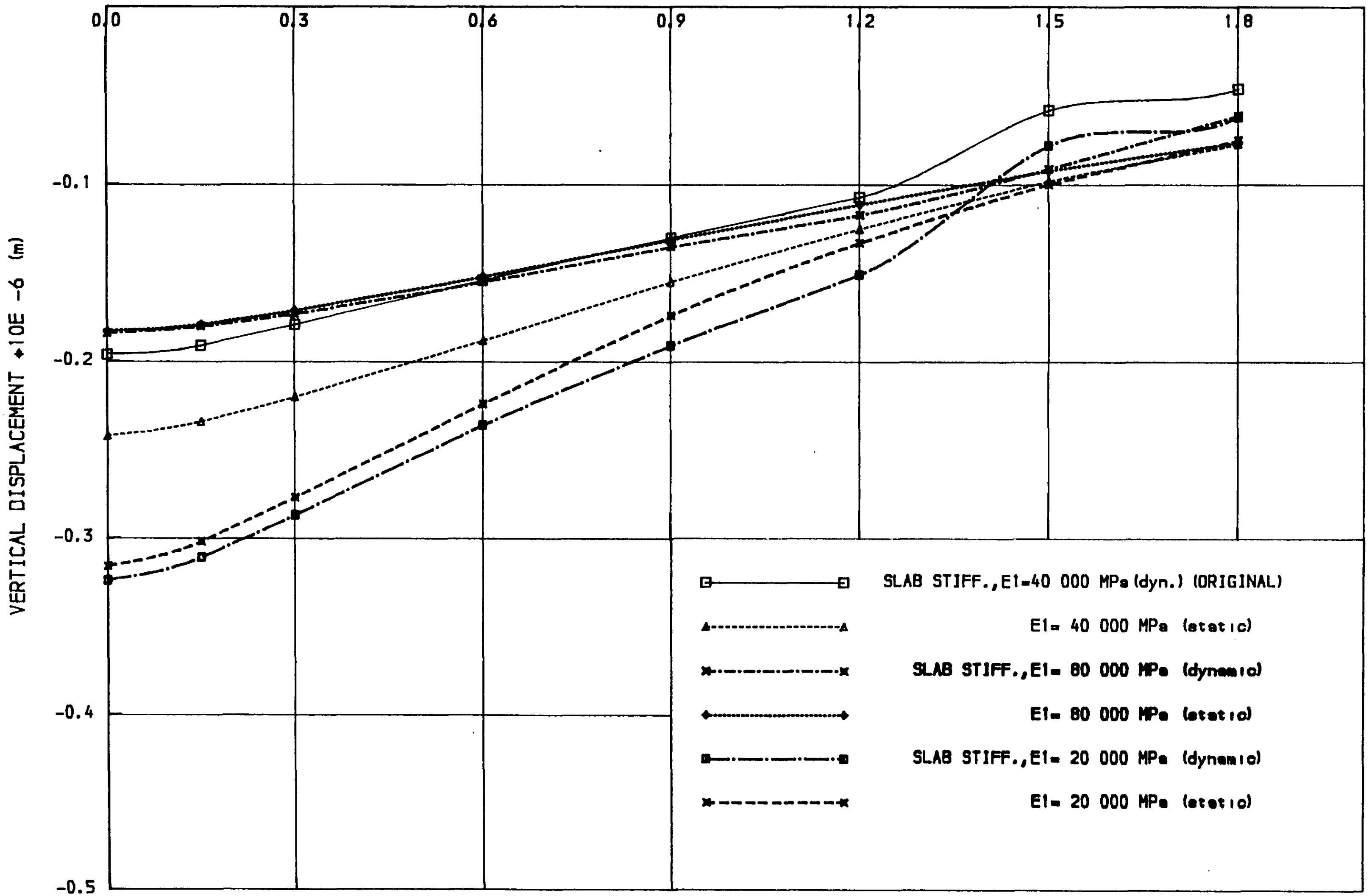

(FIG.4.22a)

RIGID AIRPORT RUNWAY *** TWO-LAYER SYSTEM

DEFLECTION BASINS (SLAB STIFFNESS ANALYSIS)

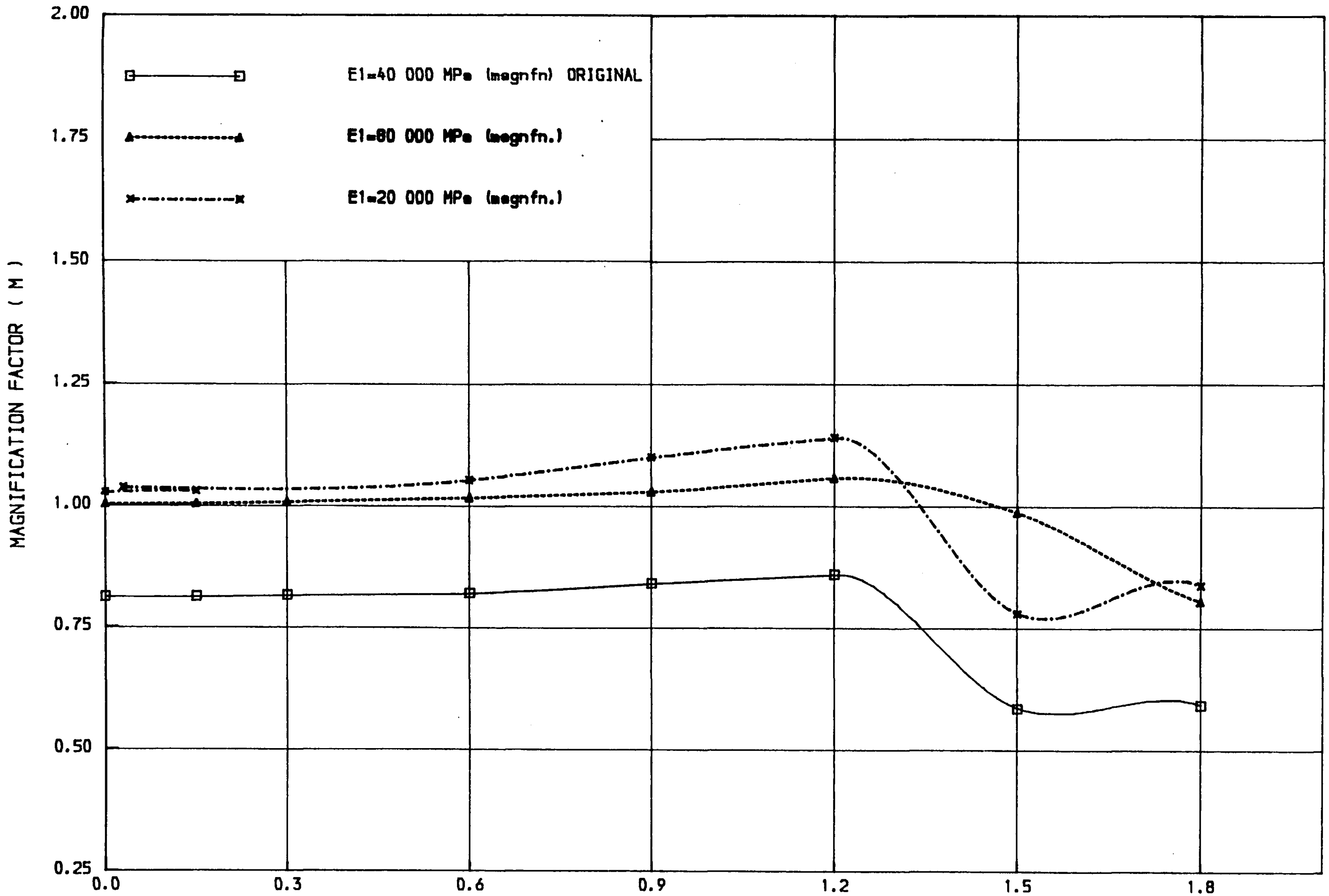

(FIG.4.22b) TP= 40 msec , PERIOD T= 140 msec
(SLAB STIFFNESS ANALYSIS)

RIGID AIRPORT RUNWAY ♦♦♦ TWO-LAYER SYSTEM

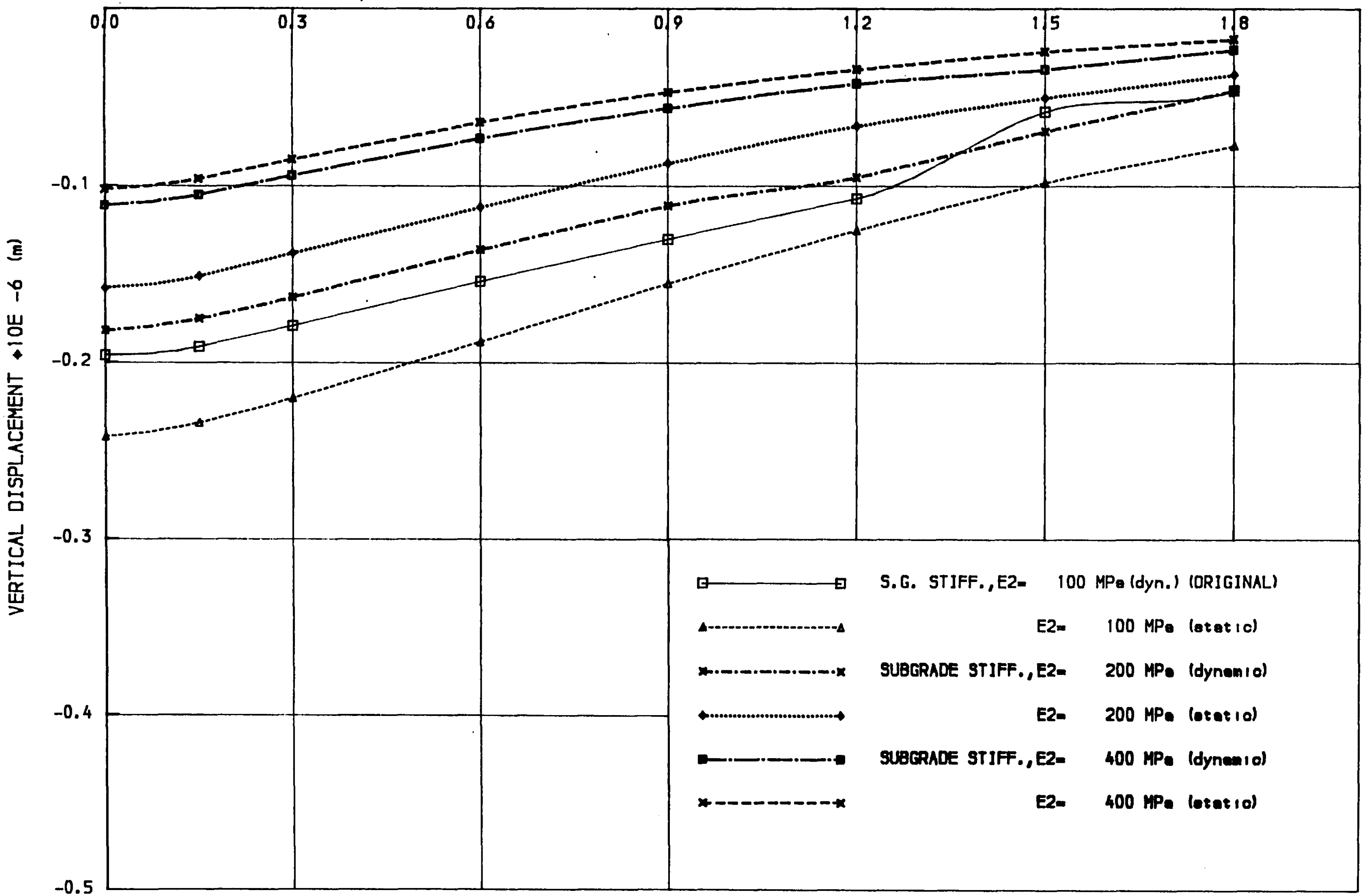

(FIG.4.23.a)

RIGID AIRPORT RUNWAY *** TWO-LAYER SYSTEM

DEFLECTION BASINS (SUBGRADE STIFFNESS ANALYSIS)

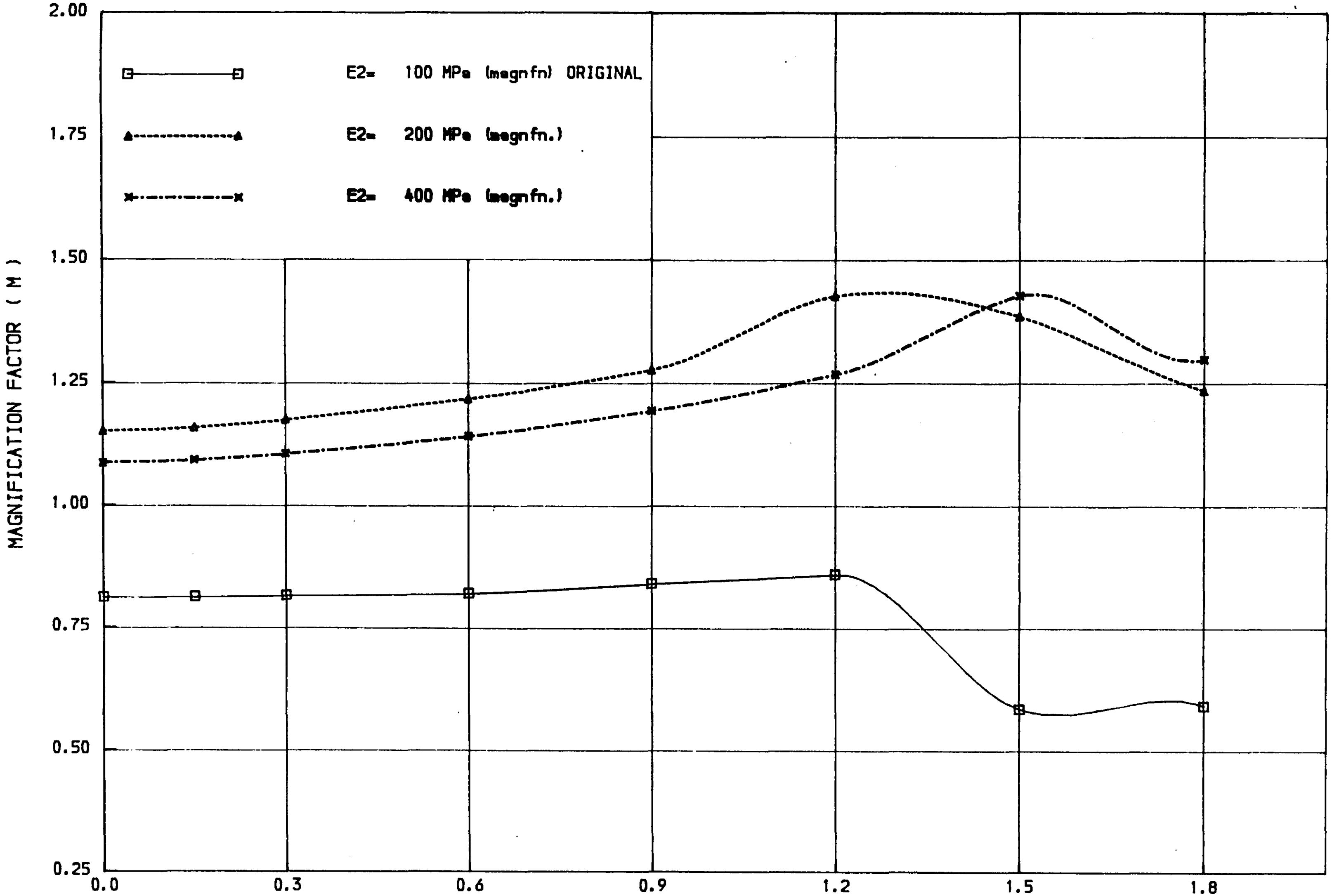

(FIG. 4.23.b)

TP= 40 msec , PERIOD T= 140 msec
(SUBGRADE STIFFNESS ANALYSIS)

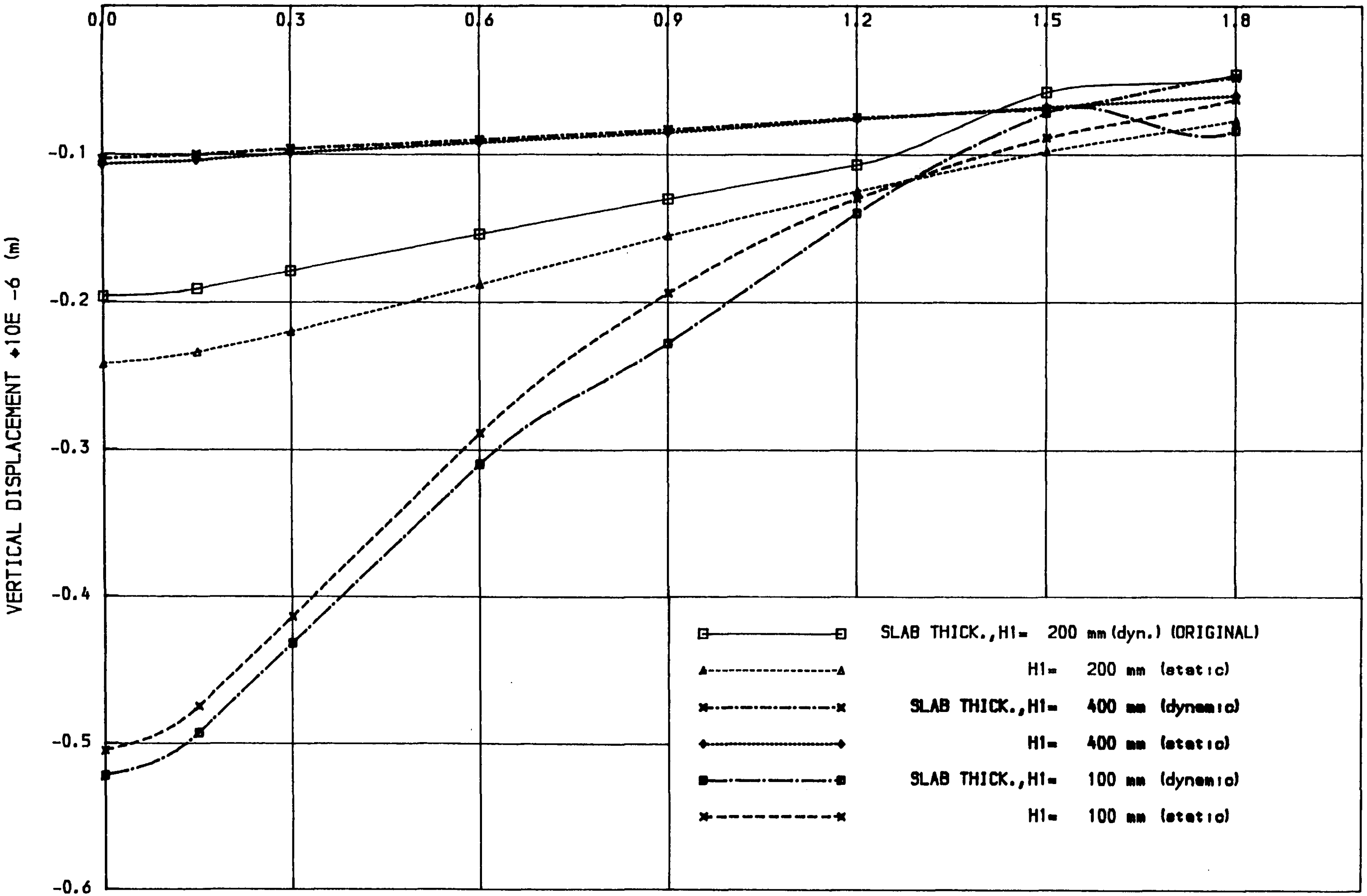

(FIG.4.24a)

RIGID AIRPORT RUNWAY *** TWO-LAYER SYSTEM

RADIUS (m)

DEFLECTION BASINS (SLAB THICKNESS ANALYSIS)

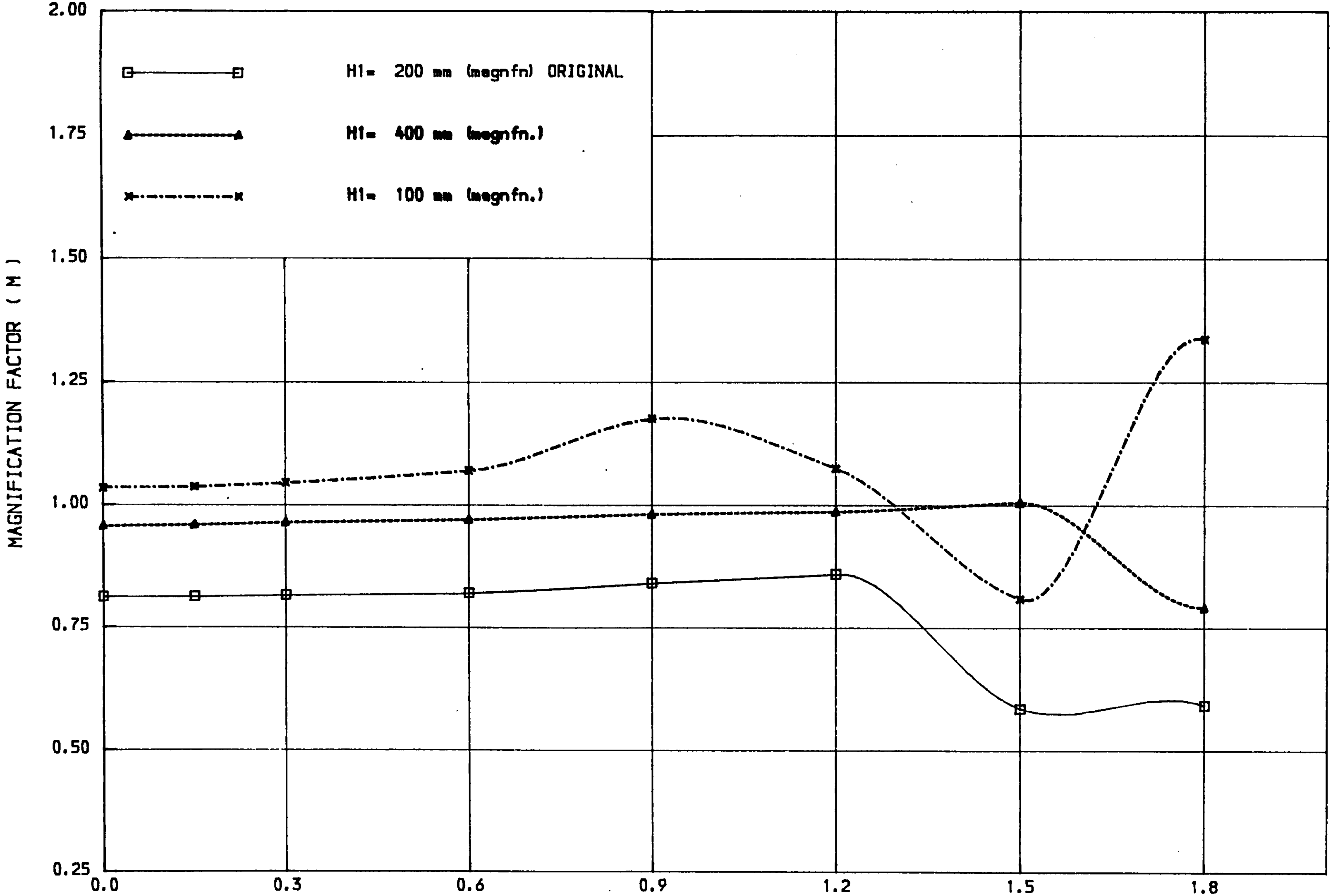

(FIG. 4.24.b) TP= 40 msec , PERIOD T= 140 msec
(SLAB THICKNESS ANALYSIS)

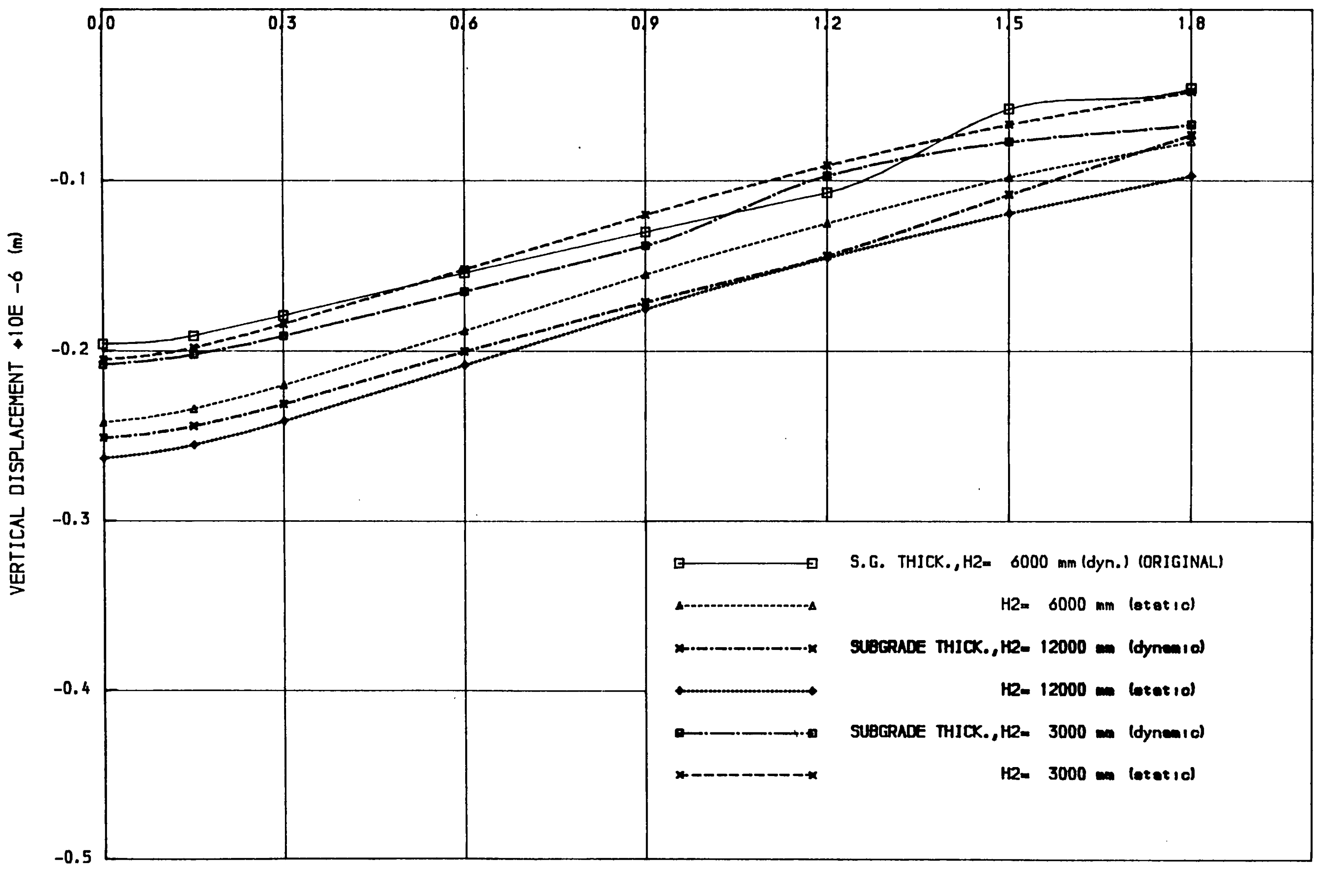

(FIG.4.25a)

DEFLECTION BASINS (SUBGRADE THICKNESS ANALYSIS)

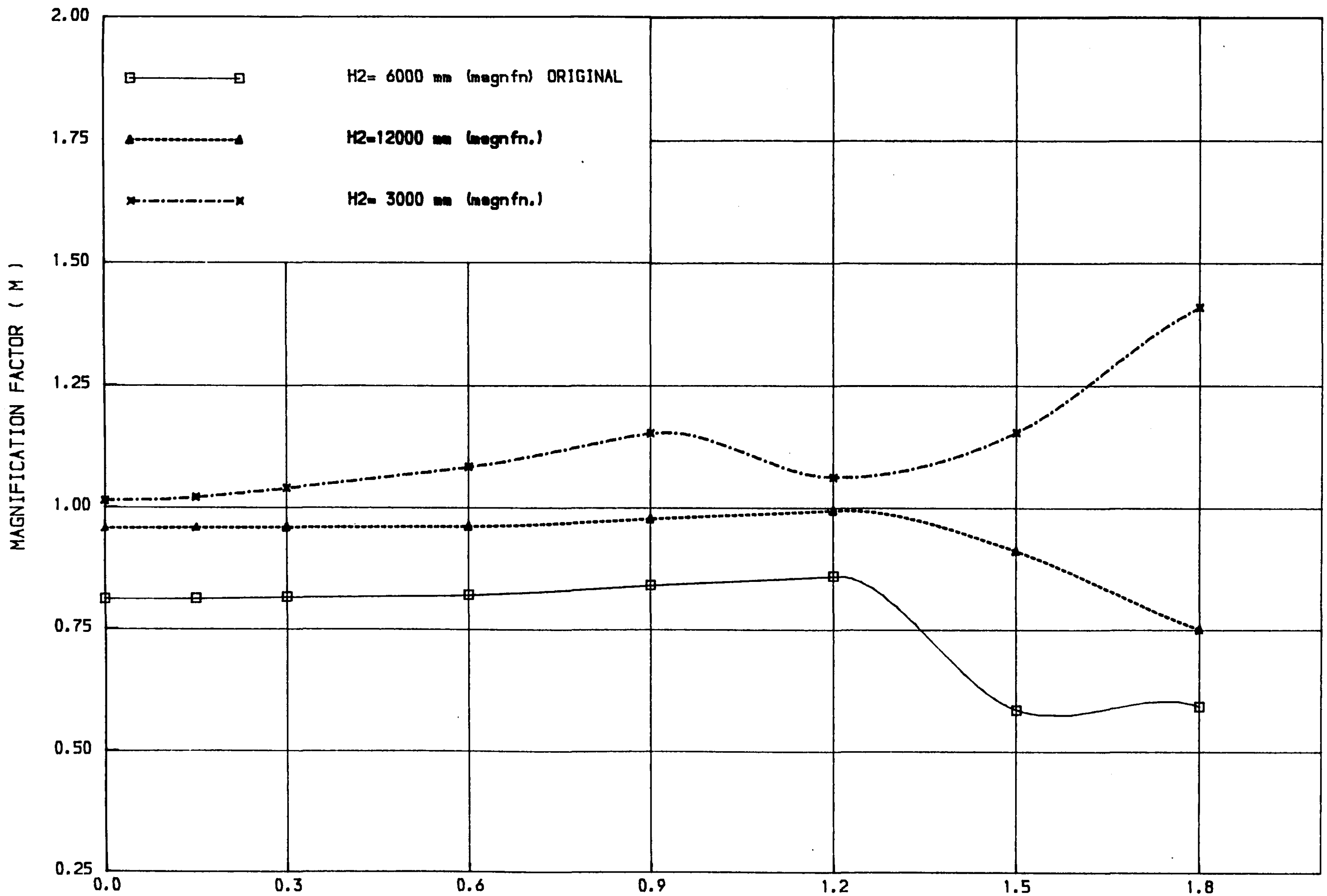

(FIG.4.25.b) RIGID AIRPORT RUNWAY ♦♦♦ TWO-LAYER SYSTEM

TP= 40 msec , PERIOD T= 140 msec

(SUBGRADE THICKNESS ANALYSIS)

FOUR LAYER FLEXIBLE PAVEMENT

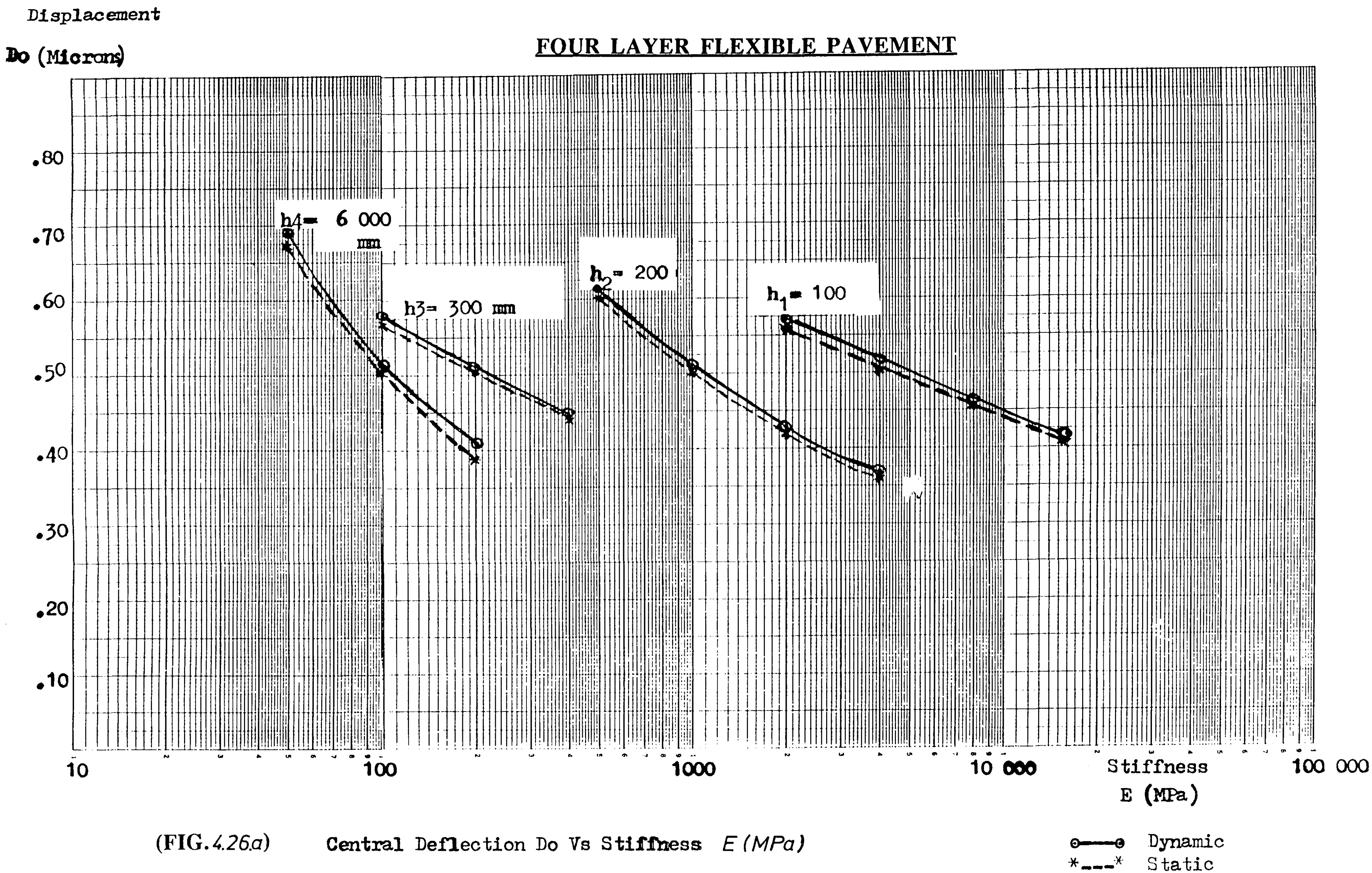

(FIG. 4.26a) Central Deflection Do Vs Stiffness E (MPa)

THREE -LAYER FLEXIBLE PAVEMENT

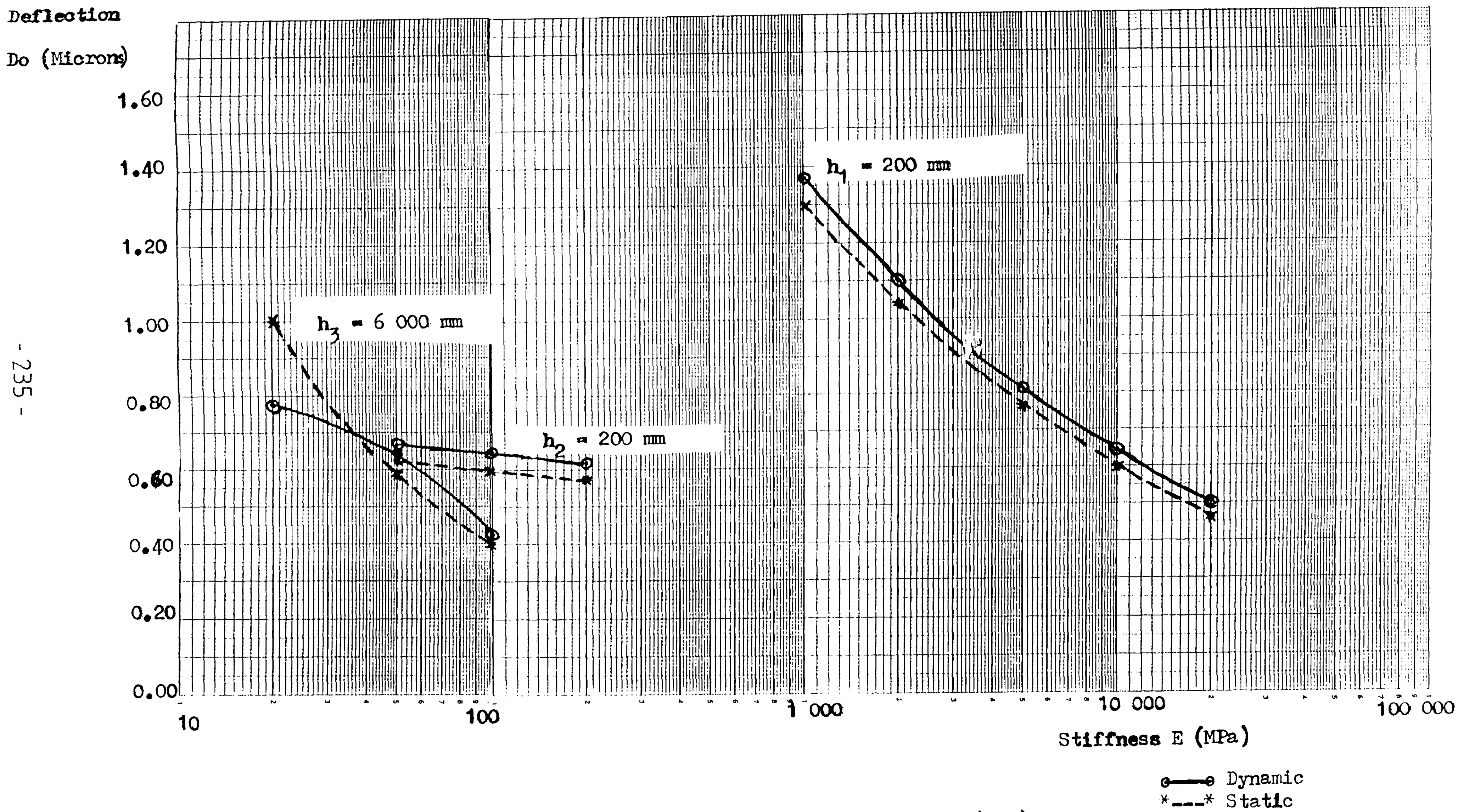

(FIG.4.26.b) Central Deflection Do Vs Stiffness E (MPa)

THREE -LAYER RIGID PAVEMENT

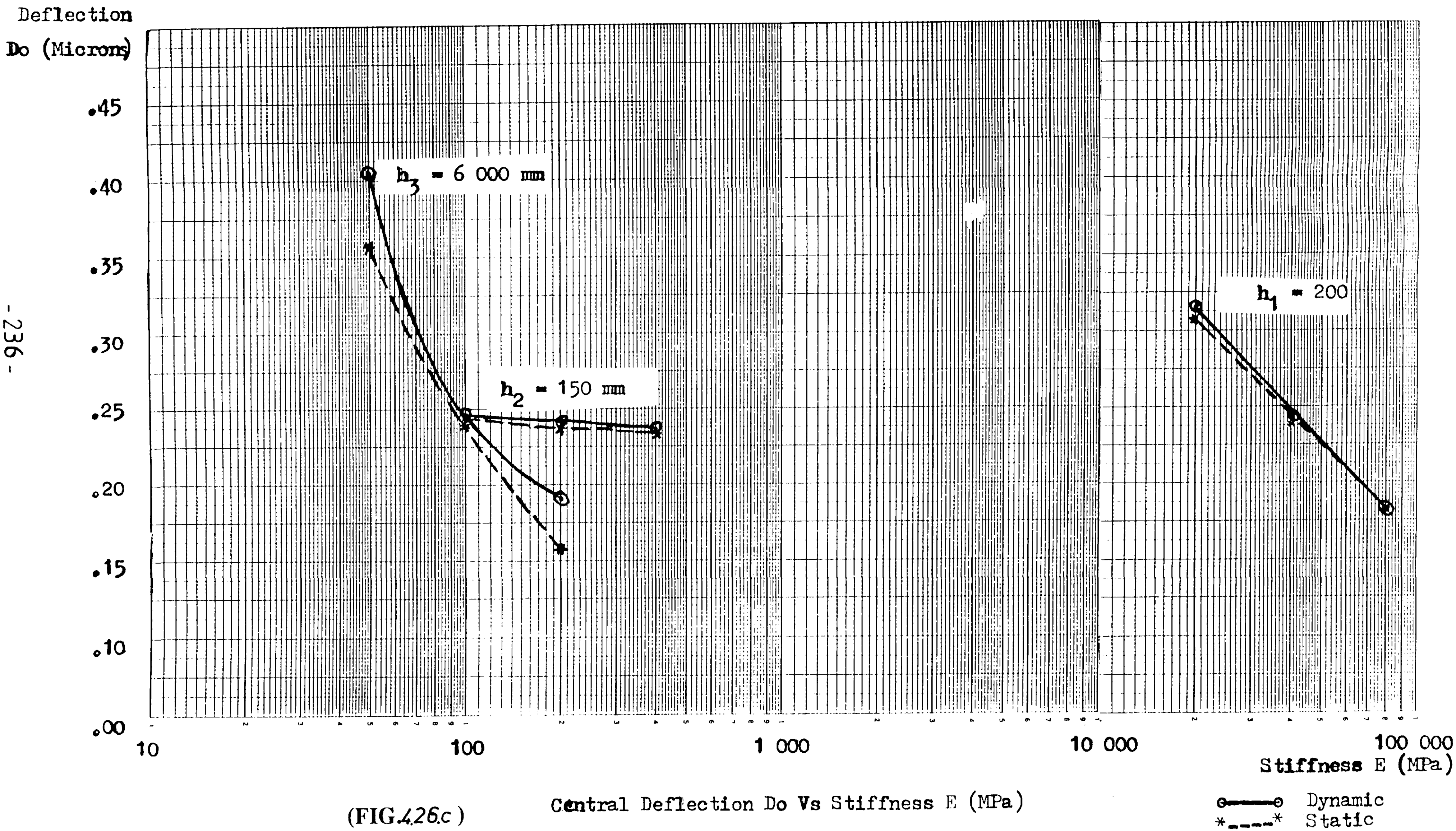

Central Deflection Do Vs Stiffness E (MPa)

(FIG.4.26.c)

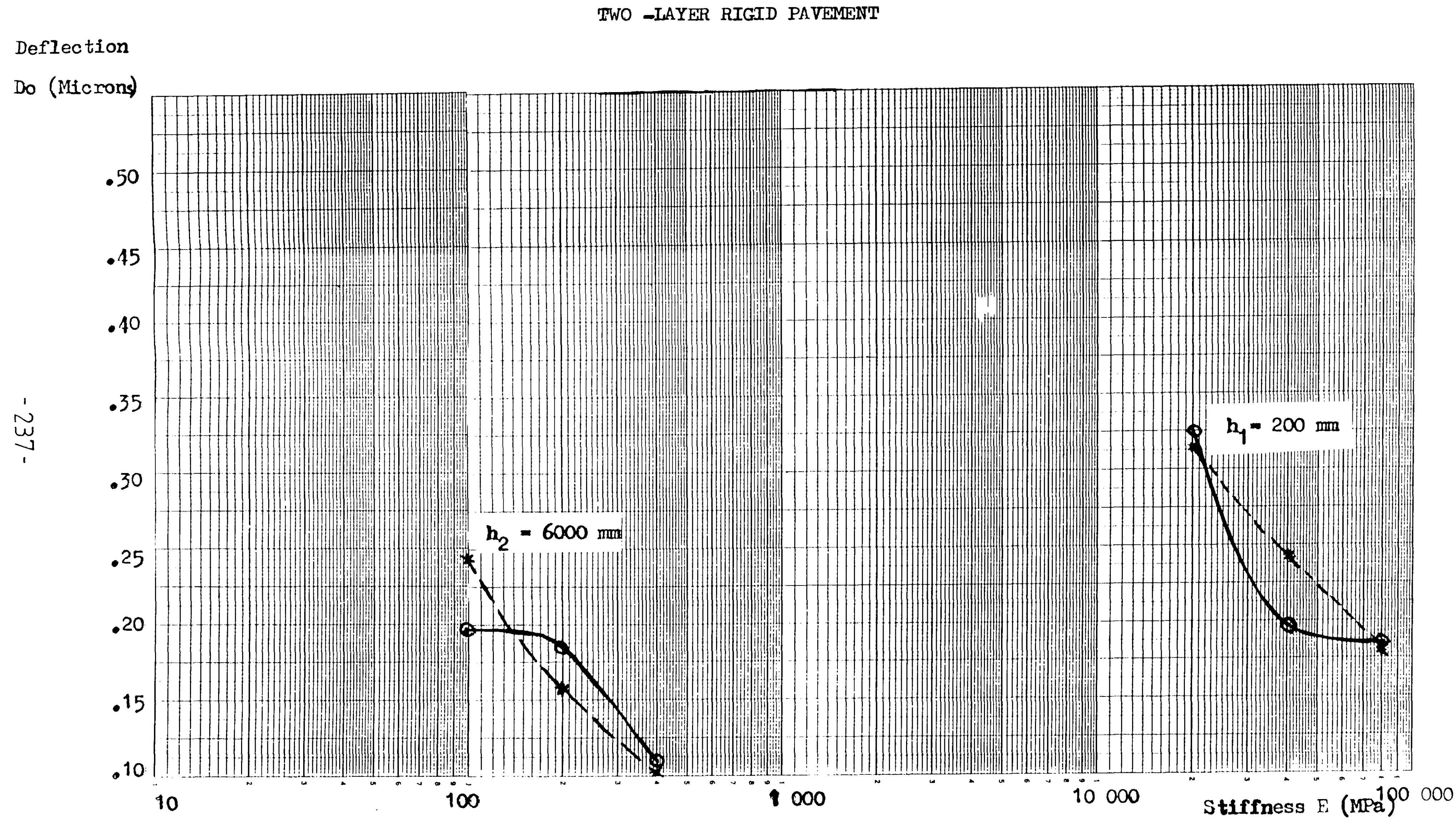

(FIG.4.26d) Central Deflection Do Vs Stiffness E (MPa)

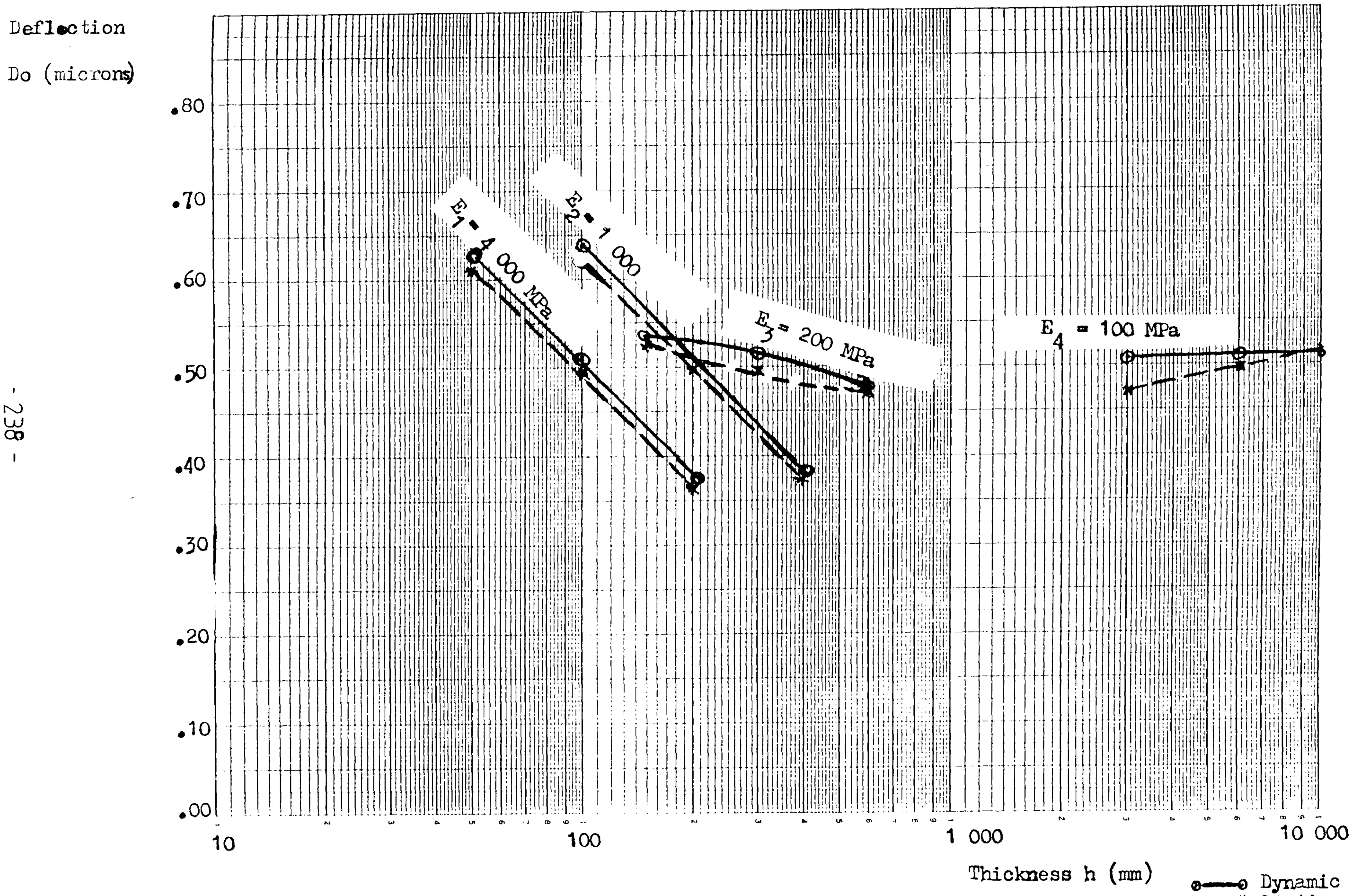

(FIG.4.27a) **Central Deflection Do Vs Layer Thickness h (mm)**

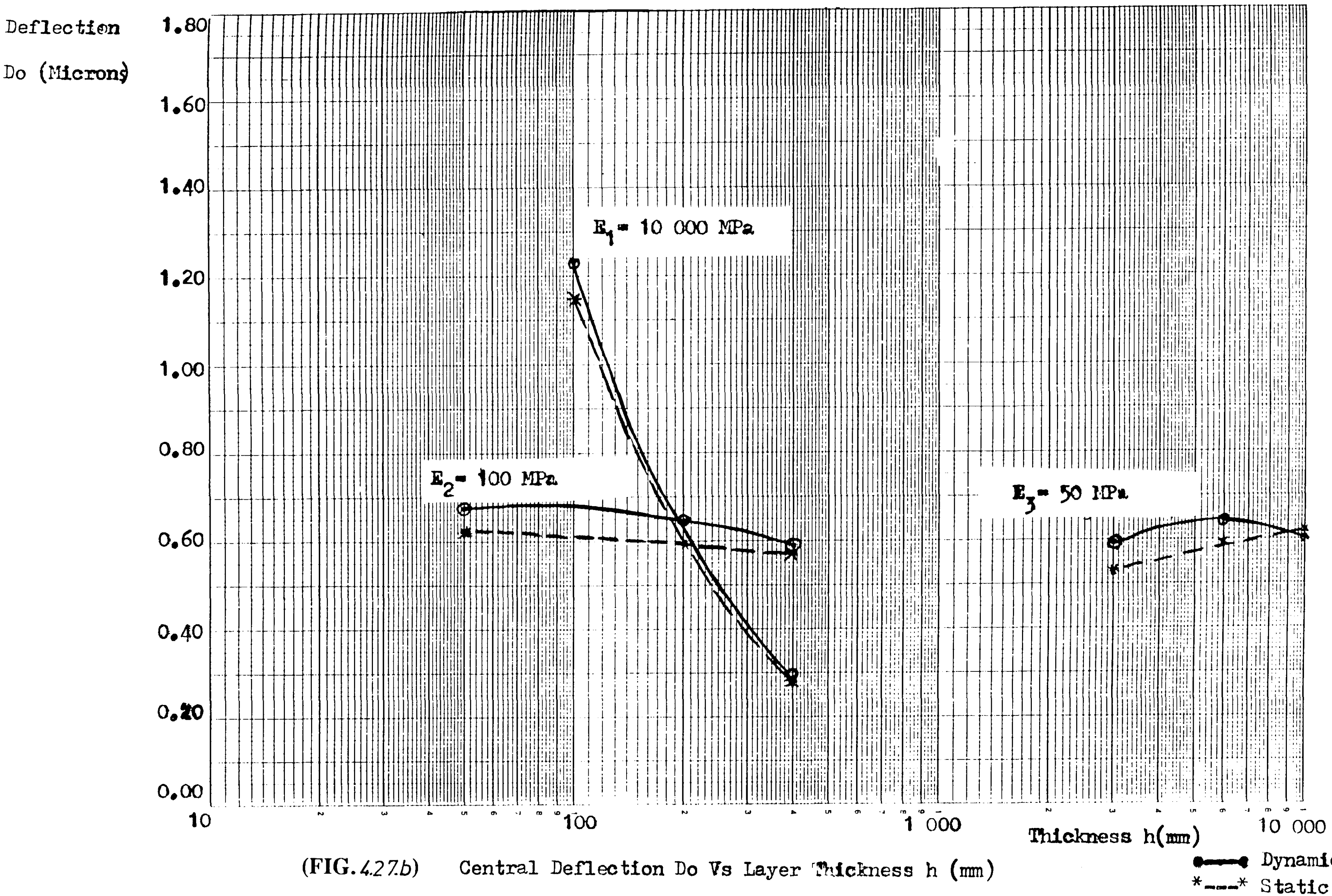

(FIG. 4.27b) Central Deflection Do Vs Layer Thickness h (mm)

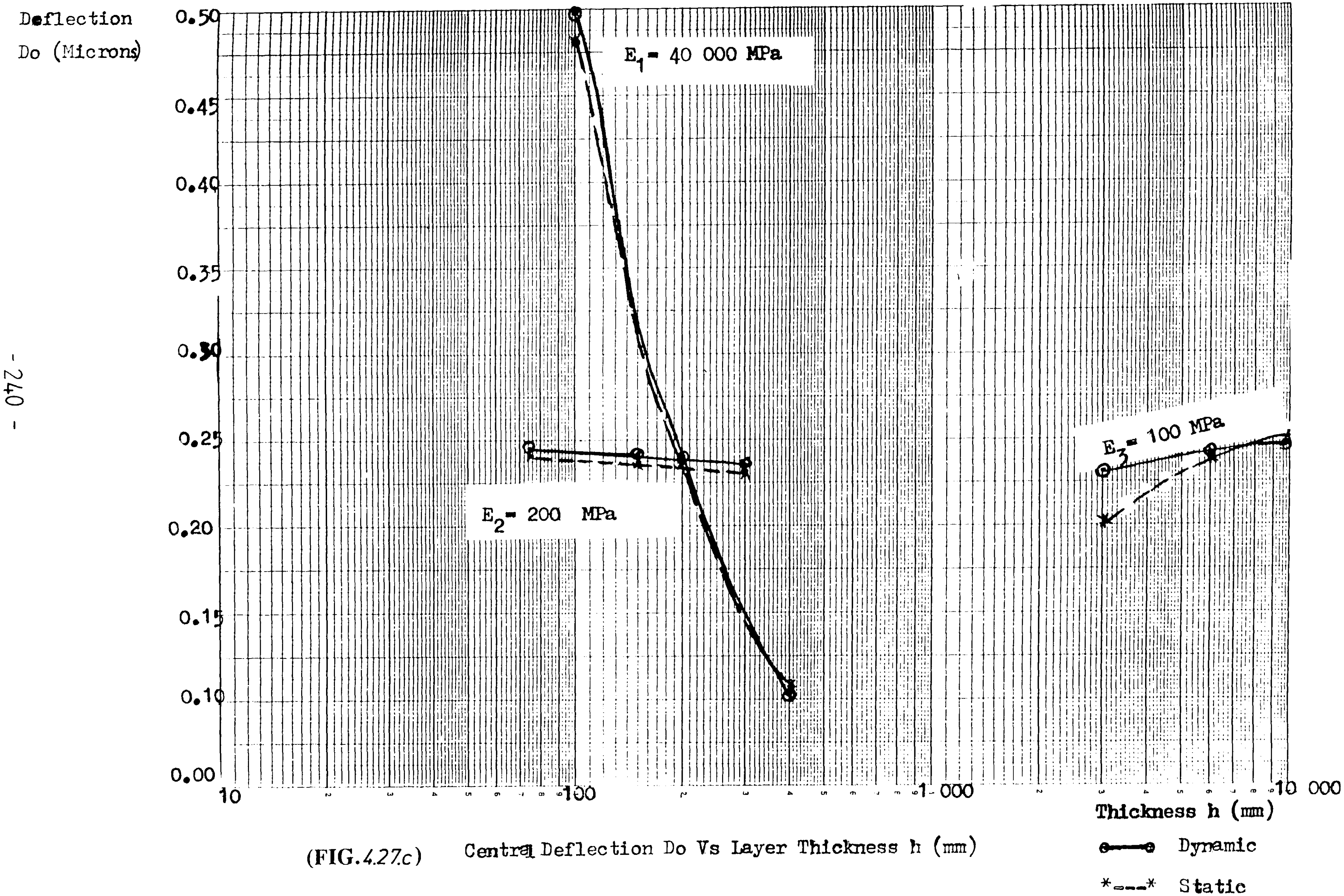

(FIG.4.27.c) Central Deflection Do Vs Layer Thickness h (mm)

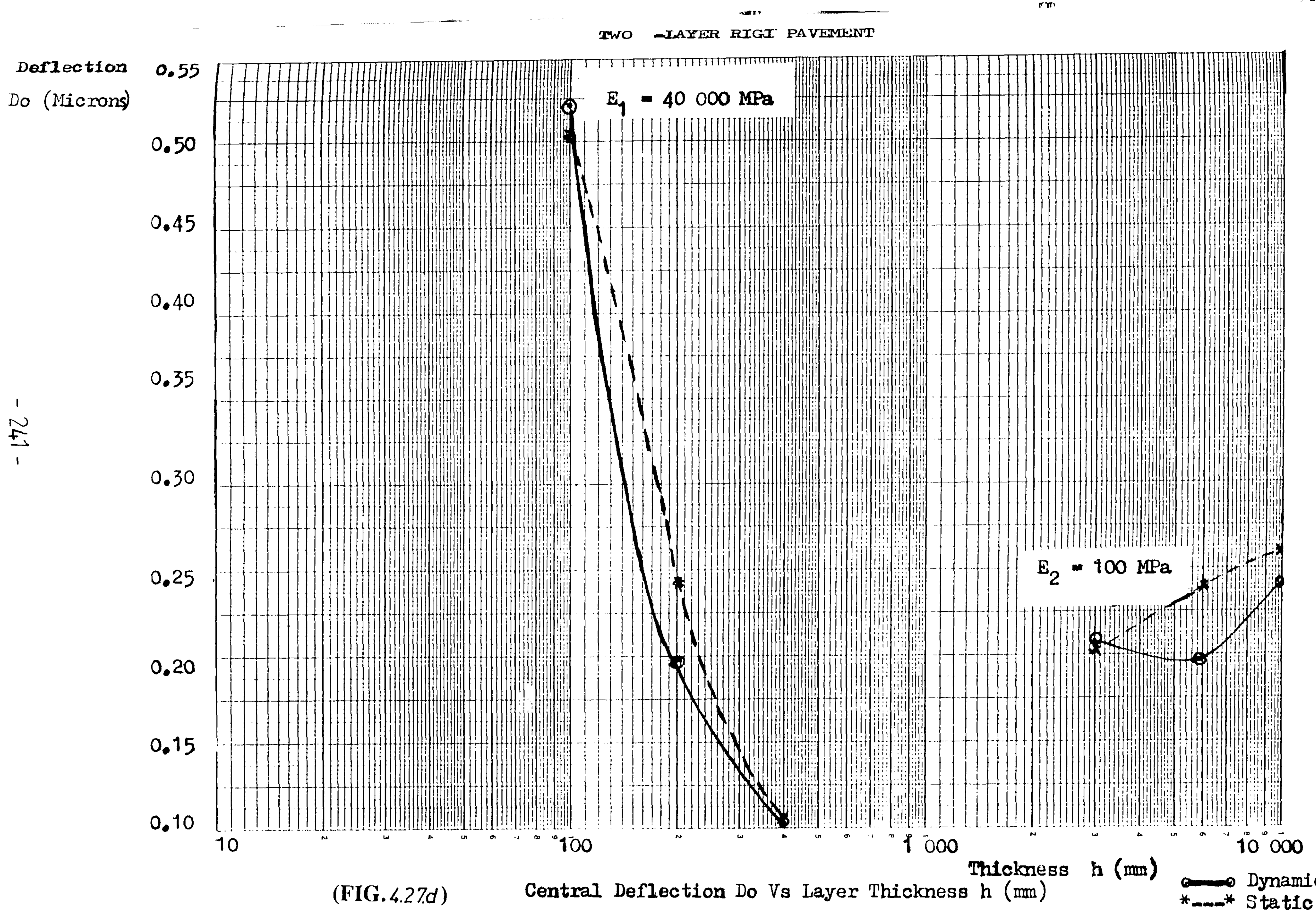

(FIG. 4.27d) Central Deflection Do Vs Layer Thickness h (mm)

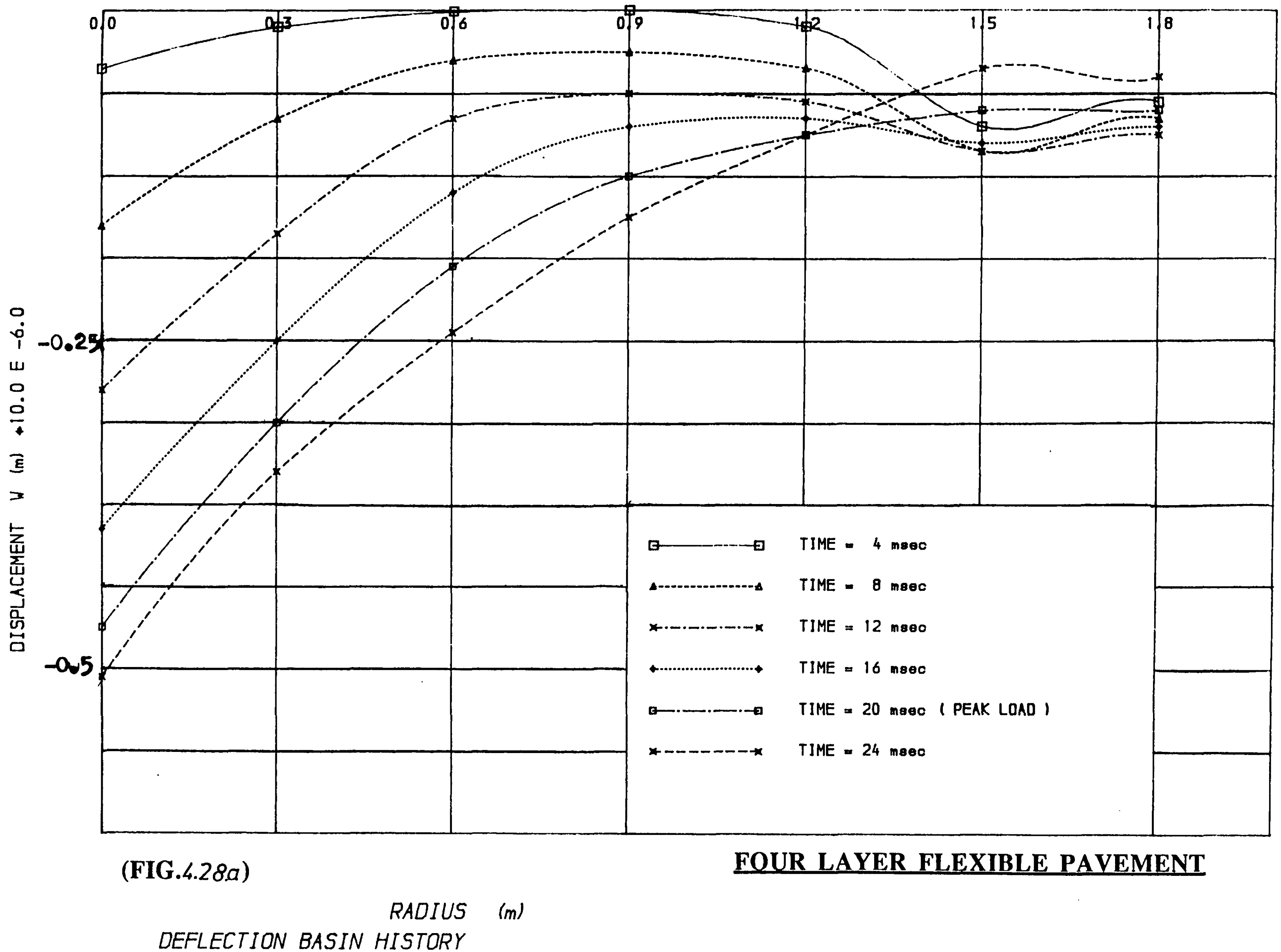

(FIG.4.28a)

FOUR LAYER FLEXIBLE PAVEMENT

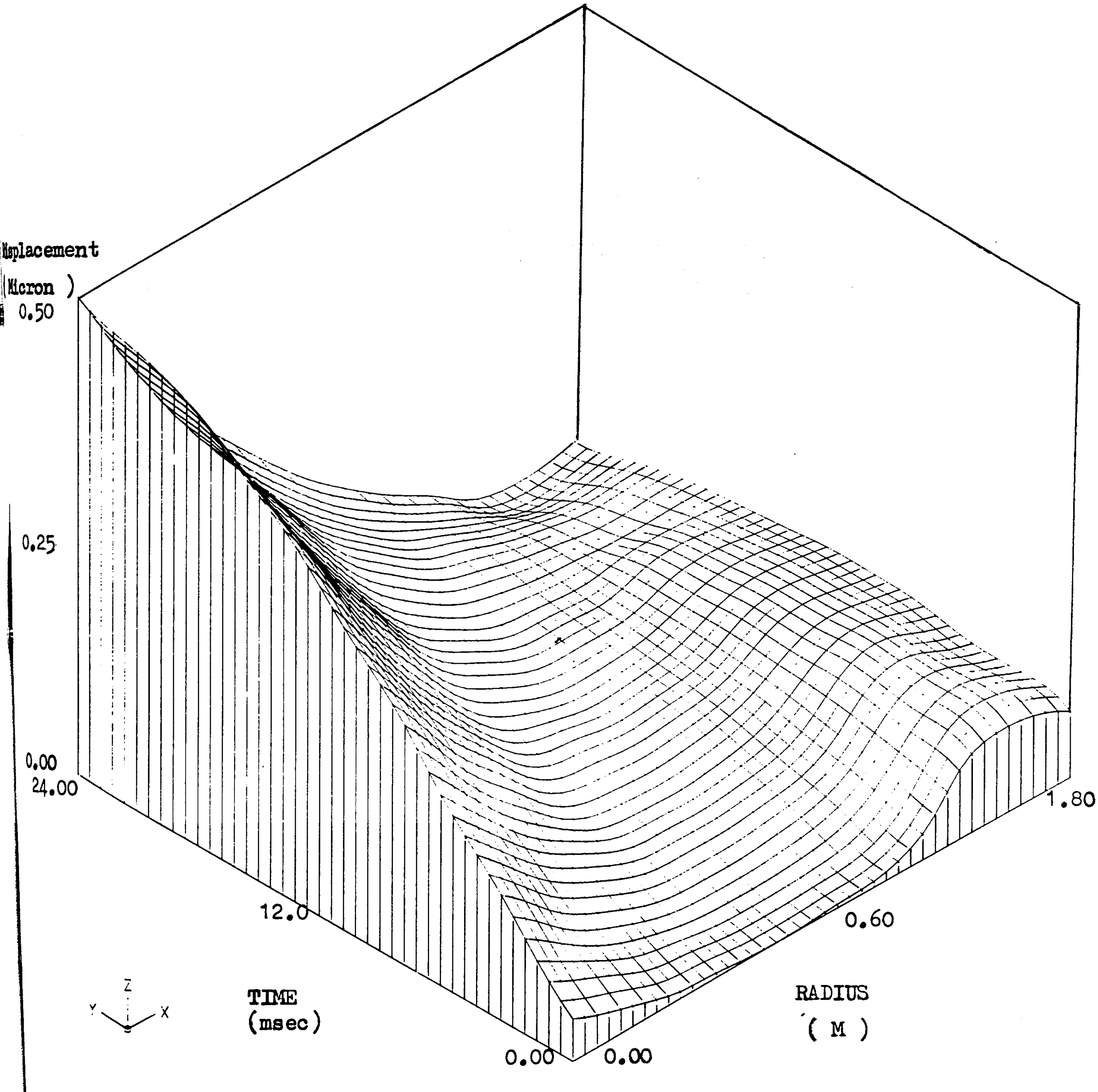

(FIG.4.28.b) DEFLECTION BASIN HISTORY

FOUR LAYER FLEXIBLE PAVEMENT

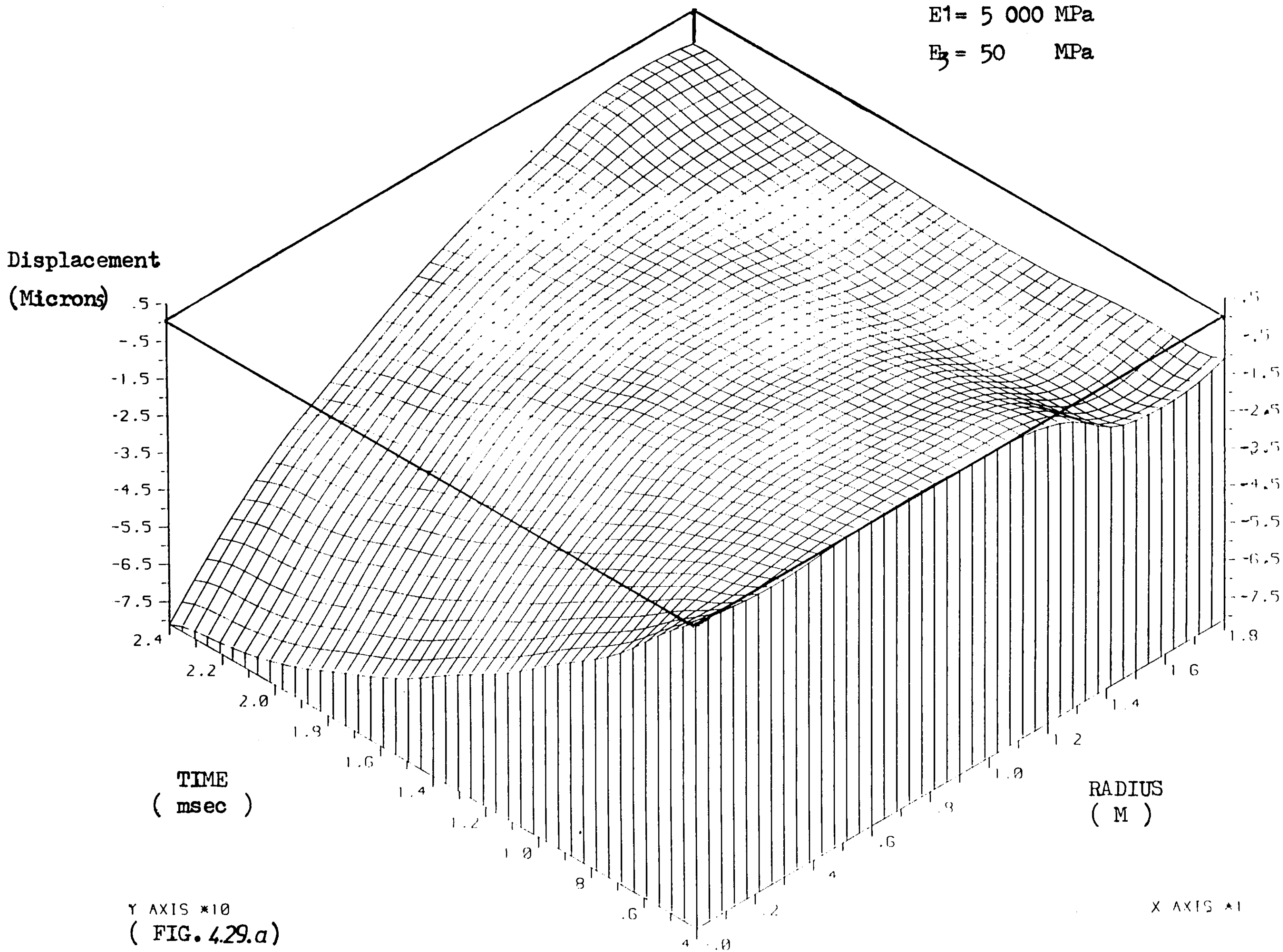

(FIG. 4.29.a)

DEFLECTION BASIN HISTORY

THREE LAYER FLEXIBLE PAVEMENT

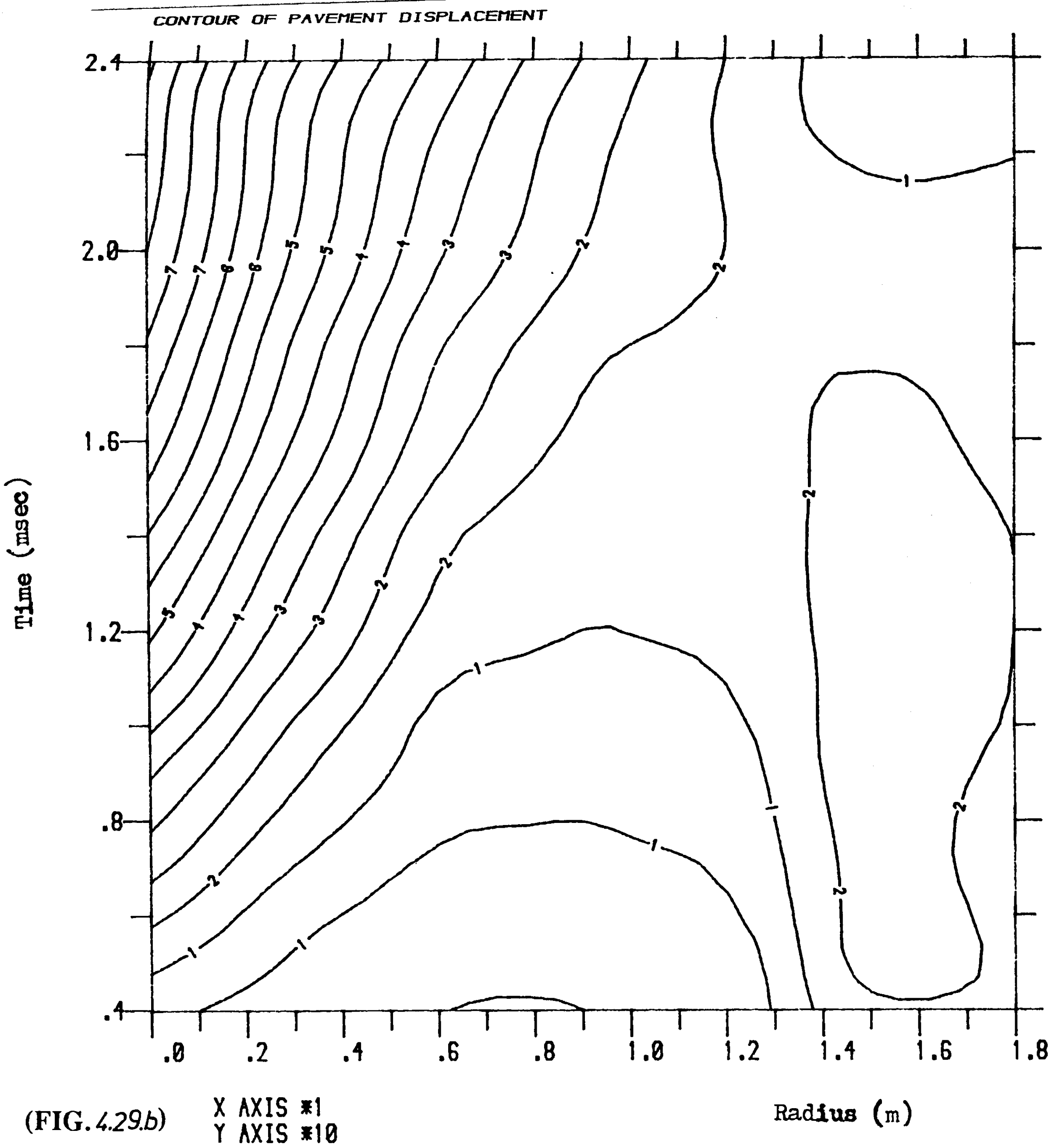

(FIG. 4.29.b)

THREE LAYER FLEXIBLE PAVEMENT

E_1 = 5 000 MPa

E_3 = 50 MPa

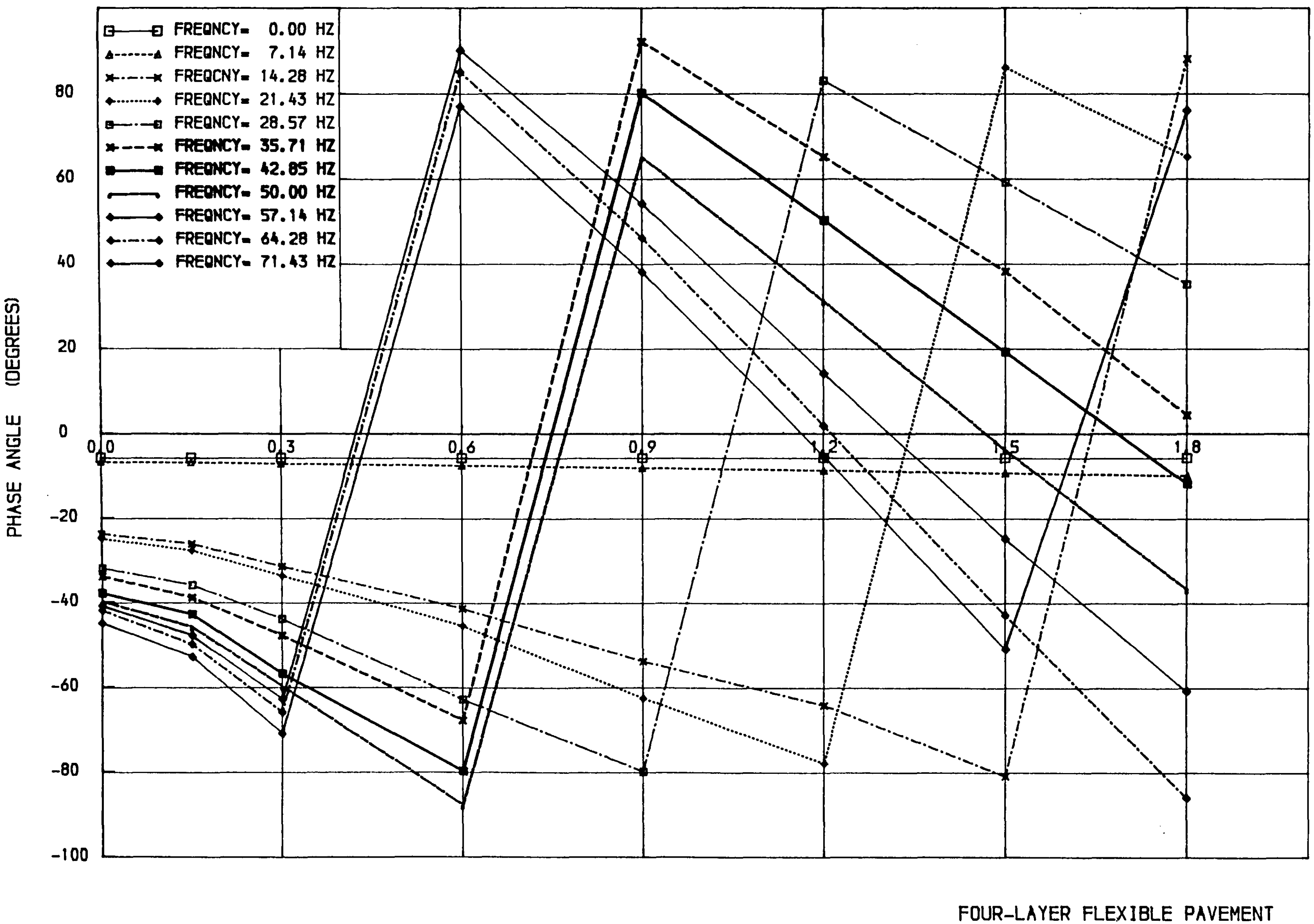

(FIG. 4.30) (ANALYSIS OF PHASE DIFFERENCE)

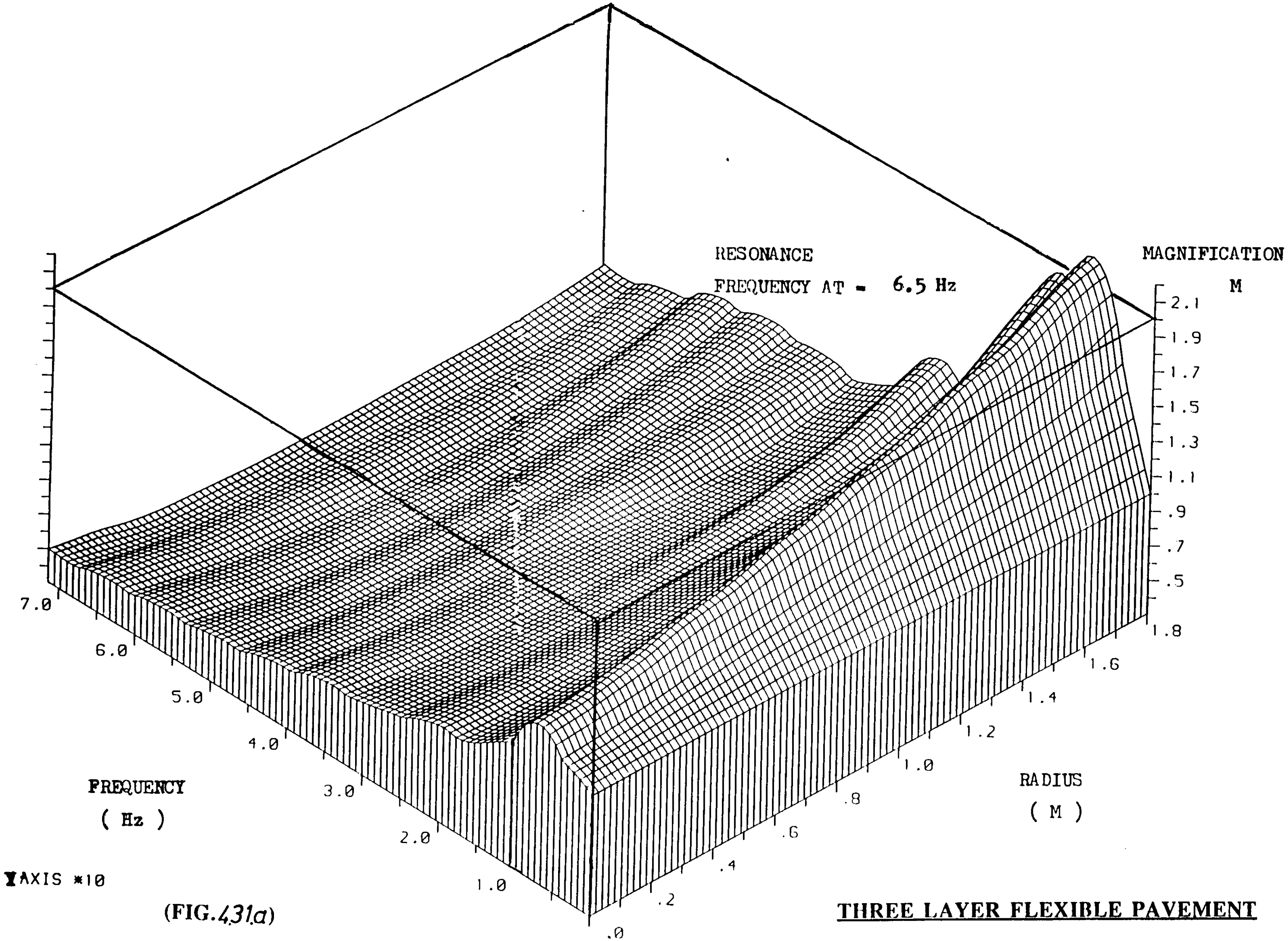

(FIG.4.31a)

DYNAMIC / STATIC SURFACE DISPL.

THREE LAYER FLEXIBLE PAVEMENT

E_1 = 10 000 MPa , E_3 = 50 MPa

CONTOUR OF THE MAGNIFICATION FACTOR M

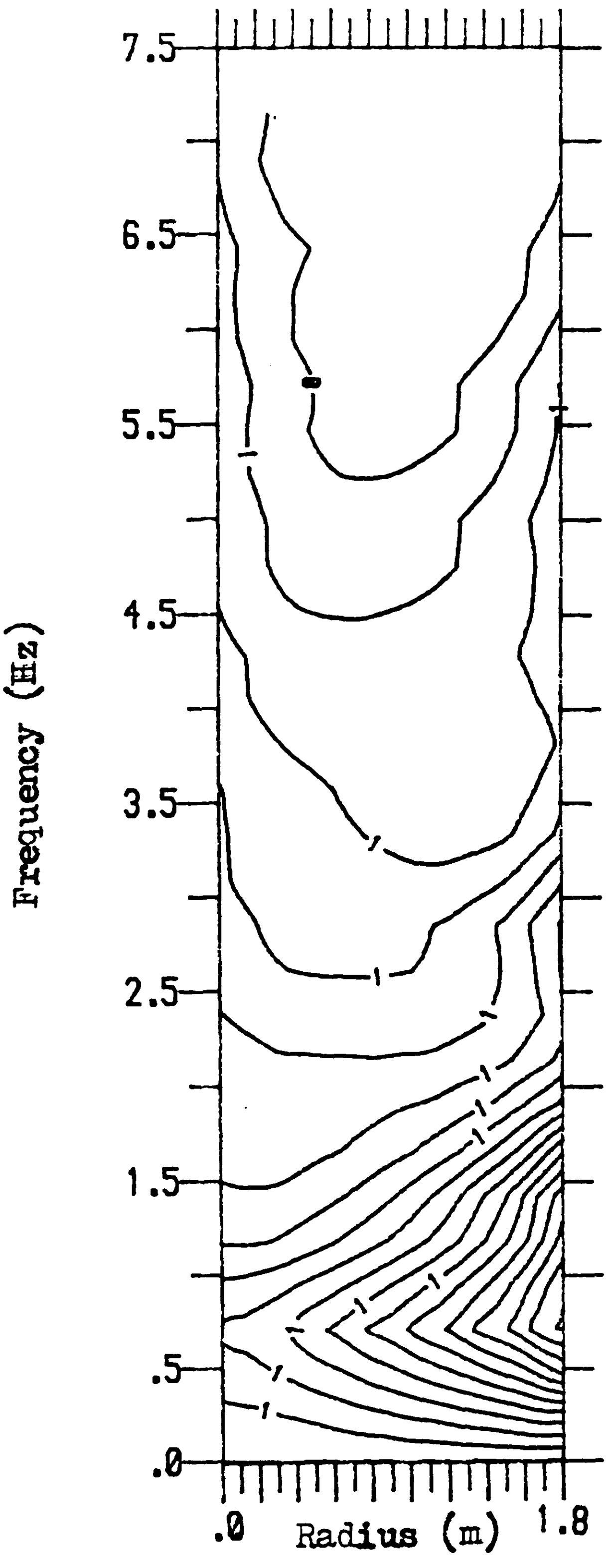

X AXIS *1
Y AXIS *10

THREE LAYER FLEXIBLE PAVEMENT

E_1 = 10 000 MPa

E_3 = 50 MPa

(FIG. 4.31.b)

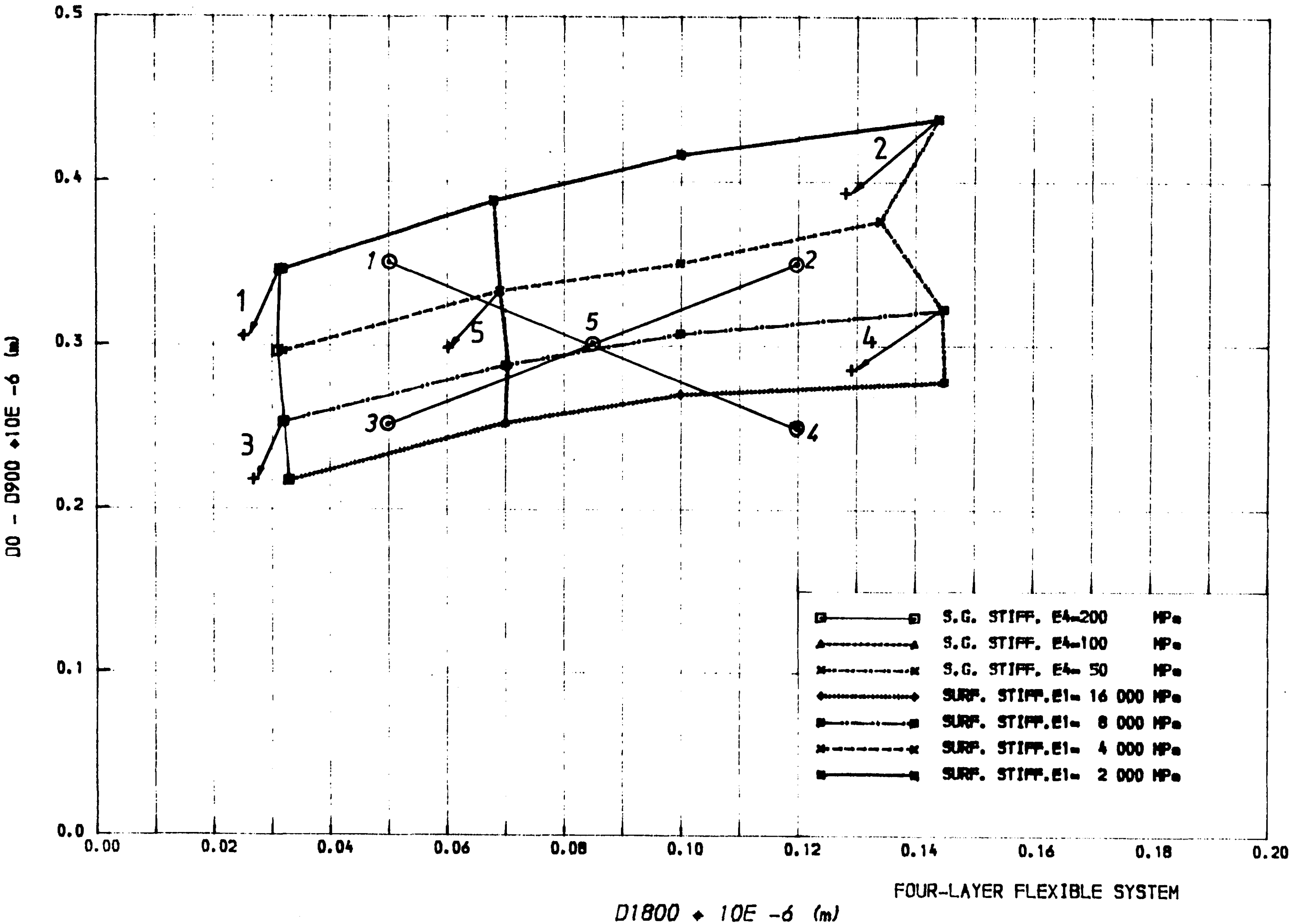

(FIG. 4.32.a) (STATIC ANALYSIS CHART)

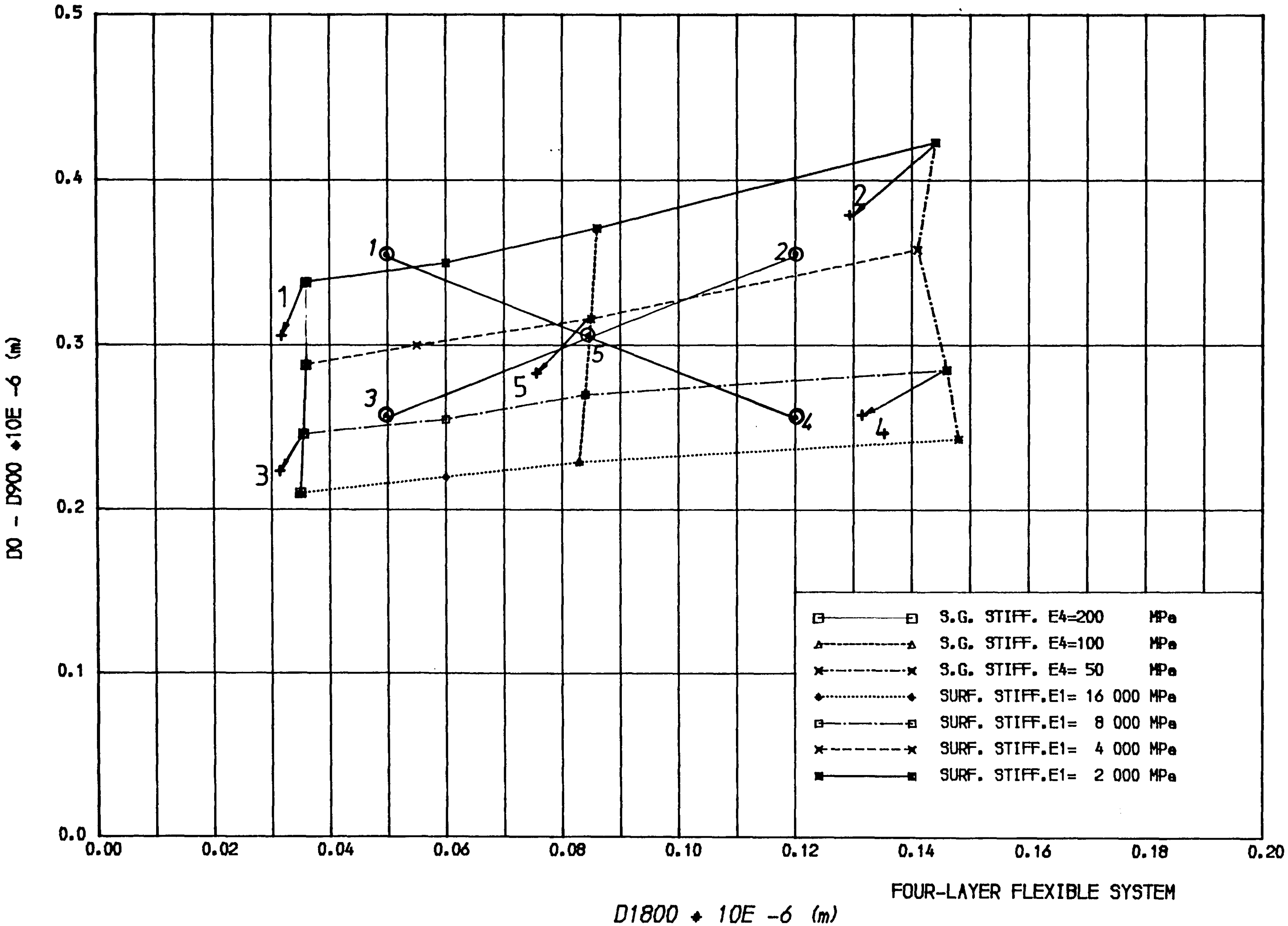

(FIG.4.32.b.) (DYNAMIC ANALYSIS CHART)

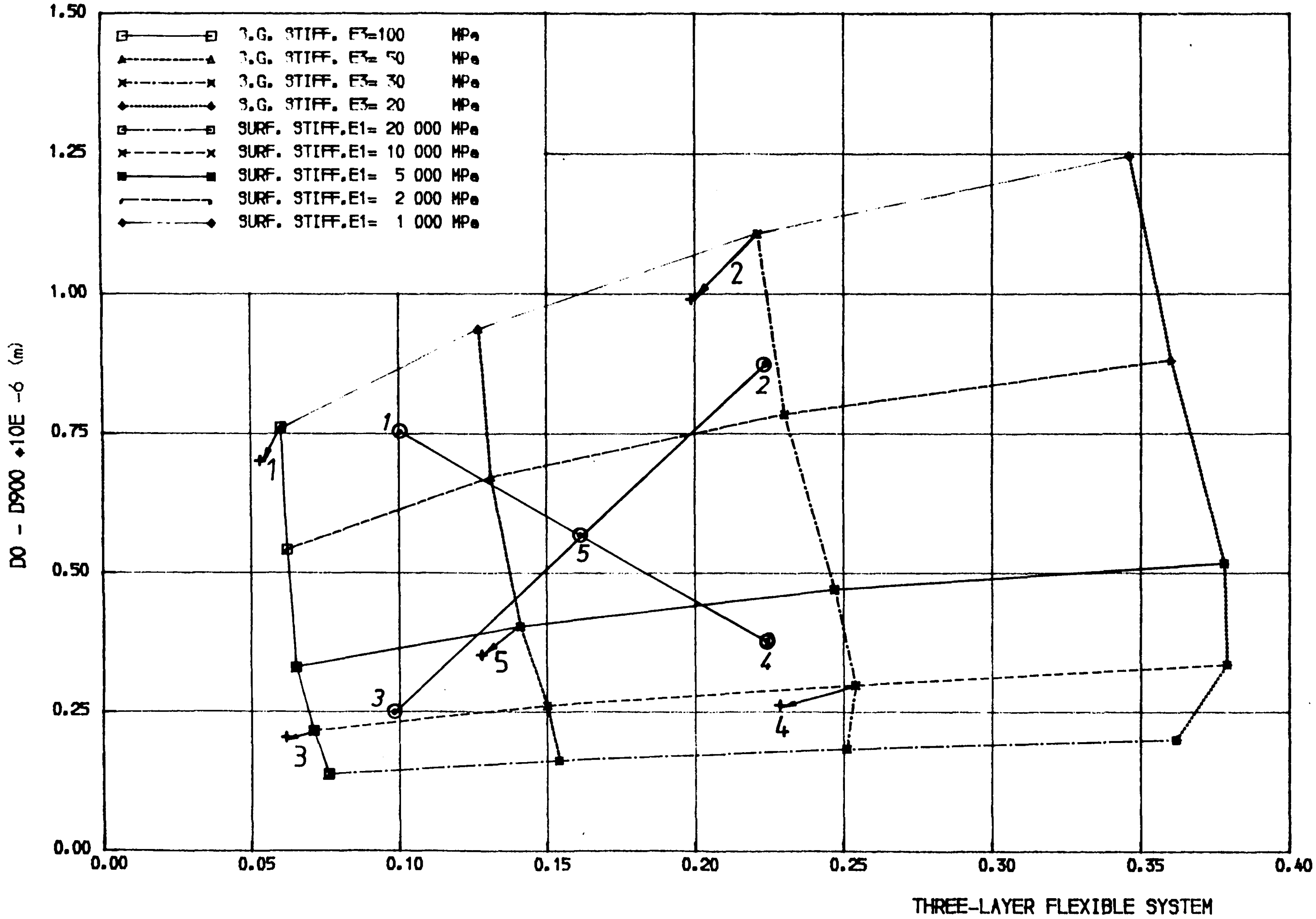

(FIG. 4.33.a) (STATIC ANALYSIS CHART)

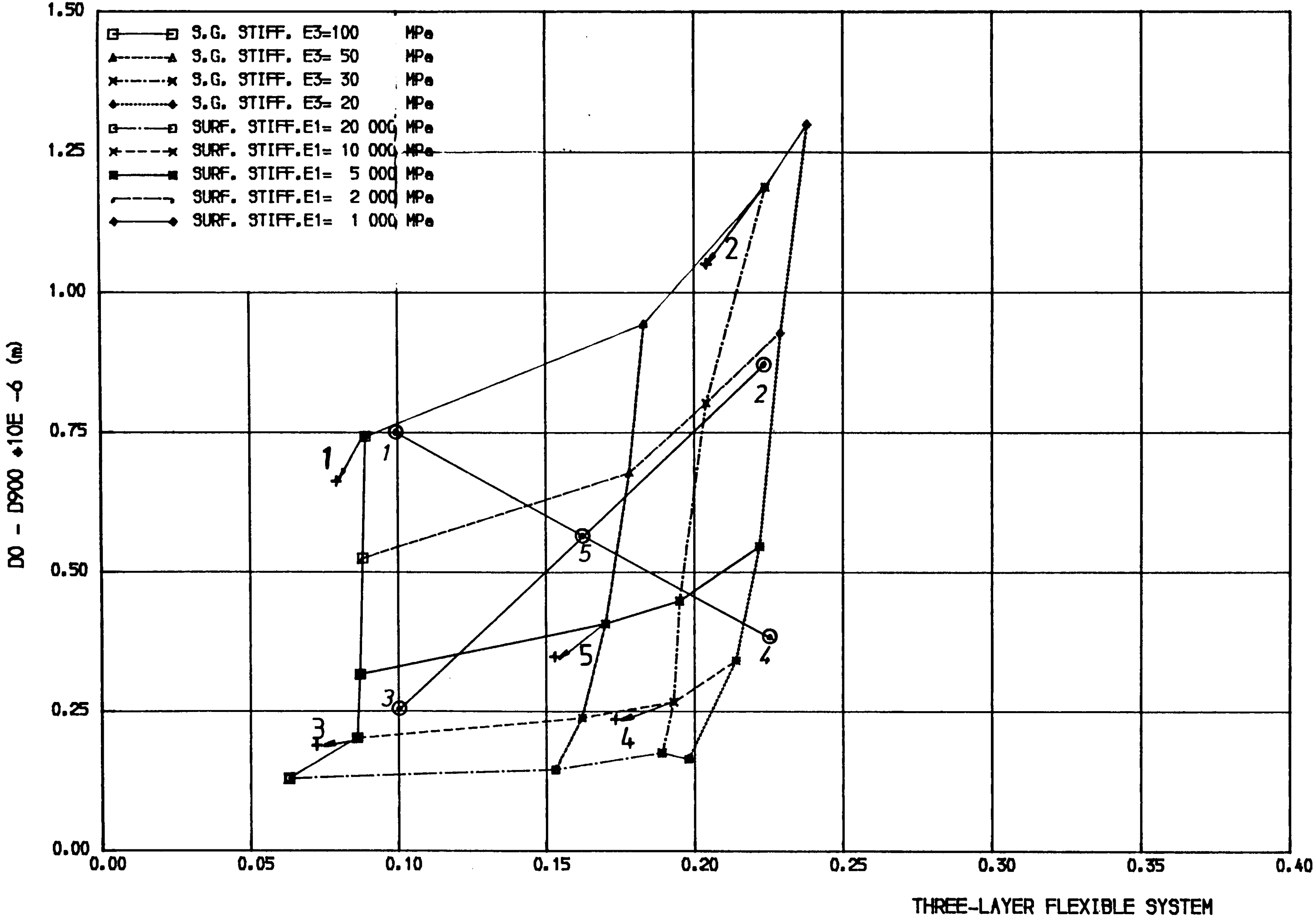

(FIG. 4.33.b) (DYNAMIC ANALYSIS CHART)

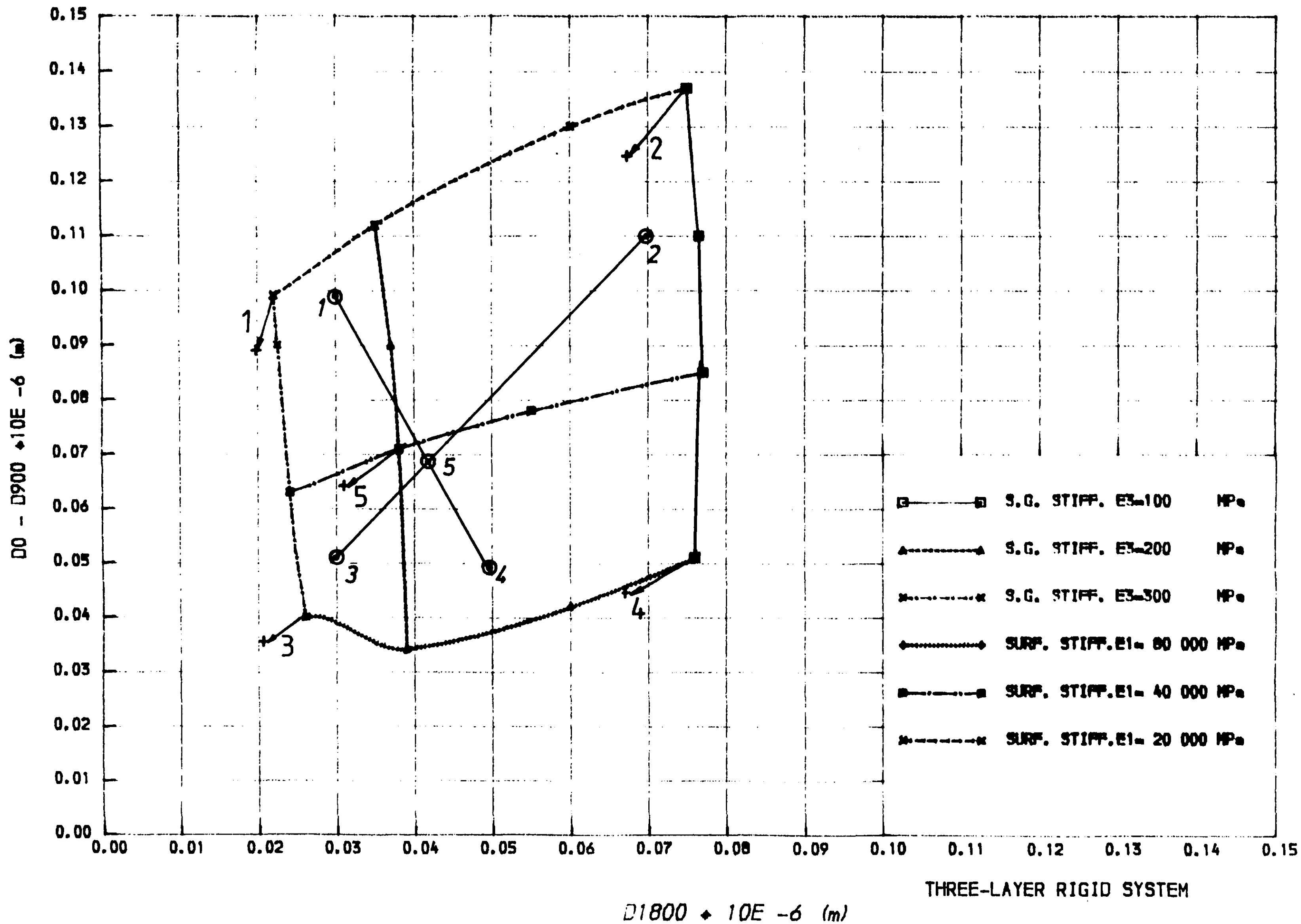

(FIG. 4.34.a) (STATIC ANALYSIS CHART)

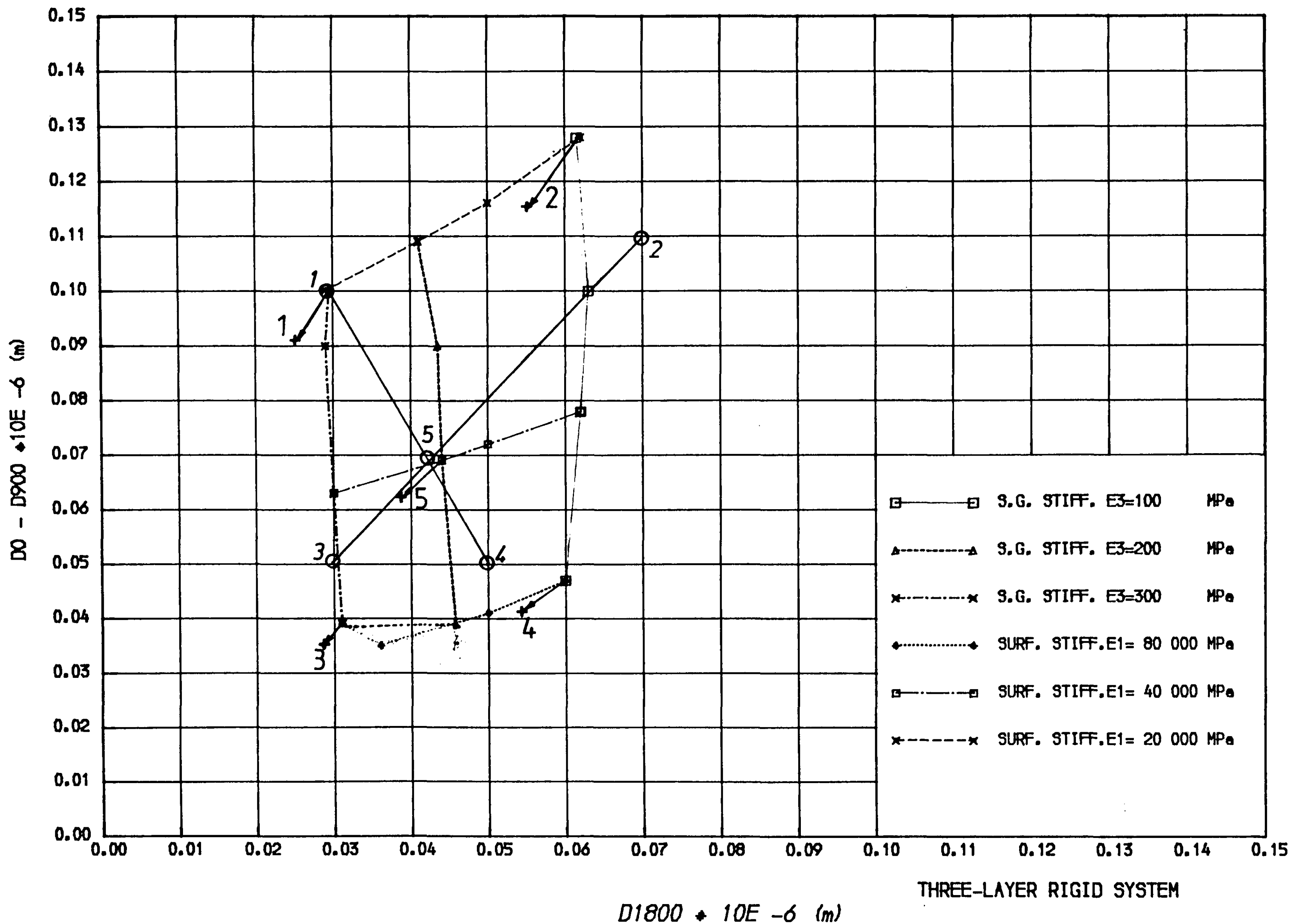

(FIG. 4.34.b) (DYNAMIC ANALYSIS CHART)

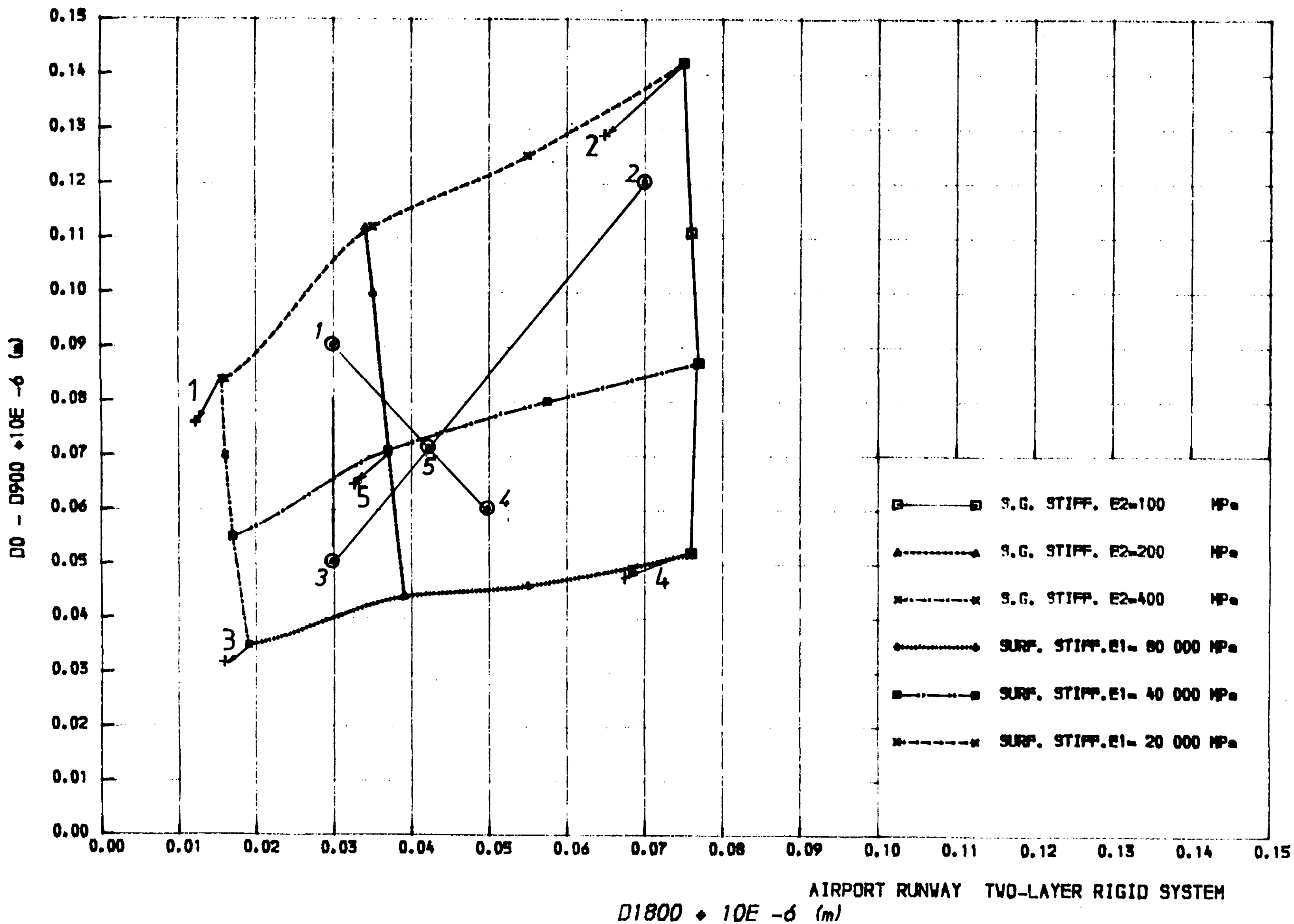

(FIG. 4.35.a) (STATIC ANALYSIS CHART)

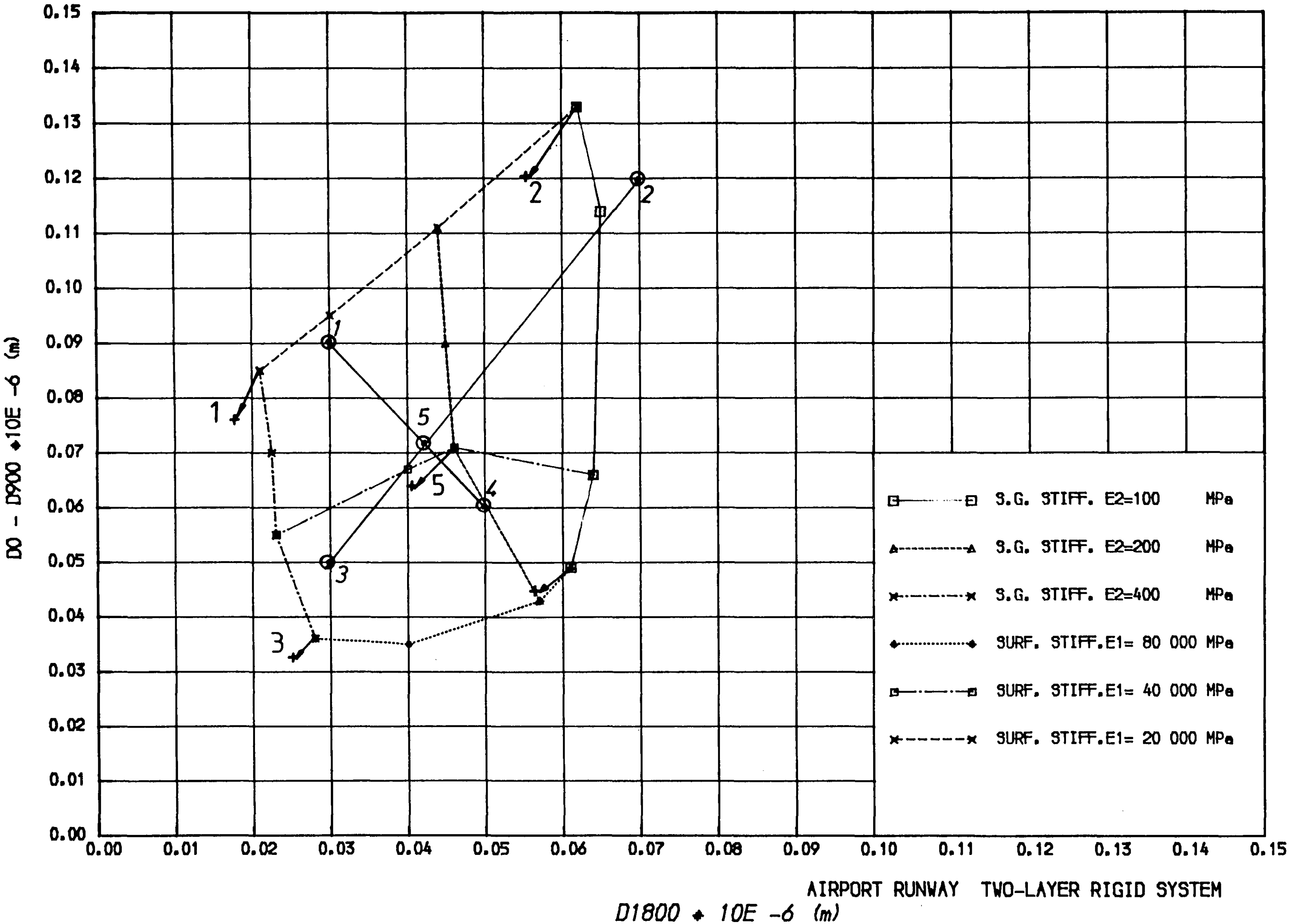

(FIG. 4.35.a) (DYNAMIC ANALYSIS CHART)

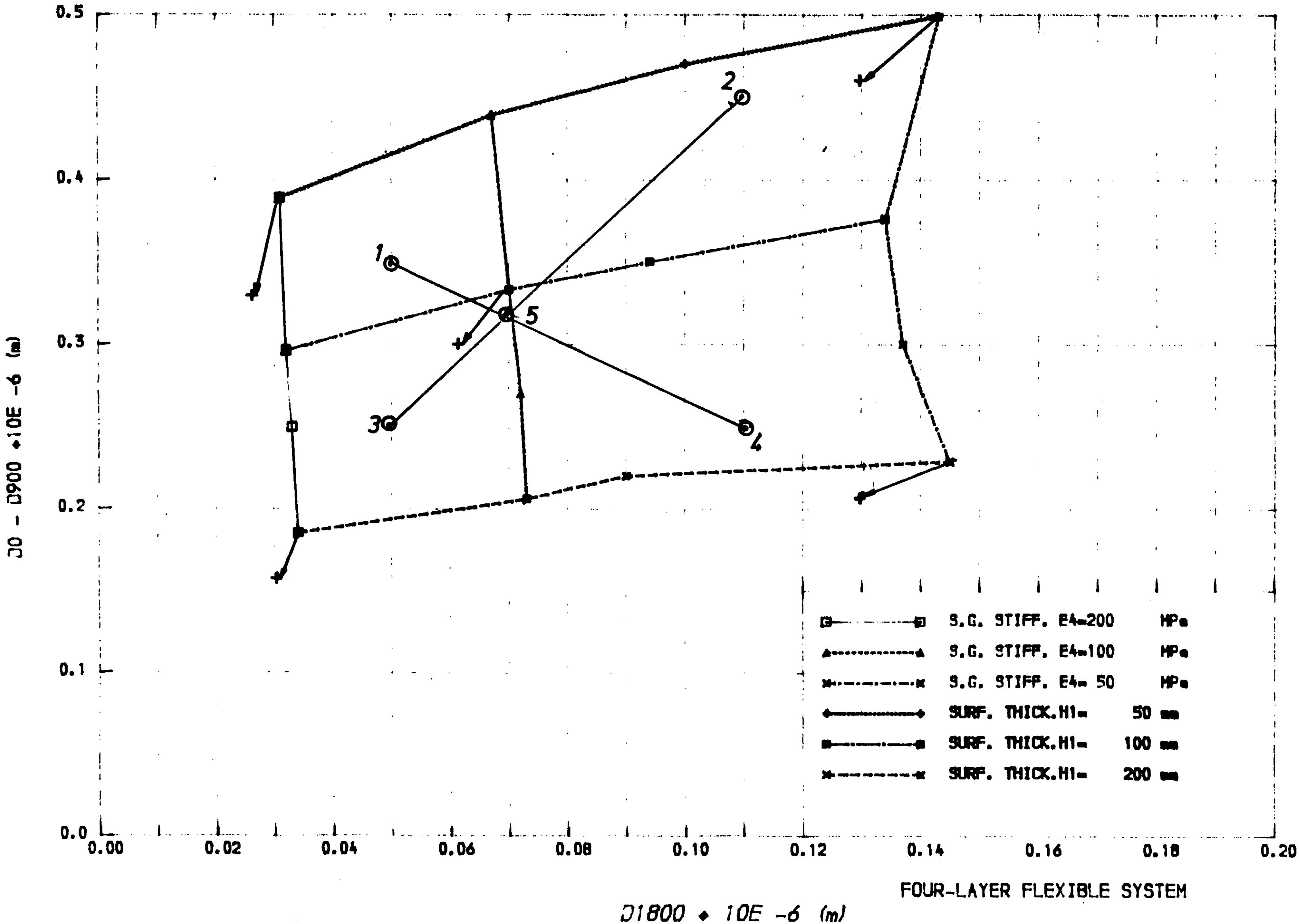

(FIG. 4.36.a)(STATIC ANALYSIS CHART)

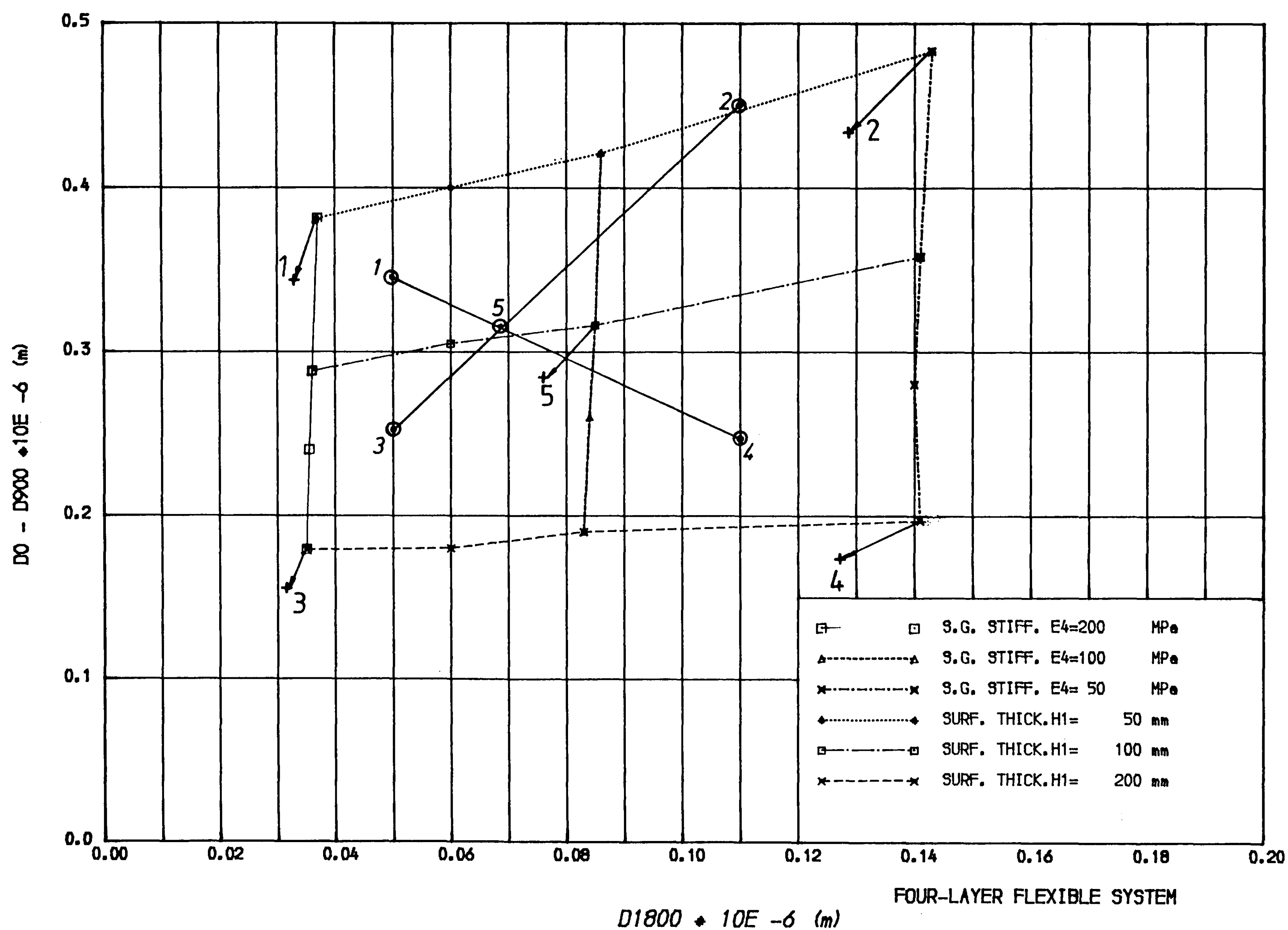

(FIG . 4.36.b) (DYNAMIC ANALYSIS CHART)

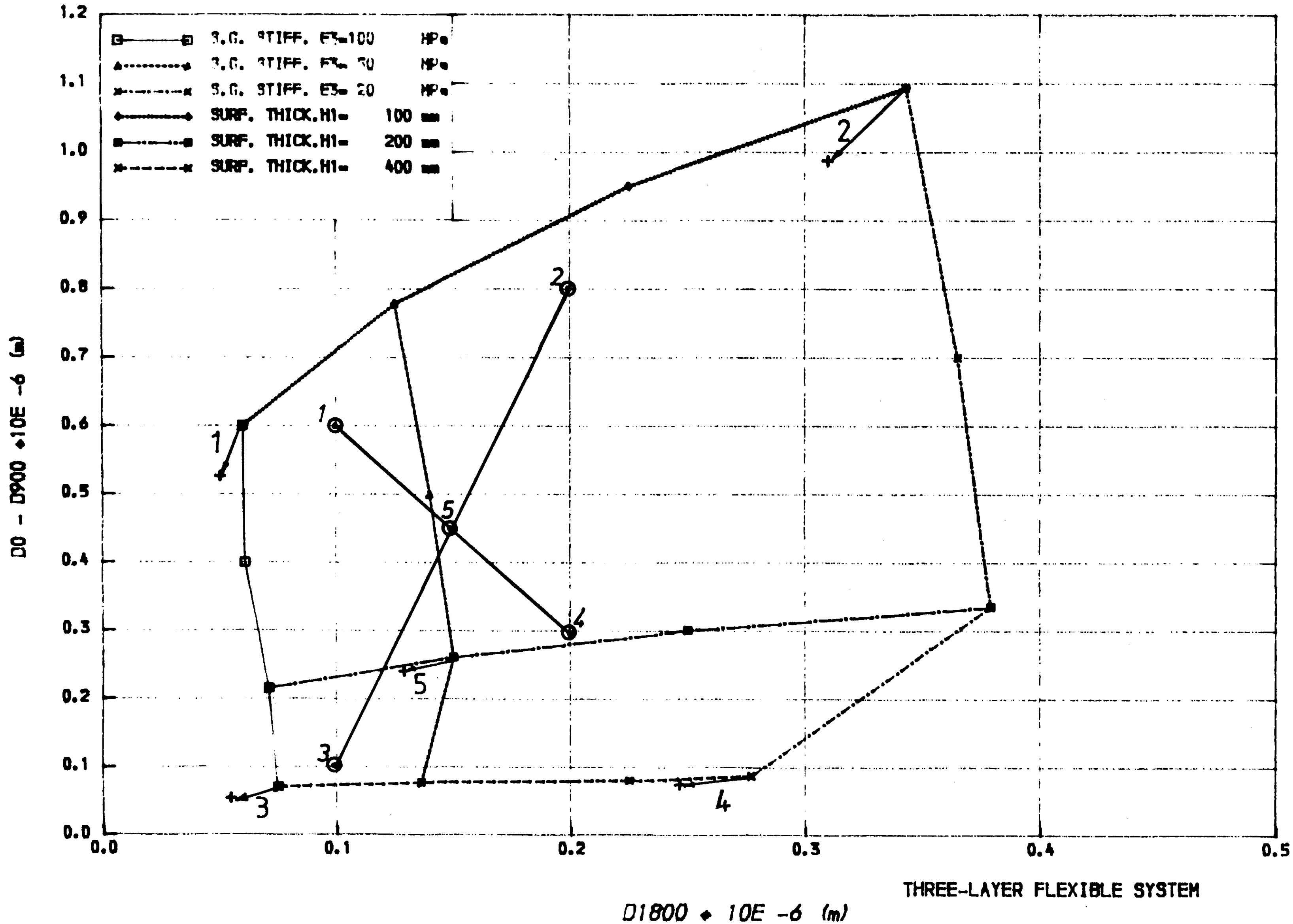

(FIG. 4.37.a) (STATIC ANALYSIS CHART)

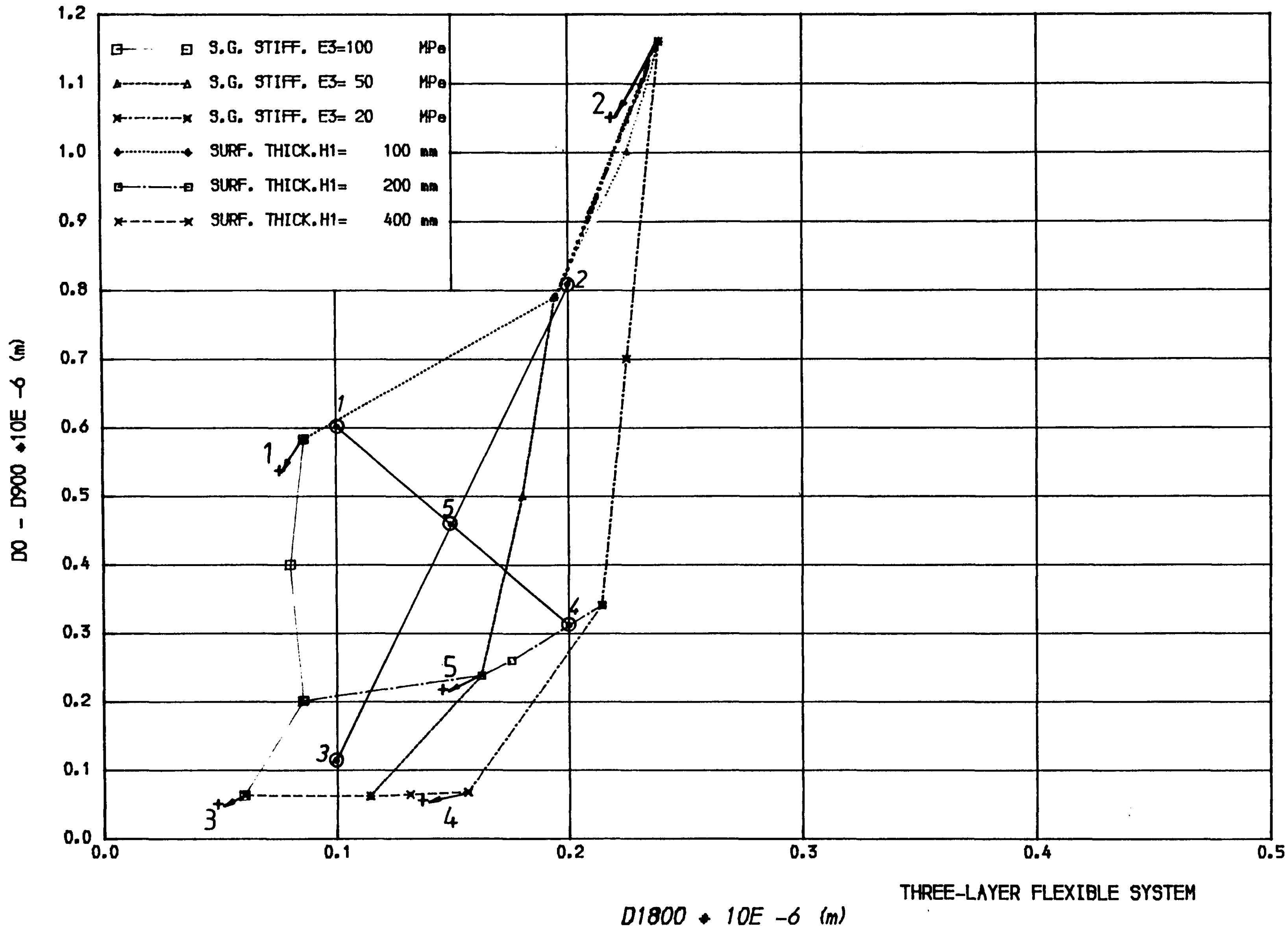

(FIG. 4.37.b)(DYNAMIC ANALYSIS CHART)

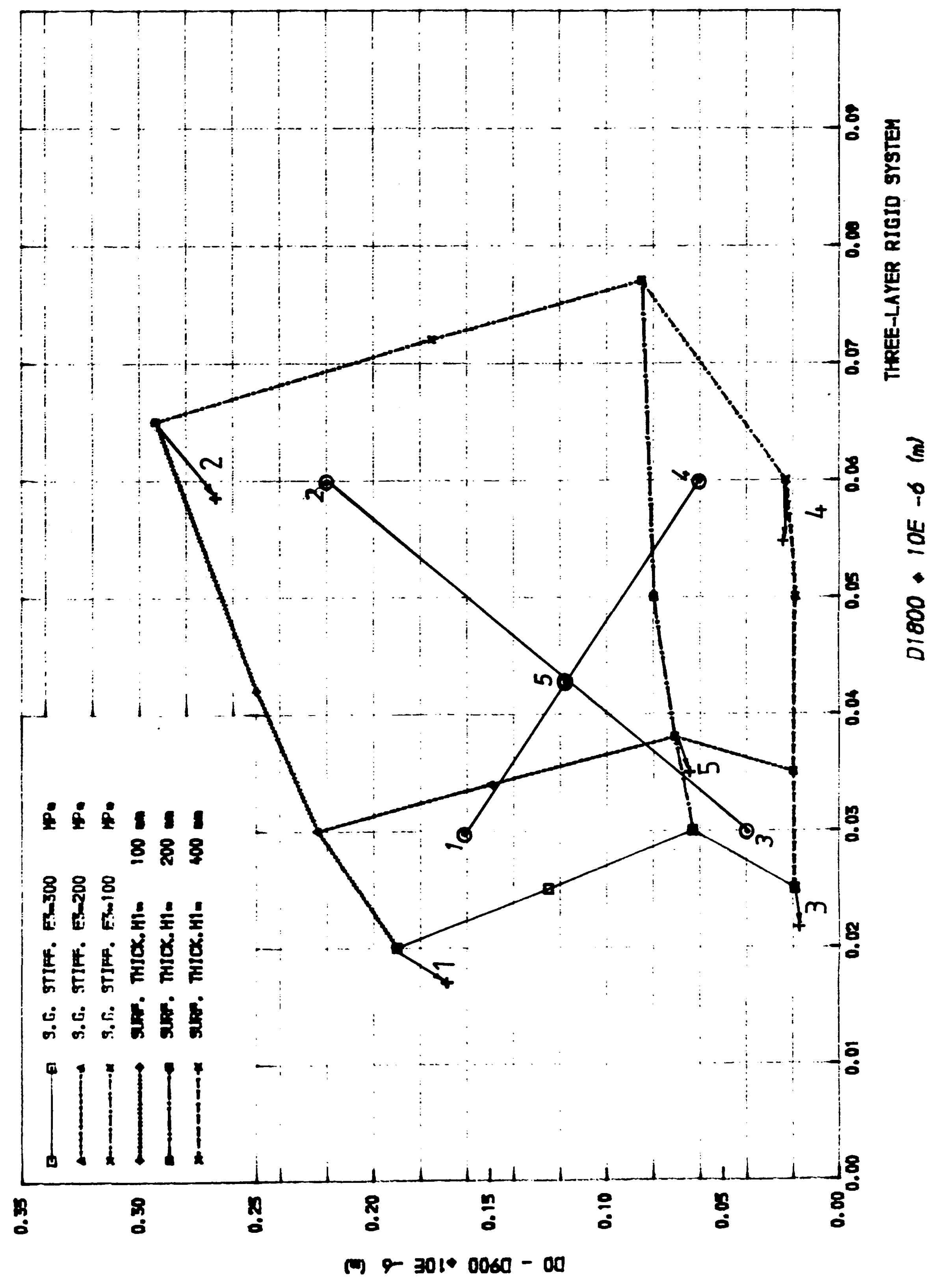

(FIG. 4.38.a) (STATIC ANALYSIS CHART)

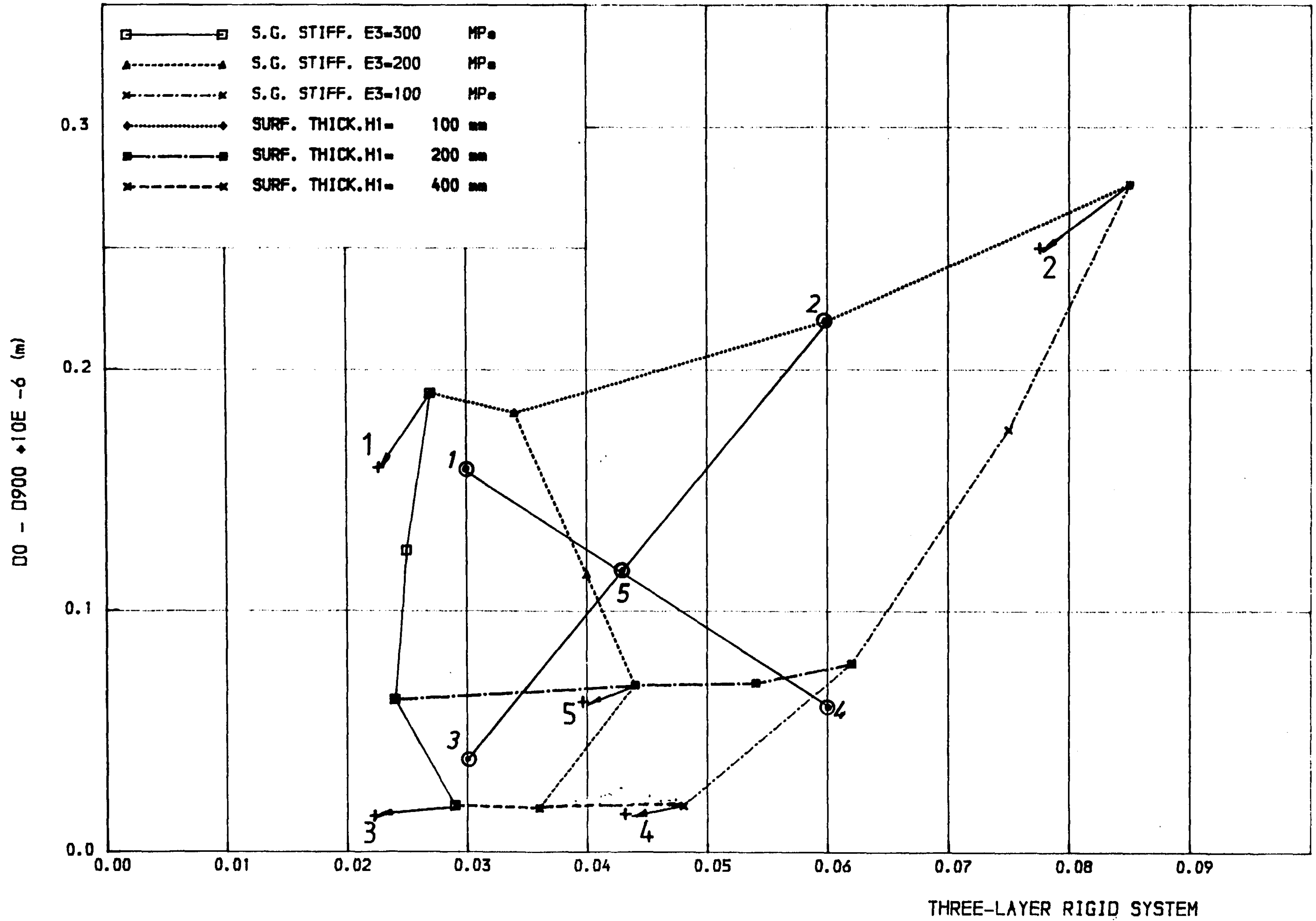

(FIG. 4.38.b) (DYNAMIC ANALYSIS CHART)

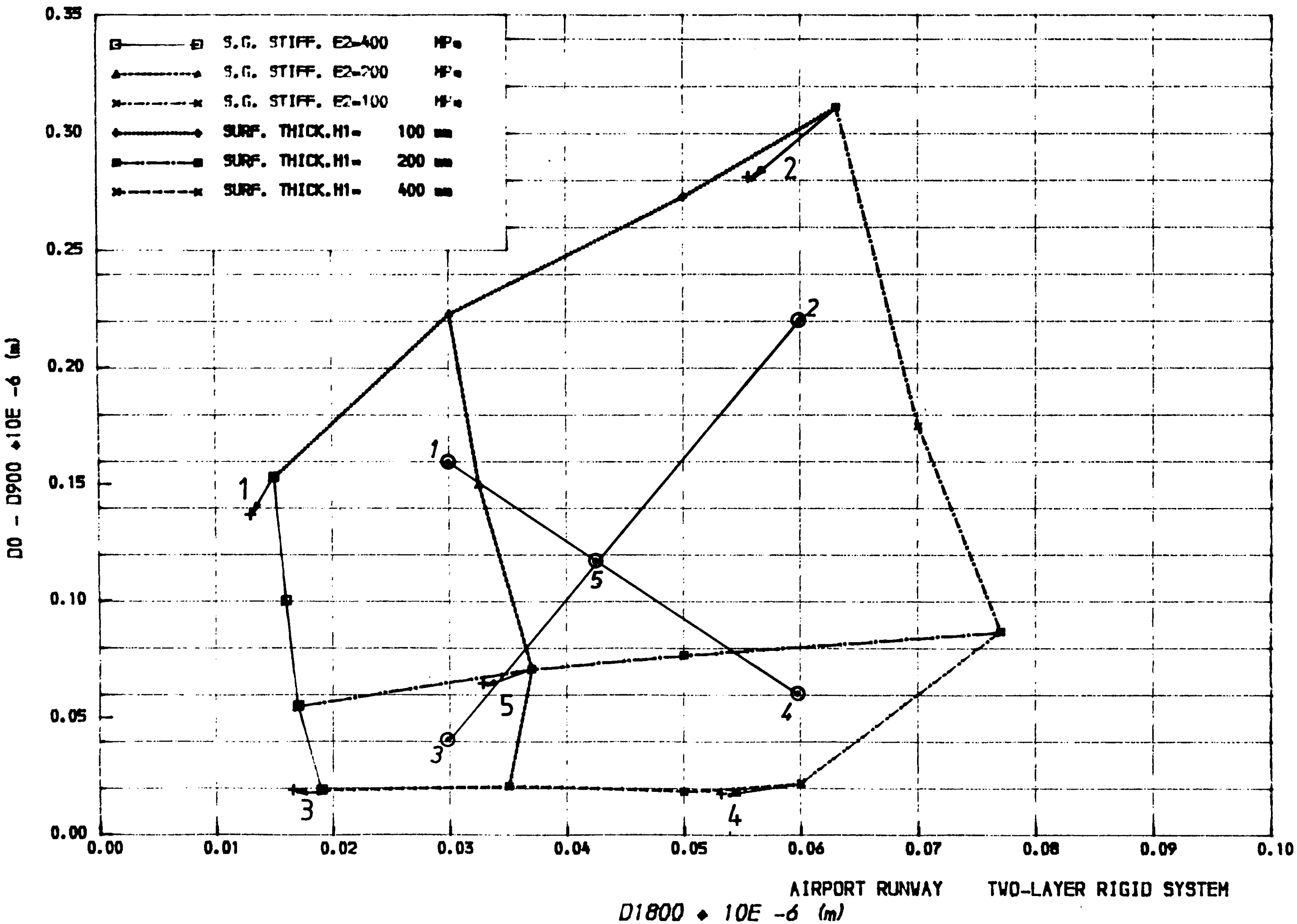

(FIG. 4.39.a) (STATIC ANALYSIS CHART)

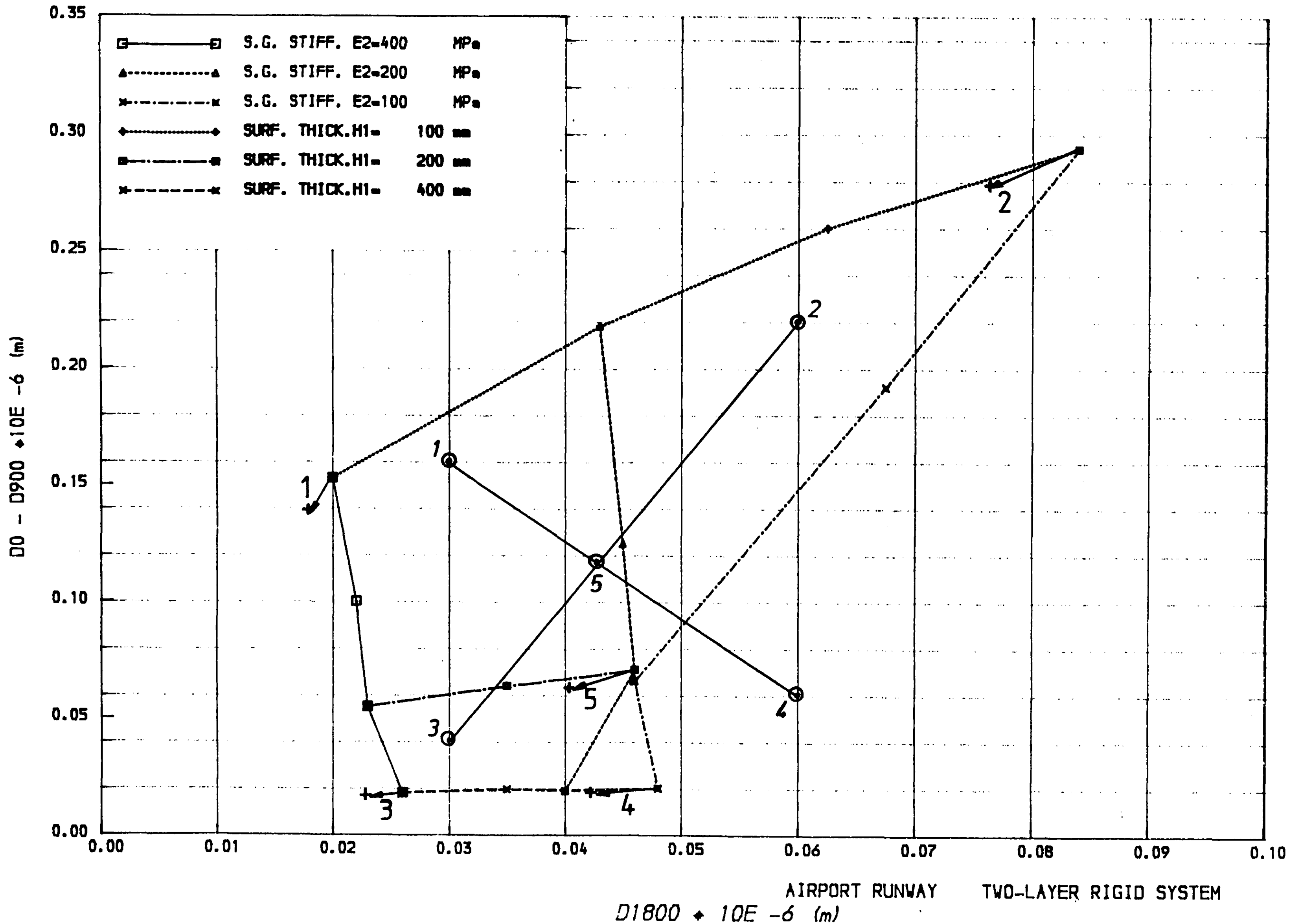

(FIG. 4.39.b) (DYNAMIC ANALYSIS CHART)

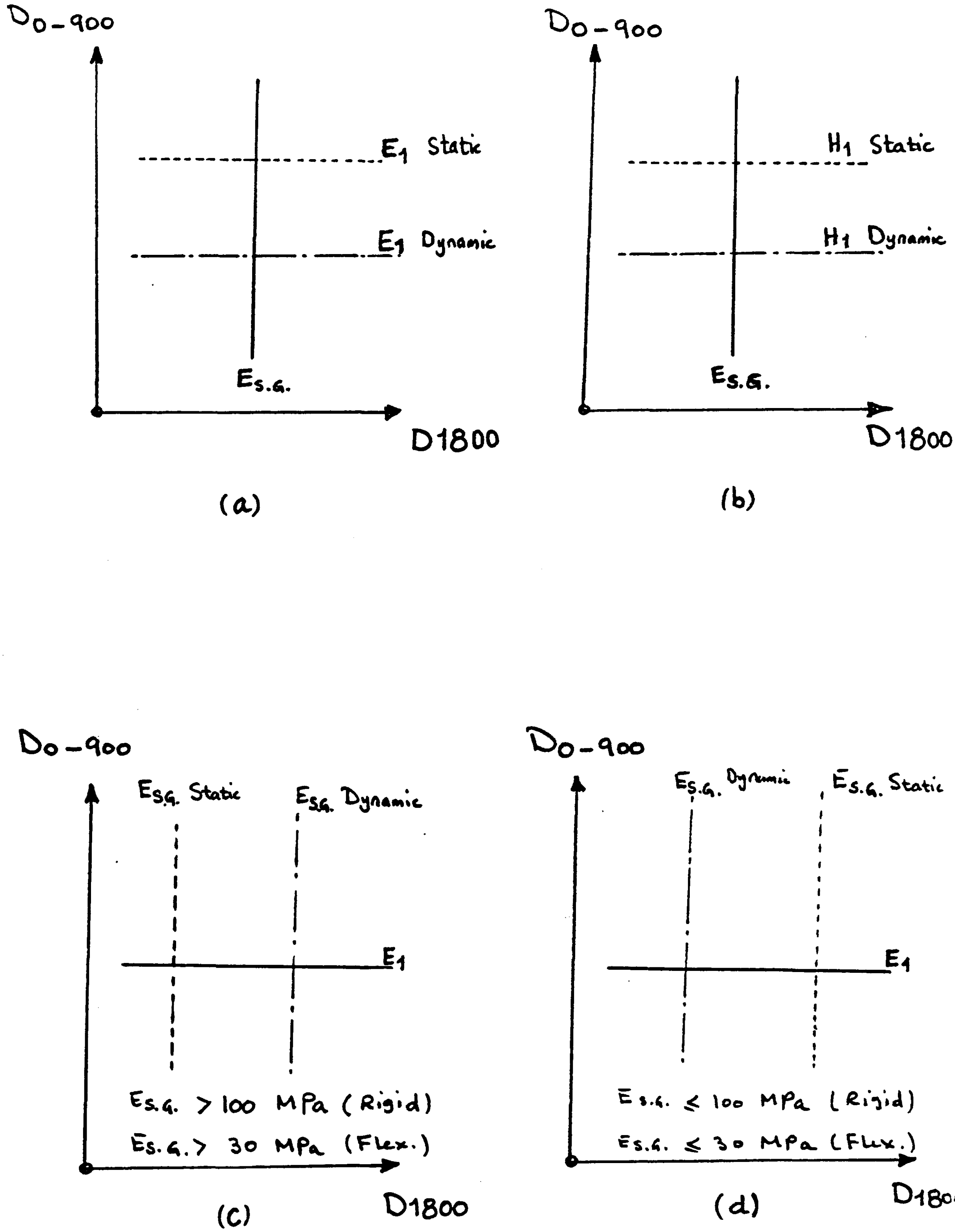

FIG. 4.40 Chart Features

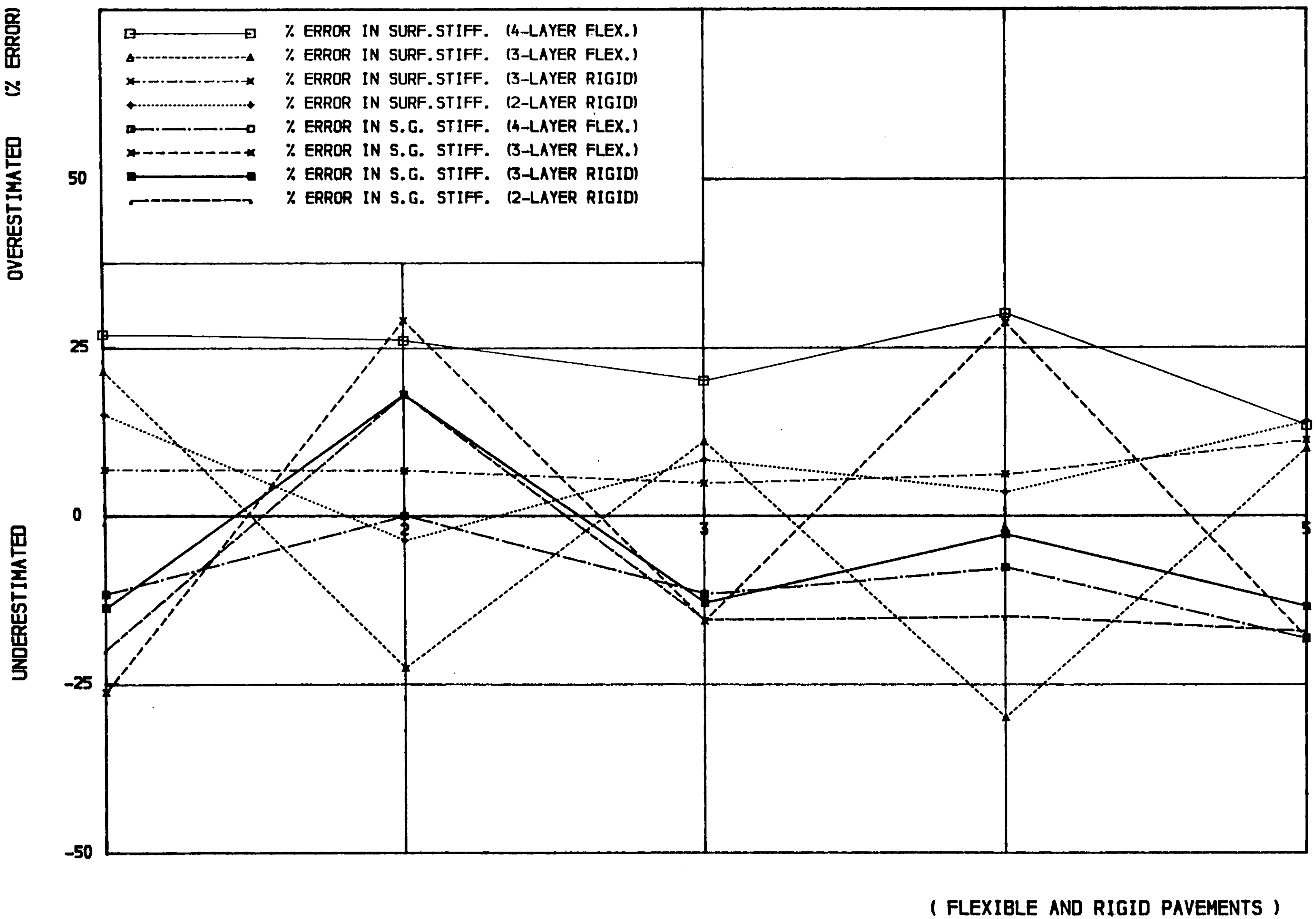

(FIG.4.41) (INVESTIGATION OF STATIC ANALYSIS OF THE F.W.D)

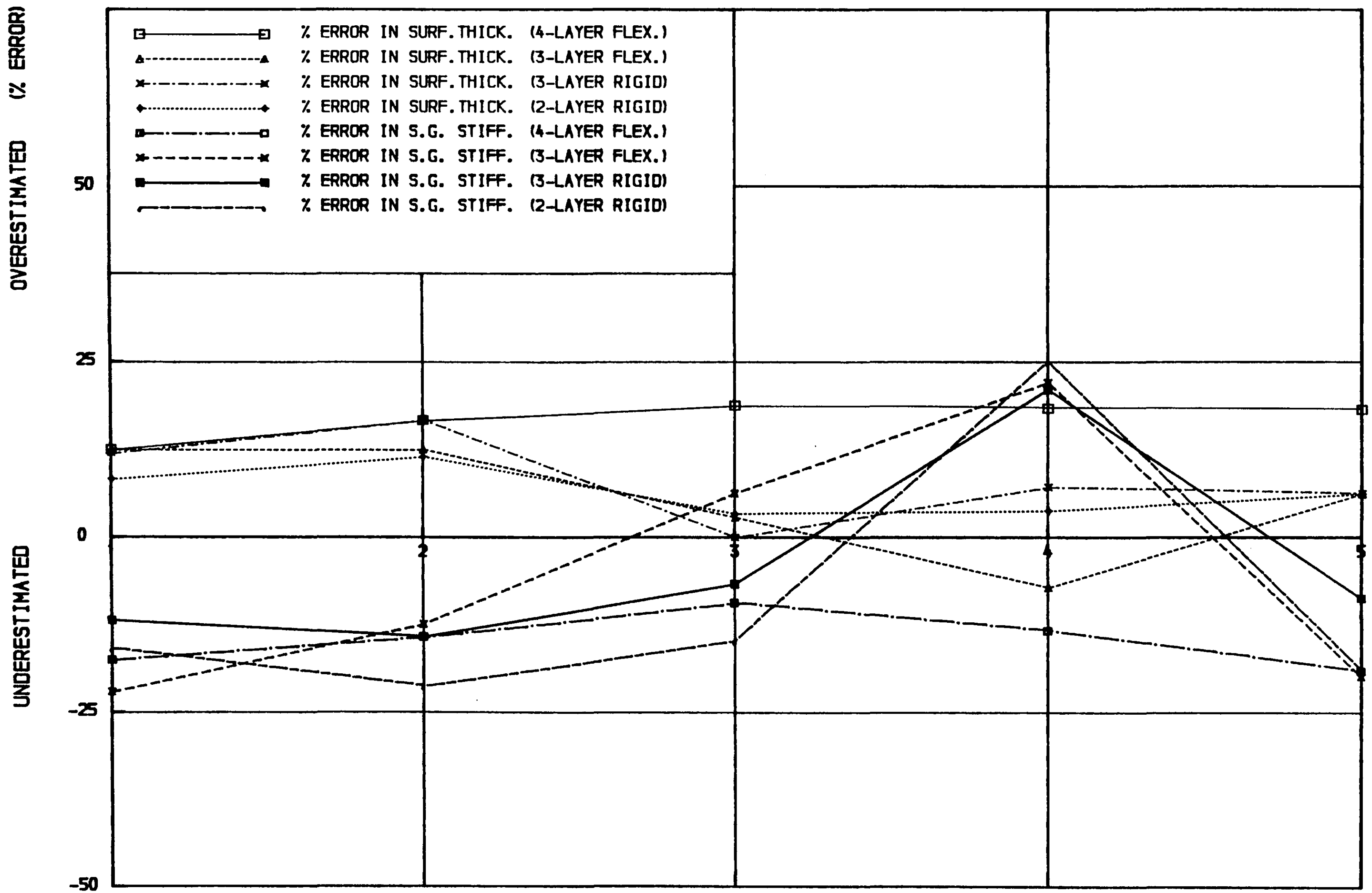

(FLEXIBLE AND RIGID PAVEMENTS)

LOCATION ON THE CHARTS

(FIG. 4.42) (INVESTIGATION OF STATIC ANALYSIS OF THE F.W.D)

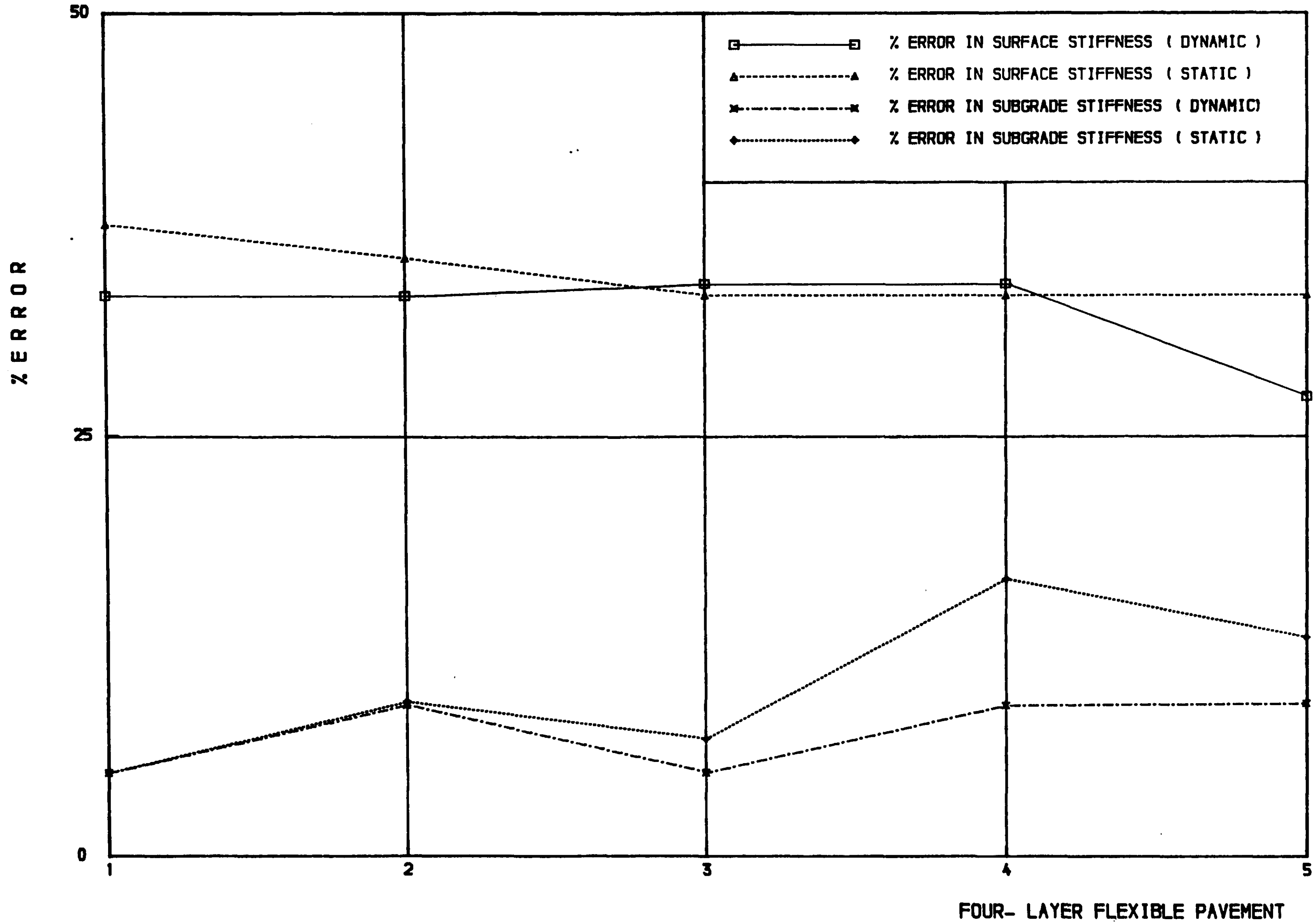

LOCATION ON THE CHARTS

(FIG.4.43) ERROR IN STIFFNESSES DUE TO 10% ERROR IN FWD DEFLECTION MEASUREMENTS

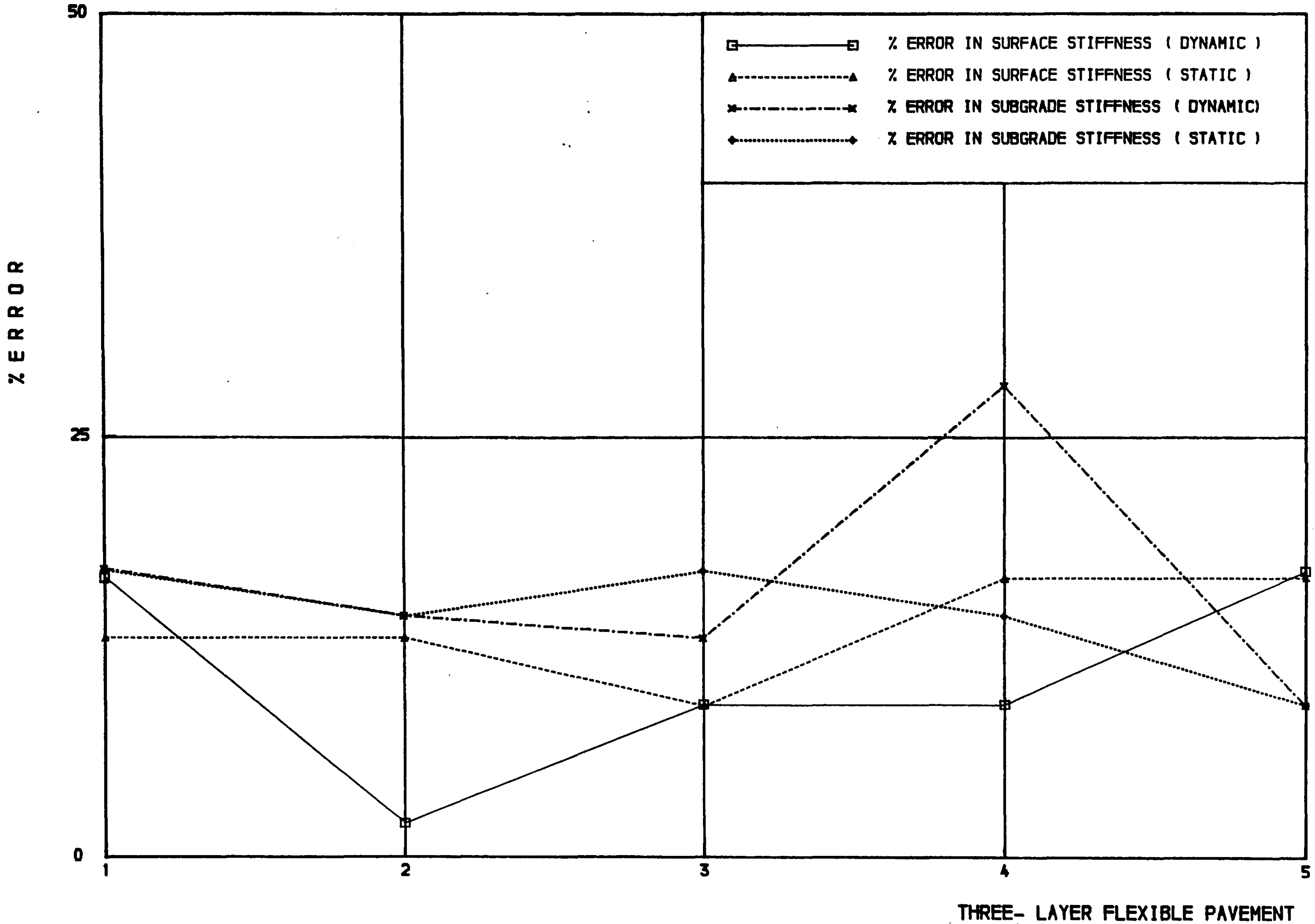

(FIG. 4.44) ERROR IN STIFFNESSES DUE TO 10% ERROR IN FWD DEFLECTION MEASUREMENTS

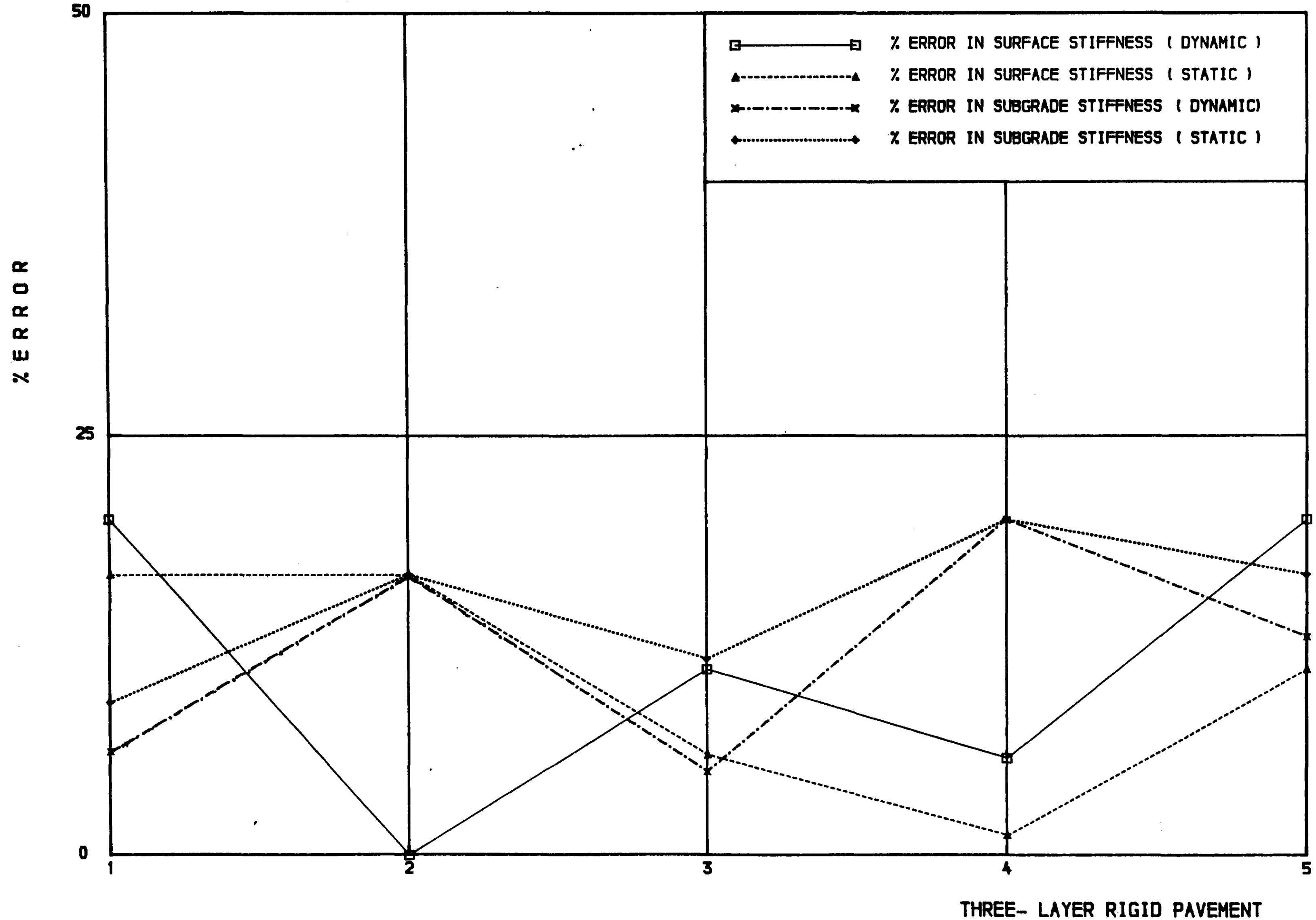

LOCATION ON THE CHARTS

(FIG.4.45) ERROR IN STIFFNESSES DUE TO 10% ERROR IN FWD DEFLECTION MEASUREMENTS

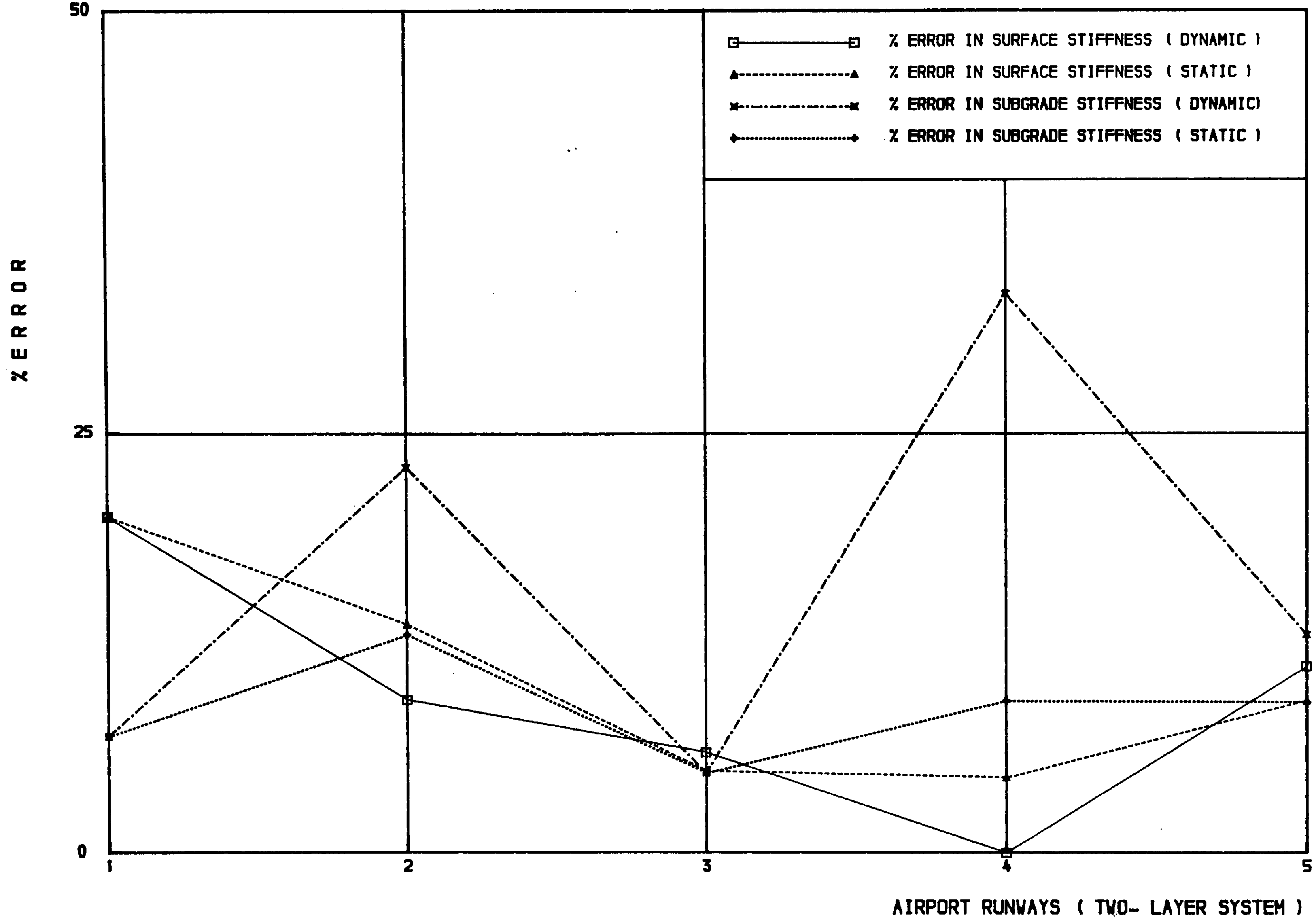

LOCATION ON THE CHARTS

(FIG.4.46) ERROR IN STIFFNESSES DUE TO 10% ERROR IN FWD DEFLECTION MEASUREMENTS

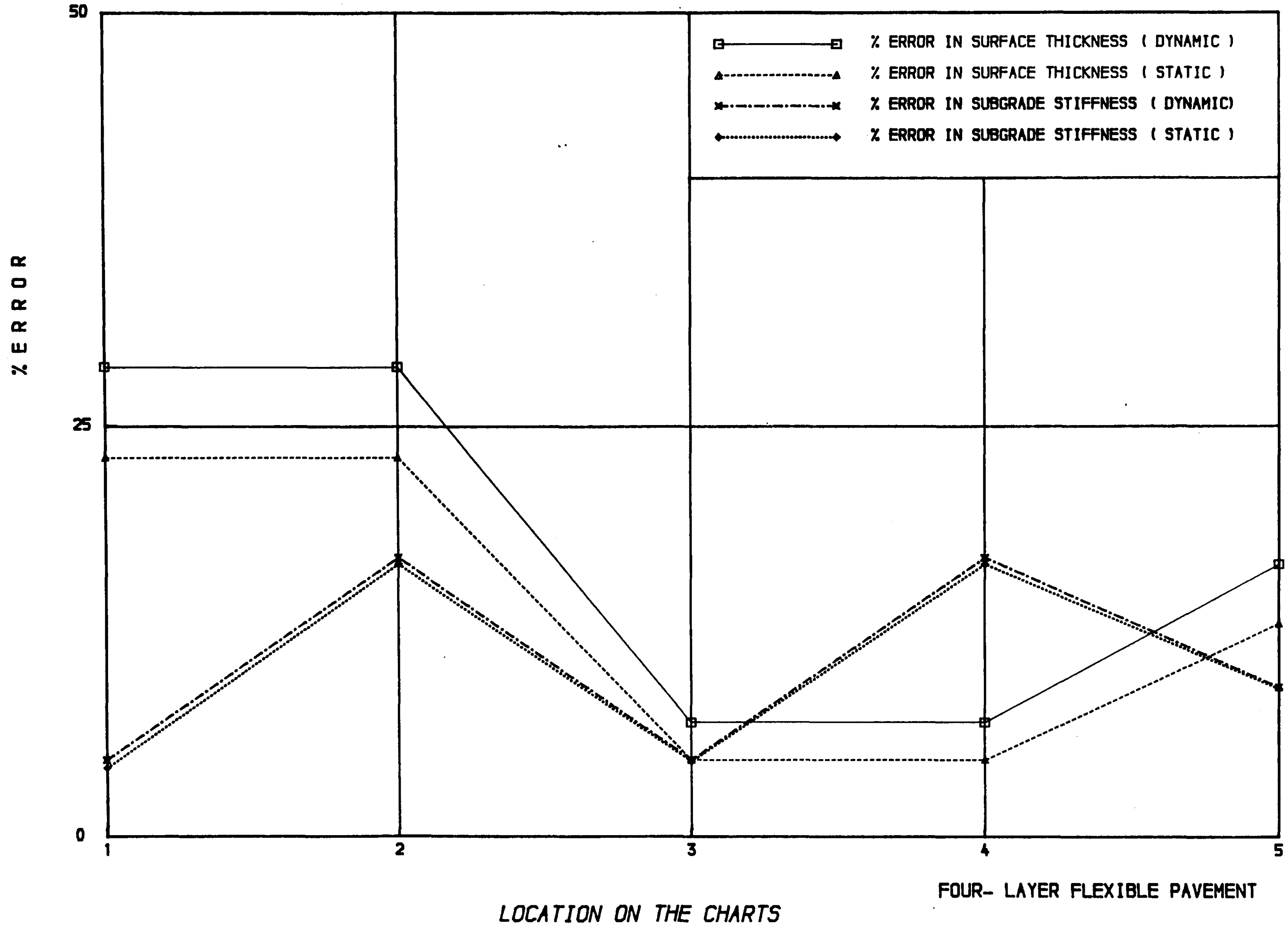

(FIG.4.47) ERROR IN STIFF. AND THICK. DUE TO 10% ERROR IN FWD DEFLn. MEASUREMENTS

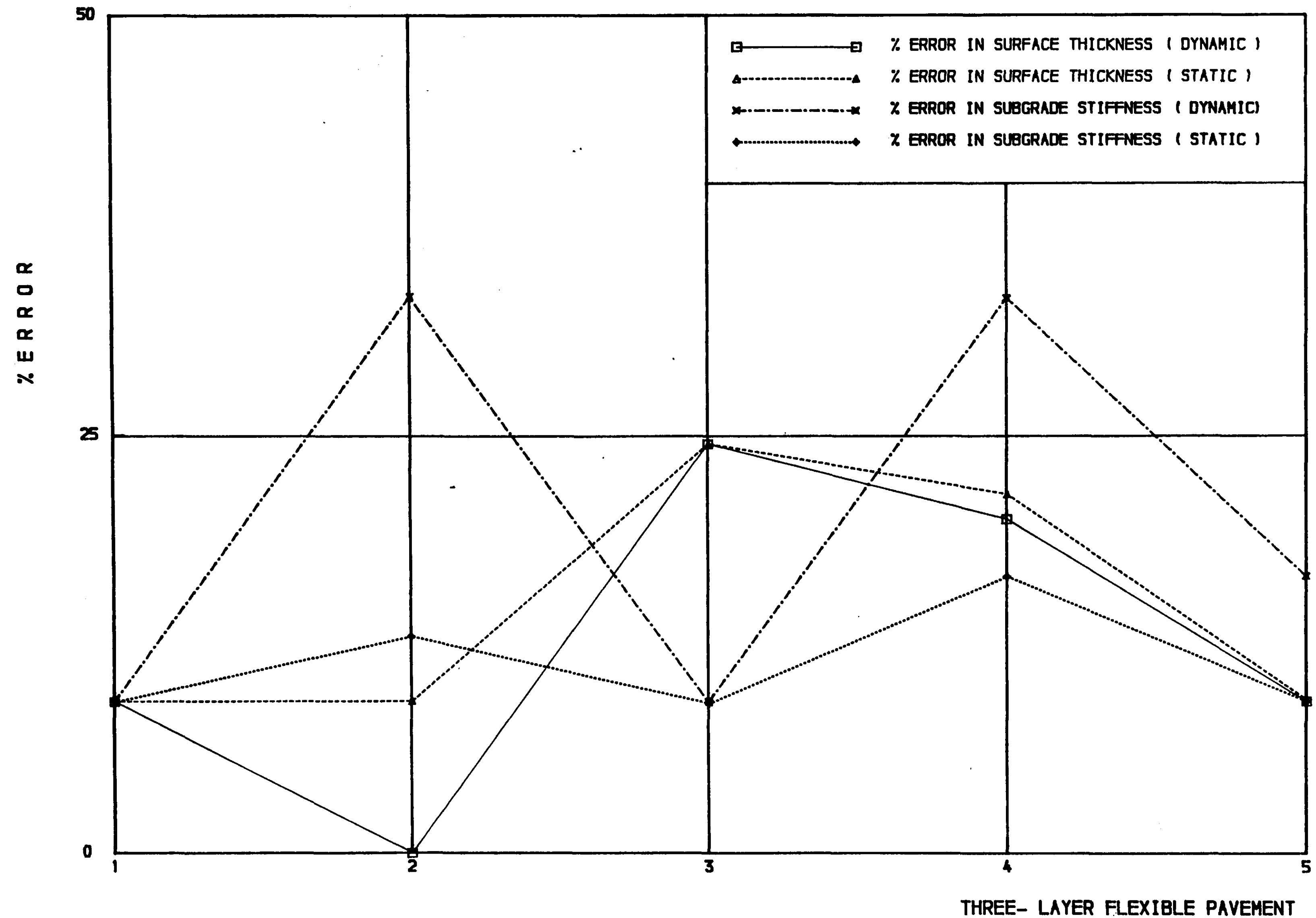

(FIG.4.48) ERROR IN STIFF. AND THICK. DUE TO 10% ERROR IN FWD DEFLn. MEASUREMENTS

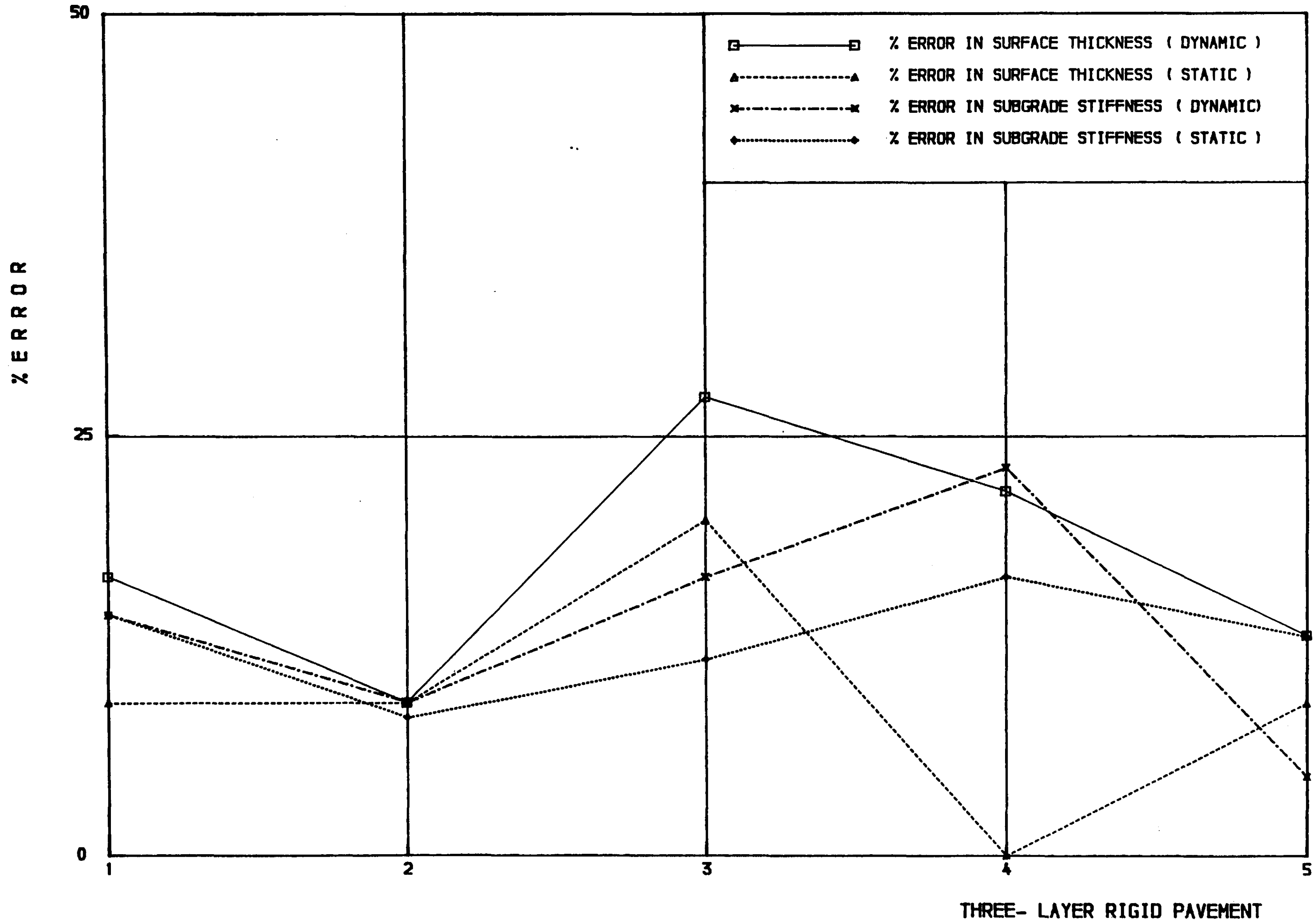

(FIG.4.49) ERROR IN STIFF. AND THICK. DUE TO 10% ERROR IN FWD DEFLn. MEASUREMENTS

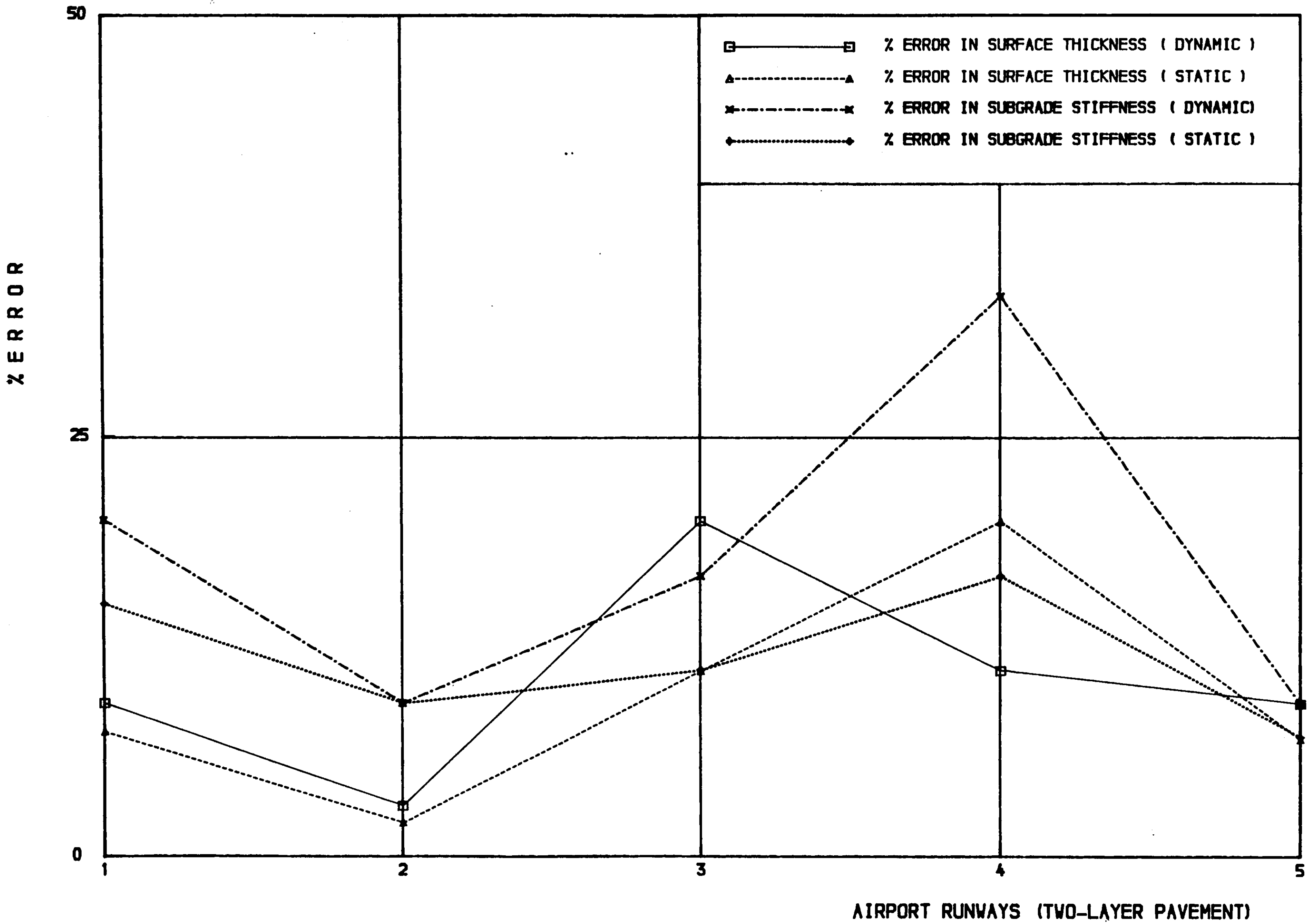

LOCATION ON THE CHARTS

(FIG.4.50) ERROR IN STIFF. AND THICK. DUE TO 10% ERROR IN FWD DEFLn. MEASUREMENTS

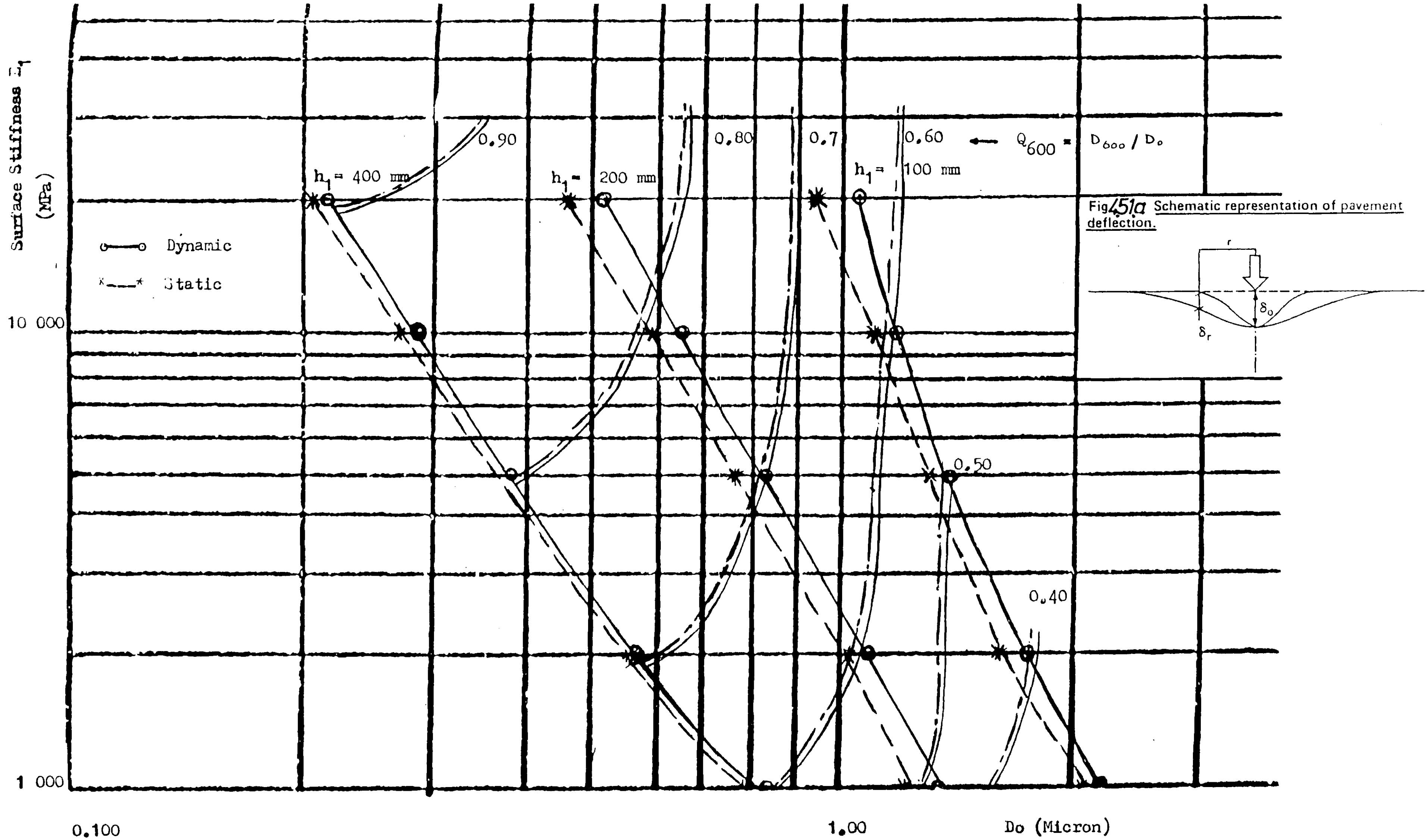

Fig 4.51a Schematic representation of pavement deflection.

(FIG. 4.51b) Deflection Interpretation Chart

THREE- LAYER FLEXIBLE PAVEMENT

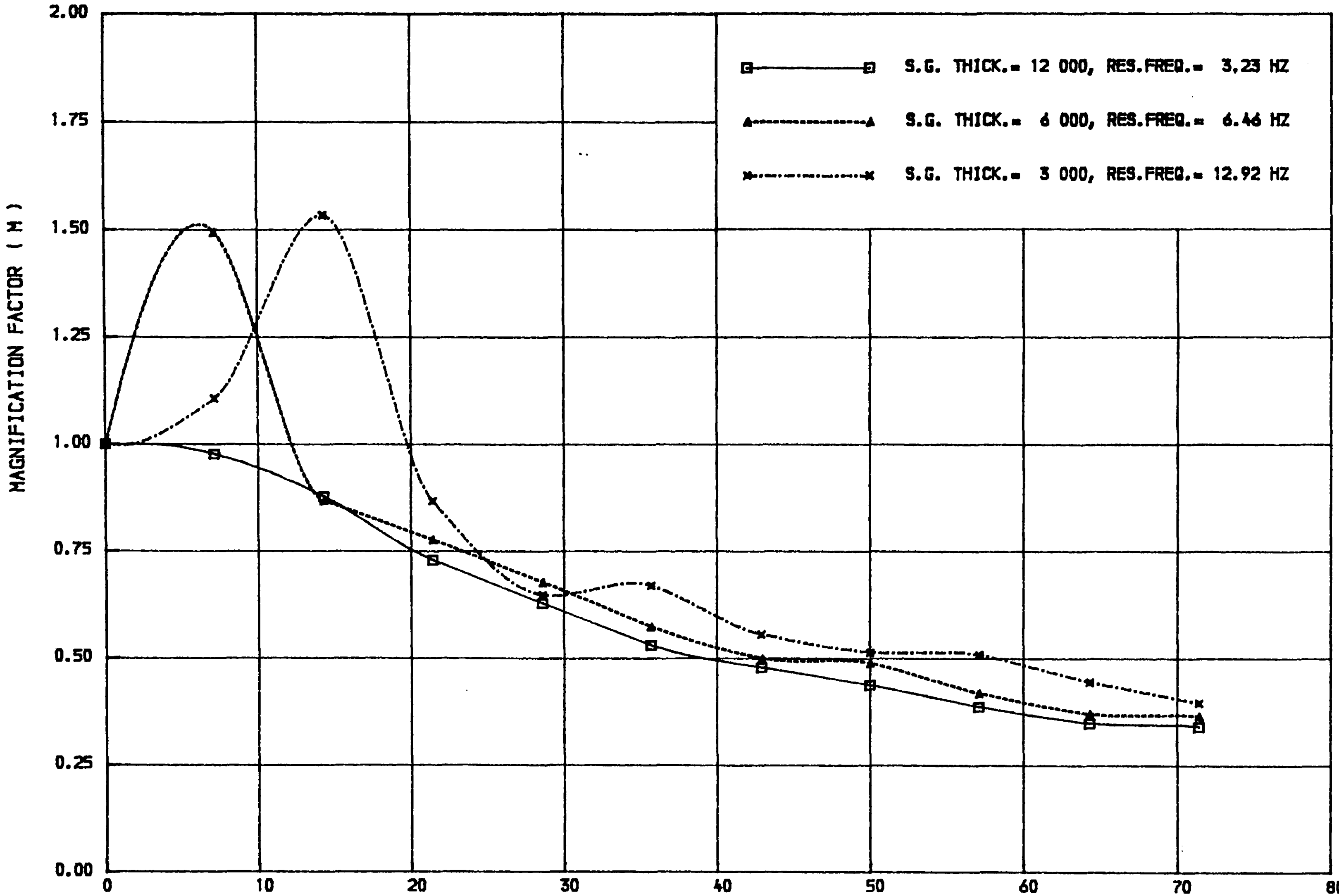

(FIG.4.52)

(SUBGRADE THICKNESS ANALYSIS)

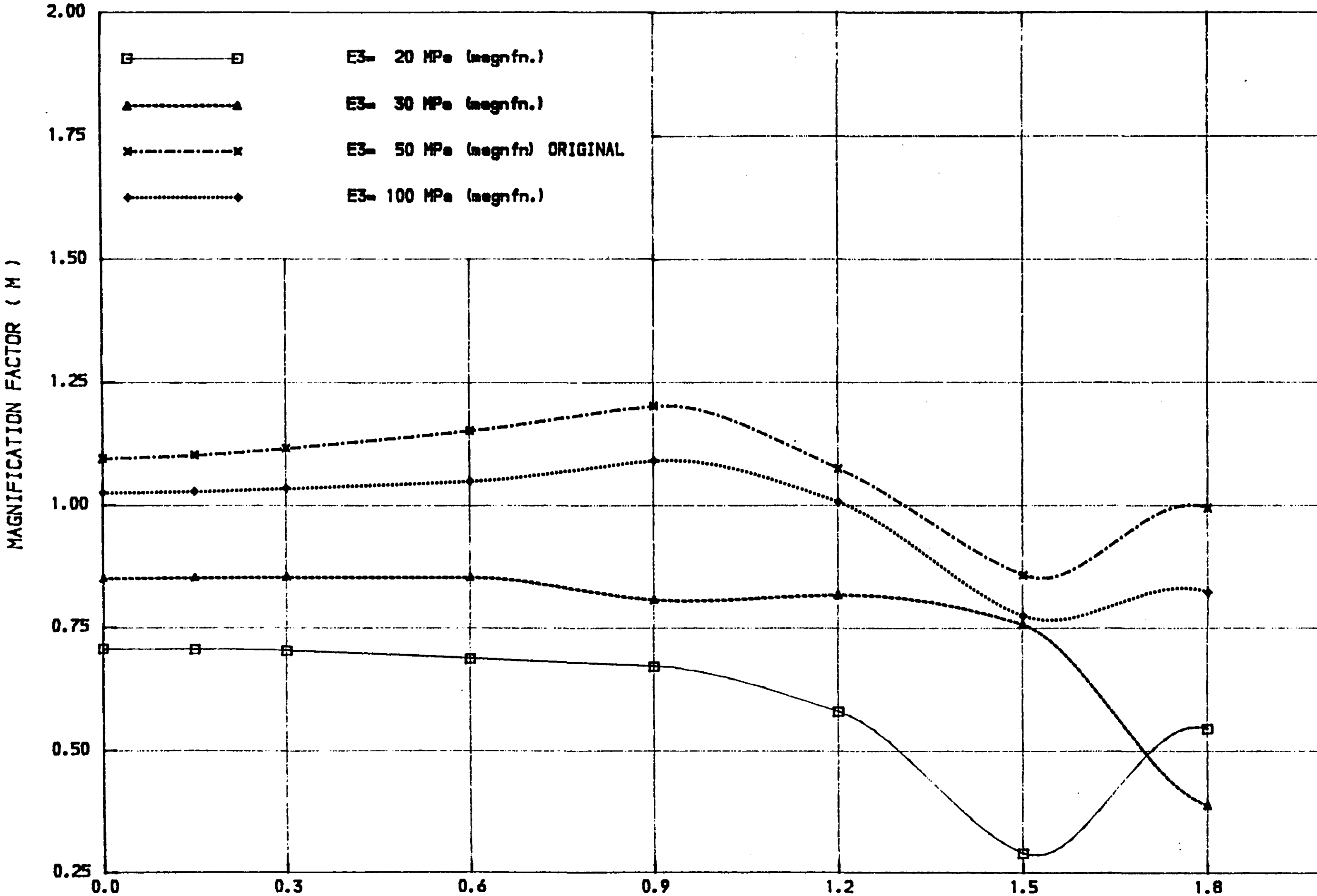

(FIG.4.53)

THREE-LAYER SYSTEM

RADIUS (M) E1= 20 000 MPa

(SUBGRADE STIFFNESS ANALYSIS)

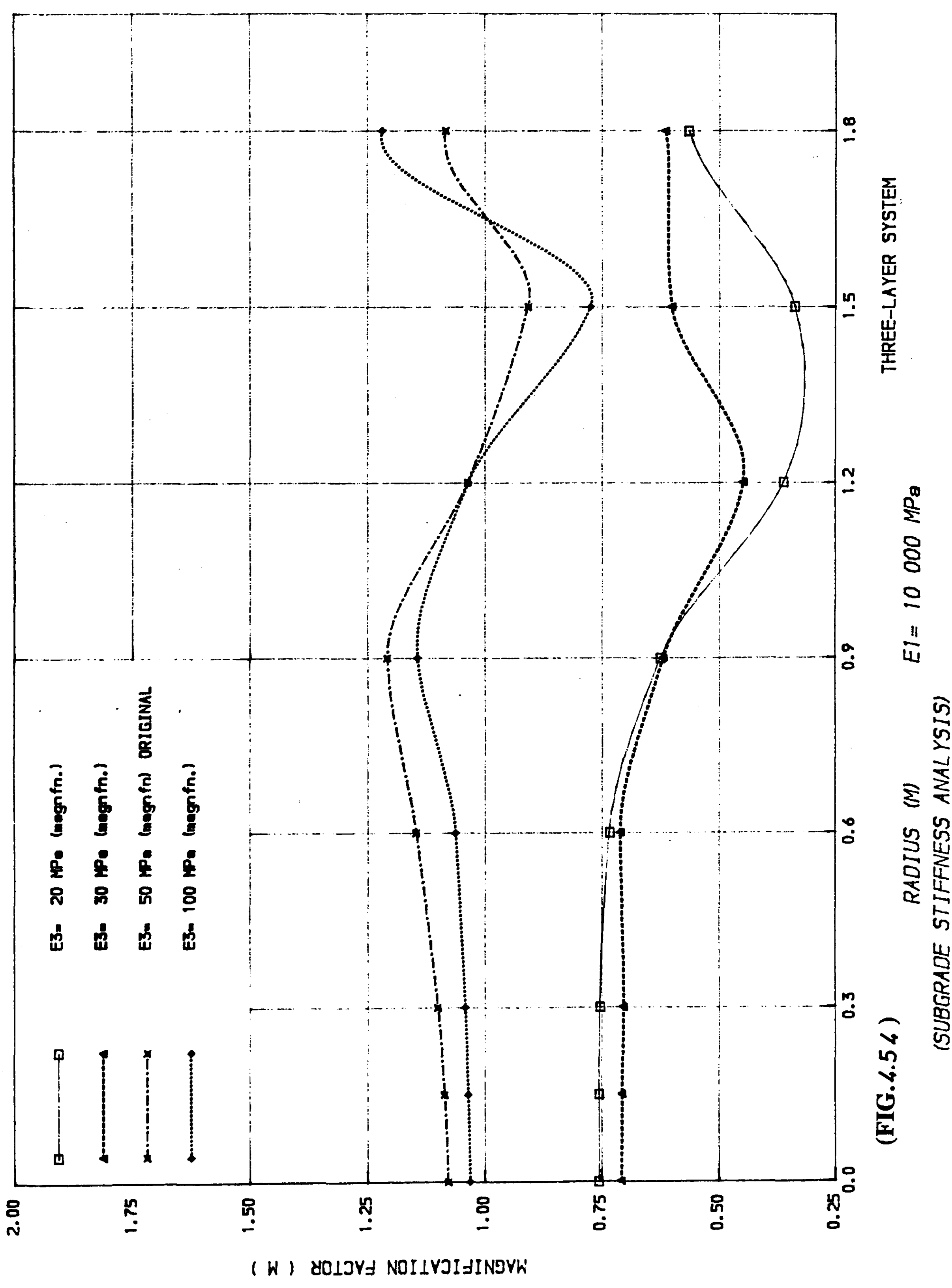
E3= 20 MPa (magnfn.)
E3= 30 MPa (magnfn.)
E3= 50 MPa (magnfn) ORIGINAL
E3= 100 MPa (magnfn.)
MAGNIFICATION FACTOR (M)
2.00
1.75
1.50
1.25
1.00
0.75
0.50
0.25
0.0
0.3
0.6
0.9
1.2
1.5
1.8
THREE-LAYER SYSTEM
RADIUS (M)
E1= 10 000 MPa
(SUBGRADE STIFFNESS ANALYSIS)

(FIG.4.54)

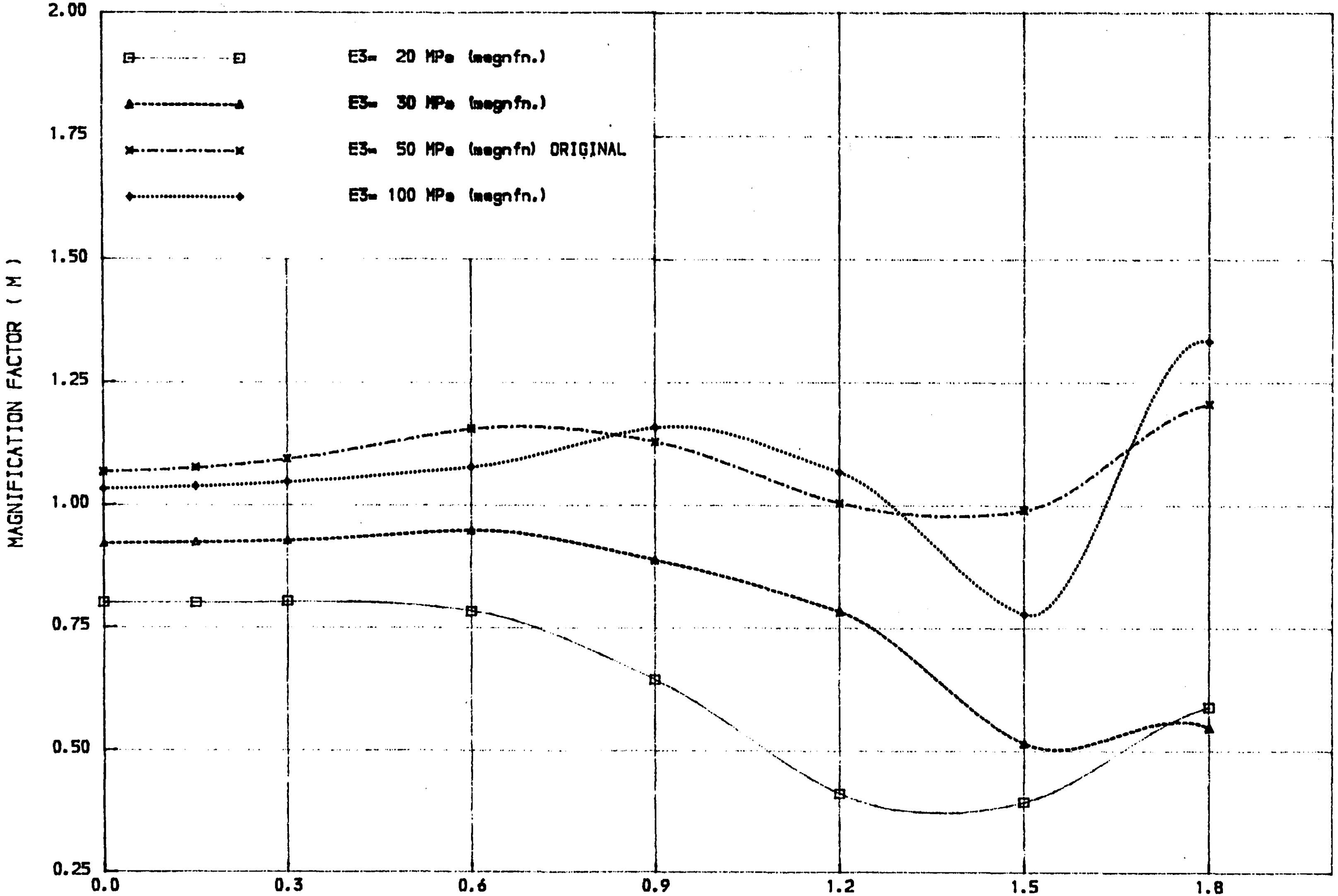

(FIG. 4.55)

THREE-LAYER SYSTEM

RADIUS (M) *E1= 5 000 MPa*

(SUBGRADE STIFFNESS ANALYSIS)

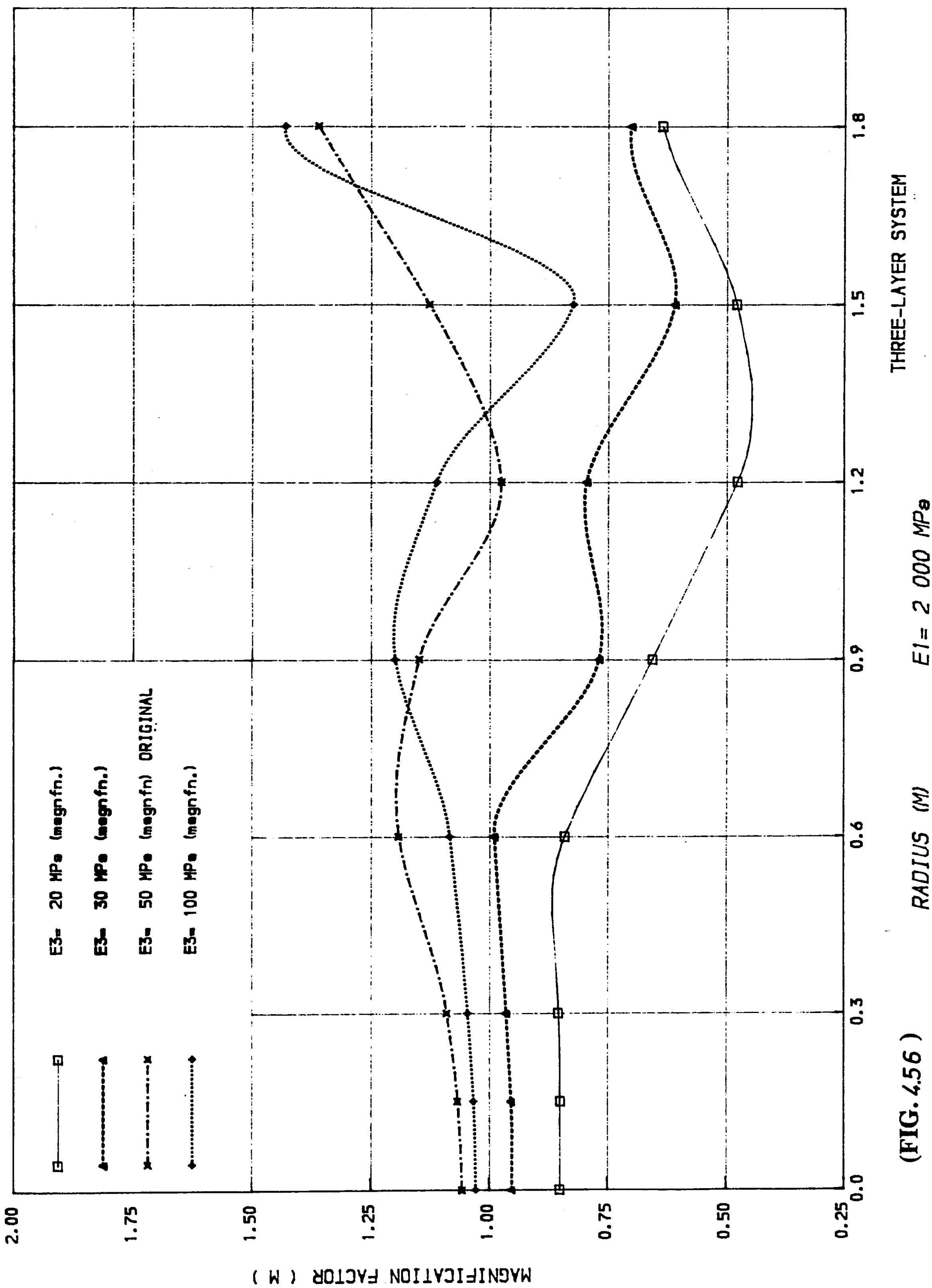

(FIG. 4.56)
(SUBGRADE STIFFNESS ANALYSIS)

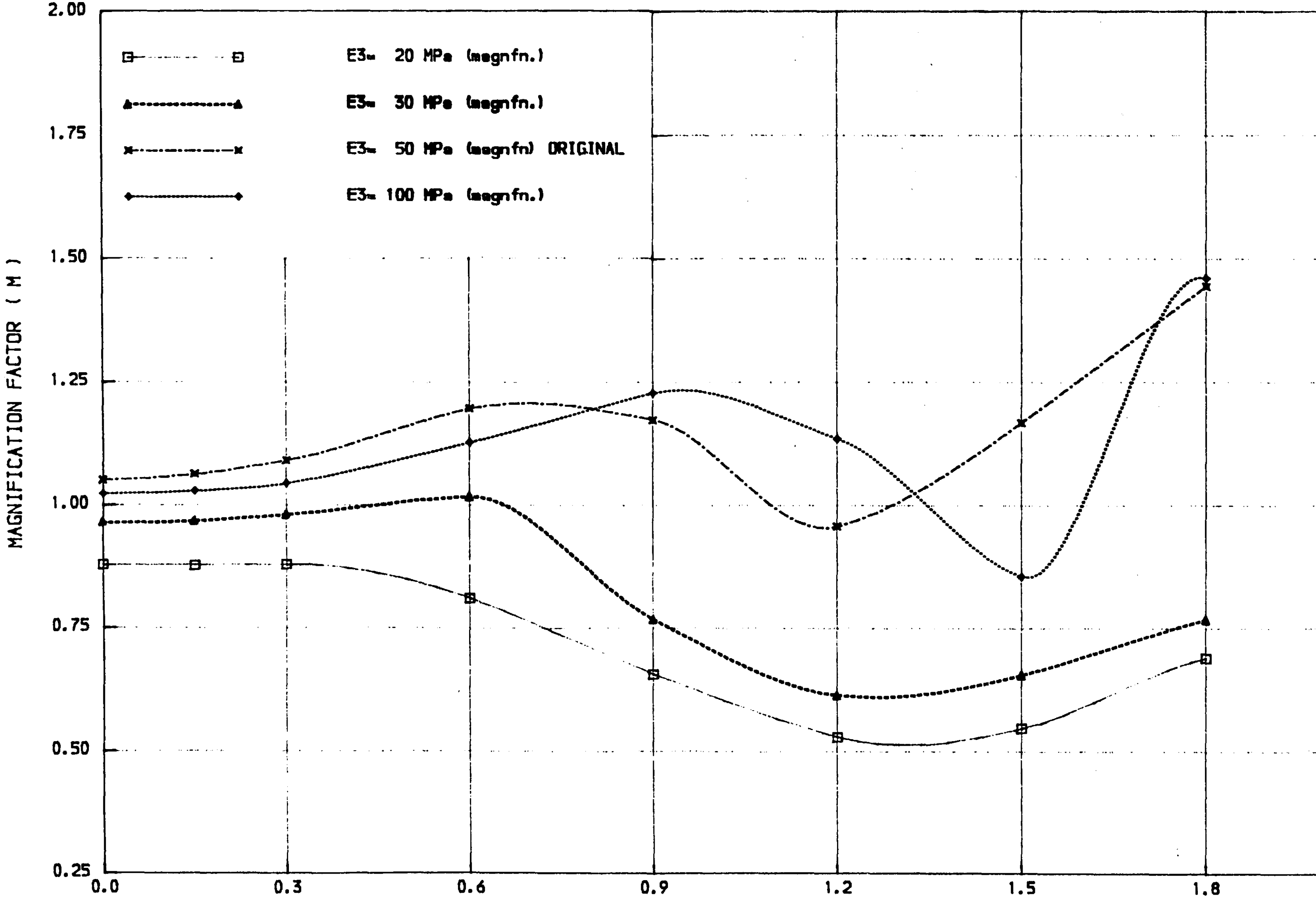

(FIG.4.57)

THREE-LAYER SYSTEM

RADIUS (M) E1= 1 000 MPa

(SUBGRADE STIFFNESS ANALYSIS)

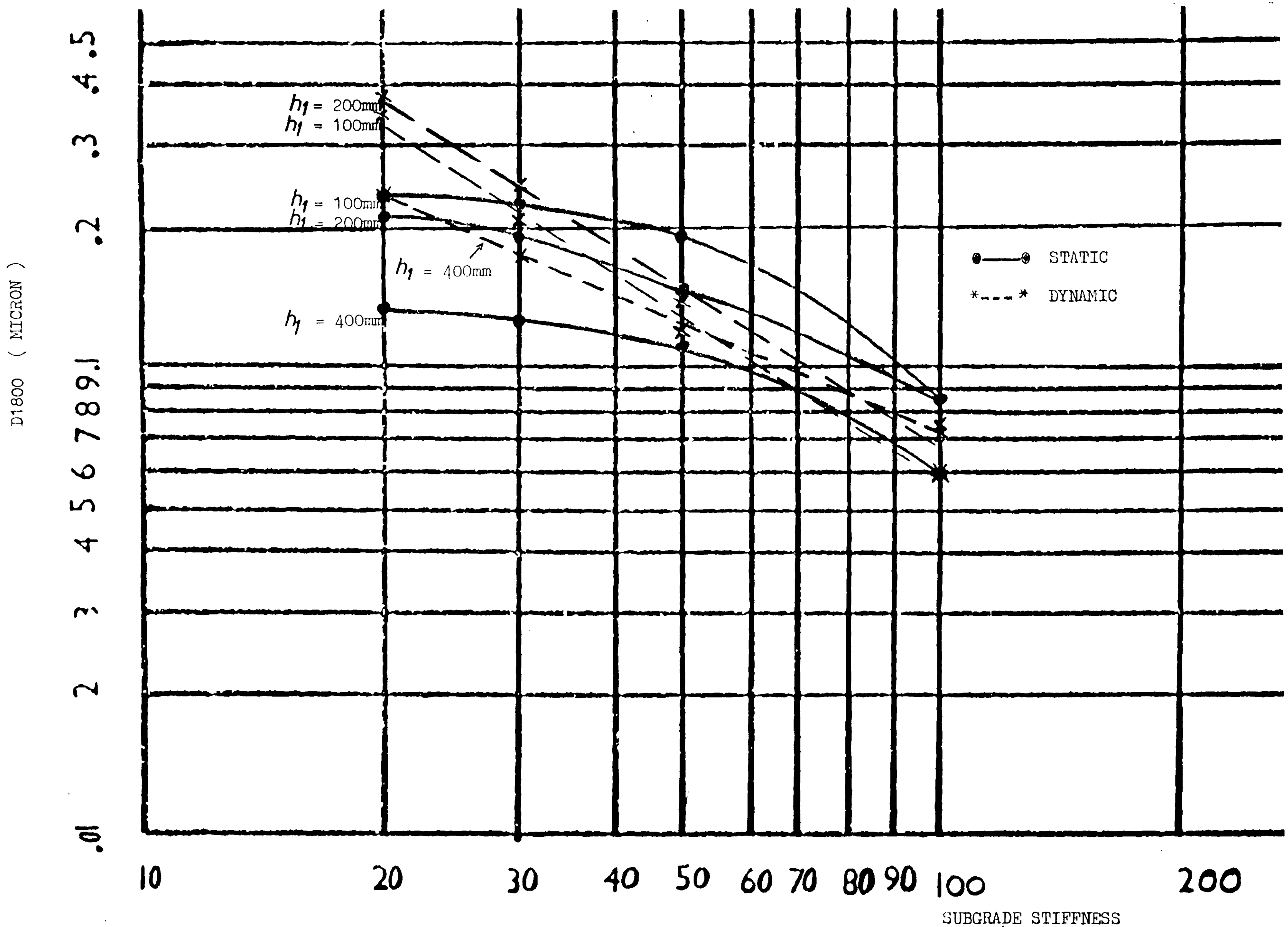

(FIG.4.58) **THREE LAYER FLEXIBLE PAVEMENT**

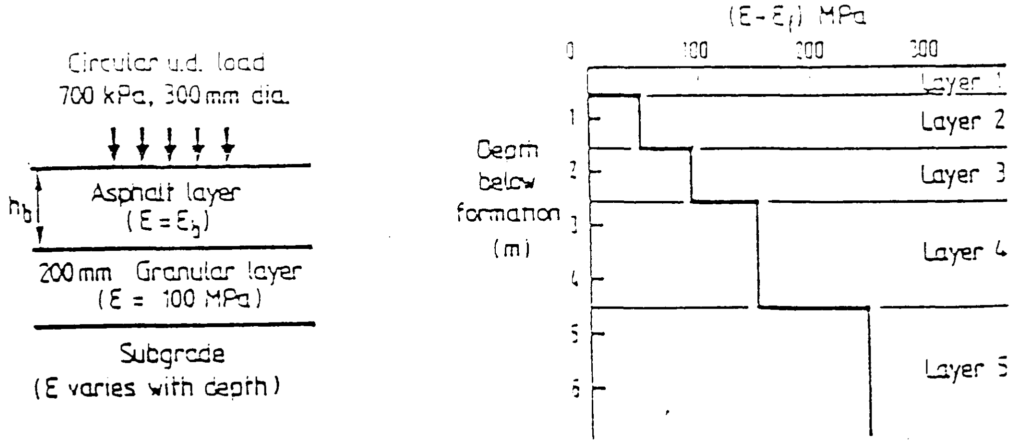

FIG. 4.59 Structural arrangement for back analysis [5]

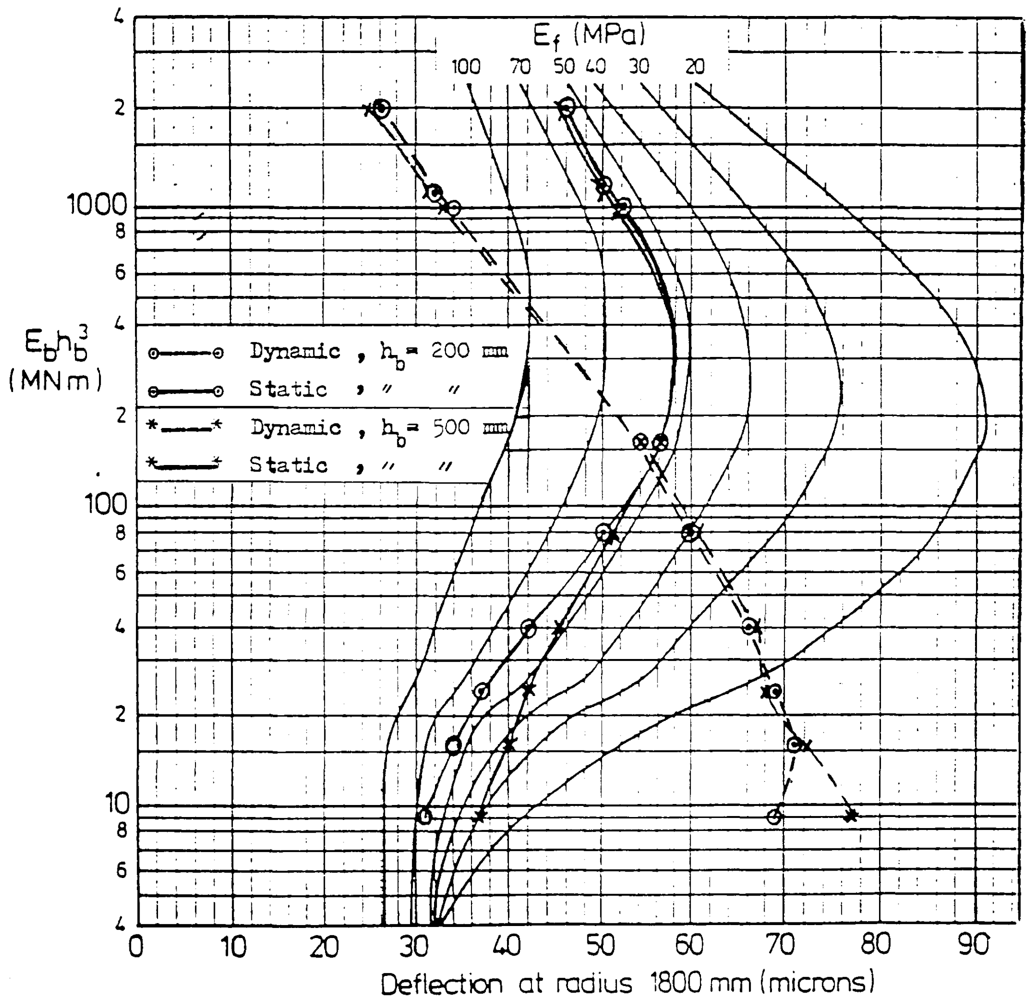

THREE LAYER FLEXIBLE PAVEMENT

(FIG. 4.60) Chart for determination of elastic stiffness at formation level (E_f)

THREE LAYER FLEXIBLE PAVEMENT

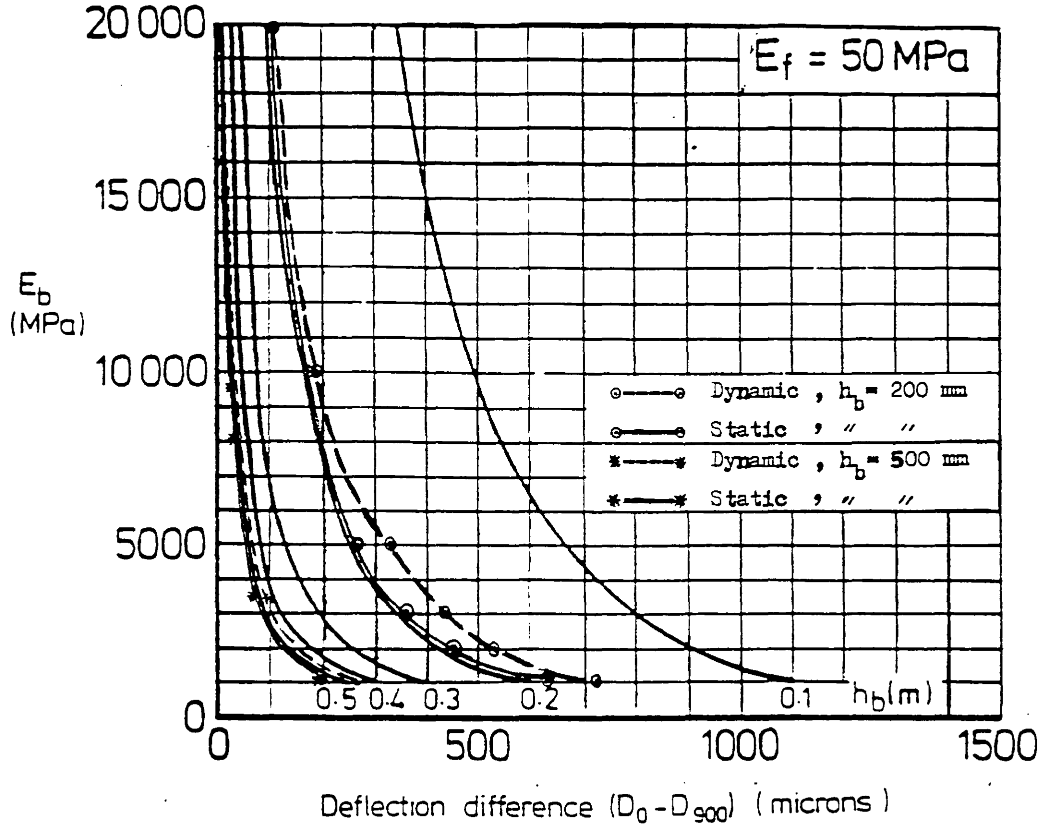

(FIG.4.61) Chart for determination of elastic stiffness (E_b)

TABLES

4 - LAYER FLEXIBLE PAVEMENT

Pavement Layer	Thickness h(mm)	Stiffness E(MPa)	STIFFNESSES, E(MPa)									
			1	2	3	4	5	6	7	8	9	10
SURFACE	100	4,000	16,000	8,000	2,000							
ROADBASE	200	1,000				4,000	2,000	500				
SUBBASE	300	200							400	100		
SUBGRADE	6,000	100									200	50

TABLE (4.1.a) LAYER STIFFNESS VARIATION

Pavement Layer	Thickness h(mm)	Stiffness E(MPa)	THICKNESSES, h(mm)							
			1	2	3	4	5	6	7	8
SURFACE	100	4,000	200	50						
ROADBASE	200	1,000			400	100				
SUBBASE	300	200					600	150		
SUBGRADE	6,000	100							12,000	3,000

TABLE (4.1.b) LAYER THICKNESS VARIATION

3- LAYER FLEXIBLE PAVEMENT

Pavement Layer	Thickness h(mm)	Stiffness E(MPa)	STIFFNESSES, E (MPa)									
			1	2	3	4	5	6	7	8	9	10
SURFACE	200	10,000	20,000	5,000	2,000	1,000	500	250				
BASE	200	100							200	50		
SUBGRADE	6,000	50									100	20

TABLE (42a)LAYER STIFFNESS VARIATION

Pavement Layer	Thickness h(mm)	Stiffness E(MPa)	THICKNESSES, h (mm)					
			1	2	3	4	5	6
SURFACE	200	10,000	400	100				
BASE	200	100			400	50		
SUBGRADE	6,000	50					12,000	3,000

TABLE (4.2b) LAYER THICKNESS VARIATION

3- LAYER RIGID PAVEMENT

Pavement Layer	Thickness h(mm)	Stiffness E(MPa)	STIFFNESSES, E (MPa)					
			1	2	3	4	5	6
SLAB	200	40,000	80,000	20,000				
BASE	150	200			400	100		
SUBGRADE	6,000	100					200	50

TABLE (4.3a) LAYER STIFFNESS VARIATION

Pavement Layer	Thickness h(mm)	Stiffness E(MPa)	THICKNESSES, h (mm)					
			1	2	3	4	5	6
SLAB	200	40,000	400	100				
BASE	150	200			300	75		
SUBGRADE	6,000	100					12,000	3,000

TABLE (4.3.b) LAYER THICKNESS VARIATION

2 - LAYER RIGID PAVEMENT

(AIRPORT RUNWAYS)

Pavement Layer	Thickness h(mm)	Stiffness E(MPa)	STIFFNESSES, E (MPa) 1	2	3	4
SLAB	200	40,000	80,000	20,000		
SUBGRADE	6,000	100			200	400

TABLE (44.a) LAYER STIFFNESS VARIATION

Pavement Layer	Thickness h(mm)	Stiffness E(MPa)	THICKNESSES, h (mm) 1	2	3	4
SLAB	200	40,000	400	100		
SUBGRADE	6,000	100			12,000	3,000

TABLE (44.b) LAYER THICKNESS VARIATION

stiffness of layer i	dynamic (static) displ. changes due to stiffness changes by:		dist. over which dynamic (static) displ. changes are significant	range of M over 1800 mm dist.
Ei (MPa)	+ 100%	- 50%	(mm)	
E1	- 12%	+ 12%	0 - 300	1.05-1.26
E2	- 21%	+ 23%	0 - 600	1.04-1.27
E3	- 19%	+ 20%	0 - 900	1.02-1.29
E4	- 20%	+ 28%	0 - 1800	1.03-1.45

Table 4.5.a Effect of layer STIFFNESS variation on the dynamic (static) displacement (4LFP)

thickness of layer i	dynamic (static) displ. changes due to thickness changes by:		dist. over which dynamic (static) displ. changes are significant	range of M over 1800 mm dist.
hi (MPa)	+ 100%	- 50%	(mm)	
h1	- 26%	+ 21%	0 - 600	1.03-1.28
h2	- 27%	+ 27%	0 - 900	1.00-1.30
h3	- 8%	+ 8%	0 - 900	1.01-1.27
h4	- 2%	+ 2%	0 - 1800	0.98-1.78

Table 4.5.b Effect of layer THICKNESS variation on the dynamic (static) displacement (4LFP)

stiffness of layer i	dynamic (static) displ. changes due to stiffness changes by:		dist. over which dynamic (static) displ. changes are significant	range of M over 1800 mm dist.
Ei (MPa)	+ 100%	- 50%	(mm)	
E1	- 25%	+ 25%	0 - 600	1.10-1.40
E2	- 4%	+ 4%	0 - 900	1.12-1.20
E3	- 33%	+ 19%	0 - 1800	1.01-1.23

Table 4.6.a Effect of layer STIFFNESS variation on the dynamic (static) displacement (3LFP)

thickness of layer i	dynamic (static) displ. changes due to thickness changes by:		dist. over which dynamic (static) displ. changes are significant	range of M over 1800 mm dist.
hi (MPa)	+ 100%	- 50%	(mm)	
h1	- 56%	+ 49%	0 - 900	1.05-1.21
h2	- 3%	+ 3%	0 - 900	1.08-1.26
h3	- 5%	+ 5%	0 - 1800	1.03-1.24

Table 4.6.b Effect of layer THICKNESS variation on the dynamic (static) displacement (3LFP)

stiffness of layer i	dynamic (static) displ. changes due to stiffness changes by:		dist. over which dynamic (static) displ. changes are significant	range of M over 1800 mm dist.
Ei (MPa)	+ 100%	- 50%	(mm)	
E1	- 29%	+ 25%	0 - 900	1.02-1.11
E2	- 2%	+ 2%	0 - 1200	1.03-1.12
E3	- 30%	+ 36%	0 - 1800	1.03-1.40

Table 4.7.a Effect of layer STIFFNESS variation on the dynamic (static) displacement (3LRP)

thickness of layer i	dynamic (static) displ. changes due to thickness changes by:		dist. over which dynamic (static) displ. changes are significant	range of M over 1800 mm dist.
hi (MPa)	+ 100%	- 50%	(mm)	
h1	- 60%	+ 50%	0 - 900	1.01-1.26
h2	- 1%	+ 1%	0 - 1200	1.02-1.12
h3	- 6%	+ 6%	0 - 1800	1.08-1.48

Table 4.7.b Effect of layer THICKNESS variation on the dynamic (static) displacement (3LRP)

stiffness of layer i	dynamic (static) displ. changes due to stiffness changes by:		dist. over which dynamic (static) displ. changes are significant	range of M over 1800 mm dist.
Ei (MPa)	+ 100%	- 50%	(mm)	
E1	- 26%	+ 25%	0 - 900	0.77-1.12
E2	- 35%	+ 26%	0 - 1800	0.80-1.40

Table 4.8.a Effect of layer STIFFNESS variation on the dynamic (static) displacement (2LRP)

thickness of layer i	dynamic (static) displ. changes due to thickness changes by:		dist. over which dynamic (static) displ. changes are significant	range of M over 1800 mm dist.
hi (MPa)	+ 100%	- 50%	(mm)	
h1	- 56%	+ 55%	0 - 900	0.80-1.30
h2	- 8%	+ 8%	0 - 1800	0.80-1.40

Table 4.8.b Effect of layer THICKNESS variation on the dynamic (static) displacement (2LRP)

4 - LAYER FLEXIBLE PAVEMENT

Pavement Layer	Thickness h(mm)	Stiffness E(MPa)	STIFFNESSES, E(MPa)		
			1	2	3
SURFACE	100	4,000	16,000	8,000	2,000
ROADBASE	200	1,000			
SUBBASE	300	200			
SUBGRADE	6,000	50,100,200	50,100,200	50,100,200	50,100,200

TABLE (4.9a) LAYER STIFFNESS VARIATION

Pavement Layer	Thickness h(mm)	Stiffness E(MPa)	THICKNESSES, h(mm)	
			1	2
SURFACE	100	4,000	200	50
ROADBASE	200	1,000		
SUBBASE	300	200		
SUBGRADE	6,000	50,100,200	50,100,200	50,100,200

TABLE (4.9b) LAYER THICKNESS VARIATION

3- LAYER FLEXIBLE PAVEMENT

Pavement Layer	Thickness h(mm)	Stiffness E(MPa)	STIFFNESSES, E (MPa) 1	2	3	4	5	6
SURFACE	200	10,000	20,000	5,000	2,000	1,000	500	250
BASE	200	100						
SUBGRADE	6,000	20,30,50,100	<---		20,30,50,100	--->		

TABLE (4.10a) LAYER STIFFNESS VARIATION

Pavement Layer	Thickness h(mm)	Stiffness E(MPa)	THICKNESSES, h (mm) 1	2
SURFACE	200	10,000	400	100
BASE	200	100		
SUBGRADE	6,000	20,30, 50,100	20,30, 50,100	20,30, 50,100

TABLE (4.10b) LAYER THICKNESS VARIATION

3- LAYER RIGID PAVEMENT

Pavement Layer	Thickness h(mm)	Stiffness E(MPa)	STIFFNESSES, E (MPa) 1	2
SLAB	200	40,000	80,000	20,000
BASE	150	200		
SUBGRADE	6,000	100,200,300	100,200,300	100,200,300

TABLE (4.11a) LAYER STIFFNESS VARIATION

Pavement Layer	Thickness h(mm)	Stiffness E(MPa)	THICKNESSES, h (mm) 1	2
SLAB	200	40,000	400	100
BASE	150	200		
SUBGRADE	6,000	100,200,300	100,200,300	100,200,300

TABLE (4.11.b) LAYER THICKNESS VARIATION

2 - LAYER RIGID PAVEMENT

(AIRPORT RUNWAYS)

Pavement Layer	Thickness h(mm)	Stiffness E(MPa)	STIFFNESSES, E (MPa) 1	2
SLAB	200	40,000	80,000	20,000
SUBGRADE	6,000	100,200,400	100,200,400	100,200,400

TABLE (4.12a) LAYER STIFFNESS VARIATION

Pavement Layer	Thickness h(mm)	Stiffness E(MPa)	THICKNESSES, h (mm) 1	2
SLAB	200	40,000	400	100
SUBGRADE	6,000	100,200,400	100,200,400	100,200,400

TABLE (4.12b) LAYER THICKNESS VARIATION

LOCATION	STIFFNESS CHARTS	THICKNESS CHARTS
1	soft surface; stiff subgrade	thin surface; stiff subgrade
2	,, ,, ; soft subgrade	,, ,, ; soft subgrade
3	stiff surface; stiff subgrade	thick surface; stiff subgrade
4	,, ,, ; soft subgrade	,, ,, ; soft subgrade
5	medium ,, ; medium ,,	medium ,, ; medium ,,

Table 4.13 Definition of locations on stiffness and thickness charts

location on chart	static E1	static E4	dynamic E1	dynamic E4	%difference E1	%difference E4
1	2700	150	1900	170	26.9	-11.7
2	5000	60	3700	60	26.0	0
3	10000	150	8000	170	20.0	-7.7
4	20000	60	14000	65	30.0	-7.7
5	7500	80	6500	98	13.3	-18.4

Table 4.14.a Percentage difference between static and dynamic STIFFNESSES (4LFP)

location on chart	static h1	static E4	dynamic h1	dynamic E4	% difference h1	% difference E4
1	80	140	70	170	12.5	-17.6
2	60	60	50	70	16.7	-14.3
3	160	145	130	160	18.8	- 9.4
4	190	65	155	75	18.4	-13.4
5	110	105	90	130	18.2	-19.2

Table 4.14.b Percentage difference between static and dynamic THICKNESSES AND STIFFNESSES (4LFP)

location on chart	static E1	static E3	dynamic E1	dynamic E3	% difference E1	% difference E3
1	1400	70	1100	95	21.4	-26.3
2	1700	31	2200	22	-22.7	29.0
3	9000	80	8000	95	11.1	-15.7
4	7000	35	10000	25	-30.0	28.6
5	3000	45	2700	55	10.0	-18.2

Table 4.15.a Percentage difference between static and dynamic STIFFNESSES (3LFP)

location on chart	static h1	static E3	dynamic h1	dynamic E3	% difference h1	% difference E3
1	120	70	105	90	12.5	-22.2
2	120	35	105	40	12.5	-12.5
3	360	80	350	75	2.8	6.3
4	195	32	210	25	-7.2	22.0
5	160	48	150	60	6.3	-20.0

Table 4.15.b Percentage difference between static and dynamic THICKNESSES AND STIFFNESSES (3LFP)

location on chart	static E1	static E3	dynamic E1	dynamic E3	% difference E1	% difference E3
1	22000	250	20500	290	6.8	-13.8
2	30000	110	2800	90	6.7	18.0
3	63000	270	60000	310	4.8	-13.0
4	65000	175	61000	180	6.2	- 2.8
5	45000	190	40000	220	11.2	-13.6

Table 4.16.a Percentage difference between static and dynamic STIFFNESSES (3LRP)

location on chart	static h1	static E3	dynamic h1	dynamic E3	%difference h1	%difference E3
1	125	220	110	250	12.0	-12.0
2	120	120	100	140	16.7	-14.3
3	310	270	310	290	0	- 6.7
4	280	120	260	95	7.2	21.0
5	160	260	150	285	6.3	- 8.8

Table 4.16.b Percentage difference between static and dynamic THICKNESSES AND STIFFNESSES (3LRP)

location	static		dynamic		%difference	
on chart	E1	E2	E1	E2	E1	E2
1	27000	240	23000	300	15.0	-20.0
2	26000	110	27000	90	- 3.7	18.0
3	60000	270	55000	320	8.3	-15.6
4	57000	170	55000	200	3.5	-15.0
5	43000	190	37000	230	14.0	-17.4

<u>Table 4.17.a Percentage difference between static and dynamic STIFFNESSES (2LRP)</u>

location	static		dynamic		% difference	
on chart	h1	E2	h1	E2	h1	E2
1	120	210	110	250	8.3	-16.0
2	130	110	115	140	11.5	-21.4
3	300	230	290	270	3.3	-14.8
4	260	120	250	90	3.8	25.0
5	160	170	150	210	6.3	-19.0

<u>Table 4.17.b Percentage difference between static and dynamic THICKNESSES AND STIFFNESSES (2LRP)</u>

LOCATION	UNDERESTIMATED	OVERESTIMATED
1	subgrade stiffness	surface stiffness
2	surface stiffness	subgrade stiffness
3	subgrade stiffness	surface stiffness
4	,, ,,	,, ,,
5	,, ,,	,, ,,

Table 4.18 Static analysis of FWD (obtained from Fig. 4.41)

LOCATION	UNDERESTIMATED	OVERESTIMATED
1	subgrade stiffness	surface thickness
2	,, ,,	,, ,,
3	,, ,,	,, ,,
4	surface thickness	subgrade stiffness
5	subgrade stiffness	surface thickness

Table 4.19 Static analysis of FWD (obtained from Fig. 4.42)

error	static		% error		dynamic		% error	
location	E'1	E'4	E'1	E'4	E'1	E'4	E'1	E'4
1	3200	210	37.5	5.0	3000	210	33.3	5.0
2	3100	55	35.5	9.0	3000	55	33.3	9.0
3	12000	215	33.5	7.0	12000	210	34.0	5.0
4	12000	60	33.3	16.5	12000	55	34.0	9.0
5	6000	115	33.3	13.0	5500	110	27.3	9.1

Table 4.20.a Percentage error in STIFFNESSES due to 10% deviation in FWD measurements (4LFP)

error	static		% error		dynamic		% error	
location	h'1	E'4	h'1	E'4	h'1	E'4	h'1	E'4
1	65	210	23.1	4.2	70	210	28.6	4.7
2	65	60	23.1	16.6	70	60	28.6	17.0
3	210	210	4.7	4.6	215	210	7.0	4.7
4	210	60	4.7	16.6	215	60	7.0	17.0
5	115	110	13.0	9.0	120	110	16.6	9.1

Table 4.20.b Percentage error in STIFFNESSES and THICKNESSES due to 10% deviation in FWD measurements (4LFP)

error location	static E'1	static E'3	% error E'1	% error E'3	dynamic E'1	dynamic E'3	% error E'1	% error E'3
1	1150	120	13.0	17.0	1200	120	16.6	17.1
2	1150	35	13.0	14.3	1020	35	2.0	14.3
3	11000	120	9.0	17.0	11000	115	9.1	13.0
4	12000	35	16.6	14.3	11000	42	9.1	28.0
5	6000	55	16.6	9.0	6000	55	17.1	9.0

Table 4.21.a Percentage error in STIFFNESSES due to 10% deviation in FWD measurements (3LFP)

error location	static h'1	static E'3	% error h'1	% error E'3	dynamic h'1	dynamic E'3	% error h'1	% error E'3
1	110	110	9.1	9.1	110	110	9.1	9.1
2	110	23	9.1	13.0	90	30	0	33.3
3	530	110	24.5	9.0	530	110	24.5	9.1
4	510	24	21.5	16.6	500	30	20.0	33.3
5	220	55	9.2	9.1	220	60	9.1	16.6

Table 4.21.b Percentage error in STIFFNESSES and THICKNESSES due to 10% deviation in FWD measurements (3LFP)

error	static		% error		dynamic		% error	
location	E'1	E'3	E'1	E'3	E'1	E'3	E'1	E'3
1	24000	330	16.7	9.1	25000	320	20.0	6.2
2	24000	120	16.7	16.7	20000	120	0	16.6
3	85000	340	6.0	11.7	90000	315	11.1	5.0
4	81000	125	1.2	20.0	85000	125	5.8	20.0
5	45000	240	11.1	16.7	50000	230	20.0	13.0

Table 4.22.a Percentage error in STIFFNESSES due to 10% deviation in FWD measurements (3LRP)

error	static		% error		dynamic		% error	
location	h'1	E'3	h'1	E'3	h'1	E'3	h'1	E'3
1	110	350	9.1	14.3	120	350	16.6	14.3
2	110	109	9.1	8.2	110	110	9.1	9.1
3	500	340	20.0	11.7	550	360	27.3	16.6
4	400	120	0	16.6	510	130	21.5	23.1
5	220	230	9.1	13.0	230	210	13.1	4.7

Table 4.22.b Percentage error in STIFFNESSES and THICKNESSES due to 10% deviation in FWD measurements (3LRP)

error location	static E'1	static E'2	% error E'1	% error E'2	dynamic E'1	dynamic E'2	% error E'1	% error E'2
1	25000	430	20.0	7.0	25000	430	20.0	7.0
2	23000	115	13.6	13.0	22000	130	9.1	23.0
3	84000	420	4.9	4.8	85000	420	6.0	4.8
4	84000	110	4.5	9.1	80000	150	0	33.3
5	44000	220	9.1	9.0	45000	230	11.1	13.0

Table 4.23.a Percentage error in STIFFNESSES due to 10% deviation in FWD measurements (2LRP)

error location	static h'1	static E'2	% error h'1	% error E'2	dynamic h'1	dynamic E'2	% error h'1	% error E'2
1	108	470	7.4	15.0	110	500	9.1	20.0
2	102	110	2.0	9.1	103	110	3.0	9.1
3	450	450	11.1	11.1	500	480	20.0	16.7
4	500	120	20.0	16.7	450	150	11.1	33.3
5	215	215	7.0	7.1	220	220	9.1	9.1

Table 4.23.b Percentage error in STIFFNESSES and THICKNESSES due to 10% deviation in FWD measurements (2LRP)

CHAPTER FIVE GENERAL CONCLUSIONS and SUGGESTIONS FOR FUTURE WORK

5.1 GENERAL CONCLUSIONS

A rigorous elasto-dynamic analysis of pavement response to Falling Weight Deflectometer (FWD) testing has been used to undertake a comprehensive parametric study of the problem. The study has included an investigation into the effect of changes in pavement layer stiffnesses and thicknesses on pavement response to FWD testing as well as the effect of changes in the FWD loading rate. A wide variety of flexible and rigid pavement sections have been analysed and the results have been used to develop design charts.

The computer program PULSE developed for this study is based on the Fourier synthesis of a numerical solution (due to Kausel and Peek) for harmonic loading of multi-layered visco-elastic horizontally layered strata. The program calculates pavement deflections resulting from FWD impact directly beneath the load and at arbitrary selected points elsewhere on the pavement surface. Verification of the accuracy of the program (conducted by means of a convergence study) resulted in the following findings:-

(i) Reasonable accuracy can be obtained when the pavement layers are divided into approximately 25 sub-layers.

(ii) About 10 terms of the Fourier series are adequate in order to achieve a fair degree of precision for nominal loading periods of up to approximately 400 msec. For longer loading periods, a higher number of terms (15-30 depending on the duration of the loading period) is required to preserve accuracy.

(iii) Varying the pulse width has far greater influence on the peak surface displacement than varying the nominal loading period. The peak surface displacements increase by about 8% for every 10 msec increase in the pulse duration while the peak surface displacements increase by less than 0.5% for every 10 msec increase in the loading period.

(iv) Long rest periods between FWD blows (typically 300 msec) enable pavements to recover fully. The time taken to reach a quiescent state is primarily a function of subgrade thickness and stiffness.

The parametric studies (in which emphasis has been given to elastic stiffness E and layer thickness H) revealed that the upper pavement layers predominantly influence the local region (up to a radial distance of 600mm). The lower layers (the subgrade in particular) exert the greatest influence further away from the load (900-1800 mm). Changes in the subgrade stiffness result in changes to the whole deflection bowl. Typically, a 50% reduction in the subgrade stiffness results in a 25-30% increase in pavement deflections. Changes in subgrade thickness have very little influence on the shape of deflection bowls but may alter the fundamental resonant frequency of the pavement.

Design charts, derived from deflection basins, revealed that the deflection response of pavements to dynamic loading may be significantly different (by 25-30%) from the static deflection response. The study also showed that in most types of pavements, static analysis of the FWD overestimates the stiffness (and thickness) of surface layers and underestimates the stiffness (and thickness) of subgrade layers by approximately 20-30%.

Sensitivity studies carried out on the design charts showed that small experimental errors can lead to large errors in the determination of pavement properties (i.e. stiffness and thickness). Relatively large errors (in the order of 20-40% for flexible pavements and 10-25% for rigid pavements) in the design charts can result from small deviations (about 10%) in the FWD deflection measurements. This finding diminishes the credibility of claims that surface and subgrade stiffness can be determined (using back-analysis procedures) within 10%. The study further revealed that for practical purposes, stiff thick surface layers and stiff subgrades (i.e. rigid pavements) yield the lowest error in the determination of pavement properties.

These results confirm earlier findings that inertial effects can be significant in FWD testing and that there is no simple means of correlating pavement response to static loading with pavement response to FWD testing. Dynamic deflections may be greater or lesser than "corresponding" static deflections, depending on radial distance from the FWD as well as pavement layer stiffnesses and thicknesses. Consequently, the back-analysis procedures (based on static analyses) which have been presented in the literature for evaluating pavement layer stiffnesses from measured surface deflection values can yield erroneous results. A detailed investigation into this important practical aspect of FWD testing suggests that neglect of the dynamic dimension of the problem leads to errors of the order of 20% in the prediction of the stiffnesses of the upper pavement layers and errors of the order of 30% in the prediction of the stiffness of the subgrade. In view of the many other sources of error in FWD testing and data interpretation, pavement engineers should exercise caution in interpreting the results of FWD tests. Parametric sensitivity studies, allied with a recognition of the importance of the dynamic effects described in this thesis, should however prove helpful in bracketting back-analyses predictions within useful bounds.

continued.....

5.2 RECOMMENDATIONS FOR FUTURE RESEARCH WORK

In order to gain a better insight into the dynamic response of pavements to FWD's successive blows, further investigation into the deflection basins' history (progressive deformation of pavement surface with time) is necessary. The study should explore the causes of the evolution of some distortions at remote locations (1500-1800 mm) from the loaded area in conjunction with the establishment of optimum quiescent values for various pulse widths. For the latter, distortions tend to occur at late stages of the rest period (100-300 msec beyond pulse widths). The study of wave reflection/refraction at pavement layer interfaces may prove helpful in the investigation of the above phenomena.

The sensitivity of deflection values to variation in stiffness of a particular layer can be assessed more easily by producing deflection charts using the concept of "normalised deflection difference (D/D_o)", [i.e. the difference between each two adjacent deflection points (e.g. $D_{12} = D_1 - D_2$, etc.) divided by the centroidal deflection D_o as the vertical axis versus stiffness values of a particular layer, e.g. sensitivities of D_{12} and D_{78} to variation of upper and lower layer stiffnesses, respectively. Some preliminary work has been presented in Chapter Four, Figures 4.26.a - 4.27.d.

The design charts presented in this thesis cater only for a limited number of (flexible and rigid) pavement sections with prescribed thicknesses. Thus, for a wider application of these charts, it is necessary to extend the data in parametric studies to include a wider range of intermediate pavement layer thicknesses. This would also reduce the possibility of obtaining erroneous results due to the existing interpolation method.

Finally, a less critical case is the modification of the computer program 'PULSE' to compute surface deflections for pavements of low subgrade stiffnesses (less than 20 MPa for flexible pavements and less than 100 MPa for rigid pavements). Similarly, for very stiff surfaces in rigid pavements (greater than 80,000 MPa). To achieve this, the number of iteration steps in the subroutine 'RAYLGH' (where convergence failure occurs) should be increased.

REFERENCES

1. **Bohn A. (1967)**
Danish experiments with the French falling ball deflectometer.
2nd Int Conf Struct Des Asphalt Pavements, Ann Arbor 647-659

2. **Bohn A. Ullidtz P. Stubstad R. & Sorenson A. (1972)**
Danish experiments with the French falling weight deflectometer.
Proc 3rd Int Conf Struct Des Asphalt pavements 1 London 1119-1128

3. **Brown S F. & Pell P S. (1967)**
An experimental investigation of stress, strain and deflections in a layered pavement structure subjected to dynamic loads.
Proc 2nd Int Conf Struct Des Asphalt Pavements, Ann Arbor 487-504

4. **Brown S F. & Bush D I. (1972)**
Dynamic response of model pavement structure.
J ASCE 109 TE4 1005-1022

5. **Brown S F. (1987)**
Pavement evaluation and overlay design using falling weight deflectometer - Chapter J.
Analt Des Eval Bituminous Pavements, Course given at Glasgow University

6. **Brown S F. & Brunton J M. (1987)**
An introduction to the analytical design of bituminous pavements.
3rd Ed Nottingham University 26-36

7. **Bush A J. & Alexander R R. (1982)**
Pavement evaluation using deflection basin measurements and layered theory.
TRB 1022 16-25

8. **Claessen A I M. Valkering C P. & Ditmarsch R. (1976)**
Pavement evaluation with falling weight deflectometer.
Proc Assoc Asphalt Paving Tech 45 122-157

9. **Claessen A I M. & Ditmarsch R. (1977)**
Pavement evaluation and overlay design - The shell method. Proc 4th Int Conf Struct Des Asphalt Pavements, Ann Arbor 649-661

10. **Clough R W. & Penzien J. (1975)**
Dynamics of structures.
McGraw Hill New York N.Y.

11. **Croney D. (1971)**
The design and performance of road pavements.
Chapter 12 John Wiley & Son Inc

12. **Davies T G. & Mamlouk M S. (1985)**
Theoretical response of multilayer pavement systems to dynamic non-destructive testing.
TRB 1022 1-7

13. **Davies T G. & Salahi R. (1987)**
Dynamic analysis of pavement response to falling weight deflectometer testing.
Research report, Civil Eng Dept Glasgow University

14. **Dorman G M. & Metcalf C T. (1965)**
Design curves for flexible pavements based on layered system theory.
HRR 71 Publ 1255 69-84

15. **Duncan J M. Monismith C L. & Wilson E L. (1968)**
Finite element analysis of pavements.
HRB 228 18-33

16. **Eringen A C. & Suhubi E S. (1975)**
Elasto-dynamics, Linear theory.
Academic press, Vol. 2, New York N.Y.

17. **Foxworthy P T. & Darter M I. (1986)**
Preliminary concept for falling weight deflectometer testing and evaluation of rigid airfield pavements.
TRB 1070 77-89

18. **Hall R J. & Richart F E. (1963)**
Dissipation of elastic wave energy in granular soils.
J ASCE 89 SM6 27-52

19. **Heisey J S. Stokoe K H. & Meyer A H. (1982)**
Moduli of pavement system from spectral analysis of surface wave.
TRB 852 22-31

20. **Hoffman M S. & Thompson M R. (1981)**
Non-destructive testing of flexible pavements.
Civil Eng Ser 31 Univ Illinois 32-39

21. **Hoffman M S. & Thompson M R. (1982)**
Comparative study of selected non-destructive testing devices.
TRB 852 32-41

22. **Hoffman M S. & Thompson M R. (1982)**
Backcalculating non-linear resilient moduli from deflection data.
TRB 852 42-51

23. **Hoffman M S. (1983)**
Loading mode effects on pavement deflections.
J ASCE 109 TE5 651-668

24. **Heukelom W. & Foster C R. (1960)**
Dynamic testing of pavements.
J ASCE 86 SM1 1-28

25. **Irwin L H. (1977)**
Determination of pavement layer moduli from surface deflection data for pavement performance evaluation.
Proc 4th Int Conf Struct Des Asphalt Pavements 1 Univ Michigan 831-840

26. **Kausel E. & Peek R. (1982)**
Dynamic loads in the interior of a layered stratum - an explicit solution.
Bull Seis Soc Am. Vol. 72 Part 5 1459-1481

27. **Kennedy C K. (1987)**
Pavement evaluation and overlay design using deflectograph - Chapter I.
Conf Analt Des Eval Bituminous Pavements, Course given at Glasgow University.

28. **Koole R C. (1979)**
Overlay design based on falling weight deflectometer measurements.
TRB 700 59-72

29. **Kulkarni R M. Alviti E. & Connor B. (1986)**
Uses of falling weight deflectometer data in predicting fatigue cracking.
TRB 1070 69-76

30. **Lysmer M. & Richart F E. (1966)**
Dynamic response of footing to vertical loading.
J ASCE 92 SM1 65-92

31. **Mamlouk M S. & Davies T G. (1984)**
Elasto-dynamic analysis of pavement deflections.
J ASCE 110 TE6 536-550

32. **McCullough B F. & Taute A. (1982)**
Use of deflection measurements for deterimning pavement material properties.
TRB 852 8-14

33. **Nazarian S. Stokoe K H. & Hudson W R. (1983)**
Uses of spectral analysis of surface wave method for determination of moduli and thickness of pavement system.
TRB 930 38-45

34. **Nazarian S. & Stokoe K H. (1986)**
Use of surface wave in pavement evaluation.
TRB 1070 132-144

35. **Nelson M. & Isada M. (1970)**
Impulsive load stiffness of flexible pavements.
J ASCE 96 SM2 639-650

36. **Peattie K R. (1979)**
The design of overlays - Chapter G.
Conf Analt Des Flexible Pavements, Course given at Glasgow University.

37. **Ramaswamy R. (1988)**
Flexible pavement design - the French practice.
J IHT No. 1 Vol. 35 26-29

38. **Richart F E. Hall J R. & Woods R D. (1970)**
Vibration of soils and foundations.
Prentice Hall, Englewood Cliffs N.J.

39. **Road note 29 (1970)**
Method of flexible pavement design.
BS 594 note 2 para 8.47-8.116

40. **Roesset J M. & Shao K. (1985)**
Dynamic interpretation of dynaflect and falling weight deflectometer tests.
TRB 1022 7-16

41. **Sebaaly B E. Davies T G. & Mamlouk M S. (1985)**
Dynamics of the falling weight deflectometer.
J ASCE 111 TE6 618-632

42. **Sebaaly B E. Mamlouk M S. & Davies T G. (1986)**
Dynamic analysis of falling weight deflectometer data.
TRB 1070 63-68

43. **Sharpe G W. Southgate H F. & Deen R C. (1981)**
Dynamic pavement deflections.
J ASCE 107 TE2 162-181

44. **Shell pavement design manual (1978)**
Asphalt pavements and overlays for road traffic.
Shell Int Petroleum Co

45. **Soydemir C. Werner E. & Schmid M. (1970)**
Deformation and stability of visco-elastic media.
J ASCE 96 SM6 2081-2099

46. **Szendrei M E. & Freeme C R. (1970)**
Road Response to vibration tests.
J ASCE 96 SM6 2099-2123

47. **Tam W S. & Brown S F. (1988)**
Back-analysed elastic stiffnesses : comparison between different evaluation procedures.
1st Int Symp NDT Pavements & Back-calculation of moduli Baltimore Maryland U.S.A. 1-21

48. **Uddin W. Meyer A H. & Hudson W R. (1986)**
Rigid bottom consideration of non-destructive evaluation of pavements.
TRB 1070 21-29

49. **Ullidtz P. & Stubstad R N. (1985)**
Analytical-Empirical pavement evaluation using the falling weight deflectometer.
TRB 1022 36-44

50. **Walker R S. & Hudson W R. (1971)**
Practical uses of spectral analysis with surface dynamic road profilometer.
HRB 362 104-119

51. **Weiss R A. (1977)**
Subgrade elastic moduli determined from vibratory testing of pavements.
Tech. Report S-77-19, U.S. Army Eng Waterway Exp Station, Vicksburg Miss.

52. **Weiss R A. (1979)**
Pavement evaluation and overlay design.
TRB 700 20-34

53. **Yoder E J. & Witczak M W. (1975)**
Principles of pavement design.
Chapters 14-17 John Wiley & Son Inc

APPENDICES

<u>APPENDIX - A -</u>

The Fourier series constants are:

$$a_o = \frac{2}{T} \int_0^T f(t).\ dt \tag{1}$$

$$a_n = \frac{2}{T} \int_0^T f(t).\ \cos\left(\frac{2\pi n}{T}\right) t\ \ dt \tag{2}$$

$$b_n = \frac{2}{T} \int_0^T f(t).\ \sin\left(\frac{2\pi n}{T}\right) t\ dt \tag{3}$$

The function f(t) is defined as follows:

$$f(t) = \begin{cases} \sin\left(\frac{\pi}{T_p}\right)t & 0 \leqslant t \leqslant T_p \quad (4) \\ 0 & T_p \leqslant t \leqslant T \quad (5) \end{cases}$$

Hence

$$a_o = \frac{2}{T} \int_0^{T_p} \sin\left(\frac{\pi}{T_p}\right)t\ dt + \frac{2}{T} \int_{T_p}^{T} 0.\ dt \tag{6}$$

$$= \frac{4}{\pi}.\frac{T_p}{T} \tag{7}$$

Note: Clearly the second term in the Equation (6) is zero and hence these terms are neglected in the sequel.

$$a_n = \frac{2}{T} \int_0^{T_p} \sin\ (\ A\ )\ t\ \ \cos\ (\ \ B\ \ )\ t\ dt \tag{8}$$

where

$$\underline{A = \frac{\pi}{T_p}} \quad \text{and} \quad \underline{B = \frac{2\pi n}{T}}$$

Integration yields:

$$a_n = -\frac{1}{T}\left[\frac{\cos(A-B)t}{A+B} + \frac{\cos(A+B)t}{A+B}\right]_0^{T_p} \qquad (9)$$

Noting that:

$$\cos(AT_p - BT_p) \equiv -\cos(B\,T_p) \qquad (10)$$

and

$$\cos(AT_p + BT_p) \equiv -\cos(BT_p) \qquad (11)$$

We obtain, after some algebra:

$$a_n = \frac{2A}{T}\left(\frac{\cos(BT_p) + 1}{A^2 - B^2}\right) \qquad (12)$$

The final set of constants are obtained similarly:

$$b_n = \frac{2}{T}\int_0^{T_p} \sin(A)t \ \sin(B)t \ dt \qquad (13)$$

$$= \frac{1}{T}\left[\frac{\sin(A-B)t}{A-B} - \frac{\sin(A+B)t}{A+B}\right]_0^{T_p} \qquad (14)$$

$$= \frac{2A}{T}\left[\frac{\sin(B\,T_p)}{A^2 - B^2}\right] \qquad (15)$$

APPENDIX - B -

Exponential form of the Fourier series

With the aid of the Euler formula:

$$e^{ix} = \cos x + i\sin x \tag{1}$$

it can be shown that the Fourier series may be written as:

$$F(t) = Re\left\{ \sum_{n=-\infty}^{+\infty} C_n . e^{(B)t} \right\} \tag{2}$$

where

$$\begin{aligned} B &= \omega n \\ &= \frac{2\pi n i}{T} \end{aligned} \tag{3}$$

The coefficients Cn are defined by the equation

$$C_n = \frac{1}{T} \int_0^T f(t) .\ e^{-Bt}\ dt \tag{4}$$

For FWD loading:

$$f(t) = \begin{cases} \sin (A)t & 0 \leqslant t \leqslant T_p \\ 0 & T_p \leqslant t \leqslant T \end{cases} \tag{5}$$

where

$$A = \frac{\pi}{T_p} \tag{6}$$

Substituting Equations (5) and (6) into Equation (4) we obtain:

$$C_n = \frac{1}{T} \int_0^{T_p} \sin (A)t\ .\ e^{(-B)t}\ dt \tag{7}$$

$$= \frac{A}{T\left(A^2 + B^2\right)} \left[e^{-BT_p} + 1 \right] \tag{8}$$

Substitution of Equation (8) back into Equation (2) and performing the indicated summation yields the synthesised function F(t). In practice, ten terms is sufficient for engineering accuracy if the symmetry of the terms about the zero axis is exploited.

APPENDIX - C -

The enhanced part of the computer program PULSE.

```
      PROGRAM PULSE
C************************
C     THIS PROGRAM CALCULATES THE DISPLACEMENTS OF A MULTI-LAYERED
C     SYSTEM SUBJECTED TO AN IMPULSIVE LOADING.
C
C     TRANSIENT DYNAMIC
C*************************
C
      IMPLICIT REAL*8 (A-H,O-Y)
      COMPLEX*16 Z,ZUT
C
      DIMENSION A(20),XTIME(20),XDISPL(20),FMAG(20)
      DIMENSION QUMOD(30,10),QUTET(30,10),TIME(30),UDISP(30,10)
C
      COMMON/XTRA/PRESSR,IOFLAG
      COMMON/QA/IQNL,IQNN(30),QHH(30),QWW(30),
     +                   QES(30),QPO(30),QBT(30)
      COMMON/QB/QRR,QR2(10),IQNU,IQNUU(10),IQNP,IQNPP(10),
     +         IQNFR,IQNOM,QDOM,IQNR,IQNRR,QOM
      COMMON/QC/IQN,QTA,IQNTA,QTB,IQNTB,QFP
      COMMON/QD/QFREQ(35),QFMOD(35),QFPHI(35)
      COMMON/QE/QUMODA(30),QUTETA(30),QPRESS
      COMMON/QF/STATC(20), USTATC(20),FMAGN(20),WREAL(20)
      COMMON/QG/COUNT
      COMMON/QH/HGRADE,WGRADE,EGRADE,PGRADE,RESFRQ
C
      IOFLAG=0
      PI=3.14159D0
      CALL DATAIN
      NTP=IQNTA+IQNTB+1
C
      CALL FOURIR
      NP1=IQN+1
      COUNT=0.0D0
C
      DO 50 I=1,NP1
      QPRESS=QFMOD(I)
      QOM=QFREQ(I)
      CALL KAUSEL
      COUNT=COUNT+1.D0
      DO 5 J=1,IQNR
      QUMOD(I,J)=QUMODA(J)
      QUTET(I,J)=QUTETA(J)
 5    CONTINUE
 50   CONTINUE
C
      DTA=QTA/DBLE(IQNTA)
      DTB=(QTB-QTA)/DBLE(IQNTB)
      NTP=IQNTA+IQNTB+1
      NTAP=IQNTA+1
      NTAQ=IQNTA+2
C
      DO 10 I=1,NTAP
      TIME(I)=DBLE(I-1)*DTA
 10   CONTINUE
C
      DO 20 I=NTAQ,NTP
      TIME(I)=QTA+DBLE(I-NTAP)*DTB
 20   CONTINUE
C
```

```
      DO 30 I=1,NTP
      T=TIME(I)
      DO 45 K=1,IQNR
      ZUT=0.D0
C
      DO 40 J=1,NP1
      WT=QFREQ(J)*(2.D0*PI)*T
      PHI=QFPHI(J)
      THETA=QUTET(J,K)
      Z=CMPLX(0.D0,(WT-PHI+THETA))
      ZUT=ZUT+QUMOD(J,K)*EXP(Z)
 40   CONTINUE
C
      UDISP(I,K)=REAL(ZUT)
   45 CONTINUE
 30   CONTINUE
C     IF(COUNT.GE.0.D0) GO TO 600
C
      WRITE(6,400)
C       WRITE(6,410)
      WRITE(6,415)
      WRITE(6,515)
C
      WRITE(6,510) (QR2(I),I=1,IQNR)
C
      WRITE(6,420)
      DO 60 I=1,NTP
      WRITE(6,500) TIME(I),(UDISP(I,K),K=1,IQNR)
 60   CONTINUE
C
C***********************************
C
C     THE NEXT SUBROUTINE CALCULATES THE MAXIMUM DISPLACEMENT IN THE
C     RANGE OF 40 MSEC APPLIED. PULSE.
C***********************************
C
      WRITE(6,415)
      WRITE(6,515)
      WRITE(6,510) (QR2(I),I=1,IQNR)
C
      DO 115 I=1,IQNR
      DO 120 J=1,NTAP
      A(J)=UDISP(J,I)
120   CONTINUE
      CALL DMAX(A,NTAP,DTA,TMX,AMX)
      XTIME(I)=TMX
      XDISPL(I)=AMX
115   CONTINUE
C
      WRITE(6,506)
      WRITE(6,505) (XTIME(K),K=1,IQNR)
C
      WRITE(6,507)
      WRITE(6,505)(XDISPL(K),K=1,IQNR)
C
      WRITE(6,508)
      WRITE(6,505) (USTATC(K),K=1,IQNR)
C
      DO 300 JJ=1,IQNR
      FMAG(JJ)=XDISPL(JJ)/USTATC(JJ)
```

```
300     CONTINUE
C
        WRITE(6,509)
        WRITE(6,510)  (FMAG(K),K=1,IQNR)
C
        WRITE(6,511)
        WRITE(6,512)  RESFRQ
C
        WRITE(6,513)
        WRITE(6,514)  HGRADE,EGRADE
C
 400    FORMAT(//,11X,'TIME',25X,'TOTAL  DISPLACEMENT',/)
C   410 FORMAT(/,22X,'(REAL)',6X,'(IMAG)',/)
  500   FORMAT(8X,1PE10.2,2X,1P10E13.2)
505     FORMAT(21X,1P10E13.2)
506     FORMAT(//,2X,'TIME  :-  ')
507     FORMAT(//,'MAX.  DISPL.')
508     FORMAT(//,'STATIC  DISPL.')
509     FORMAT(//,'MAGNFN.  FACTOR')
510     FORMAT(19X,8(5X,F8.3),//)
511     FORMAT(/,'RESONANACE  DUE  TO  HARMONIC  LOADING  OCCURS  AT  :')
512     FORMAT(50X,F10.4,4X,'  HZ  ',//)
513     FORMAT(/,'SUBGRADE  THICKNESS  AND  STIFFNESS  =   ')
514     FORMAT(40X,1P2E13.2)
415     FORMAT(//,1X,'RADIUS  :- ')
 420    FORMAT(8X,'--------------------------------------------------------------',
     + '--------------------------------------------------------------')
 515    FORMAT(1X,6(1H*))
C
C600     CONTINUE
        STOP
        END
        SUBROUTINE  DMAX(A,NTAP,DTA,TMX,AMX)
C****************************************************
C
        IMPLICIT  REAL*8(A-H,O-Z)
        DIMENSION  A(20)
C
        AM=0.D0
        N=NTAP
        DT=DTA
C
        DO  20  I=1,N
        AA=ABS(A(I))
        IF(AA.LT.AM)  GO  TO  10
        IA=I
        AM=AA
 10     CONTINUE
 20     CONTINUE
C
        IF(IA.GT.1.AND.IA.LT.N)  GO  TO  30
        IF(IA.EQ.1)  AMX=A(1)
        IF(IA.EQ.N)  AMX=A(N)
        RETURN
 30     CONTINUE
C
C*****=======FINITE  DIFFERENCE==============
C       ===CALCULATE  CONSTANTS  ==================
C
        A2=(A(IA-1)-2.D0*A(IA)+A(IA+1))/(2.D0*DT*DT)
```

```
      A1=(A(IA+1)-A(IA-1))/(2.D0*DT)
      A0=A(IA)
C
C======CALCULATE TIME===================
C
      ZC=-A1/(2.D0*A2)
C
C***===FORM QUADRATIC EQUATION FOR THE PARABOLA========
C
      AMX=(A2*ZC*ZC)+(A1*ZC)+A0
C
C********  CALCULATE MAX. TIME ************
C
      TMX=DBLE(IA-1)*DT+ZC
      RETURN
      END
      SUBROUTINE DATAIN
C************************
      IMPLICIT REAL*8 (A-H,O-Z)
C
      COMMON/XTRA/PRESSR,IOFLAG
      COMMON/QA/IQNL,IQNN(30),QHH(30),QWW(30),
     +                    QES(30),QPO(30),QBT(30)
      COMMON/QB/QRR,QR2(10),IQNU,IQNUU(10),IQNP,IQNPP(10),
     +         IQNFR,IQNOM,QDOM,IQNR,IQNRR,QOM
      COMMON/QC/IQN,QTA,IQNTA,QTB,IQNTB,QFP
C
      COMMON/QH/HGRADE,WGRADE,EGRADE,PGRADE,RESFRQ
C
C     READ LAYER PROPERTIES
C
      WRITE(6,102)
      WRITE(6,105)
      READ(5,*) IQNL
C
      DO 3 I=1,IQNL
      READ(5,*) IQNN(I),QHH(I),QWW(I),QES(I),QPO(I),QBT(I)
 3    CONTINUE
C
      ACCG=1.D0
      HT=0.D0
C
      DO 4 J=1,IQNL
      NN=IQNN(J)
      HH=QHH(J)
      WW=QWW(J)
      ES=QES(J)
      POI=QPO(J)
      AT=QBT(J)
      GG=0.5D0*ES/(1.D0+POI)
      CS=GG*ACCG/WW
      CS=SQRT(CS)
      CLA=1.D0-2.D0*POI+1.D-20
      CLA=2.D0*POI*GG/CLA
      WRITE(6,103) J,HH,HT,WW,CS,GG,ES,CLA,POI,AT
   4  HT=HT+HH
      WRITE(6,106)
      WRITE(6,104)HT
C
      READ(5,*) HGRADE,WGRADE,EGRADE,PGRADE
```

```
      GGRADE= 0.5D0*EGRADE/(1.D0+ PGRADE)
      CGRADE= GGRADE*ACCG/WGRADE
      CGRADE= SQRT(CGRADE)
      RESFRQ= 0.40D0*CGRADE/HGRADE
C
      IQNFR= 1
      IQNOM= 1
      QDOM= 0.D0
C
      READ(5,*)  IQNR,IQNRR
      READ(5,*)  (QR2(I),I= 1,IQNR)
C
C       QRR= QR2(IQNRR)
      QRR= QR2(IQNRR)/2.D0
C
      IQNP= 1
      IQNPP(1)= 1
C
C       IQNU= 1
C       IQNUU(1)= 1
C
C********READ PAVEMENT LEVEL WHERE DISPLACEMENTS ARE REQUIRED.
      READ(5,*)  IQNU,(IQNUU(I),I= 1,IQNU)
C
      READ(5,*)  IQN
      READ(5,*)  QTA,QTB
      READ(5,*)  IQNTA,IQNTB
      READ(5,*)  QFP
C
      WRITE(6,100)  IQNL
      WRITE(6,130)  IQNR
      WRITE(6,204)  QRR
      WRITE(6,140)  (QR2(I),I= 1,IQNR)
      WRITE(6,145)  (IQNUU(I),I= 1,IQNU)
C
 100  FORMAT(/,5X,'NUMBER OF LAYERS=  ',I3,/)
 140  FORMAT(/,3X,'DISTANCE FROM THE CENTROID OF DISK=  ',2X,10F8.3,/)
 145  FORMAT(/,3X,'LEVEL(S) AT WHICH DISPL. ARE TO BE CALCULATED',
     + 30I5,/)
 130  FORMAT(/,5X,'NUMBER OF RADIAL DISTANCES=  ',I3,/)
204   FORMAT(//,4X,' RADIUS OF DISK LOAD= ',F10.4,/)
C
102   FORMAT(//,1H ,'SOIL PROPERTIES',/,1X,15(1H*),//,2X,
     + 'LAYER',2X,' THICKNESS',
     1'     DEPTH          SPEC.WEIGHT    SH.WAVE VEL   SHR MODULUS     YNGS',
     1' MOD       LAME CONST     POISS.RATIO      DAMPING',/)
 103  FORMAT(1X,I4,1P9E13.2)
104   FORMAT(//,1H ,'TOTAL DEPTH= ',10X,1PE8.2,/)
 105  FORMAT(/,2X,'————————————————————————————————',
     + '————————————————————————————————')
 106  FORMAT(23X,'————')
C
      RETURN
      END
      SUBROUTINE FOURIR
C***********************
C
      IMPLICIT REAL*8 (A- H,O- Y)
      COMPLEX*16 Z,ZFT,ZFS
C
```

```
      DIMENSION  TIME(35),F(35),FS(35),ANCOS(35),BNSIN(35)
      DIMENSION  PHI(35),FPHI(35),FMOD(35),FPMOD(35)
C       DIMENSION  FS1(35),FS2(35),ZFS(35)
      DIMENSION  ZFS(35)
      DIMENSION  CC(35),SS(35)
C
      COMMON/QC/IQN,QTA,IQNTA,QTB,IQNTB,QFP
      COMMON/QD/QFREQ(35),QFMOD(35),QFPHI(35)
C
      PI= 3.14159D0
      IFLAG= 1
      WRITE(6,700)
C
      N= IQN
      WRITE(6,800)  N
      TA= QTA
      TB= QTB
      TR= TB- TA
      WRITE(6,900)TA,TR
      NTA= IQNTA
      NTB= IQNTB
      WRITE(6,905)NTA,NTB
      FP= QFP
      WRITE(6,909)  FP
C
      DTA= TA/DBLE(NTA)
      DTB= (TB- TA)/DBLE(NTB)
      NTP= NTA+ NTB+ 1
      NTAP= NTA+ 1
      NTAQ= NTA+ 2
C
      DO  10  I= 1,NTAP
      TIME(I)= DBLE(I- 1)*DTA
      T= TIME(I)
      A= PI/TA
      X= T*A
      F(I)= SIN(X)*FP
   10 CONTINUE
C
      DO  20  I= NTAQ,NTP
      TIME(I)= TA+ DBLE(I- NTAP)*DTB
      T= TIME(I)
      F(I)= 0.D0
   20 CONTINUE
C
C      CALCULATE  CONSTANT,  A0
C
      W= TA/TB
      A0D2= 2.D0*W/PI
      A= PI/TA
      BDN= 2.D0*PI/TB
C
C      CALCULATE  TERMS  OF  THE  F.S.  FOR  'N'  TERMS
C
      DO  70  I= 1,N
      B= BDN*DBLE(I)
      IF(ABS(A- B).LT.1.0D- 4)  A= B+ 1.0D- 4
C       DEN= TB*(A*A- B*B)
      DEN= TB*((A- B)*(A+ B))
      CC1= COS(B*TA)
```

```
      CC(I)= CC1+ 1.D0
      AN= 2.D0*A*CC(I)/DEN
      SS(I)= SIN(B*TA)
      BN= 2.D0*A*SS(I)/DEN
      ANCOS(I)= AN
      BNSIN(I)= BN
      FPHI(I)= ATAN(BN/AN)
      IF(AN.GT.0.D0) GO TO 17
      IF(BN.LT.0.D0) FPHI(I)= FPHI(I)- PI
      IF(BN.GT.0.D0) FPHI(I)= PI+ FPHI(I)
 17   CONTINUE
      IF(FPHI(I).LT.0.D0) FPHI(I)= (2*PI)+ FPHI(I)
      PHI(I)= 57.3D0*FPHI(I)
      AN2= ANCOS(I)*ANCOS(I)
      BN2= BNSIN(I)*BNSIN(I)
      FMOD(I)= SQRT(AN2+ BN2)
      FPMOD(I)= FMOD(I)*FP
 70   CONTINUE
C
      IF(IFLAG.EQ.1) GO TO 75
      WRITE(6,810)
      WRITE(6,950) (CC(I), I=1,N)
      WRITE(6,820)
      WRITE(6,950) (SS(I), I=1,N)
      WRITE(6,910)
      WRITE(6,950) A0D2
      WRITE(6,915)
      WRITE(6,950) (ANCOS(I),I=1,N)
      WRITE(6,925)
      WRITE(6,950) (BNSIN(I),I=1,N)
 75   CONTINUE
      WRITE(6,935)
      WRITE(6,950) (PHI(I),I=1,N)
      WRITE(6,945)
      WRITE(6,950) (FPMOD(I),I=1,N)
C
C     LOOP OVER TIME 'T' AND CALCULATE F(T)
C
      DO 90 IA=1,NTP
      T= TIME(IA)
      FT= A0D2
      FT1= FT
      FT2= 0.D0
      ZFT= CMPLX(FT1,0.D0)
C
      DO 80 I=1,N
      B= BDN*DBLE(I)
      Z= CMPLX(0.D0,((B*T)- FPHI(I)))
      FT= FT+ ANCOS(I)*COS(B*T)+ BNSIN(I)*SIN(B*T)
C       FT1= FT1+ FMOD(I)*COS((B*T)- FPHI(I))
C       FT2= FT2+ FMOD(I)*SIN((B*T)- FPHI(I))
      ZFT= ZFT+ FMOD(I)*EXP(Z)
 80   CONTINUE
C
      FS(IA)= FT*FP
C       FS1(IA)= FT1
C       FS2(IA)= FT2
      ZFS(IA)= ZFT*FP
 90   CONTINUE
      WRITE(6,930)
```

```
      WRITE(6,980)
C
      DO 200 I=1,NTP
C       WRITE(6,940) TIME(I),F(I),FS(I),FS1(I),FS2(I),ZFS(I)
      WRITE(6,940) TIME(I),F(I),FS(I),ZFS(I)
 200  CONTINUE
C
      QFREQ(1)=0.001D0/TB
      QFMOD(1)=A0D2*FP
      QFPHI(1)=0.D0
      PHI(1)=0.D0
C
      DO 300 I=1,N
      QFREQ(I+1)=DBLE(I)/TB
      QFMOD(I+1)=FMOD(I)*FP
      QFPHI(I+1)=FPHI(I)
      PHI(I+1)=57.3D0*QFPHI(I+1)
 300  CONTINUE
C
      WRITE(6,600)
C
      DO 400 I=1,N+1
      WRITE(6,610) QFREQ(I),QFMOD(I),PHI(I)
 400  CONTINUE
C
 600  FORMAT(//,25X,'FREQUENCY',7X,'AMPLITUDE',3X,'PHASE ANGLE (DEG)',/)
 610  FORMAT(17X,1P10E16.2)
C
 700
FORMAT(//,3X,'==============================================

+ '===============================================
 800  FORMAT(/,3X,'MAX. VALUE OF N USED IN THE TERMS OF THE F.S.',2X,I3)
 900  FORMAT(//,3X,'PULSE DURATION          TP= ',5X,F5.2,3X,'SEC',/,4X,
     .'REST DURATION          TR= ',5X,F5.2,3X,'SEC',/)
 905  FORMAT(/,3X,'NO. OF INTERVALS IN THE PULSE PHASE',3X,I4,/,
     .3X,'NO. OF INTERVALS IN THE RESTING PHASE',3X,I2,/)
  909 FORMAT(/,3X,'PEAK PRESSURE DUE TO THE PULSE=  ',7X,F8.2,/)
 910  FORMAT(1X,'CONSTANT A0D2:')
 930  FORMAT(//,8X,'TIME',13X,'FUNCTION',8X,'FUNCTION ',
     .11X,'COMPLEX FUNCTION')
C     .5X,'IN PHASE FN.',
C     .3X,'OUT-OF-PHASE FN.',6X,'COMPLEX FUNCTION')
980   FORMAT(41X,'VALUES',12X,'(REAL)',10X,'IMAG)',//)
C 980  FORMAT(41X,'VALUES',8X,' VALUES (RE)',5X,' VALUES (IM)',6X,
C     .'(REAL)',10X,'(IMAG)',//)
 915  FORMAT(1X,'COEFFT.AN:')
 940  FORMAT(3X,1PE11.2,3X,1P10E16.2)
 925  FORMAT(1X,'COEFFT.BN:')
 935  FORMAT(1X,'ANGLE PHI(DEG):')
 945  FORMAT(1X,'MODULUS FN:')
 950  FORMAT(15X,1P10E11.2,//)
 810  FORMAT(/,2X,'(COS(B*TA)+1.0) = ',/)
 820  FORMAT(/,2X,'SIN(B*TA) = ',/)
      RETURN
      END
```